

Generalized Quantum Mean-Field Systems and their Application to Ultracold Atoms

Von der Fakultät für Mathematik und Physik
der Gottfried Wilhelm Leibniz Universität Hannover
zur Erlangung des Grades
Doktorin der Naturwissenschaften

Dr. rer. nat.

genehmigte Dissertation

von

Dipl.-Phys. Friederike Annemarie Trimborn-Witthaut

geboren am 15.08.1983

in Ludwigshafen am Rhein

2011

Referent: Prof. Dr. R. F. Werner

Koreferent: apl. Prof. Dr. H. J. Korsch

Tag der Promotion: 18.11.2011

Abstract

Strongly interacting many-body systems consisting of a large number of indistinguishable particles play an important role in many areas of physics. Though such systems are hard to deal with theoretically since the dimension of the respective Hilbert space increases exponentially both in the particle number and in the number of system modes. Therefore, approximations are of considerable interest. The mean-field approximation describes the behaviour in the macroscopic limit $N \rightarrow \infty$, which leads to an effective nonlinear single-particle problem. Although this approximation is widely used, rigorous results on the applicability and especially on finite size corrections are extremely rare. One prominent example of strongly interacting many-body systems are ultracold atoms in optical lattices, which are a major subject of this thesis. Typically these systems consist of a large but well-defined number of particles, such that corrections to the mean-field limit can be systematically studied.

This thesis is divided into two parts: In the first part we study generalized quantum mean-field systems in a C^* -algebraic framework. These systems are characterized by their intrinsic permutation symmetry. In the limit of infinite system size, $N \rightarrow \infty$, the intensive observables converge to the commutative algebra of weak*-continuous functions on the single particle state space. To quantify the deviations from the mean-field prediction for large but finite N , we establish a differential calculus for state space functions and provide a generalized Taylor expansion around the mean-field limit. Furthermore, we introduce the algebra of macroscopic fluctuations around the mean-field limit and prove a quantum version of the central limit theorem. On the basis of these results, we give a detailed study of the finite size corrections to the ground state energy and establish bounds, for both the quantum and the classical case. Finally, we restrict ourselves to the subspace of Bose-symmetric states and discuss their representation by quantum phase space distributions in terms of generalized coherent states. In particular, this allows for an explicit calculation of the evolution equations and bounds for the ground state energy.

In the second part of this thesis we analyse the dynamics of ultracold atoms in optical lattices described by the Bose-Hubbard Hamiltonian, which provide an important example of the generalized quantum mean-field systems treated in the first part. In the mean-field limit the dynamics is described by the (discrete) Gross-Pitaevskii equation. We give a detailed analysis of the interplay between dissipation and strong interactions in different dynamical settings, where we especially focus on the relation between the mean-field description and the full many-particle dynamics given by a master equation.

Keywords: Ultracold Atoms; Quantum Mean-Field Systems; Dissipative Quantum Systems; Finite Size Corrections

Zusammenfassung

Stark wechselwirkende Vielteilchensysteme spielen in vielen Gebieten der Physik eine herausragende Rolle. Die theoretische Beschreibung ist jedoch sehr aufwändig, da die Dimension des Hilbertraums exponentiell mit der Anzahl der Teilchen und der Anzahl der Moden skaliert. Daher sind Näherungen von großem Interesse. Die mean-field Näherung beschreibt das System im Grenzwert $N \rightarrow \infty$ als effektives nichtlineares Einteilchensystem. Auch wenn diese Näherung oft angewendet wird, gibt es nur wenige mathematisch rigorose Ergebnisse. Ein wichtiges Beispiel für ein solches System sind ultrakalte Atome in optischen Gittern, die in dieser Arbeit untersucht werden. Typischerweise bestehen diese Systeme aus einer großen, aber wohlbestimmten Anzahl an Atomen, so dass Abweichungen von mean-field Grenzwert systematisch analysiert werden können.

Diese Arbeit gliedert sich in zwei Teile: Im ersten Teil befassen wir uns mit der Beschreibung von verallgemeinerten mean-field Systemen mithilfe von C^* -Algebren, die durch ihre Permutationssymmetrie charakterisiert sind. Im makroskopischen Grenzwert $N \rightarrow \infty$ konvergieren intensive Observablen gegen die kommutative Algebra der schwach $*$ -stetigen Funktionen auf dem Einteilchenzustandsraum. Um die Abweichungen von einer solchen Beschreibung für große, aber endliche Systemgrößen zu quantifizieren führen wir einen Differentialkalkül für Funktionen auf dem Zustandsraum ein, mit dessen Hilfe wir eine verallgemeinerte Taylorentwicklung um den mean-field Extremwert definieren können. Darüber hinaus diskutieren wir die Algebra der Fluktuationen um den Grenzwert und beweisen einen nicht-kommutativen zentralen Grenzwertsatz. Mithilfe dieser Ergebnisse analysieren wir die Korrekturen aufgrund der endlichen Systemgröße für das Grundzustandsproblem und ermitteln Schranken für den klassischen und den quantenmechanischen Fall. Im letzten Kapitel des ersten Teils betrachten wir Bose-symmetrische Zustände und deren Phasenraumdarstellungen mithilfe verallgemeinerter kohärenter Zustände. Diese Darstellung ermöglicht es unter anderem die Bewegungsgleichungen und Schranken für die Grundzustandsenergie zu bestimmen.

Im zweiten Teil dieser Arbeit beschäftigen wir uns mit der Dynamik von ultrakalten Atomen in optischen Gittern, welche durch das Bose-Hubbard-Modell beschrieben werden und eine wichtige Anwendung der verallgemeinerten mean-field Systeme darstellen. Im mean-field Grenzwert wird die Dynamik durch die Gross-Pitaevskii-Gleichung beschrieben. Wir stellen eine detaillierte Analyse des Zusammenspiels von Dissipation und starker Wechselwirkung zwischen den Teilchen vor. Insbesondere befassen wir uns mit der Beziehung zwischen den Vorhersagen der mean-field Näherung und der vollen Vielteilchendynamik, welche durch eine Mastergleichung beschrieben wird.

Stichwörter: Ultrakalte Atome; Quanten Mean-Field Systeme; Dissipative Quantensysteme; Korrekturen aufgrund endlicher Systemgröße

Contents

Abstract	iii
Zusammenfassung	v
I Generalized Mean-Field Systems	1
1 Mathematical preliminaries	3
1.1 C^* -Algebras	3
1.1.1 Composed systems	5
1.1.2 States on C^* -algebras	5
1.2 CCR-algebra and quasi-free states	7
1.3 Tools from functional analysis	8
2 Introduction to mean-field systems	9
2.1 Mean-field observables: Basic concepts	9
2.2 Strictly symmetric sequences	10
2.3 Approximately symmetric sequences	12
2.4 The limiting algebra	14
2.5 Symmetric states	18
2.5.1 Størmer's theorem and the mean-field limit	19
2.5.2 Finite quantum de Finetti theorem	19
3 Mean-field differential calculus	23
3.1 Introduction to the calculus of state space functions	23
3.2 Higher order derivatives	25
3.3 Extremal problems	28
3.4 Taylor expansion	31

4	The algebra of fluctuations	35
4.1	Quantum fluctuations	35
4.2	Central limit theorem	38
4.3	Expansion in fluctuation operators	41
5	The ground state problem	47
5.1	Introduction	47
5.2	Some illustrative examples from statistical mechanics	49
5.2.1	The mean-field Heisenberg Model	49
5.2.2	Mean-field Ising Model with transverse field	51
5.3	Relations to other problems	52
5.3.1	Finite de Finetti theorems	53
5.3.2	Spin squeezing inequalities and entanglement detection	54
5.4	Inner bound in terms of fluctuations	59
5.4.1	Minimization of the fluctuation Hamiltonian	62
5.4.2	Determination of the mean-field limit of the corrections	63
5.4.3	Illustrative example	66
5.5	Classical ground state problem	67
5.6	Conclusion and outlook	73
6	Quantum phase space	75
6.1	Generalized coherent states	76
6.1.1	Glauber states	77
6.1.2	$SU(M)$ -coherent states	78
6.2	Differential algebra	79
6.2.1	Flatland	80
6.2.2	From the plane to the sphere	81
6.3	Quantum dynamics in phase space	82
6.3.1	Quantum phase space distributions	83
6.3.2	Expectation values	83
6.3.3	Evolution equations	85
6.3.4	Numerical simulation using phase space ensembles	87
7	Relation to the general theory	89
7.1	The Bose-Hubbard model as a quantum mean-field system	89
7.1.1	Formulation in symmetric operators	90
7.1.2	The ground state problem	91
7.2	Mean-field dynamical semigroups	94

7.2.1	Hamiltonian flows	94
7.2.2	Limiting dynamics for the Bose-Hubbard Hamiltonian	97
7.2.3	Symplectic structure	100
7.2.4	Some comments on dissipative systems	102
7.3	Applications of the phase space approach	104
7.3.1	A quantum de Finetti theorem starting from differential operators	104
7.3.2	A quantum de Finetti theorem in phase space	108
7.3.3	Discussion of the bounds	114
7.3.4	A note on quantum phase space entropies	115
7.3.5	The ground-state variational problem	116
 II Dynamics of Ultracold Atoms in Optical Lattices		121
 8 Ultracold atoms in optical lattices – models and methods		123
8.1	Bose-Einstein condensation	123
8.2	Experimental overview	127
8.2.1	From laser cooling to the creation of a BEC	127
8.2.2	Trapping by light	129
8.3	The Bose-Hubbard model	130
8.4	The mean-field limit and beyond	133
8.4.1	The time-independent Gross-Pitaevskii equation	133
8.4.2	Bogoliubov theory	135
8.4.3	The time-dependent Gross-Pitaevskii equation	137
8.4.4	Dynamics beyond mean-field	139
8.5	Noise and dissipation in a trapped Bose-Einstein condensate	141
8.5.1	Master equation	142
8.5.2	Monte Carlo wave function method	144
 9 Dynamics of an open two-mode Bose-Einstein condensate		147
9.1	Ultracold atoms in a double-well trap	147
9.2	Dissipative mean-field dynamics	151
9.2.1	Relation to the non-hermitian Gross-Pitaevskii equation	151
9.2.2	Analysis of fixed points	154
9.2.3	Metastable dynamics	156
9.3	Dissipation induced coherence and stochastic resonance	157
9.3.1	Dissipation induced coherence in a weakly-interacting Bose-Einstein condensate	158

9.3.2	Stochastic resonance of a driven Bose-Einstein condensate	164
9.3.3	Dissipation induced coherence in a strongly-interacting Bose-Einstein condensate	167
9.4	Conclusion	170
10	Landau-Zener transitions and Bloch oscillations in optical lattices	171
10.1	Interacting BEC in a time-varying double-well trap	173
10.1.1	Nonlinear Landau-Zener tunneling	175
10.1.2	Landau-Zener tunneling in phase-space	177
10.1.3	Number squeezing during the transition	180
10.1.4	Influence of interactions onto the Landau-Zener transition probability	182
10.1.5	Semiclassical and adiabatic limit	184
10.1.6	Influence of phase noise	185
10.2	Bloch oscillations	187
10.3	Interacting BEC in a bichromatic lattice	190
10.3.1	Stability of Bloch bands	191
10.3.2	Nonlinear Zener tunneling	195
10.3.3	Depletion of the condensate	198
10.3.4	Bloch-Zener oscillations	200
10.3.5	Coupling of bands by a periodic driving	200
10.4	Concluding remarks	202
11	Decay of a Bose-Einstein condensate in an optical lattice	205
11.1	Dissipative mean-field dynamics and beyond	206
11.2	Inhibition of quantum tunneling	211
11.3	Boundary dissipation	212
11.4	Localized loss	215
11.5	Engineering quantum states by dissipation	218
11.6	Outlook	221
	Bibliography	223

Part I

Generalized Mean-Field Systems

Chapter 1

Mathematical preliminaries

Many particle-systems consisting of a large number of subsystems play an important role in many areas of physics. Symmetry under permutation of subsystems, as it is e.g. implied by the indistinguishability of particles, has a wide range of consequences. In the special case of quantum mean-field systems the subsystems can be assumed to be approximately independent in the limit of an infinite number of subsystems and their behaviour can be described by an effective single-particle theory. The consequences of this description and especially the case of a large, but finite number of subsystems will be analysed in detail in the following chapters. In this chapter we briefly introduce the mathematical framework, provide the basic notations and discuss the fundamental concepts.

1.1 C^* -Algebras

The description of a system in terms of its observable algebra, respective its C^* -algebra, allows for the treatment of both quantum and classical systems, as well as finite and infinite dimensional systems on the same ground. This is especially useful if one is interested in the macroscopic limit and the transition between large, but finite systems and their infinite mean-field counterpart. In this description the C^* -algebra is taking over the role of continuous functions on the space of elementary outcomes, while the probability measures are given by its expectation functionals. Still if one feels more comfortable with linear operators on Hilbert spaces, the Gelfand-Naimark-Segal theorem promises that there is always a representation in the usual language of quantum mechanics even if this representation might not be unique.

In this section, we will give a rough introduction to C^* -algebras and explain the fundamental concepts. To this end, we will partly follow the textbook [1], which gives a basic introduction to quantum systems. For a detailed discussion especially focusing on the relation to statistical physics, as well as for the proofs omitted here, we recommend the seminal books [2, 3].

Definition 1. A C^* -algebra \mathcal{A} is a complex, normed, complete $*$ -algebra with its norm satisfying

$$\|A^*A\| = \|A\|^2, \quad \forall A \in \mathcal{A}. \quad (1.1)$$

In detail, a C^* -algebra \mathcal{A} is a vector space over the field of complex numbers \mathbb{C} , closed under addition $\mathcal{A} \times \mathcal{A} \ni (A, B) \mapsto A + B \in \mathcal{A}$ and multiplication $\mathcal{A} \times \mathcal{A} \ni (A, B) \mapsto AB \in \mathcal{A}$, which in general does not have to be commutative. Furthermore, it is closed under the adjoint operation $\mathcal{A} \ni A \mapsto A^* \in \mathcal{A}$, which fulfills

$$\begin{aligned} (A^*)^* &= A, \\ (\lambda A + \nu B)^* &= \bar{\lambda}A^* + \bar{\nu}B^* \quad \lambda, \nu \in \mathbb{C}, \\ (AB)^* &= B^*A^*, \end{aligned} \quad (1.2)$$

where $\bar{\nu}, \bar{\lambda}$ denote the complex conjugation of ν, λ . Note that the adjoint operation is sometimes also referred to as star operation or involution. In the physics literature the adjoint is often denoted as A^\dagger .

In addition to the usual definition of a norm,

$$\begin{aligned} \|A\| \geq 0 \quad \text{and} \quad \|A\| = 0 &\Rightarrow A = 0, \\ \|\lambda A\| = |\lambda| \|A\| \quad \text{and} \quad \|A + B\| &\leq \|A\| + \|B\|, \end{aligned} \quad (1.3)$$

and the requirement for a Banach algebra,

$$\|AB\| \leq \|A\| \|B\|, \quad (1.4)$$

the norm $\|\cdot\|$ of a C^* -algebra fulfills the C^* -condition (1.1).

Note that a C^* -algebra does not necessarily feature an identity $\mathbb{1}$, though we will be only concerned with unital C^* -algebras in the following.

The case of finite dimensional C^* -algebras is already covered by the obvious example of matrix algebras:

Proposition 2. Any finite dimensional C^* -algebra is isomorphic to a direct sum of square matrix algebras \mathcal{M}_d ,

$$\mathcal{A} \simeq \bigoplus_{j=1}^n \mathcal{M}_{d_j}. \quad (1.5)$$

Other examples for C^* -algebras are e.g. the algebra of compact operators $\mathcal{C}(\mathcal{H})$, as well as the algebra of bounded operators $\mathcal{B}(\mathcal{H})$ on a separable Hilbert space \mathcal{H} equipped with the operator norm

$$\|A\|_\infty := \sup\{\|A\psi\|; \psi \in \mathcal{H}, \|\psi\| = 1\}, \quad (1.6)$$

where $\|\psi\|^2 = \langle \psi | \psi \rangle$ is determined by the scalar product on \mathcal{H} . Later on, we will see that in fact every C^* -algebra is isomorphic to a norm-closed algebra of bound operators on a (generally not separable) Hilbert space.

To analyse the structure of a C^* -algebra the notion of the center of a C^* -algebra,

$$\mathcal{Z}(\mathcal{A}) = \{A \in \mathcal{A} | AB = BA, \forall B \in \mathcal{A}\}, \quad (1.7)$$

consisting of the subset of all commuting elements is useful. The algebra is commutative or abelian if and only if $\mathcal{Z}(\mathcal{A}) = \mathcal{A}$. While non-commuting observables are a fundamental characteristic of quantum systems, classical systems are commutative. The mean-field systems studied in the following are represented by asymptotically abelian C^* -algebras. This explains why these are sometimes denoted as classical.

One particular example for a commutative C^* -algebra is the set of all complex-valued, continuous functions on a compact space X . The following theorem by Gelfand states that this is already the general case:

Theorem 3 (Gelfand). *Any commutative unital C^* -algebra \mathcal{A} is isomorphic to the algebra $\mathcal{C}(X)$ of continuous complex functions on a compact Hausdorff space X . This space is called spectrum of \mathcal{A} and is uniquely determined up to homomorphisms.*

1.1.1 Composed systems

This thesis is focused on composed quantum systems consisting of a finite number of identical subsystems and their asymptotic behaviour in the limit of infinite system size. In general, the tensor product of two C^* -algebras is given by

$$\mathcal{A} \otimes \mathcal{B} = \text{closure}\{A \otimes B | A \in \mathcal{A} \text{ and } B \in \mathcal{B}\}. \quad (1.8)$$

The composed systems forms again a C^* -algebra. This can be seen easily:

$$\begin{aligned} (A \otimes B)^* &= A^* \otimes B^* \\ (A_1 \otimes B_1)(A_2 \otimes B_2) &= A_1 A_2 \otimes B_1 B_2 \quad \forall A_1, A_2 \in \mathcal{A}, B_1, B_2 \in \mathcal{B}. \end{aligned} \quad (1.9)$$

As established in the next section, every C^* -algebra is isomorphic to a norm-closed subalgebra of bounded operators $\mathcal{B}(\mathcal{H})$ on a suitable Hilbert space. For finite dimensional Hilbert spaces, the tensor product of bounded operators corresponds to taking the tensor product of Hilbert spaces,

$$\mathcal{B}(\mathcal{H}_1) \otimes \mathcal{B}(\mathcal{H}_2) \equiv \mathcal{B}(\mathcal{H}_1 \otimes \mathcal{H}_2). \quad (1.10)$$

For a finite number of subsystems, the generalization to more than two subsystems is straightforward. One possibility for treating the case of an infinite number of subsystems is introduced in chapter 2.

1.1.2 States on C^* -algebras

By $\langle \cdot, \cdot \rangle$, we denote the canonical bilinear form between the algebra \mathcal{A} and its dual \mathcal{A}^* . In the case of a finite dimensional algebra the canonical bilinear form is simply given by the trace.

A linear functional $\omega : \mathcal{A} \rightarrow \mathbb{C}$ is called positive, if $\omega(A^*A) \geq 0$ for all $A \in \mathcal{A}$ and normalised if $\omega(\mathbb{1}) = 1$.

Definition 4. A state on a C^* -algebra \mathcal{A} is a positive, linear and normalised functional $\omega : \mathcal{A} \mapsto \mathbb{C}$. The state space $\mathcal{S}(\mathcal{A})$ is defined as the set of all states on \mathcal{A} .

Any convex combination of states $\omega_1, \omega_2 \in \mathcal{S}(\mathcal{A})$,

$$\omega = \lambda\omega_1 + (1 - \lambda)\omega_2 \in \mathcal{S}(\mathcal{A}) \quad \text{with} \quad 0 \leq \lambda \leq 1, \quad (1.11)$$

is again a state. Thus, the state space forms a convex set. A state is called a pure state if it cannot be decomposed in this way, i.e. $\omega = \omega_1 = \omega_2$. Otherwise it is called a mixed state.

A state on a composed system $\mathcal{A} \otimes \mathcal{B}$ is called separable, respectively classically correlated if it can be decomposed as

$$\omega = \sum_k \lambda_k \omega_k^{\mathcal{A}} \otimes \omega_k^{\mathcal{B}}, \quad (1.12)$$

with $\omega_k^{\mathcal{A}} \in \mathcal{S}(\mathcal{A})$, $\omega_k^{\mathcal{B}} \in \mathcal{S}(\mathcal{B})$ and $\sum_k \lambda_k = 1$. Otherwise it is called entangled.

In the case of a finite dimensional C^* -algebra $\mathcal{A} \simeq \mathcal{M}_d$ any state can be rewritten as a positive and normed density matrix D_ω , with $D_\omega \geq 0$ and $\text{tr}(D_\omega) = 1$, such that

$$\omega(A) = \text{tr}(D_\omega A). \quad (1.13)$$

In the general case, a state which admits a density operator representation is called normal.

Definition 5. A representation of a C^* -algebra \mathcal{A} on a Hilbert space \mathcal{H} is a linear map $\pi : \mathcal{A} \rightarrow \mathcal{B}(\mathcal{H})$ fulfilling the following conditions:

$$\begin{aligned} \pi(AB) &= \pi(A)\pi(B), \\ \pi(A^*) &= \pi(A)^*, \\ \pi(\mathbb{1}) &= \mathbb{1}. \end{aligned} \quad (1.14)$$

The Gelfand-Naimark-Segal theorem (GNS) states that every abstract quantum probability space (\mathcal{A}, ω) has a realisation in terms of a Hilbert space, where the connection between abstract description and the concrete realisation is given by a representation π . This allows to rephrase questions from the abstract setting of C^* -algebras in the language of quantum mechanics based on operators on Hilbert spaces.

Theorem 6 (Gelfand-Naimark-Segal). For any given state ω on a C^* -algebra \mathcal{A} , there exists a Hilbert space \mathcal{H}_Ω , a unit vector $\Omega \in \mathcal{H}$ and a representation $\pi : \mathcal{A} \mapsto \mathcal{B}(\mathcal{H}_\Omega)$, such that

$$\begin{aligned} \omega(A) &= \langle \Omega, \pi(A)\Omega \rangle \quad \forall A \in \mathcal{A} \quad \text{and} \\ \pi(\mathcal{A}) &\text{ is dense in } \mathcal{H}_\Omega. \end{aligned} \quad (1.15)$$

1.2 CCR-algebra and quasi-free states

In chapter 4 we will analyse the algebra of fluctuations and in particular show that this is an example for an algebra fulfilling canonical commutation relations (CCR). As the algebraic formulation in terms of Weyl operators is not yet common standard we will provide the basic concepts needed to follow the discussion here. As the notation has proven to be most convenient for the discussion of quantum fluctuation operators, we closely follow the presentation in [4, 5] and borrow some notation from [6].

Let H be a real linear space equipped with a bilinear form σ . (H, σ) is called a real symplectic space with a symplectic form σ if the bilinear form satisfies

$$\sigma(x, y) = -\sigma(y, x) \quad \forall x, y \in H. \quad (1.16)$$

The symplectic form σ is called non-degenerate if $\sigma(x, y) = 0$ for every $y \in H$ implies $x = 0$.

The canonical example for a symplectic space which one should keep in mind in the following is a complex Hilbert space $H = \mathcal{H}$ with the nondegenerate symplectic form been given by the imaginary part of the scalar product, that is

$$\sigma(f, g) = \Im\langle f, g \rangle \quad \forall f, g \in \mathcal{H}. \quad (1.17)$$

The CCR-algebra is generated by the Weyl elements $\{W(f) \mid f \in H\}$, where the involution is given by

$$W(f)^* = W(-f) \quad (1.18)$$

and the product is given by

$$W(f)W(g) = W(f + g)e^{-\frac{i}{2}\sigma(f, g)}. \quad (1.19)$$

Thus $W(0)$ is equal to the identity and all elements are unitary.

For a nondegenerate symplectic space (H, σ) this is already sufficient to define a C^* -algebra, which is even unique up to isomorphisms (cf. e.g. theorem 2.1 in [6]). Still, for a degenerate space, we have to do some more work. In this case we can only conclude from the above definition that the free vector space $\Delta(H, \sigma)$, composed of all finite linear combinations of Weyl elements $W(f)$, is a $*$ -algebra. However, if we consider the completion of $\Delta(H, \sigma)$ in the minimal regular norm, that is

$$\|a\| = \sup\{\psi(a^*a)^{\frac{1}{2}} \mid \psi \text{ is a state}\} \quad \forall a \in \Delta(H, \sigma), \quad (1.20)$$

this defines a C^* -algebra which we identify with the CCR-algebra.

A state ω , i.e. a linear, positive and normalised functional on the CCR-algebra $\Delta(H, \sigma)$ is called regular if the map

$$\mathbb{R} \ni \lambda \mapsto \omega\left(W(\lambda f + g)\right) \quad (1.21)$$

is continuous. From this property it follows (for the technical details see e.g. chapter 5.2 and especially lemma 5.2.12 in [3]) that there exist a linear map $B_\pi : H \rightarrow \mathcal{L}(\mathcal{H}_\omega)$ from H to the set of linear operators on the Hilbert space of the corresponding GNS-representation $(\pi, \omega, \mathcal{H}_\omega)$, such that $B_\pi(f)^* = B_\pi(f)$ is self-adjoint for all $f \in H$ and

$$\pi\left(W(tf)\right) = e^{itB_\pi(f)} \quad \forall t \in \mathbb{R}. \quad (1.22)$$

Since the map $B_\pi(f)$ satisfies the commutation relation

$$[B_\pi(f), B_\pi(g)] = i\sigma(f, g)\mathbb{1} \quad \forall f, g \in H, \quad (1.23)$$

it is called a Bose-field or a field operator.

A quasi free state ω_s on the CCR-algebra as defined above is a state which fulfills

$$\omega_s\left(W(f)\right) = e^{-\frac{1}{2}s(f,f)}, \quad (1.24)$$

where $s(\cdot, \cdot)$ is a real symmetric positive bilinear form on H with

$$\frac{1}{4}|\sigma(f, g)|^2 \leq s(f, f)s(g, g) \quad \forall f, g \in H. \quad (1.25)$$

Note that a quasi free state is an example for a regular state.

For a more detailed introduction we recommend the book [6], while we refer to the seminal books [2, 3] for a rigorous mathematical treatment.

1.3 Tools from functional analysis

Definition 7. Let X, Y be real vector spaces and choose $A \subset X$ to be a convex subset of X . A function $f : A \rightarrow Y$ is called *convex-linear* iff for every $\lambda, \mu \geq 0$ with $\lambda + \mu = 1$ and for all $x, y \in A$, $f(\lambda x + \mu y) = \lambda f(x) + \mu f(y)$ holds.

A simple example for a convex-linear function is the restriction of a linear functions to a convex set.

Theorem 8 (Minmax-Theorem [7]). Let X, Y be two real vector spaces with arbitrary topologies, and $A \subset X, B \subset Y$ two non-empty, convex and compact subspaces. If $f : A \times B \rightarrow \mathbb{R}$ is upper-semicontinuous in A and continuous in B , as well as convex-linear in both arguments, then

$$\sup_{a \in A} \inf_{b \in B} f(a, b) = \inf_{b \in B} \sup_{a \in A} f(a, b). \quad (1.26)$$

For more details, as well as a sketch of the proof, we refer to [8].

Chapter 2

Introduction to mean-field systems

2.1 Mean-field observables: Basic concepts

In this thesis, we want to study many-particle systems and their behaviour with growing system size. Each single system is described by its observable algebra \mathcal{A} . In the case of ultracold atoms, this can be thought of as the single-particle observables, while for a lattice spin system this would refer to the single-site algebra of a quantum lattice system.

The observable algebra for the n -particle system is given by the n -fold minimal C^* -tensor product

$$\underbrace{\mathcal{A} \otimes \mathcal{A} \otimes \cdots \otimes \mathcal{A}}_{n \text{ times}} = \mathcal{A}^{\otimes n} := \mathcal{A}^n. \quad (2.1)$$

The special choice of the norm in which the completion necessary for the definition of the tensor product has to be taken has several technical implications, e.g. on the continuity of linear functionals on the tensor products. However, in the case of a finite C^* -algebra with which we are mostly concerned, the different definitions of the norm on the tensor product coincide and thus the resulting C^* -norm is unique. More details on these questions can be found in [9], whereas a first introduction to the problem is given in [10].

As we are interested in the macroscopic behaviour, we need to relate the different systems with growing particle numbers. To this end we use the embedding $\mathcal{A}^m \hookrightarrow \mathcal{A}^n$ for $m < n$ by the identification of $A \in \mathcal{A}^m$ with

$$A \otimes \mathbb{1}_{n-m} \in \mathcal{A}^n, \quad (2.2)$$

where

$$\mathbb{1}_m = \underbrace{\mathbb{1} \otimes \mathbb{1} \otimes \cdots \otimes \mathbb{1}}_{m \text{ times}}$$

denotes the tensor product of m consecutive identities $\mathbb{1} \in \mathcal{A}$. To indicate the observable $A \in \mathcal{A}$ of a special subsystem of \mathcal{A}^n , we use the notation

$$A^{(i)} = \underbrace{\mathbb{1} \otimes \cdots \otimes \mathbb{1}}_{(i-1) \text{ times}} \otimes A \otimes \underbrace{\mathbb{1} \otimes \cdots \otimes \mathbb{1}}_{(n-i) \text{ times}}. \quad (2.3)$$

We are especially interested in the thermodynamic limit of statistical mechanics, where both the number of particles, as well as the system size tend to infinity. The subject of the next section will be the question how to use the embedding (2.2) not only to consider \mathcal{A}^m as a subalgebra of \mathcal{A}^n , but to rigorously describe the mean field limit in algebraic terms as elements of the inductive limit space.

The common characteristic of all mean-field systems is the underlying symmetry of the interaction which is invariant under a permutation of the subsystems. Both examples from above, ultracold atoms as well as spin systems, feature an intrinsic symmetry which strongly influences the behaviour in the thermodynamic limit. In the case of ultracold atoms the permutation symmetry results directly from the fact that all particles are indistinguishable, whereas in the case of spin systems we explicitly assume that the systems are translationally invariant.

In statistical mechanics we typically face systems with few-body interactions. The typical example for a mean-field system with pairwise interactions is given by the hamiltonian density

$$H_n = \frac{1}{n} \sum_n E^{(i)} + \frac{1}{n(n-1)} \sum_{i \neq j} V^{(i,j)}. \quad (2.4)$$

Here, $E^{(i)} \in \mathcal{A}$ denotes the one-particle energy of the i -th system and $V^{(i,j)} \in \mathcal{A} \otimes \mathcal{A}$ denotes the energy of interaction between the i -th and j -th particle.

The notion *mean-field* refers to the fact that the hamiltonian density H_n , respectively the energy per particle or subsystem, is obtained by averaging over all possible permutations of the onsite energy $E^{(i)}$ and the interaction term $V^{(i,j)}$, that is by taking the average over all possible sites to which $E^{(i)}$ and $V^{(i,j)}$ can be permuted.

In the language of statistical mechanics, the energy density H_n is an intensive observable, while the total energy of the system, respectively the expectation value of the Hamiltonian $\langle nH_n \rangle$ is an extensive quantity. Extensive quantities diverge in the macroscopic limit $n \rightarrow \infty$, while intensive quantities do not scale with the system size, but constitute specific quantities characterising the system. In this language, mean-field observables are intensive quantities.

2.2 Strictly symmetric sequences

The preceding argument constitutes the heuristic basis for the abstract description of mean-field systems and their thermodynamic limit. To define and analyze general mean-field observables, going beyond the example of pairwise-interactions (2.4), we

use the formalism of symmetric sequences introduced in [11]. While this description was first aimed at the rigorous derivation of a variational formula for the free energy per particle in the thermodynamic limit, the framework is far more general and has proven to be beneficial in many applications ranging from ground-state problems to dynamical questions [12, 13]. There are several notations, which have proven to be useful depending on the context they are used in. Here, we will closely follow the introduction in [12].

For all $m, n \in \mathbb{N}$ with $n \geq m$ we introduce the symmetrization maps, $\text{sym}_n : \mathcal{A}^m \rightarrow \mathcal{A}^n$, as the consecutive application of the natural embedding

$$\mathcal{A}^m \hookrightarrow \mathcal{A}^n : A_m \mapsto A_m \otimes \mathbb{1}_{n-m} \quad (2.5)$$

and a symmetrization with respect to all permutations of n sites. Explicitly, this means

$$\text{sym}_n(A_m \otimes \mathbb{1}_{n-m}) = \frac{1}{n!} \sum_{\pi \in S_n} \pi(A_m \otimes \mathbb{1}_{n-m}), \quad (2.6)$$

where the sum is taken over all permutations $\pi \in S_n$ of the factors of the tensor product in \mathcal{A}^n and S_n denotes the symmetric group on n letters. Wherever possible without loss of clarity, the notation will be shortened to $\text{sym}_n(A_m)$ in the following.

Since $\mathcal{A}_{\text{sym}}^n$ is a family indexed by a direct set and the homomorphism $\text{sym}_n : \mathcal{A}_{\text{sym}}^m \mapsto \mathcal{A}_{\text{sym}}^n$ fulfills

$$\begin{aligned} \text{sym}_n(\text{sym}_n(A_k)) &= \text{sym}_n(A_k) \\ \text{sym}_n(\text{sym}_m(A_k)) &= \text{sym}_n(A_k) \quad \forall k \leq m \leq n, \end{aligned} \quad (2.7)$$

The symmetrized spaces $\mathcal{A}_{\text{sym}}^n := \text{sym}_n(\mathcal{A}^n)$ together with the symmetrization $\text{sym}_n : \mathcal{A}_{\text{sym}}^m \rightarrow \mathcal{A}_{\text{sym}}^n$ form an inductive system of vector spaces.

As stated earlier, we are especially interested in the thermodynamic limit of statistical mechanics, where both the number of particles, as well as the system size tend to infinity. If we consider \mathcal{A}^m as a subalgebra of \mathcal{A}^n via the embedding (2.2) this limit can be described in algebraic terms as elements of the inductive limit space

$$\mathcal{A}^\infty = \overline{\bigcup_n \mathcal{A}_{\text{sym}}^n}. \quad (2.8)$$

Whenever it is convenient, we will consider $\mathcal{A}_{\text{sym}}^n$ as a subalgebra of \mathcal{A}^∞ in this sense. The inductive system is associated with a natural seminorm,

$$\|A\| = \inf_{n \geq 0} \sup_{m \geq n} \|A_m\| = \limsup_{n \geq 0} \|A_n\|. \quad (2.9)$$

In this description, $\text{sym}_n(A_n)$ and $\text{sym}_{n+m}(A_n)$ can be identified as elements of the same equivalence class. The elements of the inductive limit space are the strictly symmetric sequences, which are defined as follows:

Definition 9. *Sequences of observables for which $A_n = \text{sym}_n(A_{n_0})$ for all $n \geq n_0$ with $A_{n_0} \in \mathcal{A}_{\text{sym}}^{n_0}$ are called strictly symmetric of degree n_0 . The set of strictly symmetric observables is denoted as \mathcal{Y} .*

These are exactly the sequences $\mathbb{N} \mapsto A_n \in \mathcal{A}^n$ considered in the original treatment of mean-field dynamics [14] and obviously include the example

$$H_n = \text{sym}_n(E) + \text{sym}_n(V), \quad (2.10)$$

which gives rise to a strictly symmetric sequence of degree 2 (cf. equation (2.4)). Wherever we refer to the sequence in general and not to a special element of the sequence, we will suppress the index to shorten the notation.

At this point it is worth to pause for a moment: What characterises a mean-field observable is its scaling behaviour with the system size. Starting from the few-particle operators acting on a fixed number of particles, as e.g. the two particle interaction term in equation (2.4), one can write down the many-particle observable for every system size n just by averaging over all possible permutations.

2.3 Approximately symmetric sequences

Although we now have a formal definition of mean-field observables there is a fundamental drawback: The set of strictly symmetric sequences \mathcal{Y} is obviously closed under addition, but generally not under multiplication. This can already be seen by the simple example of a multiplication of the symmetrisation of two single-particle operators $A, B \in \mathcal{A}$:

$$\begin{aligned} & \text{sym}_n(A) \text{sym}_n(B) \\ &= \frac{1}{n} \left(\sum_i A^{(i)} \right) \frac{1}{n} \left(\sum_j B^{(j)} \right) \\ &= \frac{1}{n^2} \left(\sum_{i \neq j} A^{(i)} B^{(j)} + \sum_i AB^{(i)} \right) \\ &= \frac{1}{n(n-1)} \left(\sum_{i \neq j} A^{(i)} B^{(j)} \right) + \frac{1}{n} \left(\frac{1}{n} \sum_i AB^{(i)} - \frac{1}{n(n-1)} \sum_{i \neq j} A^{(i)} B^{(j)} \right) \\ &= \text{sym}_n(A \otimes B) + \frac{1}{n} (\text{sym}_n(AB) - \text{sym}_n(A \otimes B)) \end{aligned} \quad (2.11)$$

Hence, the set of all strictly symmetric sequences \mathcal{Y} does not form a closed algebra providing a suitable framework for a rigorous analysis.

To overcome the problem, we need to analyse it in more detail. Therefore, we consider the product of two strictly symmetric observables of arbitrary, but fixed degree k, ℓ ,

e.g. $\text{sym}_n(A_k)$ and $\text{sym}_n(B_\ell)$ with $\text{sym}_k A_k = A_k$ and $\text{sym}_\ell B_\ell = B_\ell$. Moreover, we assume that $n \geq k + \ell - 1$. Thus, multiplication of the observables yields

$$\begin{aligned} \text{sym}_n(A_k) \cdot \text{sym}_n(B_\ell) &= \text{sym}_n(A_k \otimes \mathbb{1}_{n-k}) \text{sym}_n(B_\ell \otimes \mathbb{1}_{n-\ell}) \\ &= \text{sym}_n \left(\frac{1}{n!} \sum_{\pi} (A_k \otimes \mathbb{1}_{n-k}) \pi (B_\ell \otimes \mathbb{1}_{n-\ell}) \right). \end{aligned} \quad (2.12)$$

Here we have just used the definition of the symmetrisation operation by the sum over all possible permutations π of indices (cf. equation (2.6)). All the terms with the same number of common sites on which A_k and B_ℓ act give exactly the same contribution to the product under the symmetrization operation. Hence, we can reorder the summands according to the overlap r between A_k and B_ℓ ,

$$\text{sym}_n(A_k) \text{sym}_n(B_\ell) = \sum_{r=0}^{\max(k,\ell)} c_n(k, \ell, r) \text{sym}_n((A_k \otimes \mathbb{1}_{\ell-r})(\mathbb{1}_{k-r} \otimes B_\ell)). \quad (2.13)$$

For $r = 0$ there is no overlap, while for $r > 0$ there are exactly r sites on which both A_k and B_ℓ act. These are sometimes referred to as ‘collision terms’.

The factor $c_n(k, \ell, r)$ can be determined by a simple combinatoric argument, as it is given by the fraction of the number of summands featuring r intersections and the total number of permutations,

$$c_n(k, \ell, r) = \frac{k! \ell! (n - k!) (n - \ell!)}{n! r! (k - r)! (\ell - r)! (n + r - k - \ell)!}. \quad (2.14)$$

Obviously, for $n \rightarrow \infty$ only the term with $r = 0$ contributes and thus the product of two strictly symmetric observables, $\text{sym}_n(A_k) \text{sym}_n(B_\ell)$, is to leading order symmetric,

$$\lim_{n \rightarrow \infty} \|\text{sym}_n(A_k) \text{sym}_n(B_\ell) - \text{sym}_n(A_k \otimes B_\ell \otimes \mathbb{1}_{n-k-\ell})\| = 0. \quad (2.15)$$

A closer analysis shows that the factor c_n decreases exponentially with the overlap r in the limit of large system size:

$$\lim_{n \rightarrow \infty} n^r c_n(k, \ell, r) = r! \binom{k}{r} \binom{\ell}{r}. \quad (2.16)$$

Hence, for finite n there is a whole hierarchy of corrections including all kinds of collision terms, where the scaling of the corrections depends on the overlap r . A careful evaluation of the sum of all summands with $r \neq 0$ shows that the error of the approximation of the product $\text{sym}_n(A_k) \text{sym}_n(B_\ell)$ by the strictly symmetric operator $\text{sym}_n(A_k \otimes B_\ell)$ as given by the summand with $r = 0$ is bounded by

$$\|\text{sym}_n(A_k) \text{sym}_n(B_\ell) - \text{sym}_n(A_k \otimes B_\ell \otimes \mathbb{1}_{n-k-\ell})\| \leq \frac{k\ell}{n} \|A_k\| \|B_\ell\|, \quad (2.17)$$

(cf. Lemma IV.1 in [11]). This clearly shows that the set of strictly symmetric sequences \mathcal{Y} is not closed under multiplication. Hence, to obtain a closed algebra we have to weaken the symmetry condition with the constraint that in the limit of an infinite number of subsystems the observables are still symmetric. To make this notion rigorous we introduce the definition of approximately symmetric sequences:

Definition 10. *The set of approximately symmetric sequences is defined as the closure of the set of strictly symmetric sequences with respect to the seminorm (2.9) and will be referred to as $\tilde{\mathcal{Y}}$ in the following.*

Note that this definition is reminiscent of the set of microstates in statistical mechanics, which differ on the microscopic level, but contribute to the same macrostate. By definition, all approximately symmetric sequences $A_n \in \mathcal{A}^n$ can be uniformly approximated by a strictly symmetric sequence,

$$\lim_{n > m \rightarrow \infty} \|A_n - \text{sym}_n A_m\| = 0. \quad (2.18)$$

This is why the approximately symmetric sequences are sometimes referred to as mean-field convergent. The completion can be interpreted as the set of intensive observables including microscopic perturbations even though these do not influence the macroscopic behaviour.

The product of two symmetric sequences (2.13) is an example of an approximately symmetric sequence. This remains true when multiplying two approximately symmetric sequences. Thus, the set of approximately symmetric sequences $\tilde{\mathcal{Y}}$ is closed under multiplication and therefore again a C^* -algebra.

Moreover, we have seen that each approximately symmetric sequence can (for large n) be uniformly approximated by a strictly symmetric sequence and the product of two strictly symmetric sequences (2.13) is to leading order given by

$$\text{sym}_n (A_k \otimes B_\ell) = \text{sym}_n (B_\ell \otimes A_k). \quad (2.19)$$

Hence, the set of approximately symmetric sequences $\tilde{\mathcal{Y}}$ is asymptotically abelian, i.e.

$$\lim_{n \rightarrow \infty} \|A_n B_n - B_n A_n\| = 0 \quad (2.20)$$

for all $A_n, B_n \in \tilde{\mathcal{Y}}$. In this sense, the many-particle structure does no longer play a dominant role in the limit of an infinite number of particles and due to the asymptotic commutativity, the system can be considered as classical in the macroscopic limit.

In the next section we will see how the formalism presented here allows for an approximate treatment of the system in the limit of infinite particle numbers as a single particle system under the influence of a mean interaction potential, which yields an effective nonlinearity.

2.4 The limiting algebra

In the preceding sections we have seen that the approximately symmetric sequences provide a set of intensive observables because of their scaling behaviour with growing system size. By construction, the set of approximately symmetric sequences is the completion of the set of strictly symmetric sequences under the seminorm (2.9), which

thus form a dense subset of the approximately symmetric sequences. In other words, the set \mathcal{Y} contains exactly the sequences in the limiting space of the inductive system (cf. equation (2.7)). Due to their permutation symmetry and their scaling properties the approximately symmetric sequences can be identified with the observables of quantum mean-field systems.

In this section we will have a closer look at the behaviour of approximately symmetric sequences in the limit of infinite system size. This can be interpreted as the thermodynamic limit of intensive observables for mean-field systems. According to a common heuristic argument, it is sufficient to treat the many-particle problem as an effective single-particle problem in the macroscopic limit, which is subject to an effective mean-field potential given by the averaged interaction over all other particles. Here we will explain how we can put this argument on more solid grounds. Still we can only give a rough introduction following the presentation in [12, 13]. A much more detailed discussion can be found in [11].

In the first chapter we have introduced the state space $\mathcal{S}(\mathcal{A}) \subset \mathcal{A}^*$ as the subset of the dual of \mathcal{A} , which contains all positive, normalized linear functionals on \mathcal{A}

$$\mathcal{S}(\mathcal{A}) = \{\rho \in \mathcal{A}^* \mid \rho \geq 0, \langle \rho, \mathbb{1} \rangle = 1\}. \quad (2.21)$$

As above, $\langle \cdot, \cdot \rangle$ denotes the canonical bilinear form between the algebra \mathcal{A} and its dual \mathcal{A}^* . In the following we will also use the common notation $\rho(A)$ from operator algebra theory for the expectation value of an observable A in the state ρ wherever this notation seems more convenient. As defined in section 1.1.2 $\rho^n = \rho^{\otimes n} \in \mathcal{S}(\mathcal{A}^{\otimes n})$ will denote the n -fold homogeneous product state.

With these preliminary considerations we can define a functional $A_\infty : \mathcal{S}(\mathcal{A}) \rightarrow \mathbb{C}$ for each sequence $A_n \in \mathcal{A}^{\otimes n}$ by

$$A_\infty(\rho) = \lim_{n \rightarrow \infty} \langle \rho^{\otimes n}, A_n \rangle. \quad (2.22)$$

It is easy to see that this map defines a continuous function on the single-particle state space $\mathcal{S}(\mathcal{A})$, e.g. $A_\infty \in \mathcal{C}(\mathcal{S}(\mathcal{A}))$, when $\mathcal{S}(\mathcal{A})$ is equipped with its weak*-topology.

However from a more abstract viewpoint, the map (2.22) can be interpreted as a map $\tilde{\mathcal{Y}} \rightarrow \mathcal{C}(\mathcal{S}(\mathcal{A}))$ assigning to each approximately symmetric sequence $A_n \in \tilde{\mathcal{Y}}$ the function $A_\infty(\cdot)$, that is

$$\tilde{\mathcal{Y}} \ni A_n \mapsto \left(\rho \mapsto \lim_{n \rightarrow \infty} \langle \rho^{\otimes n}, A_n \rangle \right) \in \mathcal{C}(\mathcal{S}(\mathcal{A})). \quad (2.23)$$

In the following we will have a closer look at the set of all limits A_∞ and show that the latter interpretation yields not only a simple map, but an isometric homomorphism. In conclusion, the algebra of approximately symmetric sequences $\tilde{\mathcal{Y}}$ can be identified with the commutative algebra of weak*-continuous functions on the single-particle state space, $\mathcal{C}(\mathcal{S}(\mathcal{A}))$. Thus, in the macroscopic limit the many-particle system can be approximately treated as a single-particle system, which is commutative and therefore behaves like a classical system.

First of all, we note that each element A_∞ can be seen as an equivalence class containing all mean-field convergent sequences which do not differ in the seminorm (2.9), e.g.

$$A_n \sim B_n \quad \Leftrightarrow \quad \lim_{n \rightarrow \infty} \|A_n - B_n\| = 0. \quad (2.24)$$

In this sense, A_∞ can be understood as an element of the inductive limit space (2.8). Still note that the existence of the limit alone does not imply that the sequence is approximately symmetric.

For a strictly symmetric sequence of degree r , $\text{sym}_n(A_r) \in \mathcal{Y}$, the functional (2.22) becomes independent of n for all $n > r$:

$$\begin{aligned} A_\infty(\rho) &= \lim_{n \rightarrow \infty} \langle \text{sym}_n(A_r), \rho^{\otimes n} \rangle \\ &= \langle \rho^{\otimes r}, A_r \rangle \quad \forall A_r \in \mathcal{Y}. \end{aligned} \quad (2.25)$$

Thus, we can conclude that the image of strictly symmetric sequences under the homomorphism (2.23) defines a subalgebra of polynomials on the state space of \mathcal{A} . Because each element of $\tilde{\mathcal{Y}}$ can be uniformly approximated by a strictly symmetric sequence, this subset is dense.

Obviously, the set of all limiting elements A_∞ is a vector space, as

$$\begin{aligned} \lim_{n \rightarrow \infty} (\alpha A_n + \beta B_n)(\rho) &= \langle \rho^{\otimes n}, \alpha A_n + \beta B_n \rangle \\ &= \alpha A_\infty(\rho) + \beta B_\infty(\rho) \end{aligned} \quad (2.26)$$

holds for all $\alpha, \beta \in \mathbb{C}$ and $A_n, B_n \in \tilde{\mathcal{Y}}$.

Because of the seminorm properties, $\|\text{sym}_m(A_n)\| \leq \|A_n\|$ is decreasing and hence convergent. Hence, A_∞ equipped with the supremum norm

$$\|A_\infty\| = \lim_{n \rightarrow \infty} \|A_n\| \quad (2.27)$$

is a Banach space. Moreover, this shows that the map (2.22) is an isometry.

In the preceding section, we have already seen that the n -fold product of two approximately symmetric sequences is again approximately symmetric. Furthermore, for two strictly symmetric sequences, the product $\text{sym}_n(A_k)\text{sym}_n(B_\ell)$ is to leading order given by $\text{sym}_n(A_k \otimes B_\ell)$ and therefore asymptotically commutative. Transferring this result to the limit space spanned by the elements A_∞ , this space becomes an abelian algebra. This reasoning also explains the choice of the n -fold product state $\rho^{\otimes n}$ as the reference state in (2.22), since in the limit $n \rightarrow \infty$ this defines a multiplicative functional on the n -fold product. Moreover, one can show that one can construct all pure states on $\mathcal{C}(\mathcal{S}(\mathcal{A}))$ in this way (for more details see [11]).

Finally, we verify the C^* -condition (1.1), which can be directly carried over from the properties of the C^* -algebra \mathcal{A} ,

$$\|A_\infty^* A_\infty\| = \lim_{n \rightarrow \infty} \|A_n^* A_n\| = \lim_{n \rightarrow \infty} \|A_n\|^2 = \|A_\infty\|^2. \quad (2.28)$$

Summarizing the above results we conclude that the map (2.23) preserves the algebraic structure and therefore yields an isometric homomorphism from $\tilde{\mathcal{Y}}$ to $\mathcal{C}(\mathcal{S}(\mathcal{A}))$. Since the set of all strictly symmetric sequences is dense in $\tilde{\mathcal{Y}}$, the subalgebra of polynomials on the state space of \mathcal{A} is dense in $\mathcal{C}(\mathcal{S}(\mathcal{A}))$. Hence, by the Stone-Weierstrass theorem, the homomorphism is onto $\mathcal{C}(\mathcal{S}(\mathcal{A}))$: The image must be a closed subalgebra and contains the linear functionals on $\mathcal{S}(\mathcal{A})$. In other words, $\mathcal{C}(\mathcal{S}(\mathcal{A}))$ is the Hausdorff completion of the inductive system.

In conclusion the algebra of approximately symmetric sequences $\tilde{\mathcal{Y}}$ is isometric and homomorphic with the commutative algebra of weak*-continuous functions $\mathcal{C}(\mathcal{S}(\mathcal{A}))$. Note, that the homomorphism property can be extended to a whole C^* -functional calculus (more details can be found in the appendix of [11]).

The following theorem summarizes the argument presented in this section. It provides the basis for the abstract description of general mean-field systems, as well as the starting point for the analysis of the fluctuations around the mean-field limit. Here, $A \in \tilde{\mathcal{Y}}$ refers to the sequence $n \mapsto A_n \in \mathcal{A}^n$, and not to a special element $A_n \in \mathcal{A}^n$ of the sequence.

Theorem 11 (Generalized mean-field systems [12, 13]).

1. For all $A \in \tilde{\mathcal{Y}}$ the seminorm $\|A\| = \lim_{n \rightarrow \infty} \|A_n\|$ exists and $\tilde{\mathcal{Y}}$ is the completion of \mathcal{Y} in the seminorm (2.9). Furthermore, $\tilde{\mathcal{Y}}$ is closed within the set of all sequences $n \mapsto A_n \in \mathcal{A}^n$ in this seminorm.
2. $\tilde{\mathcal{Y}}$ is an algebra with the operations of n -wise addition $(A + B)_n = A_n + B_n$ and n -wise multiplication $(AB)_n = A_n B_n$, which is commutative under the seminorm (2.9) in the sense that

$$\|AB - BA\| = \lim_{n \rightarrow \infty} \|A_n B_n - B_n A_n\| = 0. \quad (2.29)$$

3. For all $A \in \tilde{\mathcal{Y}}$, $A_\infty(\rho) := \lim_{n \rightarrow \infty} \text{sym}_n(A_n)(\rho^{\otimes n})$ exists uniformly for all $\rho \in \mathcal{S}(\mathcal{A})$.
4. The map $\tilde{\mathcal{Y}} \ni A \mapsto A_\infty \in \mathcal{C}(\mathcal{S}(\mathcal{A}))$ is an isometric *-homomorphism from $\tilde{\mathcal{Y}}$ onto $\mathcal{C}(\mathcal{S}(\mathcal{A}))$.

A detailed introduction to the general theory of quantum mean-field systems can be found in the seminal paper [11]. A thorough study of the limiting dynamical semigroup addressing several fundamental questions ranging from the conditions for the existence of the limit to an analysis of the stability properties, is given in [12]. In the last chapter of part I, we will give a short introduction to the application of these results to hamiltonian systems following [13] and discuss the relation to the phase space description for Bose symmetric systems. In particular we will show that the theory of differential operators introduced in section 6.2 provides an efficient way to explicitly calculate and analyse the limiting phase space flow predicted by the general theory.

The ideas presented in this chapter can be extended to study local dynamics to analyse the interactions between a small amount of tagged sites and the bulk [15]. Moreover, this framework is not restricted to homogeneous mean-field systems, but can be generalized to treat inhomogeneous mean-field systems. In these systems each single-site algebra \mathcal{A} carries an additional label, describing e.g. a position or different types of species, which influences the interaction. If these labels are given by points in a compact space X with a limiting distribution which fulfills some specific conditions, one can carry through the theory considering $\mathcal{C}(X, \mathcal{A})$ instead of $\mathcal{C}(\mathcal{S}(\mathcal{A}))$ [16]. One important example for such a system is the BCS-model without the strong coupling assumption. These systems are treated in [17]. Dynamical questions in a general inhomogeneous mean-field setting are discussed in [18].

The abstract treatment of quantum mean-field systems features some fundamental connections to the theory of large deviations [19] and is closely related to the theorem by Størmer about the integral decomposition of symmetric states on an infinite tensor product of C*-algebras [20]. The relation to the results presented above will be briefly highlighted in the next section. Later on, this discussion will be taken up again from a different viewpoint in chapter 5, as well as in the context of quantum phase space distributions in chapter 6.

2.5 Symmetric states

In this section we briefly discuss the implications of the symmetry property for states. In particular, we will introduce the theorem by Størmer which provides an integral decomposition, characterising permutation symmetric states on infinite tensor products, such as the C*-inductive limit algebra

$$\mathcal{A}^\infty = \overline{\bigcup_n \mathcal{A}^n}. \quad (2.30)$$

For the time being, we will only consider finite dimensional C*-algebras, respective d -dimensional matrices $\mathcal{A} = \mathcal{M}_d$. The limit is taken along the embeddings $\mathcal{A}^m \rightarrow \mathcal{A}^n : A_m \mapsto A_m \otimes \mathbb{1}_{n-m}$.

Moreover, we will explain how one can directly obtain this result as a corollary of theorem 11 and give an alternative formulation commonly known as quantum de Finetti theorem [21–24]. This theorem is a generalization of a result from classical probability theory on the relation between the symmetry and the independent and identically distributed (i.i.d.) property [25]. Here we will follow the recommendable introduction [26]. Here we only briefly comment on the implications of the quantum de Finetti, but we will come back to this point in chapter 5. Furthermore, we will prove two similar results in the context of quantum phase space distributions in chapter 6.

2.5.1 Størmer's theorem and the mean-field limit

A state $\rho_n \in \mathcal{A}^n$ is called symmetric if it is invariant under an exchange of its subsystems, e.g. the state is not affected by any permutation π :

$$\rho_n = \pi \rho_n \pi^\dagger. \quad (2.31)$$

In the case of an infinite tensor product of C^* -algebras, as e.g. \mathcal{A}^∞ (2.30), a state $\phi \in \mathcal{S}(\mathcal{A}^\infty)$ is said to be symmetric if all restrictions to a finite sequence are symmetric, that is

$$\phi(\text{sym}_n(A_n)) = \phi(A_n) \quad \forall n \in \mathbb{N} \quad (2.32)$$

with $A_n \in \mathcal{A}^n \subset \mathcal{A}^\infty$.

Størmer's theorem [20] establishes that the set of all symmetric states on \mathcal{A}^∞ forms a simplex with the extremal states been given by product states, which yields a tractable parametrization of the infinite dimensional convex set \mathcal{A}^∞ .

Corollary 12 (Størmer's theorem [20]). *Any symmetric state ϕ on \mathcal{A}^∞ has a w^* -integral decomposition*

$$\phi = \int \mu(d\sigma) \sigma^\infty, \quad (2.33)$$

where μ is a probability measure on $\mathcal{S}(\mathcal{A})$ and σ^∞ denotes the infinite product state on \mathcal{A}^∞ .

This corollary is a consequence from the above reasoning, and especially from theorem 11. This can be seen as follows:

For each permutation symmetric state ϕ the limit $\lim_n \phi(A_n)$ exists uniformly for each $A \in \tilde{\mathcal{Y}}$ and thus defines a state on $\tilde{\mathcal{Y}}$ as promised by theorem 11. Now this space modulo the equivalence relation (2.24) is isomorphic to $\mathcal{C}(\mathcal{S}(\mathcal{A}))$. Hence, the state ϕ is equivalent to a state on $\mathcal{C}(\mathcal{S}(\mathcal{A}))$, which another way of saying that it defines a measure on $\mathcal{C}(\mathcal{S}(\mathcal{A}))$. Finally, the decomposition into pure states yields (2.33). For more details on the proof of corollary 12, as well as on the relation to the general mean-field theory we refer to [11].

In the next section, we will see how the same problem arises in a quite different context. Moreover, we will explain how one can weaken the symmetry assumptions to be able to approximate a larger class of states by the convex combination (2.33) and give explicit bounds on the error of the approximation, for a large but finite number of tensor factors N .

2.5.2 Finite quantum de Finetti theorem

All physical laws are based on a limited number of observations restricted by experimental resources. Yet we expect them to hold in general. This paradigm, which we

have to assume but which we cannot verify experimentally. It is most clearly expressed in the tomography problem [26] :

Given a large composite system consisting of N subsystems ρ_1, \dots, ρ_N where only k out of N are experimentally accessible. Now one can ask under which assumptions the physical state of the whole system can be inferred on the basis of this experimental data?

Lets first assume that the physical state of the N -partite system is composed of N independently and identically distributed (i.i.d.) copies of the same state σ , which is just another way of saying that we assume that ρ_N is a product state $\rho_N = \sigma^{\otimes N}$. Then it is possible to deduce the physical state of the composite system only by individual measurements on a small number of subsystems. However, the complete absence of any correlation can in itself not be verified experimentally, unless the whole state is accessible. On the other hand, symmetry $\rho_N = \pi \rho_n \pi^\dagger$ is often implied naturally in physical systems, e.g. by the indistinguishability of identical particles or can be enforced by random permutations of the subsystems. But still it is not clear if this assumption alone is sufficient to solve the tomography problem.

To clarify this problem one has to go back to the fundamental relation between symmetric and i.i.d. states. Bruno de Finetti was the first to address this question in the context of classical probability distributions of random variables for the special case of fixed k and $N \rightarrow \infty$ [25, 27]. In its generalized form [28], the classical de Finetti theorem makes a statement about exchangeable random variables, that is probability distributions which are invariant under permutations.

Theorem 13 (Classical de Finetti theorem [28]). *Let S be a finite set of cardinality d and P be an exchangeable probability distribution on S^N . Then there exists a probability μ on the Borel subsets of the set of probabilities on S , such that the projection P_k of P on S^k can be approximated as*

$$\|P_k - P_{\mu,k}\|_{\text{sup}} \leq \frac{dk}{N} \quad \forall k \leq N, \quad (2.34)$$

where we have defined

$$P_{\mu,k}(A) = \int p^{\otimes k}(A) \mu(dp) \quad (2.35)$$

to be a convex combination of identically and independently distributed probability measures. For sets of infinite cardinality, the error is given by

$$\|P_k - P_{\mu,k}\|_{\text{sup}} \leq \frac{k(k-1)}{2N} \quad \forall k \leq N. \quad (2.36)$$

Thus for a small sample, i.e. $k \ll N$, taking a random sample is approximately the same as sampling independently and identically distributed random variables, where the error vanishes approximately as k/N in the limit $N \rightarrow \infty$. In this limit, the analogies to corollary 12 are obvious.

There are several generalizations of de 's theorem to the quantum noncommutative case [11, 20–24], including both finite dimensional subsystems [29, 30], as well as infinite dimensional subsystems [31]. Here we are mainly concerned with finite dimensional subsystems, respectively states ρ_N on $(\mathbb{C}^d)^{\otimes N}$ and therefore we will closely follow [30].

In the quantum case, a state ρ_k is called N -exchangeable if there exists a symmetric state $\rho_N = \pi^\dagger \rho_N \pi$ on $\mathcal{H}^{\otimes N}$ with $N > k$, such that $\rho_k = \text{tr}_{N-k}(\rho_N)$. The state is said to be infinitely exchangeable if such a symmetric state ρ_n exists for all $n > k$. This is exactly the case treated in corollary 12, which promises that the state is exactly given by a convex combination of product states. In the case of finite exchangeability, the exact statement has to be replaced by an approximation:

Corollary 14 (Quantum de Finetti theorem [30]). *Let ρ_k be an N -exchangeable state, e.g. there exists a permutation invariant state ρ_N on $(\mathbb{C}^d)^{\otimes N}$ for $k \leq N$. Then the reduced state $\rho_k = \text{tr}_{N-k}(\rho_N)$ can be approximated by a convex combination of product states*

$$\tilde{\rho}_k = \int \sigma^{\otimes k} d\mu(\sigma) \quad (2.37)$$

where the error is given by

$$\|\rho_k - \tilde{\rho}_k\|_1 \leq \frac{d^2 k}{N}. \quad (2.38)$$

For Bose-symmetric states, e.g. states for which $\pi \rho_N = \rho_N$ holds for any permutation $\pi \in S_N$, the error is even tighter,

$$\|\rho_k - \tilde{\rho}_k\|_1 \leq \frac{dk}{N}. \quad (2.39)$$

For details on the proof, as well as possible generalizations we refer to [30].

A simple example shows that it is not possible to find a bound independently of d , as it is the case in the classical version of the theorem. If we consider the density operator $\rho_N = |\Psi\rangle\langle\Psi|$ where $|\Psi\rangle$ denotes the completely antisymmetric state vector for $d = N$:

$$|\Psi\rangle = \frac{1}{\sqrt{N!}} \sum_{\pi} \text{sign}(\pi) \cdot \pi \left(|0\rangle \otimes |1\rangle \otimes \cdots \otimes |N-1\rangle \right), \quad (2.40)$$

we get a mixture of singlet states for ρ_2

$$\rho_2 = \frac{2}{N(N-1)} \sum_{1 \leq i < j \leq N} (|ij\rangle - |ji\rangle)(\langle ij| - \langle ji|). \quad (2.41)$$

Thus, the trace distance of any approximation by product states never decreases below $1/4$, independently of the number of subsystems N . Note only does this prove that the bound has to depend on the dimension d of the subsystem, but also that the reduced

system is only approximately i.i.d if the number of subsystems is sufficiently large compared to the dimension d , which is obviously not the case here, as $d \sim N$.

In the following, we will be mostly concerned with the finite version of the de Finetti theorem, which is simply referred to as the de Finetti theorem wherever possible without loss of clarity. A closer analysis will show that the determination of these bounds is closely related to the first order corrections for the mean-field results. We will discuss this relation in chapter 5 for the ground state problem. There we will also give more details on the evaluation of these bounds. Moreover, we will prove a similar result in the context of phase space functions in chapter 6.

Chapter 3

Mean-field differential calculus

What we are aiming at is a general description of the macroscopic limit of mean-field observables and especially of the derivations from this limit for large, but finite system size. Hence, an expansion around the mean-field limit \mathcal{A}_∞ with the expansion parameter being the system size $1/n$ would be of major interest.

For common real or complex functions, one well-known possibility to achieve such an expansion around an arbitrary point is the Taylor expansion. For an infinitely differentiable function $f(x)$ the Taylor expansion around the point a yields the power series

$$f(x) = \sum_{n=0}^{\infty} \frac{f^{(n)}(a)}{n!} (x - a)^n, \quad (3.1)$$

where $f^{(n)}(a)$ denotes the n -th derivative evaluated at the point a and $f^{(0)}(a) = f(a)$ refers to the function itself.

However, we are not concerned with a real or complex function, but with the (generally nonlinear) functions $\mathcal{A}_\infty : \mathcal{S}(\mathcal{A}) \rightarrow \mathbb{R}$ on the single-particle state space. Thus, it is not at all obvious how to define the notion of a higher derivative, or even the first order derivative on the limiting space $\mathcal{C}(\mathcal{S}(\mathcal{A}))$, which we have identified with the set of limits of mean-field observables in the preceding chapter.

3.1 Introduction to the calculus of state space functions

To generalize the notion of a derivative to functions on the state space, as e.g. given by the mean-field limit \mathcal{A}_∞ , one has to recall the definition of the tangent space of a manifold \mathcal{M} from differential geometry. There, the basic idea relies on the composition of a chart $\delta : U \rightarrow \mathbb{R}^n$, a homeomorphism from an open subset $U \subset \mathcal{M}$ around a point $p \in \mathcal{M}$ to \mathbb{R}^n , with the local parametrization of the manifold around the point p by a curve $\gamma : (-1, 1) \rightarrow \mathcal{M}$ with $\gamma(0) = p$. Hence, the composition $(\delta \circ \gamma)$ yields

an ordinary function from $(-1, 1)$ to \mathbb{R}^n and one can apply the common definition of a derivative as the limit of the difference quotient. The tangent vector at the point p is defined as the equivalence class of all curves for which the ordinary derivative $(\delta \circ \gamma)'(0)$ coincide at 0. Furthermore, the tangent space at a point p is defined as the set of all tangent vectors and denoted by $T_p\mathcal{M}$.

Later on in this section, we will also need the notion of the total derivative. In the context of differential geometry the total derivative denotes a function $T_p\mathcal{M} \rightarrow \mathbb{R}$ which sends a tangent vector to its directional derivative and is thus itself an element of the cotangent space $T_p^*\mathcal{M}$. Note that this construction is independent of the special choice of the chart δ .

Following this reasoning, we consider the state space as a manifold, $\mathcal{M} = \mathcal{S}(\mathcal{A})$. Then the curve $\gamma : (-1, 1) \rightarrow \mathcal{S}(\mathcal{A})$ yields a parametrization of the state space, which allows to define a tangent vector at the point $\sigma(0) = \rho$ as the selfadjoint functional

$$\phi = \lim_{\varepsilon \rightarrow 0} \frac{\sigma(\varepsilon) - \sigma(-\varepsilon)}{2\varepsilon} \in T_\rho\mathcal{S}(\mathcal{A}). \quad (3.2)$$

Thus, we can identify the tangent space of $\mathcal{S}(\mathcal{A})$ at the point ρ as a subspace of the dual of \mathcal{A} containing the set of self-adjoint functionals on \mathcal{A} with

$$\langle \phi, \mathbb{1} \rangle = 0, \quad (3.3)$$

where the condition just results from the conservation of the probability in equation (3.2).

In the same manner, we can identify the elements of the cotangent space as the equivalence classes $[a] = a + \mathbb{R}\mathbb{1}$ with $a^* = a \in \mathcal{A}$. That we indeed have to treat equivalence classes $[a] = a + \mathbb{R}\mathbb{1}$ and not only self-adjoint elements $a^* = a$ of \mathcal{A} is a direct consequence of property (3.3), namely

$$\langle \phi, a + \lambda\mathbb{1} \rangle = \langle \phi, a \rangle \quad \forall \lambda \in \mathbb{R}, \quad \phi \in T_\rho\mathcal{S}(\mathcal{A}). \quad (3.4)$$

With this reasoning in mind, we can define the total derivative for a functional on the state space $\mathcal{S}(\mathcal{A})$ as follows:

Definition 15. *Total derivative [13]*

A function on the state space $f \in \mathcal{C}(\mathcal{S}(\mathcal{A}))$ is said to be **differentiable** if

1. for all $\rho \in \mathcal{S}(\mathcal{A})$ there exists an element $df(\rho) \in \mathcal{A}$ such that for all $\sigma \in \mathcal{S}(\mathcal{A})$ the derivative

$$\begin{aligned} \langle \sigma - \rho, df(\rho) \rangle &= \lim_{t \rightarrow 0} \frac{1}{t} (f((1-t)\rho + t\sigma) - f(\rho)) \\ &= \left. \frac{d}{dt} f((1-t)\rho + t\sigma) \right|_{t=0} \end{aligned}$$

exists as a weak*-continuous affine functional of σ .

2. The maps $\rho \mapsto \langle \sigma - \rho, df(\rho) \rangle$ are weak*-continuous, uniformly for $\sigma \in \mathcal{S}(\mathcal{A})$.

Due to the property (3.3), respective the property that the elements of the cotangent space form an equivalence class, we are free to choose a unique representative by fixing the expectation value of the total derivative. In the following, we will choose $\langle \rho, df(\rho) \rangle = 0$ and denote the derivative defined in this way by $\nabla_\rho f$. Hence we can always write the directional derivative as $\langle \sigma, \nabla_\rho f \rangle$ and reformulate the second condition of the definition by requiring that the map $\rho \mapsto \nabla_\rho f$ is weak*-to-norm-continuous.

As a first example, we will calculate the derivative of an arbitrary polynomial. Let $A_N = \text{sym}_N(A_k)$ be a strictly symmetric sequence of degree k , $\text{sym}_k(A_k) = A_k$. Thus the sequence is mean-field convergent and the mean-field limit

$$A_\infty(\rho) = \langle \rho^{\otimes k}, A_k \rangle \in \mathcal{C}(\mathcal{S}(\mathcal{A})) \quad (3.5)$$

defines a functional $A_\infty : \mathcal{S}(\mathcal{A}) \rightarrow \mathbb{R}$. Therefore, according to definition 15 the total derivative of the mean-field limit A_∞ can be calculated as

$$\begin{aligned} \langle \sigma, \nabla_\rho A_\infty \rangle &= \left. \frac{d}{dt} \langle (\rho + t(\sigma - \rho))^{\otimes k}, A_k \rangle \right|_{t=0} \\ &= k \langle (\sigma - \rho) \otimes \rho^{\otimes k-1}, A_k \rangle \\ &= k \langle \sigma \otimes \rho^{\otimes k-1}, A_k - \langle \rho^{\otimes k}, A_k \rangle \mathbb{1} \rangle. \end{aligned} \quad (3.6)$$

In the second line we made use of the symmetry of A_k to reorder the tensor factors. Note that in this case, we do not need to explicitly require the continuity of $\rho \mapsto \nabla_\rho A_\infty$, as the weak*-to-norm continuity already follows from the construction of the minimal C*-cross norm (for more details see [11]).

Based on the general theory of mean-field dynamical semigroups on C*-algebras [12] one can analyse the case where the generators are hamiltonian [13], in which case the mean-field limit yields a hamiltonian flow. This flow is governed by an effective Hamiltonian which is given by the first order derivative of the mean-field limit of the Hamiltonian. Moreover, the derivative can be used to define a Poisson-like bracket, which turns out to be the mean-field limit of the appropriately rescaled commutator. We will comment on this point in section 7.2.2.

3.2 Higher order derivatives

Having in mind the above reasoning it is still not clear how to iterate the construction to determine higher order derivatives. To accomplish this goal it turns out to be quite useful to make the problem even more complicated at first and consider a function $f : \mathcal{S}(\mathcal{A}) \rightarrow \mathcal{B}$ mapping the state space of the algebra \mathcal{A} to another algebra \mathcal{B} . For reasons of convenience, we will from now on use the notation $\rho(A)$ from operator algebra theory to denote the expectation value of the operator A in the state ρ .

Now we can define the gradient of such a function at a state $\rho \in \mathcal{S}(\mathcal{A})$ as a directional derivative,

$$\sigma \otimes \sigma_0(\nabla_\rho f) = \frac{d}{dt} \sigma_0\left(f((1-t)\rho + t\sigma)\right) \Big|_{t=0}, \quad (3.7)$$

with $\sigma_0 \in \mathcal{B}$, generalizing the first order derivative $\nabla_\rho f$, which is now an element of the tensor product $\mathcal{A} \otimes \mathcal{B}$.

Of course, this need not exist in general, and we define differentiability of a function precisely by the validity of this formula and the continuity of $\nabla_\rho f$ in ρ , as requested in the above definition. At first sight, this does not seem like a big change. Still if we expand the tensor product by the algebra \mathcal{B} , we are able to iterate the above construction and define the k -th order gradient $\nabla_\rho^k f \in \mathcal{A}^{\otimes k} \otimes \mathcal{B}$ to be given by

$$\sigma_k \otimes \cdots \otimes \sigma_1 \otimes \sigma_0(\nabla_\rho^k f) = \frac{\partial^k}{\partial t_k \cdots \partial t_1} \sigma_0\left(f(\rho + \sum_i t_i(\sigma_i - \rho))\right) \Big|_{t=0}. \quad (3.8)$$

This definition is readily motivated by the following construction:

$$\begin{aligned} & (\sigma_k - \rho) \otimes (\sigma_{k-1} - \rho) \otimes \cdots \otimes (\sigma_1 - \rho) \otimes \sigma_0(d^k f(\rho)) \\ &= \frac{\partial}{\partial t_k} (\sigma_{k-1} - \rho) \otimes \cdots \otimes (\sigma_1 - \rho) \otimes \sigma_0\left(d^{k-1} f(\rho - t_k(\sigma_k - \rho))\right) \Big|_{t_k=0} \\ &= \frac{\partial}{\partial t_k \cdots \partial t_1} \left(\sigma_0, f(\rho - \sum_{i=1}^k t_i(\sigma_i - \rho)) \right) \Big|_{t_i=0} \\ &:= \sigma_k \otimes \sigma_{k-1} \otimes \cdots \otimes \sigma_1 \otimes \sigma_0(\nabla^k f(\rho)). \end{aligned} \quad (3.9)$$

To simplify matters, we have defined the zeroth order derivative as the function itself, $\nabla^0 f(\rho) = f(\rho) \in \mathcal{B}$.

Since ordinary derivatives commute, the above construction (3.8) is symmetric in the parameter t_i . Thus, the gradient $\nabla_\rho^k f$ is symmetric with respect to the \mathcal{A} -factors,

$$\nabla_\rho^k f \in \mathcal{A}_{\text{sym}}^k \otimes \mathcal{B}. \quad (3.10)$$

Moreover, if we choose any one of the $\sigma_i = \rho$, the expression on the right no longer depends on t_i , and hence the derivative vanishes. This is reminiscent of the convention to choose the gradient $\nabla_\rho f$ at the point ρ such that its expectation vanishes in the state ρ . These properties are essential for the definition of the Taylor expansion and turn out to be quite beneficial for actual calculations, as we will see in the following chapters.

We will often evaluate the above expression when all $\sigma_i = \sigma$ are equal. Because of the permutation symmetry this is actually sufficient to determine $\nabla_\rho^k f$. In the case that the algebra $\mathcal{B} = \mathbb{C}$ is trivial, we get:

$$\sigma^{\otimes k}(\nabla_\rho^k f) = \frac{\partial^k}{\partial t^k} f(\rho + t(\sigma - \rho)) \Big|_{t=0}. \quad (3.11)$$

As an illustrative example, we calculate the derivatives of the mean-field limit of a strictly symmetric sequence of degree 2,

$$A_\infty(\rho) = \lim_{n \rightarrow \infty} \rho^{\otimes n} (\text{sym}_n(a \otimes b)) \quad (3.12)$$

$$\begin{aligned} &= \rho^{\otimes 2} \left(\frac{a \otimes b + b \otimes a}{2} \right) \\ &= \rho(a)\rho(b). \end{aligned} \quad (3.13)$$

Not only did we choose this example for illustrative reasons, but this calculation already covers the typical example of the Hamiltonian (2.4) with two-particle interactions.

Using the above definition of the first order derivative and following the steps of the calculation in equation (3.6), we get

$$\begin{aligned} \sigma(\nabla_\rho A_\infty) &= \frac{\partial}{\partial t} (\rho - t(\sigma - \rho))^{\otimes 2} \left(\frac{a \otimes b + b \otimes a}{2} \right) \Big|_{t=0} \\ &= (\sigma - \rho) \otimes \rho(a \otimes b + b \otimes a), \end{aligned} \quad (3.14)$$

while the second derivative yields

$$\begin{aligned} \sigma_2 \otimes \sigma_1(\nabla_\rho^2 A_\infty) &= \frac{\partial^2}{\partial t_2 \partial t_1} (\rho - t_1(\sigma_1 - \rho) - t_2(\sigma_2 - \rho))^{\otimes 2} \left(\frac{a \otimes b + b \otimes a}{2} \right) \Big|_{t_1=0=t_2} \\ &= (\sigma_2 - \rho) \otimes (\sigma_1 - \rho)(a \otimes b + b \otimes a). \end{aligned} \quad (3.15)$$

In both calculations we have benefited from the permutation symmetry of the strictly symmetric sequence.

Summarizing the results for $A_\infty(\rho) = \rho(a)\rho(b)$ the first order gradient is given by

$$\nabla_\rho A_\infty = a\rho(b) + b\rho(a) - 2\rho(a)\rho(b)\mathbb{1} \in \mathcal{A}, \quad (3.16)$$

as well as the second order gradient by

$$\nabla_\rho^2 A_\infty = 2 \text{sym}_2 \left((a - \rho(a)\mathbb{1}) \otimes (b - \rho(b)\mathbb{1}) \right) \in \mathcal{A} \otimes \mathcal{A}. \quad (3.17)$$

Moreover, as expected for a polynomial of degree 2, all higher order derivatives with $k \geq 3$ vanish.

These results can be generalized to a systematic calculation of the k -th order derivative ∇_ρ^k for a mean-field polynomial of arbitrary degree r , e.g. $A_\infty(\rho) = \langle \rho^{\otimes r}, A_r \rangle$ with $\text{sym}_r A_r = A_r$. Due to the permutation symmetry, we can use the reduced formula (3.11). Thus, the k -th order derivative can be evaluated as

$$\begin{aligned} \sigma^{\otimes k}(\nabla_\rho^k A_\infty) &= \frac{\partial^k}{\partial t^k} A_\infty(\rho - t(\sigma - \rho)) \Big|_{t=0} \\ &= \frac{\partial^k}{\partial t^k} \left\langle (\rho - t(\sigma - \rho))^{\otimes r}, A_r \right\rangle \Big|_{t=0}. \end{aligned}$$

As in the example above, we can use the permutation symmetry of A_r , which allows us to rearrange the tensor factors without changing the expectation value:

$$\sigma^{\otimes k} (\nabla_{\rho}^k A_{\infty}) = \frac{\partial^k}{\partial t^k} \left\langle \sum_{\ell=0}^r \binom{r}{\ell} t^{\ell} (\sigma - \rho)^{\otimes \ell} \otimes \rho^{\otimes r-\ell}, A_r \right\rangle \Big|_{t=0}. \quad (3.18)$$

If we now evaluate the differentiation, all terms proportional to t^{ℓ} with $\ell < k$ vanish. As a direct consequence, all higher order derivatives vanish if the order of the derivative is greater than the degree of the polynomial, thus $\nabla_{\rho}^k A_{\infty} = 0$ for all $k > r$. For $k \leq r$ we obtain

$$= \left\langle \sum_{\ell=k}^r \frac{r!}{\ell!(r-\ell)!} \frac{\ell!}{(\ell-k)!} t^{\ell-k} (\sigma - \rho)^{\otimes \ell} \otimes \rho^{\otimes r-\ell}, A_r \right\rangle \Big|_{t=0} \quad (3.19)$$

Setting t to zero further simplifies the result, as only the summand $\ell = k$ remains to be considered:

$$= \frac{r!}{r-k!} \langle (\sigma - \rho)^{\otimes k} \otimes \rho^{\otimes r-k}, A_r \rangle. \quad (3.20)$$

The last line is the starting point for the Taylor expansion, which we will construct and discuss in section 3.4. Still for actual calculations, some further transformations of the above expression are useful:

$$\begin{aligned} \sigma^{\otimes k} (\nabla_{\rho}^k A_{\infty}) &= \frac{r!}{r-k!} \left\langle \sum_{\ell=0}^k \frac{k!}{(k-\ell)!\ell!} (-1)^{\ell} \sigma^{\otimes \ell} \otimes \rho^{\otimes r-\ell}, A_r \right\rangle \\ &= \frac{r!}{r-k!} \left\langle \sigma^{\otimes k} \otimes \rho^{\otimes r}, \sum_{\ell=0}^k \frac{k!}{(k-\ell)!\ell!} (-1)^{\ell} \mathbb{1}_{k-\ell} \otimes A_r \otimes \mathbb{1}_{\ell} \right\rangle. \end{aligned} \quad (3.21)$$

In the last line, we have made use of the natural embedding $\mathcal{A}^r \hookrightarrow \mathcal{A}^{r+k}$ with $A_r \mapsto \mathbb{1}_{\ell} \otimes A_r \otimes \mathbb{1}_{k-\ell}$, as well as the normalization of the state $\langle \rho, \mathbb{1} \rangle = 1$.

In the case $r = 2$ and $k = 1$, respective $k = 2$, the result reduces to the one discussed earlier in the context of the example $A_{\infty}(\rho) = \rho(a)\rho(b)$ (cf. equation (3.16) and equation (3.17)).

3.3 Extremal problems

Since we have discussed a generalized concept of derivatives of state space functions and are going to introduce a generalized Taylor formula expansion, which allows us to expand an arbitrary state space function around a certain state, it is just natural to ask for extremal problems in this context. The determination of minima and the expansion around the extremal points will be particularly important in the context

of the ground state problem addressed in chapter 5, where we aim for the finite size corrections to the mean-field prediction for the ground state energy.

Suppose that the state space function $f : \mathcal{S}(\mathcal{A}) \rightarrow \mathbb{R}$ assumes its minimum at a point ρ , which may be well on the boundary of the state space. For ρ to be a minimizer, it is clearly necessary that for all directions towards other states the functional non-decreases, i.e., $\sigma(\nabla_\rho f) \geq 0$. Since σ is arbitrary, this just means that $\nabla_\rho f \in \mathcal{A}$ is a positive semidefinite operator.

Furthermore, for ρ to be an extremal point we need $\rho(\nabla_\rho f) = 0$, which is automatically fulfilled by the above construction. When ρ happens to be strictly positive the condition $\rho(\nabla_\rho f) = 0$ just means that the gradient $\nabla_\rho f$ itself is zero. However, if ρ is not strictly positive and thus features an eigenvalue equal to zero, we can only conclude that the gradient vanishes on the support of ρ . In particular, this is the case for a pure state and thus at the boundary of the state space.

As a condition for the second derivative, we find that for any σ such that $\sigma(\nabla_\rho f) = 0$ we must require that the second order derivative is greater or equal zero, $\sigma^{\otimes 2}(\nabla_\rho^2 f) \geq 0$. Note that this does not entail that the second derivative is a positive operator.

As an illustrative example, we consider the function

$$f(\rho) = \text{tr}(\rho^2) - 2 \quad (3.22)$$

on a qubit system, that is $\rho \in \mathbb{C}^2$. Note that this function can be interpreted as a measure of the purity of the state, where the constant offset is introduced for later convenience.

Obviously, the function (3.22) assumes its minimum for the fully mixed state, respectively at the center of the Bloch ball:

$$\rho_{\min} = \frac{1}{2}\mathbb{1} \quad \Rightarrow \quad f(\rho_{\min}) = -\frac{3}{2}, \quad (3.23)$$

whereas the maximum is assumed at the surface of the Bloch ball, respectively for any pure state,

$$\rho_{\max} = U^\dagger \begin{pmatrix} 1 & 0 \\ 0 & 0 \end{pmatrix} U \quad \Rightarrow \quad f(\rho_{\max}) = -1. \quad (3.24)$$

To calculate the first and second order derivatives, it is advantageous to transform the function (3.22) using the Pauli spin operators

$$S_1 = \begin{pmatrix} 0 & 1 \\ 1 & 0 \end{pmatrix} \quad S_2 = \begin{pmatrix} 0 & -i \\ i & 0 \end{pmatrix} \quad S_3 = \begin{pmatrix} 1 & 0 \\ 0 & -1 \end{pmatrix}. \quad (3.25)$$

A short calculation yields

$$f(\rho) = \text{tr}(\rho^2) - 2 = -\sum_{\alpha=1}^3 \text{tr}[(\rho S_\alpha)^2]. \quad (3.26)$$

With this transformation we can determine the first order derivatives $\nabla_\rho f$ according to the definition (3.11) as

$$\begin{aligned}\sigma(\nabla_\rho f) &= \left. \frac{\partial}{\partial t} f(\rho + t(\sigma - \rho)) \right|_{t=0} \\ &= - \left. \frac{\partial}{\partial t} \sum_{\alpha=1}^3 \text{tr} [(\rho + t(\sigma - \rho)) S_\alpha (\rho + t(\sigma - \rho)) S_\alpha] \right|_{t=0} \\ &= -2 \sum_{\alpha=1}^3 \text{tr} [(\sigma - \rho) S_\alpha \rho S_\alpha],\end{aligned}\tag{3.27}$$

as well as the second order derivative $\nabla_\rho^2 f$,

$$\sigma^{\otimes 2}(\nabla_\rho^2 f) = -2 \sum_{\alpha=1}^3 \text{tr} [(\sigma - \rho) S_\alpha (\sigma - \rho) S_\alpha].\tag{3.28}$$

Let us first analyse the behaviour at the minimum $\rho_{\min} = \frac{1}{2}\mathbb{1}$, which is well inside the state space. As expected the first order derivative $\nabla_{\rho_{\min}} f$ vanishes at this point, since

$$\sigma(\nabla_{\rho_{\min}} f) = 0 \quad \forall \sigma \in \mathbb{C}^2,\tag{3.29}$$

whereas the evaluation of the second order derivative yields

$$\begin{aligned}\sigma^{\otimes 2}(\nabla_{\rho_{\min}}^2 f) &= -2 \sum_{\alpha=1}^3 \text{tr} [(\sigma S_\alpha)^2] + 3 \\ &\geq 0 \quad \forall \sigma \in \mathbb{C}^2,\end{aligned}\tag{3.30}$$

which is always greater or equal 0, as required by the condition for a minimum mentioned above.

On the other hand, the maximum is assumed at the boundary of the state space. Taking for example

$$\rho_{\max} = \begin{pmatrix} 1 & 0 \\ 0 & 0 \end{pmatrix},\tag{3.31}$$

we can determine the expectation value of the first order derivative to be given in components of the state σ as

$$\begin{aligned}\sigma(\nabla_{\rho_{\max}} f) &= -2\sigma_{22} \\ &\leq 0.\end{aligned}\tag{3.32}$$

Thus the first order derivative is not positive, as required for a maximum. However, in general this expression is not equal zero – the gradient $\nabla_{\rho_{\max}} f$ only vanishes on the support of ρ_{\max} .

Finally, example (3.22) emphasizes the fact that the condition $\sigma^{\otimes 2}(\nabla_{\rho}^2 f) \geq 0$ does not mean that $\nabla_{\rho}^2 f$ has to be a positive operator, even for a vanishing gradient $\nabla_{\rho} f = 0$. To illustrate this last point, it is most convenient to write the second derivative at the point $\rho_{\min} = \frac{1}{2}\mathbb{1}$ as

$$\nabla_{\rho_{\min}}^2 f = \sum_{\alpha} S_{\alpha} \otimes S_{\alpha}. \quad (3.33)$$

That this expression is indeed equivalent to equation (3.30) can be easily verified by an evaluation in matrix elements.

If we now choose $|\Psi\rangle \in \mathbb{C}^2 \otimes \mathbb{C}^2$ to be the singlet state,

$$(S_{\alpha} \otimes \mathbb{1}) |\Psi\rangle = -(\mathbb{1} \otimes S_{\alpha}) |\Psi\rangle, \quad (3.34)$$

which is obviously neither symmetric nor a product state, we find

$$\langle \Psi | \nabla_{\rho}^2 f | \Psi \rangle = \langle \Psi | \sum_{\alpha} S_{\alpha} \otimes S_{\alpha} | \Psi \rangle = -3, \quad (3.35)$$

hence the operator $\nabla_{\rho}^2 f$ is clearly not positive.

3.4 Taylor expansion

The main motivation to introduce the calculus of state space functions was the quest for a systematic extension around the mean-field limit inspired by the well-known Taylor expansion for an analytic function (3.1).

To this end, we again consider the dense subalgebra of polynomials on \mathcal{A} , respectively the limiting elements of the strictly symmetric sequences and assume that $f : \mathcal{S}(\mathcal{A}) \rightarrow \mathbb{C}$ is a polynomial of degree r ,

$$\begin{aligned} f(\rho) &= \langle \rho^{\otimes r}, A_r \rangle \\ &= A_{\infty}(\rho) \quad \text{with} \quad A_r = \text{sym}_r A_r \in \mathcal{A}^{\otimes r}. \end{aligned} \quad (3.36)$$

Evaluating the function in the vicinity of the point $\rho \in \mathcal{S}(\mathcal{A})$ yields

$$\begin{aligned} A_{\infty}(\rho - t(\sigma - \rho)) & \\ &= \langle (\rho - t(\sigma - \rho))^{\otimes r}, A_r \rangle \\ &= \left\langle \sum_{\ell=0}^r \binom{r}{\ell} t^{\ell} (\sigma - \rho)^{\otimes \ell} \otimes \rho^{\otimes r-\ell}, A_r \right\rangle \\ &= \sum_{\ell=0}^r \frac{t^{\ell}}{\ell!} \left\langle \frac{r!}{(r-\ell)!} (\sigma - \rho)^{\otimes \ell} \otimes \rho^{\otimes r-\ell}, A_r \right\rangle, \end{aligned} \quad (3.37)$$

where we again used the permutation invariance of the expectation value to reorder the tensor factors.

A closer inspection of the last line of equation (3.37) reveals the connection with the definition of the higher order gradients $\nabla_\rho^\ell A_\infty$. In section 3.2 we derived an explicit formula for the higher order derivatives of a polynomial of degree ℓ (cf. equation (3.18) ff.):

$$\langle \sigma^{\otimes \ell}, \nabla_\rho^\ell A_\infty \rangle = \left\langle \frac{r!}{(r-\ell)!} (\sigma - \rho)^{\otimes \ell} \otimes \rho^{\otimes r-\ell}, A_r \right\rangle \quad (3.38)$$

A comparison of this result to equation (3.37) shows that we can indeed express the function $A_\infty(\rho - t(\sigma - \rho))$ evaluated in the vicinity of ρ by an expansion in terms of derivatives $\nabla_\rho^\ell A_\infty$:

$$A_\infty(\rho - t(\sigma - \rho)) = \sum_{\ell=0}^r \frac{t^\ell}{\ell!} \langle \sigma^{\otimes \ell}, \nabla_\rho^\ell A_\infty \rangle. \quad (3.39)$$

Finally, setting $t = 1$ yields the Taylor series for the function $A_\infty(\sigma)$ as an expansion around the point ρ :

$$\begin{aligned} A_\infty(\sigma) &= f(\sigma) \\ &= \sum_{\ell=0}^r \frac{1}{\ell!} \frac{\partial^\ell}{\partial t^\ell} f(\rho + t(\sigma - \rho)) \Big|_{t=0} \\ &= \sum_{\ell=0}^r \frac{1}{\ell!} \langle \sigma^{\otimes \ell}, \nabla_\rho^\ell A_\infty \rangle \\ &= \langle \sigma^{\otimes r}, A_r \rangle. \end{aligned} \quad (3.40)$$

In the same manner, we can write down the terminating Taylor series for any $N \geq k$,

$$\sigma^{\otimes N}(\text{sym}_N A_r) = \sum_{\ell=0}^k \frac{1}{\ell!} \sigma^{\otimes N}(\text{sym}_N(\nabla_\rho^\ell A_\infty)).$$

If we equalise the symmetric elements evaluated under the arbitrary state $\sigma^{\otimes N}$, we can identify the resulting operators. This yields an expansion of an arbitrary symmetric operator of degree r in terms of the derivatives of the mean-field expectation value at the point ρ ,

$$\text{sym}_N(A_r) = \sum_{\ell=0}^r \frac{1}{\ell!} \text{sym}_N(\nabla_\rho^\ell A_\infty), \quad (3.41)$$

where the ℓ -th order derivative $\nabla_\rho^\ell A_\infty$ is an element of $\mathcal{A}_{\text{sym}}^{\otimes \ell}$ as discussed earlier.

By construction the zeroth order term is given by the mean-field limit, respectively the expectation value of A_r in the product state $\rho^{\otimes r}$. As such it is just a multiple of the identity, while all higher order terms with $\ell > 1$ have vanishing expectation value. Note that the first order term is the symmetrization of a (ρ -dependent) one-site observable, the second is an symmetrized two-particle observable and so on.

A comparison to the definition of the fluctuation operator which will be discussed in chapter 5 shows that the first order term is exactly the fluctuation around the mean-field limit at the point ρ . In the same way, there is a close relation between fluctuation operators and the higher-order terms. This relation will be analysed in more detail in the next chapter.

Note that up to now equation (3.41) yields an extension in symmetrized ℓ -particle operators $\nabla_\rho^\ell A_\infty \in \mathcal{A}^{\otimes \ell}$ as we have wished for, but does not make a prediction about the scaling behaviour with the system size. This will be different for the extension in fluctuation operators.

Finally, we consider an elementary example to get a first idea how the expansion around the mean-field limit $A_\infty(\rho) = \rho(a)\rho(b)$ works in practice. To this end, we explicitly calculate the expansion of the symmetric two-particle operator

$$A_2 = \text{sym}_2(a \otimes b) = \frac{a \otimes b + b \otimes a}{2}. \quad (3.42)$$

In the preceding section, we have already explicitly calculated the first and second order derivative for this example,

$$\begin{aligned} \nabla_\rho A_\infty &= a\rho(b) + b\rho(a) - 2\rho(a)\rho(b)\mathbb{1}, \\ \nabla_\rho^2 A_\infty &= 2\text{sym}_2\left((a - \rho(a)\mathbb{1}) \otimes (b - \rho(b)\mathbb{1})\right). \end{aligned}$$

According to equation (3.18) all higher order derivatives $\nabla_\rho^k A_\infty$ with $k \geq 3$ vanish. Thus, the Taylor expansion yields a finite series.

Using these results the expansion of $A_\infty(\sigma)$ around the point ρ is given by

$$\begin{aligned} A_\infty(\sigma) &= \sum_{\ell=0}^2 \frac{1}{\ell!} \langle \sigma^{\otimes \ell}, \nabla_\rho^\ell A_\infty \rangle \\ &= A_\infty(\rho) + \langle \sigma, \nabla_\rho A_\infty \rangle + \frac{1}{2} \langle \sigma^{\otimes 2}, \nabla_\rho^2 A_\infty \rangle \\ &= \rho(a)\rho(b) + \sigma(a - \rho(a)\mathbb{1})\rho(b) + \sigma(b - \rho(b)\mathbb{1})\rho(a) \\ &\quad + \sigma(a - \rho(a)\mathbb{1})\sigma(b - \rho(b)\mathbb{1}) \\ &= \sigma(a)\sigma(b). \end{aligned} \quad (3.43)$$

By construction, the complete series sums up to the exact result.

Identifying the operators yields the Taylor expansion of the symmetric operator $\text{sym}_n(A_2)$,

$$\begin{aligned}
\text{sym}_n A_2 &= \sum_{\ell=0}^2 \frac{1}{\ell!} \text{sym}_N(\nabla_{\rho}^{\ell} A_{\infty}) \\
&= \rho(a)\rho(b)\mathbb{1}_n + \text{sym}_n \left((a - \rho(a)\mathbb{1})\rho(b) + \text{sym}_n((b - \rho(b)\mathbb{1})\rho(a)) \right. \\
&\quad \left. + \text{sym}_n((a - \rho(a)\mathbb{1}) \otimes (b - \rho(b)\mathbb{1})) \right) \\
&= \text{sym}_n(\rho(a)\rho(b)\mathbb{1}_2 + (a - \rho(a)\mathbb{1}) \otimes \rho(b)\mathbb{1} \\
&\quad + (b - \rho(b)\mathbb{1}) \otimes \rho(a)\mathbb{1} + (a - \rho(a)\mathbb{1}) \otimes (b - \rho(b)\mathbb{1})) \\
&= \text{sym}_n(a \otimes b). \tag{3.44}
\end{aligned}$$

Again we find that the zeroth order term is given by the mean-field expectation value, while the first order term is given by a single-particle operator proportional to the fluctuation around the mean-field value and the second order term is a two-particle term with vanishing expectation value in the state $\rho^{\otimes n}$.

Chapter 4

The algebra of fluctuations

In this chapter we will discuss the algebra of fluctuations, which can be used to describe the perturbations around the mean-field solution. In particular, we will see introduce the notion of states with root N fluctuations which allows to establish the relationship between microscopic fluctuations for finite system size and fluctuations on the macroscopic level. Moreover, this notation provides the basic tools to study the limiting behaviour of the fluctuations for $N \rightarrow \infty$.

Since the mean-field results describing the limit of infinite particle numbers of intensive observables obviously feature some affinities to the famous law of large numbers in classical probability theory, it is just natural to expect a quantum version of the central limit theorem to hold for quantum fluctuations. Indeed, we will find a non-commutative central limit theorem, which allows to identify the macroscopic fluctuations with a representation of the canonical commutation relations in a quasi-free state which is determined by the microscopic correlations. These questions will be addressed in section 4.2.

In the last section, we will discuss the expansion of symmetric operators in fluctuation operators, as well as the relation of this expansion to the differential calculus of functions on the state space and especially to the Taylor expansion discussed in the preceding chapter. These results and especially the expansion of a symmetric operator in fluctuation operators are a key ingredient for the determination of the bound for the ground state energy and thus play a major role in chapter 5.

4.1 Quantum fluctuations

Definition 16. *For finite N , the fluctuation algebra around the state $\rho \in \mathcal{S}(\mathcal{A})$ is generated by the (local) fluctuation operators, which are defined as*

$$\begin{aligned}\tilde{a} &= \sqrt{N} (\text{sym}_N(a) - \rho(a)\mathbb{1}) \\ &= \frac{1}{\sqrt{N}} \sum_{i=1}^N (a^{(i)} - \rho(a)\mathbb{1}) \in \mathcal{A}^N,\end{aligned}\tag{4.1}$$

where $a \in \mathcal{A}$ is an arbitrary single-particle operator.

Note that there is an implicit dependence on the system size N , which we suppress to keep the notation transparent. The local fluctuation operators are bounded if the single particle operators are bounded, but their norm diverges in the limit of infinite system size $\|\tilde{a}\| \approx \sqrt{N}\|a - \rho(a)\mathbb{1}\|$.

Here, we focus on fluctuations of single-particle observables, as e.g. the density, the momentum or the angular momentum operators. These quantities are of fundamental interest. Since they are experimentally accessible, they play a major role in part II. Moreover, we only treat normal fluctuations, which scale as $1/\sqrt{N}$, as this is the typical scaling for systems with short range interactions. However, normal fluctuations are not appropriate to describe systems featuring long-range order, as e.g. systems at low temperatures which undergo a phase transition. The algebraic structure of abnormally scaled fluctuations is analysed in detail in [32]. For the ideal Bose gas, a systematic study of the abnormal fluctuations can be found in [33]. More examples for critical fluctuations in quantum mean-field systems are discussed in [34].

The similarities of definition 16 to the concept of classical fluctuations around the mean-value of a distribution are obvious. As in the classical case, the fluctuation operators describe the deviations of the extensive observable from its mean value, where the scaling is given by the square root of the scaling parameter of the macroscopic variable $\text{sym}_N(a)$. This explains why the fluctuation operators are sometimes referred to as mesoscopic.

To define the fluctuation operators in the limit of infinite system size, we need some more considerations and do not only have to take into account observables, but also the states in which we consider the limit:

Definition 17. A sequence of states $\rho_N \in \mathcal{S}(\mathcal{A}^{\otimes N})$ is said to have root N fluctuations around ρ iff for any polynomial P in fluctuation operators $\tilde{a}_1, \dots, \tilde{a}_r \in \mathcal{A}^{\otimes N}$ the limit

$$\lim_{N \rightarrow \infty} \rho_N (P(\tilde{a}_1 \cdots \tilde{a}_k)) = \langle \Omega | P(\hat{a}_1 \cdots \hat{a}_k) \Omega \rangle \quad (4.2)$$

exists. A sequence of states $\rho_N \in \mathcal{S}(\mathcal{A}^{\otimes N})$ is said to have normal fluctuations iff these are gaussian.

The above limit defines the fluctuations \hat{a} in the limit space. In the following, we will denote the macroscopic fluctuations by \hat{a} to distinguish them from the local fluctuations \tilde{a} defined in equation (4.1).

The notion $\langle \Omega | P(\hat{a}_1 \cdots \hat{a}_k) \Omega \rangle$ already refers to the Gelfand-Naimark-Segal representation of the macroscopic fluctuations (cf. section 1.1.2). This representation can be constructed as follows:

From the properties of ρ_N it can be directly inferred that the limiting functional is again a state: Obviously $\lim_{N \rightarrow \infty} \rho_N(\mathbb{1}) = 1 = \langle \Omega | \mathbb{1} \Omega \rangle$ holds, hence the functional

$\langle \Omega | \cdot | \Omega \rangle$ is normalized. The linearity can easily be checked by

$$\begin{aligned} \langle \Omega | (\alpha \widehat{a} + \beta \widehat{b}) \Omega \rangle &= \lim_{N \rightarrow \infty} \rho_N (\alpha \widetilde{a} + \beta \widetilde{b}) \\ &= \lim_{N \rightarrow \infty} (\alpha \rho_N(\widetilde{a}) + \beta \rho_N(\widetilde{b})) \\ &= \alpha \langle \Omega | \widehat{a} \Omega \rangle + \beta \langle \Omega | \widehat{b} \Omega \rangle. \end{aligned} \quad (4.3)$$

To prove the positivity we consider an arbitrary polynomial \widetilde{F} in the local fluctuation operators \widetilde{a}_i with N -independent coefficients. Then the following relation holds:

$$\|\widehat{F}\Omega\|^2 = \lim_{N \rightarrow \infty} \rho_N(\widetilde{F}^* \widetilde{F}) \geq 0. \quad (4.4)$$

Thus, the limiting functional is indeed a state and by theorem 6 we find a representation of the macroscopic fluctuations \widehat{a} in terms of linear operators in a Hilbert space. In detail, the theorem establishes that the Hilbert space \mathcal{H}_ρ contains a unit vector $|\Omega\rangle$ and a dense subspace \mathcal{D} spanned by the elements of the form $\widehat{a}_1 \cdots \widehat{a}_k |\Omega\rangle$, whose scalar products are defined by

$$\langle \widehat{b}_1 \cdots \widehat{b}_\ell \Omega | \widehat{a}_1 \cdots \widehat{a}_k \Omega \rangle = \lim_{N \rightarrow \infty} \rho_N (\widetilde{b}_\ell^* \cdots \widetilde{b}_1^* \widetilde{a}_1 \cdots \widetilde{a}_k). \quad (4.5)$$

Note that the positivity of the scalar product in \mathcal{H}_ρ , which is implicitly claimed in the above definition, follows again from the properties of ρ_N (4.4).

In summary, the macroscopic fluctuation operator \widehat{a} is defined as an operator on \mathcal{D} , which can be constructed as

$$\widehat{a} (\widehat{a}_1 \cdots \widehat{a}_k \Omega) = \widehat{a} \widehat{a}_1 \cdots \widehat{a}_k \Omega. \quad (4.6)$$

In the next section, we will see that the sequence of product states $\rho_N = \rho^{\otimes N}$ is an example for a state with root N fluctuations around ρ . In fact the limit state is Gaussian with covariance matrix

$$\langle \Omega | \widehat{a} \widehat{b} \Omega \rangle = \rho(ab) - \rho(a)\rho(b). \quad (4.7)$$

Thus, mean-field systems as defined in chapter 2 are a prototype for systems with normal fluctuations. The reason for introducing the more general notion of states ρ_N with root N fluctuations (cf. definition 17) is that this property for the sequence of ground states will become the major step to establish an upper bound for the ground state energy. We will come to this point in section 5.4.

As a corollary of the central limit theorem proven in the next section we will show that the macroscopic fluctuation operators \widehat{a} build a CCR-algebra and thus satisfy canonical commutation relations on their common domain, namely

$$[\widehat{a}, \widehat{b}] \phi = \rho([a, b]) \phi \quad \text{for all } \phi \in \mathcal{D}. \quad (4.8)$$

This reasoning finally allows to identify the macroscopic fluctuations with Bose fields in a quasi free state.

4.2 Central limit theorem

In its simplest form, the classical central limit theorem states that for any sequences of independently and identically and distributed random variables $x_1, x_2 \dots x_N$ with expectation value μ and variance $\sigma^2 < \infty$ the fluctuation around its mean, that is

$$\frac{1}{\sqrt{N}} \left(\sum_i x_i - \mu \right) \quad (4.9)$$

converges in distribution to a normal distribution, $X \sim \mathcal{N}(0, \sigma^2)$, as given by the probability density function

$$f(x) = \frac{1}{\sqrt{2\pi\sigma^2}} e^{-\frac{x^2}{2\sigma^2}}. \quad (4.10)$$

There are various versions of this powerful theorem, which has proven to be robust under weak correlations, for more details see e.g. [35].

Additionally, there are several quantum versions of the central limit theorem which provide generalizations to the non-commutative case, see e.g. [36–40]. The general theory of non-commutative central limits for quantum fluctuations has been developed in [4, 5, 41, 42] including the time evolution. In these papers the relation between the local, microscopic fluctuations and the macroscopic fluctuations has been worked out in detail. In particular, the authors give explicit clustering conditions for a state to have normal fluctuations and present a reconstruction theorem for the CCR-algebra and the limiting functional.

Here, we are faced with a much more specific problem, namely the central limit for quantum mean-field systems. The next theorem proves that quantum mean-field systems are an example of a system with normal fluctuations. Moreover, we will show that the macroscopic fluctuations converge against Bose field operators in a quasi free state, as expected from the general theory.

Theorem 18 (Central limit theorem for quantum mean-field systems). *For every finite polynomial P of local fluctuation operators \tilde{a}_i the following limit exists*

$$\lim_{N \rightarrow \infty} \rho^{\otimes N} (P(\tilde{a}_i)) = \omega_\rho (P(\hat{a}_i)), \quad (4.11)$$

where ω_ρ is a Gaussian state with two-point function

$$\omega_\rho(\hat{a}_i \hat{a}_j) = \rho(a_i a_j) - \rho(a_i) \rho(a_j). \quad (4.12)$$

Thus, the sequence of product states has normal fluctuations.

Proof of the central limit theorem (cf. also [38]). Since ρ is assumed to be a linear functional it is sufficient to consider monomials $M(\tilde{a}_i) = \prod_{i=1}^k \tilde{a}_i$ of arbitrary degree k . The expectation value for such a monomial in the product state $\rho^{\otimes N}$ is given by

$$\rho^{\otimes N} (\tilde{a}_1 \dots \tilde{a}_k) = N^{-\frac{k}{2}} \sum_{j_1, \dots, j_k=1}^N \rho^{\otimes N} ((a_1 - \rho(a_1)\mathbb{1})^{(j_1)} \dots (a_k - \rho(a_k)\mathbb{1})^{(j_k)}), \quad (4.13)$$

where we have used the same notation as defined in (2.3). Because of the symmetry of the state $\rho^{\otimes N}$, we are only interested in the possible distributions of the k operators $a_i - \rho(a_i)\mathbb{1} \in \mathcal{A}$ over the N possible sites. Thus, we can regroup the terms according to the number of occupied sites p or respectively according to their overlap $r = k - p$:

$$\begin{aligned} \rho^{\otimes N}(\tilde{a}_1 \dots \tilde{a}_k) &= N^{-\frac{k}{2}} \sum_{p=1}^k \frac{N!}{(N-p)!} \sum_{\{S_1, \dots, S_p\}} \rho(a_{S_1}) \cdots \rho(a_{S_p}), \\ &= N^{-\frac{k}{2}} \sum_{r=0}^k \frac{N!}{(N-k+r)!} \sum_{\{S_1, \dots, S_{k-r}\}} \rho(a_{S_1}) \cdots \rho(a_{S_{k-r}}), \end{aligned} \quad (4.14)$$

where the last summation ranges over all possible partitions of $\{1, 2, \dots, k\}$ into $p = k - r$ sets $\{S_1, \dots, S_p\}$ and a_{S_i} denotes the ordered product $\prod_{i \in S_\ell} (a_i - \rho(a_i)\mathbb{1})$. The combinatorial factor can be determined by choosing $p = k - r$ different values from the set $\{1, 2, \dots, N\}$, and is thus simply given by $\frac{N!}{(N-p)!}$. Note that up to now this is just another way of writing the summation over truncated correlation functions or cumulants.

A closer inspection of the summands shows that – due to the construction of the fluctuation operators – every partition containing a singleton $\#S_i = 1$ vanishes, that is

$$\rho\left(a_i - \rho(a_i)\mathbb{1}\right) = \rho(a_i) - \rho(a_i) = 0. \quad (4.15)$$

Since all terms with an overlap r which is smaller than $k/2$ occupy more than $k/2$ sites, they must contain at least one singleton. Hence all terms with $r < k/2$, respectively $p > k/2$ vanish. On the other hand for $p \leq k/2$ the coefficient $N^{-\frac{k}{2}} \frac{N!}{(N-p)!}$ tends to zero as $N \rightarrow \infty$ unless $p = r = k/2$. In this case, which is only attained for even k , only two-point functions remain.

This reasoning yields the final result:

$$\lim_{N \rightarrow \infty} \rho^{\otimes N}(M(\tilde{a}_i)) = \begin{cases} 0 & \text{for } k \text{ odd} \\ \sum_{\substack{\{S_1, \dots, S_{k/2}\} \\ \#S_i=2}} \rho(a_{S_1}) \cdots \rho(a_{S_{k/2}}) & \text{for } k \text{ even.} \end{cases}$$

Now the notation can be simplified further: For each $S_\ell = \{i, j\}$ with $i < j$ it follows that

$$\begin{aligned} \rho(a_{S_\ell}) &= \rho((a_i - \rho(a_i)\mathbb{1})(a_j - \rho(a_j)\mathbb{1})) \\ &= \rho(a_i a_j) - \rho(a_i)\rho(a_j) \\ &\equiv \omega_\rho(\hat{a}_i \hat{a}_j). \end{aligned}$$

This finally proves the theorem. □

The next corollary shows that the limiting fluctuation operators satisfy canonical commutation relations. Thus, using the regularity of the quasi free limit state, they can be identified with Bose fields building a CCR-algebra as briefly discussed in section 1.2. For more details on this identification and a recommendable introduction to the general theory of CCR-algebras we refer to the book [6].

Corollary 19. *The commutator of two macroscopic fluctuation operators \widehat{a}_i and \widehat{a}_j is given by*

$$[\widehat{a}_i, \widehat{a}_j] = \rho([a_i, a_j]) \mathbb{1}. \quad (4.16)$$

Proof. Define $c = [a, b]$ to be the commutator of $a, b \in \mathcal{A}$ on the level of single-particle observables. With this definition, we can determine the commutator of the local fluctuations $\widetilde{a}, \widetilde{b} \in \mathcal{A}^{\otimes N}$ to be given by the mean-field observable $\text{sym}_N c$,

$$\begin{aligned} [\widetilde{a}, \widetilde{b}] &= \frac{1}{N} \sum_{i,j} a^{(i)} b^{(j)} - a^{(j)} b^{(i)} \\ &= \frac{1}{N} \sum_{i=1}^N (ab - ba)^{(i)} \\ &= \frac{1}{N} \sum_i c^{(i)} = \text{sym}_N c. \end{aligned} \quad (4.17)$$

Rewriting the last expression again as a local fluctuation

$$[\widetilde{a}, \widetilde{b}] = \rho(c) \mathbb{1} + \frac{1}{\sqrt{N}} \widetilde{c} \quad (4.18)$$

yields a constant term plus a term given by a convergent operator, which is however rescaled by $N^{-1/2}$. This reasoning allows to determine the limit

$$\begin{aligned} \lim_{N \rightarrow \infty} \rho^{\otimes N} \left(\widetilde{a}_1 \dots [\widetilde{a}, \widetilde{b}] \dots \widetilde{a}_k \right) &= \lim_{N \rightarrow \infty} \rho^{\otimes N} \left(\widetilde{a}_1 \dots \left(\rho([a, b]) \mathbb{1} + \frac{1}{\sqrt{N}} \widetilde{c} \right) \dots \widetilde{a}_k \right) \\ &= \lim_{N \rightarrow \infty} \rho^{\otimes N} \left(\widetilde{a}_1 \dots \widetilde{a}_k \right) \rho([a, b]) \\ &= \omega_\rho \left(\widehat{a}_1 \dots [\widehat{a}, \widehat{b}] \dots \widehat{a}_k \right). \end{aligned} \quad (4.19)$$

This proves the corollary. \square

In summary, we have shown that for the sequence of macroscopic fluctuations the correlation functions converge to Bose fields in the limiting functional ω_ρ . This is an example of convergence in distribution. Still it must be noted that in contrast to classical probability theory, this does not imply that the characteristic functions converge. A characteristic function version of the central limit theorem is derived in [4]. Moreover, we have treated only the case of independent operators. This condition can be significantly attenuated [5].

In the last part of this section we quantify the error of the approximation by the limiting quasi free state for finite system size to give a first idea of the convergence properties.

Corollary 20. *For an odd degree k of the polynomial M in fluctuation operators, the first order corrections to the gaussian nature of the limit state ω_ρ are of order $N^{-\frac{1}{2}}$. Explicitly, they are given by*

$$\lim_{N \rightarrow \infty} \rho^{\otimes N}(M(\tilde{a}_i)) = \frac{1}{\sqrt{N}} \sum_{\{S_1, \dots, S_{(k-1)/2}\}} \rho(a_{S_1}) \cdots \rho(a_{S_{(k-1)/2}}) + \mathcal{O}(N^{-\frac{3}{2}}) \quad (4.20)$$

For even degree, the first order corrections are of order N^{-1} and given by

$$\begin{aligned} \lim_{N \rightarrow \infty} \rho^{\otimes N}(M(\tilde{a}_i)) &= \omega_\rho(M(\hat{a}_i)) \\ &+ \frac{1}{N} \left(\omega_\rho(M(\hat{a}_i)) - \frac{k/2(k/2-1)}{2} \sum_{\{S_1, \dots, S_{k/2-1}\}} \rho(a_{S_1}) \cdots \rho(a_{S_{k/2-1}}) \right) + \mathcal{O}(N^{-2}). \end{aligned} \quad (4.21)$$

Proof. The proof is just a simple extension of the combinatorics used in the proof of the central limit theorem. \square

4.3 Expansion in fluctuation operators

In order to use the theory of fluctuations for the ground state problem, we need to expand the Hamiltonian in terms of fluctuation operators. Not surprisingly, this is related to the differential calculus of functions on the state space discussed in chapter 3, and in particular to the Taylor expansion of H_∞ around ρ , which we derived in section 3.4.

To get a first impression of the expansion in fluctuation operators we explicitly calculate for the example $A_2 = \text{sym}_2(a \otimes b)$, starting from the definition (4.1) for the local fluctuation operators:

$$\begin{aligned} \text{sym}_N(a \otimes b) &= \frac{1}{N(N-1)} \sum_{i \neq j}^N a^{(i)} b^{(j)} \\ &= \frac{1}{N(N-1)} \left(\sum_{i,j=1}^N a^{(i)} \circ b^{(j)} - \sum_{i=1}^N (a \circ b)^{(i)} \right) \\ &= \frac{1}{N(N-1)} (N\rho(a)\mathbb{1}_N + \sqrt{N}\tilde{a}) \circ (N\rho(b)\mathbb{1}_N + \sqrt{N}\tilde{b}) \\ &\quad - \frac{1}{N(N-1)} (N\rho(a \circ b)\mathbb{1}_N + \sqrt{N}\tilde{a} \circ \tilde{b}) \\ &= \rho(a)\rho(b)\mathbb{1}_N + \frac{1}{\sqrt{N}} (\tilde{a}\rho(b) + \tilde{b}\rho(a)) \\ &\quad + \frac{1}{N} (\tilde{a} \circ \tilde{b} - \rho(a \circ b)\mathbb{1}_N + \rho(a)\rho(b)\mathbb{1}_N) + \mathcal{O}(N^{-3/2}) \end{aligned} \quad (4.22)$$

To keep the notation as simple as possible we have used the definition $a \circ b \equiv \frac{1}{2}(ab + ba)$ for the symmetric product of two generally non-commuting operators $a, b \in \mathcal{A}$.

Except for the last line, this expansion is exact. In the last line we have reordered the summands according to their scaling with the number of tensor factors, respectively the system size N and only given the terms up to N^{-1} explicitly. Note that in the last term which is quadratic in the fluctuations, we recover the covariance matrix of the limiting quasi free state, $\omega_\rho(\tilde{a} \circ \tilde{b}) = \rho(a \circ b) - \rho(a)\rho(b)$ (cf. equation (4.12)).

A comparison of this result to the Taylor expansion of $\text{sym}_N(a \otimes b)$ (3.44) clearly illustrates the analogies. Again, the leading order is given by the mean-field expectation value $A_\infty(\rho) = \rho(a)\rho(b)$. Moreover, the linear term in the fluctuations is identical to the first order derivative $\nabla_\rho A_\infty$ (3.43),

$$\begin{aligned} \text{sym}_N(\nabla_\rho A_\infty) &= \text{sym}_N \left((a - \rho(a)\mathbb{1})\rho(b) + (b - \rho(b)\mathbb{1})\rho(a) \right) \\ &= \frac{1}{\sqrt{N}}(\tilde{a}\rho(b) + \tilde{b}\rho(a)). \end{aligned} \quad (4.23)$$

Still, while the Taylor expansion including the second order derivative $\nabla_\rho^2 A_\infty$ (3.43) sums up to the correct result, the expansion in fluctuation operators (4.22) does not terminate. Instead there is a whole hierarchy of corrections, as can already be seen from the above example. In particular, the error of the approximation of the second order derivative by the term quadratic in fluctuation operators is given by

$$\begin{aligned} &\text{sym}_N(\nabla_\rho^2 A_\infty) - \frac{1}{N}(\tilde{a} \circ \tilde{b} - \rho(a \circ b) + \rho(a)\rho(b)) \\ &= -\frac{1}{N}(\text{sym}_N(a \circ b) - \text{sym}_N(a \otimes b) - \rho(ab) + \rho(a)\rho(b)) \\ &= \frac{1}{N^{3/2}} \left(\widetilde{a \circ b} - \tilde{a}\rho(b) - \tilde{b}\rho(a) \right) + \mathcal{O}(N^{-2}), \end{aligned} \quad (4.24)$$

where we have continuously substituted symmetric operators by their expression in fluctuation operators.

The calculation presented above for the special case $k = 2$ can be generalized to determine the expansion in fluctuation operators for an arbitrary symmetric operator $\text{sym}_N(A_k) = \text{sym}_N(a_1 \otimes a_2 \otimes \cdots \otimes a_k)$. This results essentially in the same structure:

$$\begin{aligned} \text{sym}_N(A_k) &= \prod_{i=1}^k \rho(a_i) + \frac{1}{\sqrt{N}} \sum_j \tilde{a}_j \prod_{i \neq j} \rho(a_i) \\ &\quad + \frac{1}{N} \left(\sum_{k \neq j} (\tilde{a}_k \tilde{a}_j - \omega_\rho(\widehat{a}_k \widehat{a}_j)) \prod_{\substack{i \neq k \\ i \neq j}} \rho(a_i) \right) + \mathcal{O}(N^{-\frac{3}{2}}), \end{aligned} \quad (4.25)$$

where we have suppressed the factors $\mathbb{1}_N$ for reasons of clarity. Hence, e.g. $\rho(a)$ has to be understood as a multiple of the identity $\rho(a)\mathbb{1}_N$. Explicitly, the calculation reads:

$$\begin{aligned}
\text{sym}_N(A_k) &= \frac{(N-k)!}{N!} \sum_{\substack{i_\ell \in \{1, \dots, N\} \\ i_\ell \neq i_j \text{ for } \ell \neq j}} a_1^{(i_1)} \otimes a_2^{(i_2)} \otimes \dots \otimes a_k^{(i_k)} \\
&= \frac{(N-k)!}{N!} \sum_{i_\ell \in \{1, \dots, N\}} a_1^{(i_1)} \otimes a_2^{(i_2)} \otimes \dots \otimes a_k^{(i_k)} \\
&\quad - \frac{(N-k)!}{N!} \sum_{p=1}^{k-1} \frac{N!}{(N-p)!} \sum_{\{S_1, \dots, S_p\}} \prod_{S_i} \text{sym}_N(a_{S_i}),
\end{aligned} \tag{4.26}$$

where we have used the the same notation as in the proof of theorem 18 with the sum ranging over all partitions. Still here, in contrast to the definition above, we assume that the product $\prod_{S_i} \text{sym}_N(a_{S_i}) = \text{sym}_N(a_{S_1}) \circ \dots \circ \text{sym}_N(a_{S_i})$ is symmetric. The substitution of symmetric operators by their corresponding fluctuation operators yields:

$$\begin{aligned}
\text{sym}_N(A_k) &= \frac{(N-k)!}{N!} \prod_{i=1}^k \left(N\rho(a_i) - \sqrt{N} \tilde{a}_i \right) \\
&\quad - \frac{(N-k)!}{N!} \sum_{p=1}^{k-1} \frac{N!}{(N-p)!} \sum_{\{S_1, \dots, S_p\}} \prod_{S_i} \text{sym}_N(a_{S_i}).
\end{aligned} \tag{4.27}$$

Now, we expand the terms up to the order $1/N$,

$$\begin{aligned}
&= \left(1 + \frac{k(k-1)}{2} \frac{1}{N} + \mathcal{O}(N^{-2}) \right) \\
&\quad \times \left(\prod_{i=1}^k \rho(a_i) + \frac{1}{\sqrt{N}} \sum_j \tilde{a}_j \prod_{i \neq j} \rho(a_i) + \frac{1}{N} \sum_{k \neq j} \tilde{a}_k \circ \tilde{a}_j \prod_{\substack{i \neq k \\ i \neq j}} \rho(a_i) + \mathcal{O}(N^{-2}) \right) \\
&\quad - \frac{1}{N} \sum_{\{S_1, \dots, S_{k-1}\}} \prod_{S_i} \rho(a_{S_i}) + \mathcal{O}(N^{-2}).
\end{aligned} \tag{4.28}$$

Obviously, if one has $k - 1$ partitions of k operators, there can be only one two-point and $k - 2$ one-point functions. This yields the final result:

$$\begin{aligned}
\text{sym}_N(A_k) &= \prod_{i=1}^k \rho(a_i) + \frac{1}{\sqrt{N}} \sum_j \tilde{a}_j \prod_{i \neq j} \rho(a_i) \\
&\quad + \frac{1}{N} \left(\sum_{k \neq j} (\tilde{a}_k \circ \tilde{a}_j - \rho(a_k \circ a_j)) \prod_{\substack{i \neq k \\ i \neq j}} \rho(a_i) + \frac{k(k-1)}{2} \prod_{i=1}^k \rho(a_i) \right) \\
&\quad + \mathcal{O}(N^{-\frac{3}{2}}) \\
&= \prod_{i=1}^k \rho(a_i) + \frac{1}{\sqrt{N}} \sum_j \tilde{a}_j \prod_{i \neq j} \rho(a_i) \\
&\quad + \frac{1}{N} \left(\sum_{k \neq j} (\tilde{a}_k \circ \tilde{a}_j - \omega_\rho(\tilde{a}_k \circ \tilde{a}_j)) \prod_{\substack{i \neq k \\ i \neq j}} \rho(a_i) \right) + \mathcal{O}(N^{-\frac{3}{2}}). \quad (4.29)
\end{aligned}$$

In summary we obtain the same structure as discussed for the special example $k = 2$ – to leading order the expansion is given by the mean-field expectation $A_\infty(\rho)$, while the term proportional to $\propto N^{-\frac{1}{2}}$ is a linear combination of fluctuation operators, which is equivalent to the first order derivative $\nabla_\rho A_\infty$ of the mean-field limit. As above, the $1/N$ -correction is a quadratic expression in fluctuation operators including collision terms which are not covered by the Taylor expansion. In the remaining part of this chapter, we will analyse the relation in more detail.

The main result of section 3.4 was the generalization of the Taylor expansion for a symmetric operator $H_N = \text{sym}_k(H_k)$ in terms of the derivatives $\nabla_\rho^r H_\infty$ of the state space function $H_\infty(\rho)$:

$$\text{sym}_N(H_k) = \sum_{r=0}^k \frac{1}{r!} \text{sym}_N(\nabla_\rho^r H_\infty). \quad (4.30)$$

Due to the construction, all terms have vanishing expectation value in the state ρ , except for the zeroth-derivative, which is given by the state space function $H_\infty(\rho)\mathbb{1}_N$ itself, respectively the mean-field expectation value in the state ρ .

Thus, we are looking for an expansion in a basis with vanishing expectation value in ρ in order to generalize the reasoning in the preceding paragraph. In particular, we want to expand each term $\nabla_\rho^r H_\infty$ as follows:

$$\nabla_\rho^r H_\infty = \sum_{\alpha_1, \dots, \alpha_r=0}^{\dim \mathcal{A}-1} h(\alpha_1, \dots, \alpha_r) e_{\alpha_1} \otimes \dots \otimes e_{\alpha_r} \in \mathcal{A}^{\otimes r}, \quad (4.31)$$

where the $e_\alpha \in \mathcal{A}$ are a basis of the algebra with $e_0 = \mathbb{1}$ and $\rho(e_\alpha) = 0 \quad \forall \alpha > 0$. Note that due to the summation over all α_i , the symmetry of the operator $\nabla_\rho^r H_\infty$

is implicitly contained. As a direct consequence of the construction of derivatives all terms containing an index $\alpha_i = 0$ for $r \geq 0$ vanish. Therefore, we get the following expression in terms of fluctuation operators by a symmetrization over N sites:

$$\begin{aligned} \text{sym}_N(\nabla_\rho^r H_\infty) &= \frac{1}{N^{r/2}} \sum_{\alpha_1, \dots, \alpha_r=1}^{\dim \mathcal{A}-1} h(\alpha_1, \dots, \alpha_r) \widetilde{e}_{\alpha_1} \dots \widetilde{e}_{\alpha_r} + \text{corrections} \\ &\equiv \frac{1}{N^{r/2}} \widetilde{\nabla}_\rho^r H_\infty \in \mathcal{A}_{\text{sym}}^{\otimes N}, \end{aligned} \quad (4.32)$$

where \widetilde{e}_α is simply given by $\widetilde{e}_\alpha = N^{1/2} \text{sym}_N(e_\alpha)$, as $\rho(e_\alpha)$ vanishes by definition.

In the above example we have seen that the corrections mainly arise from the fact that the product of fluctuation operators also contains collision terms in which the two observables act on the same site, whereas these terms are not contained in the symmetrization of tensor products (4.31). In addition, we introduce an error by the replacement of the exact combinatorial factor by its leading order.

Still the explicit calculation (cf. equation (4.26) to equation (4.29)) has shown that the corrections again expressed in terms of local fluctuation operators scale as $1/\sqrt{N}$ compared with the leading term. So they do not invalidate the observation that the above treatment turns the Taylor expansion into a power series in $1/\sqrt{N}$,

$$\begin{aligned} \text{sym}_N(H_k) &= \sum_{r=0}^k \frac{1}{r!} \text{sym}_N(\nabla_\rho^r H_\infty) \\ &= \sum_{r=0}^{\infty} \frac{1}{r! N^{r/2}} \widetilde{\nabla}_\rho^r H_\infty \\ &= H_\infty(\rho) \mathbb{1}_N + \frac{1}{\sqrt{N}} \widetilde{\nabla}_\rho H_\infty + \frac{1}{2N} \widetilde{\nabla}_\rho^2 H_\infty + \mathcal{O}(N^{-3/2}), \end{aligned} \quad (4.33)$$

where $\widetilde{\nabla}_\rho^r H_\infty$ is a polynomial in fluctuation operators (4.32). It is worth stopping here for a moment: So, what we have finally got is an expression for a symmetric operator as a polynomial of fluctuation operators. Therefore, every single term $\widetilde{\nabla}_\rho^r H_\infty$ is convergent if we take the limit of infinite system size in a state with root N fluctuations (17). This allows for a determination the deviations from the limit for finite system size

$$\begin{aligned} &\lim_{N \rightarrow \infty} \rho_N(\text{sym}_N(H_k)) \\ &= \lim_{N \rightarrow \infty} \sum_{r=0}^{\infty} \frac{1}{r! N^{r/2}} \rho_N(\widetilde{\nabla}_\rho^r H_\infty) \\ &= H_\infty(\rho) + \lim_{N \rightarrow \infty} \frac{1}{\sqrt{N}} \rho_N(\widetilde{\nabla}_\rho H_\infty) \\ &\quad + \lim_{N \rightarrow \infty} \frac{1}{N} \rho_N\left(\frac{1}{2} \widetilde{\nabla}_\rho^2 H_\infty\right) + \mathcal{O}(N^{-3/2}) \\ &= H_\infty(\rho) + \frac{1}{\sqrt{N}} \langle \Omega | \widehat{\nabla}_\rho H_\infty \Omega \rangle + \frac{1}{N} \langle \Omega | \frac{1}{2} \widehat{\nabla}_\rho^2 H_\infty \Omega \rangle + \mathcal{O}(N^{-3/2}). \end{aligned} \quad (4.34)$$

This expansion will be the the key ingredient to establish an inner bound for the ground state problem in chapter 5.

Still, to quantify the deviations, we need to take into account the corrections (4.32). Note that for $r = 0$, as well as $r = 1$ there are no corrections. Here, we will not determine the exact collision corrections for general r , which would essentially result in a similar calculation to the one presented above starting from equation (4.26). However, the case $r = 2$ will be crucial for us since we are interested in an expansion around the mean-field extrema, where the second order derivatives play a major role.

In this case, the determination of the corrections is equivalent to the above calculation (4.26), with the special choice $A_2 = \sum_{\alpha,\beta} h(\alpha, \beta) \text{sym}_N(e_\alpha \otimes e_\beta)$. Thus, we get

$$\begin{aligned}
\text{sym}_N(\nabla_\rho^2 H_\infty) &= \frac{1}{N-1} \sum_{\alpha,\beta}^{\dim \mathcal{A}-1} h(\alpha, \beta) \tilde{e}_\alpha \tilde{e}_\beta - \frac{1}{N(N-1)} \sum_{\alpha,\beta}^{\dim \mathcal{A}-1} h(\alpha, \beta) e_\alpha e_\beta \\
&= \frac{1}{N} \sum_{\alpha,\beta}^{\dim \mathcal{A}-1} h(\alpha, \beta) \tilde{e}_\alpha \tilde{e}_\beta - \frac{1}{N} \sum_{\alpha,\beta}^{\dim \mathcal{A}-1} h(\alpha, \beta) \text{sym}_N(e_\alpha e_\beta) \\
&\quad - \frac{1}{N(N-1)} \left(\sum_{\alpha,\beta}^{\dim \mathcal{A}-1} h(\alpha, \beta) \text{sym}_N(e_\alpha e_\beta) - \sum_{\alpha,\beta}^{\dim \mathcal{A}-1} h(\alpha, \beta) \tilde{e}_\alpha \tilde{e}_\beta \right) \\
&\equiv \frac{1}{N} \tilde{\nabla}_\rho^2 H_\infty, \tag{4.35}
\end{aligned}$$

where we have chosen a representation for the corrections which most clearly reveals the convergence properties in the limit (4.5) we are interested in. This expression will be the starting point for the analysis of the $1/N$ corrections for the quantum ground state problem discussed in section 5.4.

Chapter 5

The ground state problem

5.1 Introduction

In this chapter we are interested in the ground state energy of an N -particle system with a mean-field interaction term described by a symmetric Hamiltonian of degree k

$$N \operatorname{sym}_N(H_N) = N \operatorname{sym}_N(H_k) \in \mathcal{A}^{\otimes N}. \quad (5.1)$$

While the total energy of the N -particle system is an extensive quantity given by the expectation value of the Hamiltonian $\langle NH_N \rangle$, $H_N = \operatorname{sym}_N H_k \in \mathcal{Y}$ denotes the hamiltonian density, respectively the energy per particle, which is an intensive quantity. For the time being we only consider strictly symmetric operators $H_N = \operatorname{sym}_N(H_k)$. Moreover, in this chapter \mathcal{A} will either be the algebra of $d \times d$ -matrices, i.e., we will be concerned with a d -level quantum system, or \mathcal{A} will be the commutative algebra of continuous functions on some compact space X , i.e. a classical system with configuration space X .

The example for such a hamiltonian density including two-particle interactions $V^{(i,j)}$

$$\begin{aligned} H_N &= \frac{1}{N} \sum_{i=1}^N E^{(i)} + \frac{1}{N(N-1)} \sum_{\substack{i,j=1 \\ i \neq j}}^N V^{(i,j)} \\ &= \operatorname{sym}_N(E) + \operatorname{sym}_N(V), \end{aligned} \quad (5.2)$$

has already been introduced in section 2.1. Here $E^{(i)} \in \mathcal{A}$ denotes the one-particle energy of the i -th system and $V^{(i,j)} \in \mathcal{A} \otimes \mathcal{A}$ denotes the interaction energy between the i -th and j -th particle. This example includes the mean-field Heisenberg model, as well as the mean-field Ising model with a transverse field as special realisations, which are briefly addressed in section 5.2.

For a general N -particle system (5.1) the size of the corresponding Hilbert space grows exponentially with the system size N , as well as with the local dimension d . Therefore an explicit calculation of the infimum of the spectrum of the hermitian operator

H_N , respectively the calculation of the smallest eigenvalue of the N -particle hermitian operator H_N in finite dimension,

$$\sigma_N(H_N) = \inf_{\rho_N \in \mathcal{S}(\mathcal{A}^N)} \langle \rho_N, H_N \rangle, \quad (5.3)$$

becomes impossible for any realistic system size. Hence, approximations are of high interest. For a quantum mean-field system it is well-known that the problem can be approximately solved in the limit of infinite system size $N \rightarrow \infty$ by a reduction to an effective single-particle problem. However, rigorous results on the relation between the mean-field solution and the original N -particle problem are extremely rare, see e.g. [43]. These relations and especially the case of large, but finite system size N illustrating the convergence towards the mean-field solution will be thoroughly discussed in this chapter.

As we have seen in chapter 2, the formalism of strictly and approximately symmetric operators allows for a rigorous treatment of such problems and especially of the limit of infinite system size. In this formalism the mean-field limit of a sequence of strictly symmetric hamiltonian densities $H_N = \text{sym}_N H_k \in \mathcal{Y}$ is described by a function $H_\infty(\rho)$ on the single-particle state space $\mathcal{S}(\mathcal{A})$,

$$H_\infty(\rho) = \lim_{N \rightarrow \infty} \langle \rho^{\otimes N}, H_N \rangle = \langle \rho^{\otimes k}, H_k \rangle. \quad (5.4)$$

We will also use the common notation from operator theory $\rho^{\otimes k}(H_k)$ for the expectation value of the observable H_k in the state $\rho^{\otimes k}$, wherever this notation is more convenient. In the limit of infinite system size the ground state energy $\sigma_N(H_N)$ defined in equation (5.3) is thus given by a variational problem on the single particle state space $\mathcal{S}(\mathcal{A})$:

$$\begin{aligned} \lim_{N \rightarrow \infty} \sigma_N(H_N) &= \inf_{\rho \in \mathcal{S}(\mathcal{A})} H_\infty(\rho) \\ &= \inf \left\{ \rho^{\otimes k}(H_k) \mid \rho \in \mathcal{S}(\mathcal{A}) \right\}. \end{aligned} \quad (5.5)$$

By a simple inclusion of domains over which the infimum is taken,

$$\left\{ \rho^{\otimes N} \mid \rho \in \mathcal{S}(\mathcal{A}) \right\} \subset \mathcal{S}(\mathcal{A}^{\otimes N}), \quad (5.6)$$

one can show that $\sigma_N(H_N) \leq \inf_{\rho} H_\infty(\rho)$. Moreover, because of the properties of the norm (1.3), the relation

$$\|H_N\| \leq \|H_{N+M}\| \quad (5.7)$$

holds. Thus, $\sigma_N(H_N)$ is monotonically increasing to its limit.

In this chapter, we are interested in the next order in $1/N$ of the approximation of the ground state energy $\sigma_N(H_N)$ by the mean-field solution $\inf_{\rho} H_\infty(\rho)$:

$$\sigma_N(H_N) = \inf_{\rho} H_\infty(\rho) - \frac{1}{N} \gamma(H_k) + o(1/N). \quad (5.8)$$

The major goal of this chapter is therefore the determination of the coefficient $\gamma(H_k)$. As a direct consequence of the convergence properties of $\sigma_N(H_N)$, this coefficient has to be positive, i.e. $\gamma(H_k) \geq 0$.

It is clear that in order to establish the value of $\gamma(H_k)$ we have to prove two bounds. Still in this case it may be confusing to speak of upper and lower bounds, since a lower bound to the ground state energy (5.8) is at the same time an upper bound to $\gamma(H_k)$, and vice versa. Instead we will refer to this bound as the **outer bound**, as it limits the set of possible values of $\rho_N(H_N)$ or $\gamma(H_k)$ from the outside, typically by establishing conditions valid for all states ρ_N . In contrast, we call the upper bound to the ground state problem (5.8), respectively the lower bound to $\gamma(H_k)$, the **inner bound**, as it sets a limit to the set of expectation values from within, typically by explicitly constructing suitable states ρ_N .

The bound we are searching for is closely related to the error predicted by the finite de Finetti theorem discussed in section 2.5. This relation will be elucidated in section 5.3.1.

5.2 Some illustrative examples from statistical mechanics

Before going into more details considering the general problem, we will discuss the implications of the ground state problem for two well-known examples from the theory of solid state physics: The mean-field Heisenberg model and the mean-field Ising model with a transverse field.

5.2.1 The mean-field Heisenberg Model

The mean-field Heisenberg model describes a system consisting of N identical spins $s \in \frac{1}{2}\mathbb{N}$, which all interact in the same way with the external field, as well as with one another. For illustrative reasons, we only consider the simplest case $s = \frac{1}{2}$, such that the single-particle algebra is given by the set of 2×2 -matrices, i.e. $\mathcal{A} = \mathbb{C}^{2 \times 2}$. In addition, we chose the external field along the z -axis, $\mathbf{B} = (0, 0, B)$. Hence, the Hamiltonian of the N -particle system in terms of the Pauli matrices S_1, S_2, S_3 (3.25) becomes

$$NH_N = B \sum_{i=1}^N S_3^{(i)} + \frac{J}{N-1} \sum_{i \neq j}^N \sum_{\alpha=x,y,z} S_\alpha^{(i)} \otimes S_\alpha^{(j)}. \quad (5.9)$$

This is an example of a mean-field quantum system with pairwise interactions (5.2) with the special choice $E = BS_3 \in \mathcal{A}$ for the term describing the interaction with the external field and $V = J \sum_{\alpha=x,y,z} S_\alpha \otimes S_\alpha \in \mathcal{A} \otimes \mathcal{A}$ for the interaction term.

A concise way to summarize the possible values of $\rho_N(H_N)$ of such a two-parameter model and in particular the ground state energies is the joint numerical range. For an arbitrary two-parameter model, e.g. $H = aA + bB$ with $a, b \in \mathbb{R}$ and $A, B \in \mathcal{A}$, the

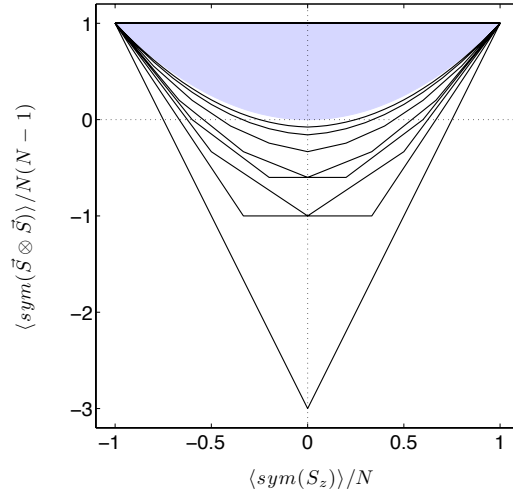


Figure 5.1: Joint numerical range ν_N (5.10) of the single-particle term $1/N \text{sym}_N(S_3)$ (horizontal axis) and the interaction term $1/(N(N-1)) \text{sym}_N(\mathbf{S} \otimes \mathbf{S})$ in the mean-field Heisenberg model (5.9) for different system sizes $N = 2, 3, 4, 5, 6, 10, 20, 40$. The shaded area depicts the region which can be accessed by mean-field states and is the intersection of all the numerical ranges ν_N for finite N . Note that for $N = 10, 20, 40$ the distance to the limiting shape is roughly halved in each step.

joint numerical range $\nu(A, B)$ of the two operators involved is defined as the compact convex set

$$\nu_N(A, B) = \{(\rho(A), \rho(B)) \in \mathbb{R}^2 \mid \rho \in \mathcal{S}(\mathcal{A}^{\otimes N})\}. \quad (5.10)$$

Then we can consider the family of parallel lines $ax + by = c$ in \mathbb{R}^2 , and find the largest and the smallest values of c such that this line meets $\nu_N(A, B)$. The smallest c will be the ground state energy of $aA + bB$. Hence determining all ground state energies of Hamiltonians in the family is equivalent to determining $\nu_N(A, B)$.

In the case of the mean-field Heisenberg model (5.9) E and V commute for all N , which can easily be checked. Thus, the Hamiltonian is diagonal in the common eigenbasis of the collective angular momenta operators

$$L_3 = \frac{1}{2} \sum_{i=1}^N S_3^{(i)} \quad \text{and} \quad \mathbf{L}^2 = \frac{1}{4} \sum_{i \neq j}^N \sum_{\alpha=x,y,z} S_\alpha^{(i)} \otimes S_\alpha^{(j)} + \frac{3N}{4} \mathbb{1}_N \quad (5.11)$$

of the tensor product representation $u \mapsto u^{\otimes N}$ of $SU(2)$. Note, that in this chapter, we do not restrict the analysis to a certain subspace, whereas in chapter 6 we only treat the projection onto the symmetric subspace.

In the common eigenbasis the eigenvalues for the collective angular momenta operators (5.11) are given by

$$L_3 |\ell, m\rangle = m |\ell, m\rangle \quad \mathbf{L}^2 |\ell, m\rangle = \ell(\ell + 1) |\ell, m\rangle. \quad (5.12)$$

with $\ell = N/2, N/2 - 1, \dots, -1/2$, respectively $\ell = N/2, N/2 - 1, \dots, 0$ depending on N being odd or even and $m = \ell, \ell - 1, \dots, -\ell$. Hence, by a simple calculation we obtain

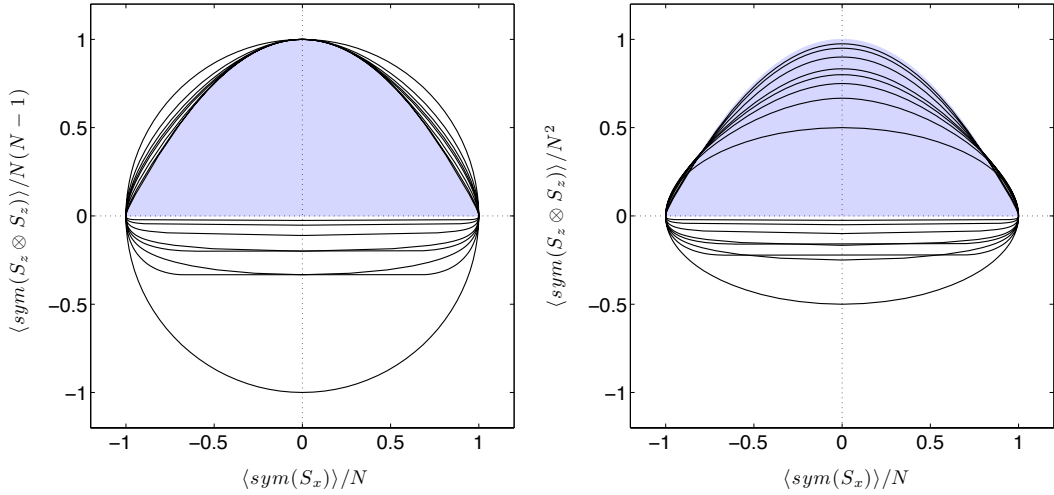


Figure 5.2: Left-hand side: Joint numerical range ν_N (5.10) of the one particle term $1/N \text{sym}_N(S_1)$ (horizontal axis) and the interaction term $1/(N(N-1)) \text{sym}_N(S_3 \otimes S_3)$ in the mean field Ising model (5.15) for $N = 2, 3, 4, 5, 6, 10, 20, 40$. Right hand side: Analogous plot for a model in which the interaction is scaled with $1/N$ rather than $1/(N-1)$.

the spectrum of the energy density H_N (5.9), which is given by

$$\begin{aligned} \langle \ell, m | H_N | \ell, m \rangle &= B \left(\frac{m}{N} \right) + J \frac{4\ell(\ell+1) - 3N}{N(N-1)} \\ &\geq -\frac{B}{2} - J. \end{aligned} \quad (5.13)$$

Because of the joint diagonalizability of L_3 and \mathbf{L}^2 the joint numerical range $\nu(L_3, \mathbf{L}^2)$ is a polytope, whose vertices are the pairs of joint eigenvalues. The result for the mean-field Heisenberg model is shown in figure 5.1. One can easily check that the vertices for ν_N are given by

$$\left\{ \left(\frac{\ell}{N}, \frac{4\ell(\ell+1) - 3N}{N(N-1)} \right) \mid \ell = N/2, N/2 - 1, \dots, -N/2 - 1, -N/2 \right\}. \quad (5.14)$$

Here the vertices on the x -axis corresponding to $\ell = 0$ reveal the convergence to the mean-field limit which is proportional to $1/(N-1)$ most clearly. The mean field accessible region is the intersection of all numerical ranges for finite particle numbers N and is shaded in blue.

5.2.2 Mean-field Ising Model with transverse field

As above, we choose $s = \frac{1}{2}$, such that the single-particle algebra is given by the set of 2×2 -matrices, i.e. $\mathcal{A} = \mathbb{C}^{2 \times 2}$. However, we now consider the case $E = BS_1 \in \mathcal{A}$ and

$V = JS_3 \otimes S_3 \in \mathcal{A} \otimes \mathcal{A}$, such that the Hamiltonian is given by

$$NH_N = B \sum_{i=1}^N S_1^{(i)} + \frac{J}{N-1} \sum_{i \neq j}^N S_3^{(i)} \otimes S_3^{(j)}. \quad (5.15)$$

In contrast to the mean-field Heisenberg model (5.9), the interaction with the external field E and the interaction term V do not commute, which makes the calculation of the spectrum a much harder task. As a direct consequence, the joint numerical range (5.10) is no longer a polytope. If we restrict the set of states to the Bose sector, then we obtain again the Bose-Hubbard system for two lattice sites, which plays a major role in the second part of this thesis. Even with this restriction, analytic solutions are not easily obtained (cf. e.g. [44] for analytic solutions based on the Bethe ansatz method). Figure 5.2 shows the numerical results. As in the first example, the shaded area represents the mean-field expectation values. As above, this area is given by the intersection of all the numerical ranges ν_N for finite N .

In addition to the strictly symmetric version (5.15) of the mean-field Ising model, we have plotted a model where the interaction term is scaled by $1/N$ instead of $1/(N-1)$. The sequence of the resulting hamiltonian densities H_N is still approximately symmetric, but the mean-field expectation values do no longer lie inside the numerical range for finite system size N . This clearly shows that the mean-field results provide only inner bounds for the expectation values if the intensive observables are strictly symmetric.

5.3 Relations to other problems

The determination of the first order corrections to the mean-field expectation value is a fundamental quantum problem. In this section we will highlight two possible applications. Finite de Finetti theorems are concerned with approximations of finitely exchangeable states, which are defined as the restrictions of permutation symmetric states (cf. section 2.5), whereas we consider the macroscopic limit of symmetric operators of finite degree. Still, we will show that there is an elementary relation between the bounds established by finite de Finetti theorems and the determination of the $1/N$ correction γ (5.8). In particular, we will see that computing γ can be interpreted as a local version of a finite de Finetti theorem.

Moreover, we will analyse the relation of the finite size corrections for the ground state (5.8) to spin squeezing inequalities. These inequalities give bounds on the set of expectation values which can be assumed by separable states. Thus, they can be interpreted as entanglement witnesses. In section 5.3.2, we will analyse this problem in more detail and show that the determination of the entanglement witnesses reduces to the computation of γ (5.8) for a suitable abelian algebra. Furthermore, we will suggest an algorithm to determine the finite size correction and discuss its applications to the examples considered in section 5.2. The algorithm will be proven to be correct to order $1/N$ in section 5.5.

5.3.1 Finite de Finetti theorems

In section 2.5 we have introduced the theorem by Størmer [20], which provides a characterization of permutation symmetric states, generalizing a result from classical probability theory by de Finetti [25] to the quantum case. There, we have also analysed the relation to the abstract theory of quantum mean-field systems and explained how this result follows as a corollary theorem 11 (for more details see [11]).

Finite de Finetti theorems [29–31] extend these results and give an explicit bound on the difference between the restriction ρ_k of a permutation symmetric state $\rho_N \in \mathcal{S}(\mathcal{A}^{\otimes N})$ and a convex combination of product states

$$\rho_{\mu,k} = \int \mu(d\sigma) \sigma^{\otimes k}, \quad (5.16)$$

where μ is a probability measure on $\mathcal{S}(\mathcal{A})$. Note that this state is sometimes referred to as a de Finetti state.

In general finite de Finetti theorems take the form of the estimate

$$\sup_{\rho_N} \inf_{\mu} \|\rho_k - \rho_{\mu,k}\|_1 \leq \frac{\gamma_k}{N}, \quad (5.17)$$

with some constant γ_k depending only on k and \mathcal{A} . In this equation and below $\|\cdot\|_1$ denotes the norm of the states (equal to the \mathcal{L}^1 -norm of probability densities or the trace norm of density operators, respectively) and it is understood that the supremum is taken over the whole set of symmetric states $\rho_N \in \mathcal{S}(\mathcal{A}^{\otimes N})$. Furthermore, ρ_k is the restriction of ρ_N to $\mathcal{A}^{\otimes k}$. For $N = \infty$, i.e., if ρ_k is the restriction of a state on infinitely many copies of N , which is invariant under finite permutations, the result reduces again to the theorem by Størmer.

Since the relation of the ground state problem (5.8) to finite de Finetti theorems (5.17) is not directly obvious, we will discuss the point in more detail. First we express the trace norm as the supremum over the set of all operators H_k with $\|H_k\| \leq 1$. Since we look for the norm of a hermitian element, it is sufficient to consider only hermitian operators $H_k^\dagger = H_k$:

$$\sup_{\rho_N} \inf_{\mu} \|\rho_{\mu,k} - \rho_k\|_1 = \sup_{\rho_N} \inf_{\mu} \sup_{H_k} (\rho_{\mu,k}(H_k) - \rho_k(H_k)).$$

As both, the element H_k , as well as its negative counterpart $-H_k$ are included in the set of elements over which the supremum is taken, we have omitted the absolute value. Now we can use the Minmax theorem presented in the mathematical introduction (cf. theorem 8), which allows to rearrange the order in which the suprema and the infimum have to be taken:

$$\sup_{\rho_N} \inf_{\mu} \|\rho_{\mu,k} - \rho_k\|_1 = \sup_{H_k} \sup_{\rho_N} \inf_{\mu} (\rho_{\mu,k}(H_k) - \rho_k(H_k)).$$

The second term is independent of the measure μ

$$\sup_{\rho_N} \inf_{\mu} \|\rho_{\mu,k} - \rho_k\|_1 = \sup_{H_k} \sup_{\rho_N} \left(\inf_{\mu} \rho_{\mu,k}(H_k) - \rho_k(H_k) \right),$$

and the first term assumes its minimum if the probability measure μ is concentrated on a point σ where the integrand assumes its minimum (see also equation (5.16)):

$$\sup_{\rho_N} \inf_{\mu} \|\rho_{\mu,k} - \rho_k\|_1 = \sup_{H_k} \left(\inf_{\sigma} \sigma^{\otimes k}(H_k) - \inf_{\rho_N} \rho_N(\text{sym}_N(H_k)) \right).$$

Note that there is no reason, why this minimum should be unique. In the last equality we introduce the notations used in equation (5.8):

$$\sup_{\rho_N} \inf_{\mu} \|\rho_{\mu,k} - \rho_k\|_1 = \sup_{H_k} \left(\inf_{\sigma} H_{\infty}(\sigma) - \sigma_N(H_N) \right) \quad (5.18)$$

To summarize the reasoning, we have found the following relation between the de Finetti constant γ_k as defined in equation (5.17) and the coefficient γ (cf. (5.8)) which we want to determine:

$$\gamma_k = \sup_{H_k} \gamma(H_k) + o(1/N). \quad (5.19)$$

Hence, in applications of the finite de Finetti theorem, in which the difference of states in equation (5.8) is only evaluated on a few observables H_k , the computation of $\gamma(H_k)$ may give more detailed information. In this sense computing $\gamma(H_k)$ is a *local* version of a finite de Finetti theorem.

5.3.2 Spin squeezing inequalities and entanglement detection

Imagine an experiment, where we measure the energy of a many-particle Hamiltonian, that is the expectation value of a N -particle Hamiltonian $H_N = \text{sym}_N(H_k)$ in some state ρ_N . If the measurement outcome is smaller than the infimum over the set of mean-field solutions $\inf_{\sigma} H_{\infty}(\sigma)$, we can conclude that the state of the system is not of de Finetti form, i.e. not given by a convex combination of homogeneous product states $\sigma^{\otimes N}$. But can we also conclude that the state is not fully separable, e.g. not a convex combination of inhomogeneous product states $\sigma_1 \otimes \cdots \otimes \sigma_N$? In other words, can we use symmetric operators as entanglement witnesses?

Clearly, it is not sufficient to consider the infimum over H_{∞} , respectively over all de Finetti states, to answer this question. Hence, we will address this problem in more detail and show that it is again closely related to the determination of the first order corrections of the mean-field limit which are summarized by the coefficient γ in equation (5.8).

In particular, we want to analyse the relation between the following variational problems: The determination of the infimum over the whole N -particle state space, respectively the minimum of the spectrum of H_N (5.3),

$$\sigma_N(H_N) = \inf \{ \rho_N(H_N) \mid \rho_N \in \mathcal{S}(\mathcal{A}^{\otimes N}) \},$$

the infimum over the set of fully separable states, i.e.

$$\inf_{\text{sep}} H_N = \inf \left\{ \rho_N(H_N) \mid \rho_N = \sum_k p_k \sigma_{k_1} \otimes \cdots \otimes \sigma_{k_N} \text{ with } \sum_k p_k = 1 \text{ and } p_k \geq 0 \right\},$$

and the infimum over the set of de Finetti states,

$$\begin{aligned} \inf_{\text{deFinetti}} H_N &= \inf \left\{ \rho_N(H_N) \mid \rho_N = \sum_k p_k \sigma_k^{\otimes N} \text{ with } \sum_k p_k = 1 \text{ and } p_k \geq 0 \right\} \\ &= \inf \{ \rho_N(H_N) \mid \rho_N = \sigma^{\otimes N} \} \\ &= \inf \{ H_\infty(\rho) \mid \rho \in \mathcal{S}(\mathcal{A}) \}, \end{aligned}$$

which is equivalent to the minimum of the mean-field expectation value.

By the inclusion of the set of states, one can directly deduce that

$$\sigma_N(H_N) \leq \inf_{\text{sep}} H_N \leq \inf_{\rho} H_\infty(\rho). \quad (5.20)$$

For an abelian algebra \mathcal{A} , the first two values coincide. Moreover, we claim that due to the symmetry of the problem, we can evaluate the separable bound in full generality by a variation over all states of an abelian algebra. This establishes the relation to the ground state problem addressed in this chapter, as the computation of the infimum over all separable states up to the first order in $1/N$ is equivalent to the determination γ for a classical problem.

To prove this claim, we introduce the map

$$j : \mathcal{A} \rightarrow \mathcal{C}(\mathcal{S}(\mathcal{A})) \quad \text{with} \quad j(a)[\sigma] \mapsto \sigma(a). \quad (5.21)$$

The set of all functions $j(a)[\sigma] = \langle \sigma, a \rangle$ on the state space forms a commutative algebra, since

$$j(a)j(b)[\sigma] = \langle \sigma, a \rangle \langle \sigma, b \rangle = \langle \sigma, b \rangle \langle \sigma, a \rangle = j(b)j(a)[\sigma] \quad \forall \sigma \in \mathcal{S}(\mathcal{A}). \quad (5.22)$$

It is easily verified that the map (5.21) is a channel, that means that it is completely positive and normalized. Obviously, j is a linear map and $j(\mathbb{1})[\sigma] = \sigma(\mathbb{1}) = 1$. To prove the complete positivity, we have to prove that not only is j a positive map, but also the composite map $j \otimes \text{id}_N$: Let $a = (a_{ij})$ be a positive $N \times N$ matrix with values in \mathcal{A} . Then the image of the composite map

$$j \otimes \text{id}_N : \mathcal{A} \otimes \mathcal{M}_N \rightarrow \mathcal{C}(\mathcal{S}(\mathcal{A})) \otimes \mathcal{M}_N \quad (5.23)$$

is isomorphic to matrices over $\mathcal{C}(\mathcal{S}(\mathcal{A}))$,

$$\begin{aligned} j \otimes \text{id}_N(a)[\sigma] &= j(a_{ij})[\sigma] \\ &= (\sigma(a_{ij}))_{i,j=1}^N \end{aligned} \quad (5.24)$$

but just as well to functions on $\mathcal{S}(\mathcal{A})$ with values in \mathcal{M}_N . Hence, if we consider the function $\sigma \mapsto (\sigma(a_{ij}))_{i,j=1}^N = \sigma \otimes \text{id}(a)$, this yields a positive map and we can conclude that j (5.21) is a completely positive map.

For a sequence of strictly symmetric observables H_N , we set $(jH)_N = j^{\otimes N}(H_N)$. Since $H_N = \text{sym}_N(H_k)$ is generated by symmetrization, this is also true for jH , i.e., $\text{sym}_N(j^{\otimes k}(H_k)) = j^{\otimes N}(\text{sym}_N(H_k))$. Therefore, we can determine the mean-field limit for this sequence to be given by

$$\begin{aligned} (jH)_\infty(\mu) &= \mu^{\otimes k}((jH)_k) = \mu^{\otimes k}(j^{\otimes k}(H_k)) \\ &= \int \mu(d\sigma_1) \cdots \mu(d\sigma_k) \sigma_1 \otimes \cdots \otimes \sigma_k(H_k) \\ &= \bar{\rho}^{\otimes k}(H_k) = H_\infty(\bar{\rho}), \end{aligned} \quad (5.25)$$

where μ is an arbitrary probability measure on $\mathcal{S}(\mathcal{A})$ and $\bar{\rho} = \int \mu(d\sigma)\sigma$ is the barycenter of μ . In particular, the infimum is identical, $\inf(jH)_\infty = \inf H_\infty$.

Then, due to the symmetry of H_N , we have

$$\begin{aligned} \inf_{\text{sep}} \text{sym}_N((H_k)) &= \inf \{ \sigma_1 \otimes \cdots \otimes \sigma_N(H_N) \mid \sigma_i \in \mathcal{S}(\mathcal{A}) \} \\ &= \inf \{ j^{\otimes N}(H_N)[\sigma_1, \dots, \sigma_N] \mid \sigma_i \in \mathcal{S}(\mathcal{A}) \} \\ &= \inf(jH)_N \\ &= \inf \text{sym}_N((jH)_k) \\ &= \inf H_\infty - \frac{1}{N} \gamma((jH)_k) + \mathcal{O}(N^{-2}). \end{aligned} \quad (5.26)$$

By the above argument $(jH)_k$ is an element of an abelian algebra (cf. equation (5.22)). This proves the claim, as we can indeed determine the infimum over all separable states up to the order $1/N$ by the computation of γ for a commutative algebra.

Later on, we will get an easy formula for $\gamma(H_k)$ in the classical case in terms of the mean-field minimizing state (cf. section 5.4.2). When the minimizer is not unique, this requires a further variation over all such minimizers. For computing \inf_{sep} this uniqueness almost always fails, since all probability measures on $\mathcal{S}(\mathcal{A})$ with the same barycenter give the same minimum.

This is best illustrated in the case $k = 2$, i.e., for two-body interactions. Because of the symmetry, we can simplify the expression over which we have to take the infimum as

$$\begin{aligned} \sigma_1 \otimes \cdots \otimes \sigma_N \left(\text{sym}_N(H_2) \right) &= \frac{1}{N(N-1)} \sum_{i \neq j} \sigma_i \otimes \sigma_j(H_2) \\ &= \frac{N}{N-1} \bar{\rho} \otimes \bar{\rho}(H_2) - \frac{1}{N(N-1)} \sum_{i=1}^N \sigma_i^{\otimes 2}(H_2) \\ &= \bar{\rho} \otimes \bar{\rho}(H_2) - \frac{1}{N(N-1)} \sum_{i=1}^N (\sigma_i - \bar{\rho})^{\otimes 2}(H_2), \end{aligned} \quad (5.27)$$

where $\bar{\rho} = (1/N) \sum_i \sigma_i$ is the barycenter of the set of states $(\sigma_1, \dots, \sigma_N)$. The expression follows by considering separately the terms with $i = j$ and $i \neq j$ for the sum on the left hand side. Here the second term is clearly of order $1/N$. The suggestive strategy for minimizing this expression is to first choose $\bar{\rho}$ minimizing the first term. In a second step, we vary over all possible choices for the components σ_i of $\bar{\rho}$. In section 5.5 we prove that this strategy yields indeed the correct infimum to order $1/N$.

A closer inspection shows that the choice of the components σ_i depends on the sign of the quadratic form $(\sigma', \sigma'') \mapsto \sigma' \otimes \sigma''(H_2)$: if this is negative-definite, it is advantageous to choose all $\sigma_i = \rho$, so that the exact minimum is attained for a homogeneous product state: $\inf_{\text{sep}} H_N = \inf_{\rho} H_{\infty}(\rho)$. On the other hand, if the quadratic form is positive-definite, the σ_i should be as far away from their mean as possible, and certainly be pure.

To illustrate this last point and the application of the algorithm, we we consider again the two examples for mean-field spin models introduced in section 5.2. For the sake of simplicity we restrict ourselves to the case without a transverse field, i.e. we set $B = 0$, and assume that the number of spins N is even. The ground state then crucially depends on the sign of the interaction constant: For $J < 0$ the spins tend to align leading to a ferromagnetic ordering, while $J > 0$ leads to an anti-ferromagnetic ordering.

We start with the Ising model (5.15). Hence, we have to minimize the mean-field term

$$H_{\infty}(\bar{\rho}) = J \langle \bar{\rho} \otimes \bar{\rho}, S_3 \otimes S_3 \rangle = J \bar{\rho}(S_3)^2. \quad (5.28)$$

For $J > 0$ the minimum is assumed for

$$J > 0 : \quad \bar{\rho}_{\min} = \begin{pmatrix} 1/2 & \rho_{12} \\ \rho_{12}^* & 1/2 \end{pmatrix}, \quad H_{\infty}(\bar{\rho}_{\min}) = 0, \quad (5.29)$$

with arbitrary coherences $|\rho_{12}| \leq 1/2$, whereas for $J < 0$ the minimum is attained by a completely polarized state:

$$J < 0 : \quad \bar{\rho}_{\min} = \begin{pmatrix} 1 & 0 \\ 0 & 0 \end{pmatrix} \text{ or } \bar{\rho}_{\min} = \begin{pmatrix} 0 & 0 \\ 0 & 1 \end{pmatrix}, \quad H_{\infty}(\bar{\rho}_{\min}) = J. \quad (5.30)$$

Now we can evaluate the $1/N$ corrections. In the ferromagnetic case $J < 0$ (5.30), the interaction Hamiltonian H_2 is negative-definite. Therefore the extremum is found for a homogeneous product state, i.e. $\sigma_i = \bar{\rho}$ for all i and we can conclude that

$$\inf_{\text{sep}} H_N = \inf_{\text{deFinetti}} H_N = J \quad \text{for } J < 0. \quad (5.31)$$

In the anti-ferromagnetic case $J > 0$ (5.29), the interaction Hamiltonian H_2 is positive-definite such that the σ_i should be chosen as far away from their mean $\bar{\rho}$ as possible. In

particular, the correction term in equation (5.27) which we have to subtract assumes its maximum for

$$\begin{aligned}\sigma_a &= \begin{pmatrix} 1 & 0 \\ 0 & 0 \end{pmatrix} \Rightarrow (\sigma_a - \bar{\rho})^{\otimes 2}(H_2) = J \quad \text{and} \\ \sigma_b &= \begin{pmatrix} 0 & 0 \\ 0 & 1 \end{pmatrix} \Rightarrow (\sigma_b - \bar{\rho})^{\otimes 2}(H_2) = J.\end{aligned}\tag{5.32}$$

In order to assure that $\bar{\rho} = (1/N) \sum_i \sigma_i$, we have to demand that half of the spins point up, $\sigma_i = \sigma_a$ and half of the spins point down, $\sigma_i = \sigma_b$.

Then equation (5.26) predicts that the infimum over the set of fully separable states is assumed for an inhomogeneous product state and that

$$\inf_{\text{sep}} H_N = -\frac{J}{N-1} \quad \text{for } J > 0.\tag{5.33}$$

Indeed, the exact ground state of the mean-field Ising model without transverse field is given by a separable state. Hence, we can conclude that $\sigma_N(H_N) = \inf_{\text{sep}} H_N$ and thus, the above results give the exact ground state energy in both cases.

For the mean-field Heisenberg model (5.9) the calculation is very similar. The mean-field term

$$H_\infty(\rho) = J \sum_{\alpha=1}^3 \langle \bar{\rho} \otimes \bar{\rho}, \sigma_\alpha \otimes \sigma_\alpha \rangle\tag{5.34}$$

assumes its minimum for

$$\begin{aligned}J > 0 : & \quad \bar{\rho}_{\min} = \frac{1}{2} \mathbb{1}_2, & H_\infty(\bar{\rho}_{\min}) &= 0, \\ J < 0 : & \quad \bar{\rho}_{\min} = U \begin{pmatrix} 1 & 0 \\ 0 & 0 \end{pmatrix} U^\dagger & H_\infty(\bar{\rho}_{\min}) &= J,\end{aligned}\tag{5.35}$$

where U is an arbitrary unitary matrix. Again, the interaction Hamiltonian H_2 is negative-definite for the ferromagnetic case $J < 0$ such that the minimum over all separable states is found for $\sigma_i = \bar{\rho} \forall i$ with

$$\inf_{\text{sep}} H_N = J \quad \text{for } J < 0.\tag{5.36}$$

In the anti-ferromagnetic case $J > 0$ the interaction Hamiltonian H_2 is positive-definite. The minimum of the $1/N$ correction term is found by choosing all σ_i as pure states under the constraint that $\bar{\rho} = (1/N) \sum_i \sigma_i$. This yields $(\sigma_i - \bar{\rho})^{\otimes 2}(H_2) = J$ for all i such that

$$\inf_{\text{sep}} H_N = -\frac{J}{N-1} \quad \text{for } J > 0.\tag{5.37}$$

The main difference to the Ising model is that the exact ground state for $J > 0$ is *not separable* but given by the entangled singlet state. As shown in section 5.2, the exact ground state energy is given by

$$\sigma_N(H_N) = -\frac{3J}{N-1}. \quad (5.38)$$

This shows that one can indeed use the expectation value of symmetric operators as e.g. the mean-field Heisenberg Hamiltonian as an entanglement witness. Moreover, the determination of the separable bound for H_N , respectively the entanglement witness is equivalent to the calculation of the first order correction γ for the corresponding abelian algebra $(JH)_N$, where the relation is given by equation (5.26).

5.4 Inner bound in terms of fluctuations

In this section we will consider an upper bound to the ground state value $\inf H_N$, respectively a lower bound for the coefficient $\gamma(H_k)$ (5.8) which arises by perturbing the minimizing mean-field solution. So throughout this section ρ will denote a one-particle state at which the state space function H_∞ attains its minimum,

$$\min_{\sigma \in \mathcal{S}(\mathcal{A})} H_\infty(\sigma) = \min_{\sigma \in \mathcal{S}(\mathcal{A})} \sigma^{\otimes k}(H_k) = H_\infty(\rho). \quad (5.39)$$

This minimum does not have to be unique and, in fact, the arguments are the same for just a local minimum.

Suppose ρ_N is a sequence of states with root N fluctuations around the state ρ , which minimizes the mean field expectation functional (5.39). Since this is a severe restriction on the set of states, it is clear that we can only obtain an upper bound for the ground state energy, e.g.

$$\inf_{\rho_N} \rho_N(\text{sym}_N(H_k)) \geq \sigma_N(H_N). \quad (5.40)$$

Now we can use expression (4.34) in terms of macroscopic fluctuations to quantify the deviations from the mean-field expectation value (5.39) for finite system size N up to the order $1/N$:

$$\begin{aligned} \lim_{N \rightarrow \infty} \rho_N(\text{sym}_N(H_k)) &= H_\infty(\rho) + \frac{1}{\sqrt{N}} \langle \Omega | \widehat{\nabla}_\rho H_\infty | \Omega \rangle \\ &\quad + \frac{1}{N} \left\langle \Omega \left| \frac{1}{2} \widehat{\nabla}_\rho^2 H_\infty \right| \Omega \right\rangle + \mathcal{O}(N^{-3/2}). \end{aligned} \quad (5.41)$$

In section 3.3 we have argued for ρ to be a minimizer of the state space functional $H_\infty(\rho)$ (5.39) the first order derivative $\nabla_\rho H_\infty$ has to be a positive semidefinite operator, $\nabla_\rho H_\infty \geq 0$. If ρ is a global minimum, e.g. in the interior of the state space $\mathcal{S}(\mathcal{A})$, we can even conclude that $\nabla_\rho H_\infty \equiv 0$. In general, we can use the condition for a minimum

to at least estimate the linear term in macroscopic fluctuations from below by zero, such that we get the following behaviour for large, but finite N :

$$\lim_{N \rightarrow \infty} \rho_N(\text{sym}_N(H_k)) \geq H_\infty(\rho) + \frac{1}{N} \left\langle \Omega \left| \frac{1}{2} \widehat{\nabla}_\rho^2 H_\infty \right| \Omega \right\rangle + \mathcal{O}(N^{-3/2}). \quad (5.42)$$

Thus, we are looking for an estimate for the quadratic term in the fluctuations. The calculation (4.35) has shown that the following considerations can be essentially split into two major parts:

$$\left\langle \Omega \left| \frac{1}{2} \widehat{\nabla}_\rho^2 H_\infty \right| \Omega \right\rangle = \langle \Omega | \widehat{H} | \Omega \rangle - \gamma_c(H_k), \quad (5.43)$$

where we have defined the Hamiltonian in the fluctuation Hilbert space,

$$\widehat{H} \equiv \frac{1}{2} \sum_{\alpha, \beta}^{\dim \mathcal{A} - 1} h(\alpha, \beta) \widehat{e}_\alpha \widehat{e}_\beta, \quad (5.44)$$

which is quadratic in the fluctuation operators even if $k > 2$ and H_∞ is not a quadratic polynomial. Note that this is the effective Hamiltonian governing the dynamics of the fluctuations for quantum mean-field systems [41].

Moreover, we have defined the coefficient $\gamma_c(H_k)$, to be given by

$$\begin{aligned} \gamma_c(H_k) &= \lim_{N \rightarrow \infty} \rho_N \left(\frac{1}{2} \sum_{\alpha, \beta} h(\alpha, \beta) \text{sym}_N(e_\alpha e_\beta) \right) \\ &= \rho \left(\frac{1}{2} \sum_{\alpha, \beta} h(\alpha, \beta) e_\alpha e_\beta \right). \end{aligned} \quad (5.45)$$

This can be interpreted as the mean-field limit of the corrections.

With these considerations we can write the bound as

$$\liminf_{N \rightarrow \infty} \rho_N(\text{sym}_N(H_k)) \geq H_\infty(\rho) + \frac{1}{N} \left(\langle \Omega | \widehat{H} | \Omega \rangle - \gamma_c(H_k) \right) + \mathcal{O}(N^{-3/2}). \quad (5.46)$$

Note that the coefficient $\gamma_c(H_k)$ does only depend on the mean-field minimizer ρ , as well as the Hamiltonian H_k , but not on the special choice of the sequence ρ_N with root N fluctuations around ρ . This is clearly different for the expectation value of the fluctuation Hamiltonian (5.44), which is strongly influenced by the choice of the sequence ρ_N . In the following sections, we will evaluate the two terms contributing to the first order corrections separately.

As a particular case, we consider the sequence $\rho_N = \rho^{\otimes N}$ of homogeneous product states. Then the sequence of expectations on the left site of equation (5.46) is just a constant, such that the $1/N$ -term on the right hand side vanish and the bound is useless. In order to improve this bound, we have to construct sequences which lead to a better

vector $|\Omega\rangle$. This is the only part which depends on the actual choice of the sequence. Still, we can give an estimate to the expectation value $\langle\Omega|\widehat{H}|\Omega\rangle$ using the ground state expectation value of \widehat{H} , which obviously yields a lower bound. Since the ground state energy of \widehat{H} only depends on its expression in terms of canonical operators \widehat{a}_α and on their commutation relations, we have found a bound which is again independent of the sequence ρ_N . Moreover, we claim that this bound is actually attained by suitable perturbations of any sequence ρ_N , including the sequence of product states. This fact is in particular important if the true ground state has root N fluctuations.

In order to prove this claim, respectively to replace (5.46) by

$$\liminf_N \rho_N(\text{sym}_N H_k) \geq H_\infty(\rho) - \frac{1}{N} \left(\gamma_c(H_k) - \inf \widehat{H} \right) + \mathcal{O}(N^{-3/2}), \quad (5.47)$$

we consider an arbitrary sequence ρ_N of states with root N fluctuations, and define

$$\widetilde{F} = \sum_{\alpha_1, \dots, \alpha_m} c(\alpha_1, \dots, \alpha_m) \widetilde{a_{\alpha_1}} \cdots \widetilde{a_{\alpha_m}} \quad (5.48)$$

to be a polynomial in fluctuation operators. Then

$$\rho_N^F(X) = \frac{\rho^{\otimes N}(\widetilde{F}^* X \widetilde{F})}{\rho^{\otimes N}(\widetilde{F}^* \widetilde{F})} \quad (5.49)$$

again defines a state with root N fluctuations. Moreover, the vector Ω^F for the modified GNS state can be realized in the same Hilbert space namely as

$$\Omega^F = \frac{1}{\|\widehat{F}\Omega\|} \widehat{F}\Omega, \quad (5.50)$$

where \widehat{F} is the same polynomial with the same coefficients as \widetilde{F} in the variables $\widehat{a_{\alpha_1}} \cdots \widehat{a_{\alpha_m}}$. By construction of the Hilbert space \mathcal{H}_Ω (cf. definition 17) the vectors of this form are dense in the unit vectors on \mathcal{H} . Hence, we conclude that we can always find a root N fluctuating sequence for which $\langle\Omega|\widehat{H}\Omega\rangle$ comes arbitrarily close to $\inf \widehat{H}$. This proves the claim.

The major reason why we only obtain an upper bound for the ground state energy, is the restriction to states with root N fluctuations (5.40). Hence, if we could prove that the true ground state of the system has root N fluctuations and the mean-field extremum is not on the boundary of the state space, we could conclude that

$$\gamma(H_k) = \gamma_c(H_k) - \inf \widehat{H}, \quad (5.51)$$

since we have argued that the infimum is actually attained. Therefore this condition allows for an replacement of the above inequality for the ground state energy (5.40) by an equality.

5.4.1 Minimization of the fluctuation Hamiltonian

In this section we have a closer look at the fluctuation Hamiltonian (5.44). In particular, want to establish a lower bound for the expectation value. This can be understood as a generalized Bogoliubov approach (cf. section 8.4).

In detail, we analyse the following problem: Suppose that \widehat{H} is an operator on a Hilbert space written in terms of other operators \widehat{a}_α on a common dense domain \mathcal{D} such that

$$\widehat{H} = \frac{1}{2} \sum_{\alpha, \beta=1}^r h^{\alpha\beta} \widehat{a}_\alpha \widehat{a}_\beta, \quad (5.52)$$

$$[\widehat{a}_\alpha, \widehat{a}_\beta] = i s_{\alpha\beta} = \rho([a_\alpha, a_\beta]), \quad (5.53)$$

where h and s are given real valued matrices, with h symmetric positive semidefinite and s antisymmetric. The problem is to establish a lower bound on $\langle \psi | \widehat{H} \psi \rangle$ for $\psi \in \mathcal{D}$ in terms of the matrices h and s .

As we will show below, one can construct a suitable basis of \mathbb{R}^r with respect to which both matrices h and s have only diagonal blocks of dimension 1 or 2. On all blocks of dimension 1, the antisymmetric matrix s vanishes, and h may be zero or non-zero. On all blocks of dimension 2 we can take

$$s = \begin{pmatrix} 0 & 1 \\ -1 & 0 \end{pmatrix} \quad \text{and} \quad h = \begin{pmatrix} 0 & \omega_\alpha \\ \omega_\alpha & 0 \end{pmatrix} \quad \text{or} \quad h = \begin{pmatrix} 1 & 0 \\ 0 & 0 \end{pmatrix} \quad \text{or} \quad h = \begin{pmatrix} 0 & 0 \\ 0 & 0 \end{pmatrix}. \quad (5.54)$$

Clearly, for the minimization problem all the blocks with $h = 0$ can be ignored and effectively just reduce the rank r . Blocks with h of the second type occur e.g., for a free particle on the line with $H = P^2$, and have also ground state energy zero. Equivalently, we can reduce r , so that the conjugate Q -variable is not considered at all and we have a diagonal block with $s = 0$. To summarize: the only relevant blocks have harmonic oscillator form and for each one we get a contribution $\omega_\alpha/2$.

Lemma 21. *Let \widehat{H} be the quadratic Hamiltonian in macroscopic fluctuations (5.52). The matrix sh is defined as*

$$(sh)_\gamma^\beta = \sum_\alpha s_{\gamma\alpha} h^{\alpha\beta}. \quad (5.55)$$

Now, sh is a skew symmetric matrix and we denote its non-zero eigenvalue pairs by $\pm i\omega_1, \dots, \pm i\omega_{r_2}$. Then, for every unit vector ψ in the domain \mathcal{D} the expectation value of the Hamiltonian \widehat{H} is bounded from below by

$$\langle \psi | \widehat{H} | \psi \rangle \geq \frac{1}{2} \sum_\alpha \omega_\alpha. \quad (5.56)$$

Proof. The idea is to consider \mathbb{R}^r as a phase space, with the symplectic matrix s , and to find a symplectic normal form of h first. Of course, s may be degenerate, e.g. there may be an index α with $s_{\alpha,\beta} = \rho([a_\alpha, a_\beta]) = 0$ for all $a_\beta \in \mathcal{A}$, even if $a_\alpha \neq 0$. Hence,

\mathbb{R}^r is not a phase space in the strict sense, but we can still use h and s to generate a linear “time evolution” in analogy to

$$\frac{d}{dt}\widehat{a}_\gamma = i[\widehat{H}, \widehat{a}_\gamma] = \sum_{\alpha,\beta=1}^r s_{\gamma\alpha} h^{\alpha\beta} \widehat{a}_\beta, \quad (5.57)$$

where we have joined two terms using that h is symmetric and s is antisymmetric. Therefore the crucial object for the dynamics is the matrix sh defined in equation (5.55), which formally generates the above “quantum” evolution, and an analogous “classical” phase space evolution $\dot{\xi} = sh\xi$ on \mathbb{R}^r , respectively on \mathbb{C}^r .

On \mathbb{C}^r , we introduce the scalar product

$$\Psi \cdot \Phi = \sum_{\alpha\beta} h^{\alpha\beta} \overline{\Psi}_\alpha \Phi_\beta, \quad (5.58)$$

which has a null space $\mathcal{N} = \{\Psi | \Psi \cdot \Phi = 0, \forall \Phi\}$ of dimension $r_0 \geq 0$. It is easily checked that the scalar product is invariant under the evolution $\exp(sh t)$ generated by sh , so we obtain a unitary operator on the $(r - r_0)$ -dimensional quotient $\mathbb{C}^r / \mathcal{N}$. Hence on the quotient space sh is a skew symmetric operator, which is hence diagonalizable. First consider a non-zero eigenvalue $i\omega$, for which there must be vectors $\Psi \in \mathbb{C}^r$, and $\chi \in \mathcal{N}$ such that $(sh - i\omega \mathbb{1})\Psi = \chi$. Since $\omega \neq 0$, we replace Ψ by $\Psi - (i/\omega)\chi$, which then is a genuine eigenvector of sh . Note that $\overline{\Psi}$ is then an eigenvector for $-i\omega$, or equivalently, we can split $\Psi = \xi + i\eta$ into real and imaginary part so that $sh\xi = -\omega\eta$ and $sh\eta = \omega\xi$. Thus, if there are r_2 pairs of eigenvalue $\pm i\omega_\alpha$ and we will choose the corresponding ξ_α, η_α as our basis vectors, conveniently normalized so that $\xi \cdot \xi = \eta \cdot \eta = 1/\omega_\alpha$.

For eigenvectors $\omega = 0$ this correction is not possible in general, and we may either have $sh\psi = 0$ or $sh\psi = \chi$ for some non-zero χ . We will take the vectors χ arising in this way as part of our basis. Finally, we can choose a basis on \mathcal{N} , consisting of “canonical pairs” of vectors connected by the symplectic matrix s , and further vectors, on which s vanishes as well.

To summarize, we have constructed a basis of \mathbb{R}^r with respect to which both matrices are block diagonal and the blocks are exactly given by the description given in equation (5.54). This proves the lemma. \square

Note that if we start from an abelian algebra, the anti-symmetric matrix s vanishes (cf. the definition in equation (5.53)). Hence, we can estimate the expectation value to be bounded from below by 0. This explains why we do not have to take into account the fluctuation Hamiltonian in the classical case treated in section 5.5.

5.4.2 Determination of the mean-field limit of the corrections

In this paragraph, we will give a more compact expression for the mean field limit of the second term (5.45). This allows to determine the functional $\gamma_c(H_k)$ starting directly from the symmetric operator H_k without making the detour of the expansion

(4.31) in the basis $\{e_\alpha\}$ with vanishing expectation values $\rho(e_\alpha) = 0$. Additionally, to simplify explicit calculations, the following considerations will reveal some fundamental differences between the ground state problem in the classical case and the quantum case, i.e. between the case where \mathcal{A} is chosen to be the commutative algebra of continuous functions on some compact space X and the general case with \mathcal{A} non-commutative.

In contrast to the representation in fluctuation operators which requires the treatment of the full N -particle system, the Taylor expansion

$$\text{sym}_N(H_k) = \sum_{\ell=0}^k \frac{1}{\ell!} \text{sym}_N(\nabla_\rho^\ell H_\infty) \quad (5.59)$$

can be determined with the knowledge of the mean-field limit alone. Thus, it would be particularly desirable to link the functional $\gamma_c(H_k)$ to the terms in the Taylor expansion and we are again faced with the problem of collision terms.

In the basis $\{e_\alpha\}$ the second order derivative is given by

$$\nabla_\rho^2 H_\infty = \sum_{\alpha, \beta}^{\dim \mathcal{A} - 1} h(\alpha, \beta) e_\alpha \otimes e_\beta. \quad (5.60)$$

By definition this does not contain any collision terms in contrast to $\gamma_c(H_k)$. This can be verified by a comparison to equation (5.45). Hence, $\gamma_c(H_k)$ does account for the error which we made by introducing the collision terms needed for the expansion in fluctuation operators.

A comparison of equation (5.45) and equation (5.60) shows that the derivative $\nabla_\rho^2 H_\infty$ is related to γ_c by

$$\gamma_c(H_k) = \frac{1}{2} \rho \left(M(\nabla_\rho^2 H_\infty) \right), \quad (5.61)$$

where M is the multiplication map, which is defined as $M : \mathcal{A} \otimes \mathcal{A} \rightarrow \mathcal{A}$ is the multiplication map $M(a \otimes b) = ab$. In the following we will present an explicit construction for the desired functional.

In section 3.2 we have derived an explicit formula for the k -th order derivatives:

$$\begin{aligned} \sigma_1 \otimes \sigma_2 \left(\nabla_\rho^2 H_\infty \right) &= \frac{\partial^2}{\partial t_1 \partial t_2} (\rho - t_1(\sigma_1 - \rho) - t_2(\sigma_2 - \rho))^{\otimes k} (H_k) \\ &= k(k-1) ((\sigma_1 - \rho) \otimes (\sigma_2 - \rho)) \otimes \rho^{\otimes(k-2)} (H_k), \\ &= k(k-1) \left((\sigma_1 \otimes \sigma_2) \otimes \rho^{\otimes(k-2)} (H_k) \right. \\ &\quad \left. - (\sigma_1 \otimes \sigma_2 + \sigma_2 \otimes \sigma_1) \otimes \rho^{\otimes(k-1)} (\mathbb{1} \otimes H_k) \right. \\ &\quad \left. + (\sigma_1 \otimes \sigma_2) \rho^{\otimes(k)} (\mathbb{1} \otimes \mathbb{1} \otimes H_k) \right), \end{aligned} \quad (5.62)$$

for arbitrary states $\sigma_1, \sigma_2 \in \mathcal{S}(\mathcal{A})$ (cf. equation (3.18)). In the last line, we have inserted the normalization of σ_i such that the entire expression becomes linear in each σ_i .

So what we are looking for is a substitution of the product state $\sigma_1 \otimes \sigma_2$ by a suitable linear combination of tensor products, which transforms the elements of the form $(e_\alpha \otimes e_\beta)$ into the expectation value of the product $\rho(e_\alpha e_\beta)$, as needed in expression (5.45), respectively in expression (5.61). Hence, the desired functional has to be a concatenation $\rho \circ M$, where the multiplication map $M : \mathcal{A} \otimes \mathcal{A} \rightarrow \mathcal{A}$ is defined as discussed above.

From the theory of matrices it is well-known that in general the product of two positive-definite matrices $A, B > 0$ is not positive-definite. Thus, in the quantum case the multiplication map is in general not positive. Still, if A and B commute, they can be jointly diagonalized and the product is again a positive definite matrix. This explains why this map is positive in the classical case. Therefore, the computation branches here.

In a first step we consider the quantum case, since we can then treat the special case of a commuting algebra in a second step. In the context of the theory of quantum information the flip operator or swap operator \mathbb{F} has to be proven quite useful in distinguishing between classical and quantum correlations [45]. The flip operator is defined as $\mathbb{F} |ij\rangle = |ji\rangle$ and can thus be written as

$$\mathbb{F} = \sum_{ij} |i\rangle\langle j| \otimes |j\rangle\langle i| \quad (5.63)$$

in suitable basis states $|ij\rangle \in \mathcal{H}^{\otimes 2}$. A short calculation shows that the flip operator satisfies the relation $\mathbb{F}(A \otimes \mathbb{1}) = (\mathbb{1} \otimes A)\mathbb{F}$. In particular, the trace of the flip operator acting on a tensor product exactly fulfills the desired property:

$$\text{tr } \mathbb{F}(A \otimes B) = \text{tr}(AB). \quad (5.64)$$

Hence, we can write the concatenation $\rho \circ M$ as

$$\begin{aligned} \rho(M(a \otimes b)) &= \text{tr}(\mathbb{F}(\rho \otimes \mathbb{1})(a \otimes b)) \\ &= \text{tr}(\mathbb{F}(\rho a \otimes b)) = \text{tr}(\rho ab) = \rho(ab), \end{aligned} \quad (5.65)$$

where by abuse of notation ρ denotes both, the state as well as the corresponding density operator $\rho(A) = \text{tr}(\rho A)$. In summary, this allows to identify the operator inducing the linear functional $\rho \circ M$ with

$$X \mapsto \rho(M(X)) = \text{tr}(\mathbb{F}(\mathbb{1} \otimes \rho)X). \quad (5.66)$$

Based on these result we can make the following substitution in (5.62) in order to introduce collision terms:

$$\begin{aligned} \sigma_1 \otimes \sigma_2 &\mapsto \mathbb{F}(\mathbb{1} \otimes \rho) = \sum_{i,j,k} \rho_{kl} |i\rangle\langle \ell| \otimes |k\rangle\langle i| \\ \sigma_1(\mathbb{1})\sigma_2 + \sigma_2(\mathbb{1})\sigma_1 &\mapsto \sum_{k,i} \rho_{ki} |k\rangle\langle i| + \sum_{i,\ell} \rho_{i\ell} |i\rangle\langle \ell| = 2\rho \\ \sigma_1(\mathbb{1})\sigma_2(\mathbb{1}) &\mapsto \sum_{ij} \delta_{ij} \langle i|\rho|j\rangle = \sum_i \rho_{ii} = 1, \end{aligned} \quad (5.67)$$

where in the second line we have taken the partial trace over the first or second tensor factor, respectively. Hence, including the factor $1/2$ introduced in the definition of γ_c , we finally get

$$\gamma_c(H_k) = \frac{k(k-1)}{2} \text{tr} \left((\mathbb{F}(\rho \otimes \mathbb{1}) \otimes \rho^{\otimes(k-2)} - \rho^{\otimes k}) H_k \right). \quad (5.68)$$

As \mathbb{F} has eigenvalues ± 1 , this functional is indeed not positive.

In the classical case H_k is a symmetric function of k variables $x_1, \dots, x_k \in X$. When X is finite we can assume that these variables are the diagonal entries in some distinguished product basis. Moreover, in the language of states, the classical ones are those which are diagonal. Thus, in the general expression (5.68), the off-diagonal terms of the flip operator do not contribute. Hence we get

$$\gamma_c(H_k) = \binom{k}{2} \left(\int_{X^{k-1}} \rho(dx_1) \cdots \rho(dx_{k-1}) H_k(x_1, x_1, x_2, \dots, x_{k-1}) - H_\infty(\rho) \right). \quad (5.69)$$

Of course, the appearance of the two equal arguments x_1, x_1 is again the direct expression of the multiplication map. The case of infinite X will be discussed below in the context of the lower bound in section 5.5.

5.4.3 Illustrative example

As an example to illustrate the quantum case, we once again consider the anti-ferromagnetic Heisenberg model (5.9) without a transversal field as discussed in section 5.3.2. We do not have to discuss the ferromagnetic case $J < 0$ in detail as its ground state is a product state such that the ground state energy is exactly given by $\min_\rho H_\infty(\rho)$ as shown earlier.

In the anti-ferromagnetic case $J > 0$, the mean-field energy assumes its minimum for

$$\rho = \frac{1}{2} \mathbb{1}_2 \quad \Rightarrow \quad H_\infty(\rho) = 0. \quad (5.70)$$

The expectation value of the Pauli matrices in this state vanishes, $\rho(S_\alpha) = 0$, $\alpha = 1, 2, 3$ such that the fluctuation operators are given by

$$\tilde{S}_\alpha = \sqrt{N} \text{sym}_N(S_\alpha). \quad (5.71)$$

The expansion into fluctuation operators around ρ (cf. equation (4.22)) thus yields

$$\begin{aligned} \text{sym}_N(H_2) &= J \sum_{\alpha=1}^3 \underbrace{\rho(S_\alpha)^2}_{=0} \mathbb{1}_N \\ &\quad + \frac{2J}{\sqrt{N}} \sum_{\alpha} \tilde{S}_\alpha \underbrace{\rho(S_\alpha)}_{=0} \\ &\quad + \frac{J}{N} \sum_{\alpha} \tilde{S}_\alpha^2 - \rho(S_\alpha^2) + \underbrace{\rho(S_\alpha)^2}_{=0} + \mathcal{O}(N^{-3/2}) \\ &= + \frac{J}{N} \sum_{\alpha} \tilde{S}_\alpha^2 - \rho(S_\alpha^2) + \mathcal{O}(N^{-3/2}). \end{aligned} \quad (5.72)$$

To obtain the $1/N$ corrections to the ground state energy we first note that $S_\alpha^2 = \mathbb{1}_2$ for $\alpha = 1, 2, 3$ such that the mean-field limit of the corrections is given by

$$\begin{aligned}\gamma_c(H_2) &= J \sum_{\alpha=1}^3 \rho(S_\alpha^2) \\ &= 3J.\end{aligned}\tag{5.73}$$

Furthermore, we have to minimize the fluctuation Hamiltonian

$$\widehat{H} = J \sum_{\alpha} \widehat{S}_\alpha^2.\tag{5.74}$$

Since the expectation values of all Pauli matrices vanishes for the mean-field minimizer $\rho = 1/2\mathbb{1}_2$, all fluctuation operators commute:

$$[\widehat{S}_\alpha, \widehat{S}_\beta] = 0 \quad \forall \alpha, \beta = 1, 2, 3.\tag{5.75}$$

Hence, the matrix s defined in equation (5.53) vanishes exactly and the ground state energy of \widehat{H} is zero.

In conclusion we find that the ground state energy of the anti-ferromagnetic Heisenberg model up to order $1/N$ is given by

$$\sigma_N(H_N) = -\frac{3J}{N} + \mathcal{O}(N^{-3/2}),\tag{5.76}$$

while the exact result is $-3J/(N-1)$. Hence, for the anti-ferromagnetic Heisenberg model the inner bound gives the correct prediction of the scaling behaviour for $1/N$.

5.5 Classical ground state problem

Now we address the classical problem, that is the case of an abelian single-particle algebra \mathcal{A} . By theorem 3 every such algebra is isomorphic to the algebra $\mathcal{C}(X)$ of continuous complex functions on a compact Hausdorff space X . In section 5.4.2 we have already briefly commented on the case of finite X . Here we will weaken this restriction and consider at least certain infinite dimensional cases, which in particular include the entanglement detection problem discussed in section 5.3.2.

Definition 22. *An element $H_k \in \mathcal{A}^{\otimes k}$ has **finite rank** or rank r if there are r elements $e_1, \dots, e_r \in \mathcal{A}$ such that*

$$H_k = \sum_{\alpha_1, \dots, \alpha_k=1}^r c(\alpha_1, \dots, \alpha_k) e_{\alpha_1} \otimes \dots \otimes e_{\alpha_k},\tag{5.77}$$

with suitable coefficients $c \in \mathbb{C}$.

If H_k has rank r , then so does $\text{sym}_N(H_k)$, provided the unity is one of the basis elements e_i , which we may assume. Moreover, if \mathcal{A} is r -dimensional, then $(jH)_k$ as defined in section 5.3.2 has rank r . Hence the case of entanglement detection for a finite dimensional single-particle algebra is covered as well.

In the classical case the pure states on $\mathcal{C}(X^N)$ are given by a tuple (x_1, \dots, x_N) represented by point measures δ_{x_i} . These form a set of extremal measures, since they cannot be written as a convex combination of probability measures. If we consider $H_k \in \mathcal{A}^{\otimes k}$ with $\mathcal{A} = \mathcal{C}(X)$ abelian, then H_N is taking its values on configurations in X^N . The expectation value of H_N in the state, respectively the probability measure μ can be simply evaluated as

$$\mu^{\otimes N}(H_N) = \int_X \mu(dx_1) \cdots \mu(dx_k) H_k(x_1, x_2, \dots, x_k). \quad (5.78)$$

A key step in the computation is to look at the particular function $H(x_1, \dots, x_N)$ with $(x_1, \dots, x_N) \in X^N$ in terms of the ‘‘empirical measure’’

$$\mu_N = \frac{1}{N} \sum_{i=1}^N \delta_{x_i} \quad (5.79)$$

associated with a tuple $(x_1, \dots, x_N) \in X^N$:

$$\mu_N^{\otimes N}(H_N) = \mu_N^{\otimes k}(H_k) = \frac{1}{N^k} \sum_{i_1, \dots, i_k} H_k(x_{i_1}, \dots, x_{i_k}). \quad (5.80)$$

In the following, we will see that the evaluation of H_N in empirical measures μ_N plays essentially the role of the expansion fluctuations in the quantum case.

The next lemma is closely related to the question of the difference between sampling with and without replacement. Therefore the proof has the flavour of the classic work of Diaconis and Freeman [28] on the subject.

Lemma 23. *Let $H_k \in \text{sym}_N(\mathcal{C}(X^k))$ be a real valued symmetric function. Then, for any tuple $(x_1, \dots, x_N) \in X^N$, and its associated empirical measure μ_N (5.79), we have*

$$\text{sym}_N(H_k)(x_1, \dots, x_N) = H_\infty(\mu_N) - \frac{1}{N} \Gamma(\mu_N) + \mathcal{O}(N^{-2}),$$

where the last term $\mathcal{O}(N^{-2})$ is bounded by $c(k)\|H_k\|/N^2$. Here $c(k)$ denotes a constant depending only on the degree k of the Hamiltonian and H_∞ and Γ are functionals defined for arbitrary (not just for empirical measures), namely

$$\begin{aligned} H_\infty(\mu) &= \mu^{\otimes k}(H_k) \\ &= \int_X \mu(dx_1) \cdots \mu(dx_k) H_k(x_1, x_2, \dots, x_k) \end{aligned} \quad (5.81)$$

and

$$\Gamma(\mu) = \binom{k}{2} \left(\int_{X^{k-1}} \mu(dx_1) \cdots \mu(dx_{k-1}) H_k(x_1, x_1, x_2, \dots, x_{k-1}) - H_\infty(\mu) \right). \quad (5.82)$$

We have introduced the special notation Γ in lemma 23 only to emphasize the dependence on μ . The comparison to the classical bound γ_c (5.69) shows that, in fact, Γ is exactly equal to the bound γ_c with the special choice $\rho = \mu$.

Proof. For the sake of simplicity, we introduce the notation

$$(\Delta H_k)(x_1, x_2, \dots, x_{k-1}) = H_k(x_1, x_1, x_2, \dots, x_{k-1}) \quad (5.83)$$

for the ‘‘diagonal embedding’’ applied to the first argument of H_k .

We begin by a rough sketch of the argument, which is enough to establish the first order correction to the mean-field limit. However, to determine the bound on the error, respectively $c(k)$ a more careful counting argument is needed. We will comment on this point after presenting the major argument.

The function $\text{sym}_N(H_k)$ evaluated at the point (x_1, \dots, x_N) is defined to be the symmetrization over all possible choices of the k arguments of H_k out of the N -tuple:

$$\text{sym}_N(H_k)(x_1, \dots, x_N) = \frac{(N-k)!}{N!} \sum_{\substack{i_1, \dots, i_k \\ \text{all different}}} H_k(x_{i_1}, \dots, x_{i_k}). \quad (5.84)$$

What we are aiming for is an expression of H_N in terms of the empirical measure (5.79). So if we drop the above restriction on the samples $(x_{i_1}, \dots, x_{i_k})$ we get:

$$\begin{aligned} \text{sym}_N(H_k)(x_1, \dots, x_N) &= \frac{(N-k)!}{N!} \sum_{\substack{i_1, \dots, i_k \\ \text{unconstrained}}} H_k(x_{i_1}, \dots, x_{i_k}) \\ &\quad - \frac{(N-k)!}{N!} \sum_{\substack{i_1, \dots, i_k \\ \text{two equal}}} H_k(x_{i_1}, \dots, x_{i_k}) - \dots \end{aligned} \quad (5.85)$$

To get the leading order corrections, we can restrict the analysis to the samples $(x_{i_1}, \dots, x_{i_k})$ which contain at most two identical arguments. Moreover, since the expression is symmetric, we can collectively express all these terms by the diagonal embedding (5.83):

$$\begin{aligned} \text{sym}_N(H_k)(x_1, \dots, x_N) &= \frac{(N-k)! N^k}{N!} \mu_N^{\otimes k}(H_k) \\ &\quad + \binom{k}{2} \frac{(N-k)! N^{k-1}}{N!} \mu_N^{\otimes(k-1)}(\Delta H_k) - \dots \end{aligned} \quad (5.86)$$

The expansion of the scaling factor up to the order $1/N^2$ finally yields:

$$\begin{aligned} \text{sym}_N(H_k)(x_1, \dots, x_N) &= \left(1 + \frac{1}{N} \binom{k}{2}\right) \mu_N^{\otimes k}(H_k) \\ &\quad - \frac{1}{N} \binom{k}{2} \mu_N^{\otimes(k-1)}(\Delta H_k) + \mathcal{O}(N^{-2}). \end{aligned} \quad (5.87)$$

This reasoning already reveals the general structure. In order to determine the constant $c(k)$ we have to do the combinatorics for the terms featuring more than one identical argument more carefully. Note that all these expressions are sums of evaluations of H_k at various arguments out of x_1, \dots, x_N , with some coefficients. Moreover, the expression is symmetric in all arguments, so that all terms with the same sizes of the clusters of equal arguments can be collected together.

The determination of $c(k)$ is closely related to the fundamental question of the total variation distance of the probability distributions of a sample with and without replacement. This is most clearly revealed in equation (5.85), where we express the average over all samples (x_1, \dots, x_k) without replacement by the average over all samples with replacement minus the cluster terms. The question of the quantification of the error for large sample sizes N was first addressed by Diaconis and Freedman [28, 46]. They proved that the error is to first order in $1/N$ given by $1/2(k(k-1))$, which is exactly the scaling with k which we obtain for the term proportional to $1/N$. However, we are now interested in the error to the next order N^{-2} . In [47] a family of explicit approximations P_r for the probability distribution for a sample without replacement has been constructed, which is given by a linear combination of uniform probability product-measures concentrated on certain submeasures. By a generalization of the argument of Freeman [46], the authors prove that the total variational distance between the exact distribution and the approximation scales as $(k^2/N)^{r+1}$ as $N \rightarrow \infty$. As the argument is quite technical we will not go into details here. Still note that the convergence of the total variational distance implies weak*-convergence of measures. For $r = 2$, their results cover exactly the case we are considering. Hence, we get

$$\begin{aligned} & \left\| \text{sym}_N(H_k)(x_1, \dots, x_N) - \left(1 + \frac{1}{N} \binom{k}{2}\right) \mu_N^{\otimes k}(H_k) - \frac{1}{N} \binom{k}{2} \mu_N^{\otimes(k-1)}(\Delta H_k) \right\| \\ & \leq \binom{k}{2}^2 \frac{N!}{(N-k+1)!} N^{-(k+1)} \|H_k\| \leq \frac{k^2}{4N^2} \|H_k\|, \end{aligned} \quad (5.88)$$

which finally proves the lemma. \square

Now we finally come to the main result of this section.

Theorem 24. *Let $H_k \in \mathcal{C}(X^k)$ be a symmetric, real valued function of finite rank. Then, the mean-field limit of the ground state of $H_N = \text{sym}_N(H_k) \in \mathcal{C}(X^N)$ is given by*

$$\lim_{N \rightarrow \infty} \inf_{(x_1, \dots, x_N) \in X^N} \text{sym}_N(H_k) = \inf_{\mu} H_{\infty}(\mu). \quad (5.89)$$

We denote by $\text{argmin } H_{\infty}$ the set of minimizers $\rho \in \mathcal{S}(\mathcal{A})$ of $H_{\infty}(\rho)$. Then the $\mathcal{O}(1/N)$ correction to the mean field ground state energy is given by

$$\begin{aligned} \gamma(H_k) &= \lim_{N \rightarrow \infty} N \left(\inf_{\mu} H_{\infty}(\mu) - \inf_{(x_1, \dots, x_N) \in X^N} \text{sym}_N(H_k) \right) \\ &= \sup \left\{ \Gamma(\mu) \mid \mu \in \text{argmin } H_{\infty} \right\}, \end{aligned} \quad (5.90)$$

where $\Gamma(\mu)$ is defined exactly as in lemma 23 (cf. equation (5.82)).

Proof. Note that, as \mathcal{A} is assumed to be abelian, it suffices to evaluate the minimum $\inf \text{sym}_N(H_k)$ on the set of pure state, respectively the tuples $(x_1, \dots, x_N) \in X^N$. The proof is divided into two major parts: The proof of the inner bound for $\gamma(H_k)$ and the proof of the outer bound based on lemma 23. Due to the finite rank condition, the result is similar to the result for the classical case (5.69) which we obtained above. Still, as this restriction is not quite satisfactory, we analyse this bound for the special case considered here and relate it to an approximation problem for empirical measures. This illustrates the reasons to introduce the finite rank condition most clearly.

Proof of the inner bound

Let μ be a probability measure which meets the description of the theorem, that is choose μ to be a minimizer of H_∞ . Our aim is to approximate it by a suitable empirical measure μ_N , for which we will provide an explicit construction in the following.

From the earlier reasoning it follows that

$$\int_X \mu(dx) A(x) - \frac{1}{N} \sum_{i=1}^N A(x_i) \rightarrow 0 \quad (5.91)$$

in the limit of infinite sample size $N \rightarrow \infty$. This is again the basic result by Freeman [46]. Thus, μ_N converges weakly towards μ , which directly implies that $\Gamma(\mu_N) \rightarrow \Gamma(\mu)$. The difficult part of the proof is to show that the approximation by the empirical measure is good enough to achieve $H_\infty(\mu_N) = H_\infty(\mu) + o(1/N)$ and hence does not disturb the convergence of $\Gamma(\mu_N) \rightarrow \Gamma(\mu)$.

This is exactly the point where we need the condition that H_k has finite rank r . Let $K \subset \mathbb{R}^r$ be the convex set spanned by the points with the coordinates $e_\alpha(x)$,

$$K = \text{span}\{e_\alpha(x) \mid x \in X\} \subset \mathbb{R}^r \quad (5.92)$$

with $\alpha = 1, \dots, r$. Then $m_\alpha = \mu(e_\alpha)$ defines a point m , which lies in the convex set K . By Carathodory's theorem [48] we can pick $r + 1$ points y_1, \dots, y_{r+1} in K such that the point $m \in K \subset \mathbb{R}^r$ lies in their convex hull. Thus, m can be expressed as a convex combination of these points, by the definition of K these points correspond to points in X , i.e.

$$m_\alpha = \mu(e_\alpha) = \sum_i^{r+1} \lambda_i y_i = \sum_i^{r+1} \lambda_i e_\alpha(x_i) \quad (5.93)$$

with convex weights $\lambda_i > 0$ and $\sum_i^{r+1} \lambda_i = 1$.

Note that due to the finite rank condition (5.77), $H_\infty(\mu)$ only depends on the expectations of the e_α :

$$\begin{aligned} H_\infty(\mu) &= \int_X \mu(dx_1) \dots \mu(dx_k) H(x_1, \dots, x_k) \\ &= \sum_{\alpha_1, \dots, \alpha_k=1}^r c(\alpha_1, \dots, \alpha_k) \prod_{i=1}^k \mu(e_{\alpha_i}). \end{aligned}$$

Thus, $H_\infty(\mu) = H_\infty(\sum_i \lambda_i \delta_{x_i})$.

Now we choose a rational approximation of the weights with denominator N , i.e., a collection of integers n_i such that

$$\left| \lambda_i - \frac{n_i}{N} \right| \leq \frac{1}{N}, \quad (5.94)$$

for all i . Indeed, we can first set $n_i = \lfloor N\lambda_i \rfloor$, and then choose a suitable subset of these numbers and add one to all elements, such that $\sum_i n_i/N = 1$. Since

$$\sum_i \lfloor N\lambda_i \rfloor \leq N \leq \sum_i \lceil N\lambda_i \rceil, \quad (5.95)$$

this strategy leads to a normalized set of weights satisfying the above inequality.

If we directly insert the estimate (5.94) into $H_\infty(\mu)$, we only get an approximation to order $1/N$, which would completely mess up the term we are interested in. In order to complete the argument, we must therefore use the property of μ , which we have chosen to be a minimizer of H_∞ . Therefore, we are again faced with an extremal problem for a state space function. As argued in section 3.3, for a minimizer the general conditions $\nabla_\mu H_\infty \geq 0$ and $\mu(\nabla_\mu H_\infty) = 0$ hold. Thus, the positive function $\nabla_\mu H_\infty$ vanishes on the support of μ . Moreover, if we take any measure μ' , whose support is contained in the support of μ , we will also get $\mu'(\nabla_\mu H_\infty) = 0$.

A closer inspection shows that this last condition is very much in line with our choice of the points y_1, \dots, y_{r+1} for the discretization of μ : In the decomposition of the point $m \in K$ (5.93), only those extremal points can have a positive weight, which lie in the same face as m . Hence the entire approximation will happen in the same face and we conclude that $\mu_N(\nabla_\mu H_\infty) = 0$. Since by definition (5.92) each point $y_i \in K$ corresponds to a certain element of $x_i \in X$, that is $y_i = e_\alpha(x_i)$, this treatment provides us with the empirical measure we were looking for.

Now the Taylor expansion (4.33) of H_∞ gives

$$H_\infty(\mu_N) - H_\infty(\mu) = (\mu_N - \mu)^{\otimes 2}(\nabla_\mu^2 H_\infty) + \mathcal{O}(N^{-3/2}).$$

This concludes the proof of the inner bound. It is to be noted that the constant of this term depends on the rank r , so it is not obvious how to generalize this result.

Proof of the outer bound

Let μ_N denote the empirical measure for every N , which corresponds to a minimizing pure state, respectively a tuple $(x_1, \dots, x_N) \in X$. Then, according to lemma 23, we have

$$\inf_{x_1, \dots, x_N} \text{sym}_N(H_k)(x_1, \dots, x_N) = H_\infty(\mu_N) - \frac{1}{N} \Gamma(\mu_N) + \mathcal{O}(N^{-2}). \quad (5.96)$$

By a simple inclusion of the domains over which the infimum is taken, we can conclude that the first term is bounded below,

$$H_\infty(\mu_N) \geq \inf_\mu H_\infty(\mu). \quad (5.97)$$

Furthermore, we have shown that there are measures attaining this value for $N \rightarrow \infty$ in the proof of the inner bound. Hence, $\lim_{N \rightarrow \infty} H_\infty(\mu_N) = \inf_\mu H_\infty(\mu)$ and any cluster point of a minimizing sequence μ_N must be a minimizer of H_∞ .

This allows to give a first estimate for the corrections γ_c ,

$$\begin{aligned} \gamma(H_k) &= \lim_{N \rightarrow \infty} N \left(\inf_\mu H_\infty(\mu) - \inf_{(x_1, \dots, x_N) \in X^N} \text{sym}_N(H_k) \right) \\ &\leq \lim_{N \rightarrow \infty} N \left(\inf_\mu H_\infty(\mu) - H_\infty(\mu_N) + \frac{1}{N} \Gamma(\mu_N) + \mathcal{O}(N^{-2}) \right) \\ &\leq \lim_{N \rightarrow \infty} \left(\Gamma(\mu_N) + \mathcal{O}(N^{-2}) \right), \end{aligned} \quad (5.98)$$

but we still need a estimate for the remaining term.

For this purpose we may pick a subsequence along which $\Gamma(\mu_N)$ converges and we will denote the limit by Γ_* . From this sequence we pick a convergent subsequence of measures μ_{N_k} which converges towards the limit μ . Since μ is a cluster point of μ_N , it minimizes H_∞ . By construction the limit along the convergent subsequence yields $\Gamma(\mu_{N_k}) \rightarrow \Gamma(\mu) = \Gamma_*$. Hence, all cluster points of $\Gamma(\mu_N)$ must be below $\{\sup \Gamma(\mu) | \mu \in \text{argmin } H_\infty\}$, as given in the theorem. □

5.6 Conclusion and outlook

In this chapter, we presented a detailed study of the finite size corrections for the ground state problem for quantum mean-field systems. The determination of the deviations from the mean-field expectation value for large, but finite systems size is a fundamental question, which is closely related to other problems. In section 5.3, we commented on two major problems in this context, namely the relation to spin squeezing inequalities and Finite de Finetti theorems. In particular, we have seen that the finite size corrections can be interpreted as an entanglement witnesses.

In section 5.4 we established an inner bound for the quantum case, where the finite corrections can be split in a mean-field part and a variational problem over a quadratic Hamiltonian in macroscopic fluctuations. In the general case, a proof for an outer bound, respectively a lower bound for the ground state energy is still missing. Thought, if the exact ground state has root N fluctuations around the mean-field minimizer we can upgrade the inner bound from an inequality to an equality.

In the last section we consider an abelian algebra and hence, the classical case. However, we have seen in section 5.3.2 that in certain quantum cases it is possible to find a suitable map from the quantum algebra to an abelian algebra, such that e.g. the quantum spin squeezing problem is covered by the classical case as well. Under the restriction that the Hamiltonian has finite rank, we can give a full characterization of the finite size corrections, which results in a variational problem over all mean-field minimizers. Up to now, it is an open question if the finite rank condition can be released.

Chapter 6

Quantum phase space

The phase space formulation of quantum mechanics is nearly as old as the theory itself and has a wide range of applications, especially in quantum optics. The formulation provides an illustrative insight into the dynamics and many techniques and methods were developed in this context. However, only a small fraction of the literature is dedicated to systems with intrinsic symmetries like the Bose-Hubbard Hamiltonian

$$\hat{H} = \sum_{i=1}^M \epsilon_i \hat{n}_i - J \sum_{i=1}^{M-1} \left(\hat{a}_i^\dagger \hat{a}_{i+1} + \hat{a}_{i+1}^\dagger \hat{a}_i \right) + \frac{U}{2} \sum_{i=1}^M (\hat{n}_i (\hat{n}_i - 1)). \quad (6.1)$$

for M sites, which plays a central role in the second part of this thesis.

In this case the dynamical group is spanned by the normally ordered operators $\hat{a}_j^\dagger \hat{a}_k$ with $j, k \in \{1, 2, \dots, M\}$ and is hence equivalent to the special unitary group $SU(M)$. This is underlined by the fact that every group element as well as the Hamiltonian itself commutes with the particle number operator $\hat{N} = \sum_{j=1}^M \hat{a}_j^\dagger \hat{a}_j$. Consequently, an analysis in terms of the flat phase space and the use of related methods, like Glauber coherent states, is not adequate because these states ignore the conservation of the total particle number. For instance, the annihilation and creation operators $\hat{a}_j, \hat{a}_j^\dagger$ lead to Hilbert spaces with different particle numbers and the order parameter $\langle \hat{a}_j \rangle$ obviously vanishes (cf. also the discussion in section 8.4.1 for more details). Since the dynamical group is no longer a direct sum of the Heisenberg-Weyl group one has to apply an extended concept of coherent states [49]. These states obey a generalized minimum uncertainty relation and stay coherent under an evolution which is linear in the generators of the dynamical group.

A general algorithm to construct phase space distribution functions for systems whose dynamical group has the structure of an arbitrary Lie group such as $SU(M)$ has been developed only about ten years ago [50]. It is based on the concept of generalized coherent states introduced by Gilmore [51] and Perelomov [49]. Starting from these states one can define a number conserving phase space description and derive exact evolution equations for the Husimi Q -function and the Glauber-Sudarshan P -function of the M -site Bose-Hubbard model. One important consequence of the use of $SU(M)$ coherent states is the different topology of the phase space, which is now isomorphic to

the $2M-2$ dimensional Bloch sphere and therefore compact. Moreover, the phase space description based on $SU(M)$ coherent states allows for a deeper analysis of the many-particle-mean-field correspondence as these states are of high physical significance. As this class of states is equivalent to the product states describing a fully condensed state, they provide an excellent tool to describe, characterize, and study deviations from the macroscopic state which determine the regional validity of the mean-field approximation.

In this chapter, we will give a short overview of phase space distributions based on generalized $SU(M)$ coherent states and introduce the definitions required for the following discussion. More details can be found in [52, 53].

6.1 Generalized coherent states

The basic ingredient which we will need in the following is the concept of generalized coherent states for systems with an arbitrary dynamical Lie group [49]. The parameter space of the generalized coherent states determines the corresponding phase space and reflects the physical properties of the system by its geometric structure. Moreover it has been shown that one can construct explicitly a family of phase-space distributions for a system with an arbitrary Lie group symmetry based on this concept [50]. In this section we will provide the basics and introduce the notations used in the following.

So, let G be the dynamical Lie group of the relevant quantum system. For reasons of simplicity we assume that G is connected, simply connected and has a finite dimension, which is the case for the group $SU(M)$. It is important to note that the general approach does not rely on these assumptions. The unitary irreducible representation of the dynamical group G acting on the Hilbert space will be denoted by T . With these preliminaries, we can define the generalized coherent states by the action of an element of the unitary irreducible representation T on a fixed normalized reference state $|\psi_0\rangle$:

$$|\psi_g\rangle = T(g) |\psi_0\rangle, \quad g \in G. \quad (6.2)$$

Even though the choice of the reference state is in principle arbitrary, it strongly influences the shape of the coherent states and the structure of the corresponding phase space. A physically motivated choice would be an extremal state of the Hilbert space like the vacuum ground state for the Heisenberg-Weyl group or the lowest/highest spin state for the case of $SU(M)$. Mathematically these states correspond to the highest/lowest weight states of the unitary irreducible representation [51].

The isotropy subgroup or maximum stability group $H \subset G$ consists of every element which leaves the reference state invariant up to a phase factor. Formally one can write

$$T(h) |\psi_0\rangle = e^{i\phi(h)} |\psi_0\rangle \quad \text{with } \phi(h) \in \mathbb{R} \quad \forall h \in H. \quad (6.3)$$

With respect to the coherent states, there is a unique decomposition for every element $g \in G$ into a product of two elements, one of the isotropy subgroup H and one of the

coset space G/H :

$$g = \Omega h, \quad g \in G, \quad h \in H \text{ and } \Omega \in G/H. \quad (6.4)$$

Hence, there is a one-to-one correspondence between the elements $\Omega(g)$ of the coset space H/G and the coherent states $|\Omega\rangle \equiv |\psi_\Omega\rangle$ which preserves the algebraic and topological properties. This construction guarantees the characteristic property of the coherent states: a coherent state stays coherent under a time evolution linear in the generators of the dynamical group.

Another important property we will need in the following is the (over)completeness of the coherent states, which leads to the resolution of the identity operator of the Hilbert space,

$$\int_{G/H} |\Omega\rangle \langle \Omega| d\mu(\Omega) = I, \quad (6.5)$$

where $d\mu(\Omega)$ denotes the invariant measure on the coset space.

6.1.1 Glauber states

The coherent states were first discussed in the context of the Heisenberg-Weyl algebra $h_4 = \{\hat{a}, \hat{a}^\dagger, \hat{a}^\dagger \hat{a} \equiv \hat{n}, I\}$, with \hat{a} and \hat{a}^\dagger being the bosonic annihilation and creation operators. One of the first applications was the description of a mode of the quantized radiation field modeled by harmonic oscillators [54]. In this case the unitary irreducible representation of an arbitrary group element $g \in H_4$ can be decomposed as

$$T(g) = e^{\alpha \hat{a}^\dagger - \alpha^* \hat{a}} e^{i(\delta \hat{n} + \phi I)} \quad \alpha \in \mathbb{C}, \quad \delta, \phi \in \mathbb{R}, \quad (6.6)$$

with the stability subgroup $U(1) \times U(1)$ being generated by $\{\hat{n}, I\}$. Therefore the phase space is isomorphic to the complex plane $H_4/U(1) \times U(1) \cong \mathbb{C}$, parametrized by the complex parameter α and the typical representative of the coset space

$$\hat{D}(\alpha) \equiv e^{\alpha \hat{a}^\dagger - \alpha^* \hat{a}} \quad (6.7)$$

is just the well-known displacement operator. With the physically motivated choice of the vacuum ground state $|0\rangle$ as the reference state one obtains the famous Glauber states

$$|\alpha\rangle \equiv \hat{D}(\alpha) |0\rangle. \quad (6.8)$$

The generalization to more than one mode is straightforward, since the multimode group $\bigoplus_{i \in \mathbb{N}} \{\hat{a}_i, \hat{a}_i^\dagger, \hat{a}_i^\dagger \hat{a}_i \equiv \hat{n}_i, I\}$ is just a direct sum of the single-mode group. Thus the multimode Glauber states can be obtained as a direct product of the single-mode Glauber states,

$$|\boldsymbol{\alpha}\rangle = \prod_{i=1}^M |\alpha_i\rangle = \prod_{i=1}^M e^{\alpha_i \hat{a}_i^\dagger - \alpha_i^* \hat{a}_i} |\mathbf{0}\rangle, \quad (6.9)$$

with $|\mathbf{0}\rangle$ being the multimode vacuum ground state. Due to this factorization the well-known properties of the single-mode Glauber states can be transferred easily to the multimode case.

6.1.2 $SU(M)$ -coherent states

In the case of the Bose-Hubbard model (6.1) with M sites, the dynamical group is equivalent to the special unitary group $SU(M)$, spanned by the generalized angular momentum operators $\hat{E}_{jk} = \hat{a}_j^\dagger \hat{a}_k$ with $j, k \in \{1, 2, \dots, M\}$. These fulfill the algebraic commutation relations

$$\left[\hat{E}_{jk}, \hat{E}_{mn} \right] = \hat{E}_{jn} \delta_{km} - \hat{E}_{mk} \delta_{nj} \quad (6.10)$$

and conserve the particle number $\hat{N} = \sum_{j=1}^M \hat{E}_{jj}$, since

$$\left[\hat{E}_{jk}, \hat{N} \right] = 0. \quad (6.11)$$

As already argued earlier in this chapter, a suitable choice of the reference state is the maximum spin state, corresponding to the state with the entire population in the first well $|N, 0, \dots, 0\rangle$. With respect to this state, an arbitrary element of the unitary irreducible representation can always be decomposed as

$$\begin{aligned} T(g) |N, 0, \dots, 0\rangle &= \exp \left(\sum_{k=2}^M (y_{k1} \hat{E}_{k1} + y_{1k} \hat{E}_{1k}) \right) \\ &\times \exp \left(\sum_{k,l=2}^M y_{kl} \hat{E}_{kl} + y_{11} \hat{E}_{11} \right) |N, 0, \dots, 0\rangle \end{aligned} \quad (6.12)$$

into an element of the coset space and an element of the stability group $U(M-1) \times U(1)$ [55]. Given that $\hat{E}_{jk} = \hat{E}_{kj}^\dagger$, we have to assume that $y_{jk}^* = y_{kj}$ in order for the argument of the exponentials to be anti-hermitian. Therefore we get the $SU(M)$ coherent states by the action of the representative of the coset space onto the reference state

$$\begin{aligned} \hat{\mathcal{R}}(\mathbf{y}) |N, 0, \dots, 0\rangle &= \exp \left(\sum_{k=2}^M (y_{k1} \hat{E}_{k1} - y_{k1}^* \hat{E}_{k1}^\dagger) \right) |N, 0, \dots, 0\rangle \\ &=: |\mathbf{y}\rangle. \end{aligned} \quad (6.13)$$

The parameter space of the coherent states is spanned by the $M-1$ complex parameters $y_k \equiv y_{k1}$ with $k \in \{2, \dots, M\}$ of the coset space and can thus be identified with the $2(M-1)$ sphere which is topologically equivalent to

$$U(M)/U(M-1) \times U(1) \cong SU(M)/U(M-1). \quad (6.14)$$

Due to this analogy one can interpret the coset representative $\hat{\mathcal{R}}(\mathbf{y})$ as a rotation of the reference state on the multidimensional sphere. To assure that the parametrization is unique one has to demand that the parameters are bounded as $\sum_{k=2}^M y_k^* y_k \leq (\pi/2)^2$. In the case of two sites the definition of the coherent states reduces to the spin coherent states or Bloch states [56, 57], which are discussed in section 9.1.

Anyhow, a parametrization by the $(M-1)$ independent complex parameters (x_2, \dots, x_M) of the site together with the real dependent parameter of the first site $x_1^* = x_1$ is physically more reasonable. These parameters represent the probability amplitudes at the respective sites, directly reflecting the particle conservation

$$x_1^2 + \sum_{k \geq 2}^M x_2^* x_2 = 1, \quad (6.15)$$

and the irrelevance of the global phase. By means of the generalized Baker-Campbell-Hausdorff formula one can show the relation

$$\hat{\mathcal{R}} \hat{a}_1^\dagger \hat{\mathcal{R}}^{-1} = \cos(\|\mathbf{y}\|) \hat{a}_1^\dagger + \frac{\sin(\|\mathbf{y}\|)}{\|\mathbf{y}\|} \sum_{k=2}^M y_k \hat{a}_k^\dagger \quad (6.16)$$

with the abbreviation $\|\mathbf{y}\|^2 \equiv \sum_{k=2}^M |y_k|^2$. This leads directly to the parameter transformation

$$x_1 = \cos(\|\mathbf{y}\|), \quad x_k = \frac{\sin(\|\mathbf{y}\|)}{\|\mathbf{y}\|} y_k, \quad k \geq 2 \quad (6.17)$$

and the representation of the $SU(M)$ coherent states in terms of the complex amplitudes (x_1, x_2, \dots, x_M) :

$$\begin{aligned} |\mathbf{y}\rangle &= \hat{\mathcal{R}} |N, 0, \dots, 0\rangle \\ &= \frac{1}{\sqrt{N!}} \hat{\mathcal{R}} \hat{a}_1^{\dagger N} |0, 0, \dots, 0\rangle \\ &= \frac{1}{\sqrt{N!}} \left(\sum_{k=1}^M x_k \hat{a}_k^\dagger \right)^N \hat{\mathcal{R}} |0, 0, \dots, 0\rangle \\ &= \frac{1}{\sqrt{N!}} \left(\sum_{k=1}^M x_k \hat{a}_k^\dagger \right)^N |0, 0, \dots, 0\rangle \\ &=: |\mathbf{x}\rangle_N, \end{aligned} \quad (6.18)$$

where we have used the commutation relation (6.16). The last relation reveals another interesting property of the $SU(M)$ coherent states. In the case of the Bose-Hubbard model these states are equivalent to the fully condensed states, since they can always be written as a product state. This characteristic trait is certainly not trivial and it cannot be generalized to other dynamical groups since it is an intrinsic property of the $su(M)$ algebra. Moreover, this fact also singles out the physical significance of an analysis in terms of phase space distributions which are based on the $SU(M)$ coherent states.

6.2 Differential algebra

In this section we present a formalism for mapping quantum observables onto differential equations acting on the continuous parameter space of the coherent states based on

the ideas of Gilmore [55]. These can be used, for example, to calculate the exact phase space dynamics for the Bose-Hubbard model, as we will see in section 6.3.3. Moreover, in section 7.3.2 we will see that the differential operators represent a genuine tool to derive a quantum de Finetti type theorem or to determine bounds on the ground state energy (cf. section 7.3.5). Note that in contrast to other approaches, for example based on the star product (see [58] and references therein), this formalism is not restricted to the case of just two sites or to the special case of some dynamical groups [51].

6.2.1 Flatland

In the field of quantum optics the modus operandi for the Heisenberg-Weyl group H_4 and the Glauber coherent states is well-known (see, e.g., [59] and references therein). Since the Glauber states expressed in Fock states $|n\rangle$,

$$|\alpha\rangle = e^{-\frac{1}{2}\alpha\alpha^*} \sum_{n=0}^{\infty} \frac{\alpha^n}{\sqrt{n!}} |n\rangle = \sum_n f_n(\alpha) |n\rangle, \quad (6.19)$$

form an overcomplete basis, one can replace the action of the bosonic creation and annihilation operators by first order linear differential equations acting on the function $f_n(\alpha) \equiv \exp(-\frac{1}{2}\alpha\alpha^*)\alpha^n/\sqrt{n!}$. This yields the differential operators \mathcal{D}^k acting on a ket state

$$\begin{aligned} \hat{A} |\alpha\rangle &= \mathcal{D}^k(\hat{A}) |\alpha\rangle \\ \text{with } \mathcal{D}^k(\hat{a}^\dagger) &= \frac{\partial}{\partial\alpha} + \frac{1}{2}\alpha^* \quad \text{and} \quad \mathcal{D}^k(\hat{a}) = \alpha. \end{aligned} \quad (6.20)$$

In what follows we are interested in phase space densities corresponding to density operators and therefore to products of functions $f_n(\alpha)f_m(\alpha^*)$, we need the differential operators \mathcal{D}^l acting from the left side on the coherent state projectors:

$$\begin{aligned} \hat{A} |\alpha\rangle \langle\alpha| &= \mathcal{D}^l(\hat{A}) |\alpha\rangle \langle\alpha| \\ \text{with } \mathcal{D}^l(\hat{a}^\dagger) &= \frac{\partial}{\partial\alpha} + \alpha^* \quad \text{and} \quad \mathcal{D}^l(\hat{a}) = \alpha. \end{aligned} \quad (6.21)$$

The generalization to operators \mathcal{D}^r acting from the right,

$$\mathcal{D}^r(\hat{A}) = \left[\mathcal{D}^l(\hat{A}^\dagger) \right]^*, \quad (6.22)$$

and to multimode Glauber states is straightforward:

$$\begin{aligned} \mathcal{D}^l(\hat{a}_i^\dagger) &= \frac{\partial}{\partial\alpha_i} + \alpha_i^* = \mathcal{D}^r(\hat{a}_i)^* \\ \mathcal{D}^l(\hat{a}_i) &= \alpha_i = \mathcal{D}^r(\hat{a}_i^\dagger)^*. \end{aligned} \quad (6.23)$$

By means of the properties of the differential operators acting on arbitrary elements of the multimode algebra \hat{A}, \hat{B} with $r, s \in \mathbb{C}$,

$$\mathcal{D}^l(r\hat{A} + s\hat{B}) = r\mathcal{D}^l(\hat{A}) + s\mathcal{D}^l(\hat{B}) \quad (6.24)$$

$$\mathcal{D}^l(\hat{A}\hat{B}) = \mathcal{D}^l(\hat{B})\mathcal{D}^l(\hat{A}) \quad (6.25)$$

$$\mathcal{D}^l([\hat{A}, \hat{B}]) = [\mathcal{D}^l(\hat{B}), \mathcal{D}^l(\hat{A})], \quad (6.26)$$

one can show that the differential operators conserve the algebraic structure. Therefore the differential operators of the generators of the Heisenberg-Weyl algebra form itself a closed (differential) algebra.

6.2.2 From the plane to the sphere

The $su(M)$ algebra is generated by the set of operators $\{\hat{E}_{jk} = \hat{a}_j^\dagger \hat{a}_k\}$ with $j, k \in \{1, 2, 3, \dots, M\}$. In the case of the multimode Glauber states, the corresponding differential operators read

$$\mathcal{D}^l(\hat{E}_{jk}) = \mathcal{D}^l(\hat{a}_k)\mathcal{D}^l(\hat{a}_j^\dagger) = \alpha_k \partial_{\alpha_j} + \alpha_k \alpha_j^*. \quad (6.27)$$

Using the transformation

$$\alpha_i = x_i \alpha e^{i\phi}, \quad \alpha = \sum_i (\alpha_i \alpha_i^*)^{\frac{1}{2}}, \quad e^{i\phi} = \frac{\alpha_1}{|\alpha_1|}, \quad (6.28)$$

to the $M-1$ complex parameters $\mathbf{x} = (x_2, x_3, \dots, x_M)^t$, the norm α and the global phase ϕ , one obtains the differential form of the generalized angular momentum operator in terms of the multimode Glauber states

$$\mathcal{D}^l(\hat{E}_{jk}) = x_k \frac{\partial}{\partial x_j} + x_k x_j^* \left(\frac{\alpha}{2} \frac{\partial}{\partial \alpha} + \alpha^2 \right) - \frac{1}{2} x_k x_j^* (\mathbf{x} \nabla + \mathbf{x}^* \nabla^*). \quad (6.29)$$

Here we have used the definition

$$\mathbf{x} \nabla + \mathbf{x}^* \nabla^* = \sum_{k=2}^M x_k \frac{\partial}{\partial x_k} + x_k^* \frac{\partial}{\partial x_k^*}. \quad (6.30)$$

The parameter $x_1 = x_1^*$ is fixed by the normalization

$$x_1 = \sqrt{1 - \sum_{k=2}^M x_k^* x_k}, \quad (6.31)$$

which leads to the following definition of the derivative with respect to the dependent parameter:

$$\frac{\partial}{\partial x_1} \equiv \frac{1}{2x_1} \left(\frac{\partial}{\partial(i\phi)} - \mathbf{x} \nabla + \mathbf{x}^* \nabla^* \right) \equiv -\frac{\partial}{\partial x_1^*}. \quad (6.32)$$

To reduce the M independent complex parameters of the multimode Heisenberg-Weyl group to the $(M - 1)$ independent complex variables parameterizing the $SU(M)$ coherent states, one has to invert the relation between the projectors for the multimode Glauber states and the $SU(M)$ coherent states $|\mathbf{x}\rangle_N$:

$$|\alpha\rangle\langle\alpha| = \sum_{L,N=0}^{\infty} e^{-|\alpha|^2} \frac{\alpha^{N+L} e^{i\phi(N-L)}}{\sqrt{N!L!}} |\mathbf{x}\rangle_N \langle\mathbf{x}|_L. \quad (6.33)$$

This can be done using the following homomorphism [55]

$$\lim_{\alpha^2 \rightarrow 0} \left(\frac{\partial}{\partial \alpha} \right)^N e^{-\alpha^2} \oint |\alpha\rangle\langle\alpha| \frac{d\phi}{2\pi} = |\mathbf{x}\rangle_N \langle\mathbf{x}|_N \quad (6.34)$$

and the relation

$$\left(\frac{\alpha}{2} \frac{\partial}{\partial \alpha} + \alpha^2 \right) e^{-\alpha^2} \frac{\alpha^{2N}}{N!} = N e^{-\alpha^2} \frac{\alpha^{2N}}{N!}. \quad (6.35)$$

A short calculation gives the desired result

$$\begin{aligned} & \lim_{\alpha^2 \rightarrow 0} \left(\frac{\partial}{\partial \alpha} \right)^N e^{-\alpha^2} \oint \mathcal{D}^l(\hat{a}_j^\dagger \hat{a}_k) |\alpha\rangle\langle\alpha| \frac{d\phi}{2\pi} \\ &= x_k \frac{\partial}{\partial x_j} + x_k x_j^* \left(N - \frac{1}{2} (\mathbf{x}\nabla + \mathbf{x}^* \nabla^*) \right) |\mathbf{x}\rangle_N \langle\mathbf{x}|_N \\ &\equiv \mathcal{D}^l(\hat{E}_{jk}) |\mathbf{x}\rangle_N \langle\mathbf{x}|_N, \end{aligned} \quad (6.36)$$

where we used the abbreviation:

$$\frac{\partial}{\partial x_1} \equiv -\frac{1}{2x_1} (\mathbf{x}\nabla - \mathbf{x}^* \nabla^*) \equiv -\frac{\partial}{\partial x_1^*}. \quad (6.37)$$

A comparison to equation (6.32) shows that the differentiation no longer depends on the global phase. This can be understood as an averaging effect of the integration over the angle ϕ , which is part of the homomorphism.

6.3 Quantum dynamics in phase space

Now we have all the tools ready to study the quantum dynamics in phase space. In this section, we first define quasi phase space distributions, the analogue to quantum states in quantum phase space. In this description the evaluation of an expectation value is equivalent to taking the statistical average of the phase space distribution. Finally, we will calculate the exact phase space evolution equations for the Bose-Hubbard model using the differential operators introduced in the preceding section.

6.3.1 Quantum phase space distributions

With the help of the generalized coherent states, which will be denoted $|\Omega\rangle$ in the following (independently of the corresponding dynamical group or parametrization), one can readily introduce quasi phase space distributions: The Glauber-Sudarshan P -distribution is defined as the diagonal representation of the density operator $\hat{\rho}$ in terms of the generalized coherent states

$$\hat{\rho} = \int_X P(\Omega) |\Omega\rangle \langle\Omega| d\mu(\Omega), \quad (6.38)$$

where Ω represents the respective parametrization and $d\mu(\Omega)$ stands for the invariant measure on the respective phase space, denoted by X . Due to the overcompleteness of the coherent states the P -function does always exist but is usually not unique. Furthermore it is not positive definite and often highly singular. On the other hand, the Husimi Q -function defined as the expectation value of the density operator in generalized coherent states,

$$Q(\Omega) = \langle\Omega| \hat{\rho} |\Omega\rangle, \quad (6.39)$$

is unique, regular and positive definite. However, the Q -function does not give the correct marginal distributions. Thus the Q -function is especially suited for illustrations, while both quasi distribution functions will be used for actual calculations.

The relation between the Q - and P -function is in general be given by a convolution with the overlap of the coherent states $|\Omega\rangle$ and $|\Omega'\rangle$,

$$Q(\Omega) = \int d\mu(\Omega') P(\Omega') |\langle\Omega|\Omega'\rangle|^2. \quad (6.40)$$

Note that it is also possible to define the Wigner function on a spherical phase space but this leads to much more complicated expressions than the P - and Q -function, since such constructions use harmonic functions on the respective phase space. This makes actual calculations a hard task even for two lattice sites corresponding to $SU(2)$ (see, e.g., the contradictory results in [60] and [61]) and is almost impossible for larger systems. A positive P -representation respecting $SU(M)$ symmetry has been introduced and analyzed in [62]. In the following chapters we will mostly focus on the Q -function, not only due to its illustrative advantages, but also because of numerical stability.

6.3.2 Expectation values

The expectation value of an arbitrary operator \hat{B} in terms of Q - and P -functions is given by the statistical average of the phase space distribution

$$\begin{aligned} \langle\hat{B}\rangle &= \int P_{\hat{B}}(\Omega) Q(\Omega) d\mu(\Omega) \\ &= \int P(\Omega) Q_{\hat{B}}(\Omega) d\mu(\Omega), \end{aligned} \quad (6.41)$$

where $P_{\hat{B}}(\Omega)$ denotes the diagonal representation of the operator \hat{B} in generalized coherent states

$$\hat{B} \equiv \int P_{\hat{B}}(\Omega) |\Omega\rangle \langle\Omega| d\mu(\Omega) \quad (6.42)$$

and $Q_{\hat{B}}(\Omega)$ represents the expectation value of the operator \hat{B} in coherent states

$$Q_{\hat{B}}(\Omega) \equiv \langle\Omega| \hat{B} |\Omega\rangle. \quad (6.43)$$

These representations are usually referred to as Weyl symbols of the operator \hat{B} . Hence, the expectation values cannot be expressed in terms of one phase space distribution alone as one always needs both distributions. However, the differential algebra formalism also allows for the calculation of the expectation values in terms of the Q -function and the differential operator without using the P -representation and vice versa:

$$\begin{aligned} \langle\hat{B}\rangle &= \text{Tr}(\hat{B}\hat{\rho}) \\ &= \text{Tr}\left(\int \hat{B} |\Omega\rangle \langle\Omega| \hat{\rho} d\mu(\Omega)\right) \\ &= \int \mathcal{D}^l(\hat{B}) Q(\Omega) d\mu(\Omega) \\ &= \int \tilde{\mathcal{D}}^l(\hat{B}) P(\Omega) d\mu(\Omega). \end{aligned} \quad (6.44)$$

In the last line $\tilde{\mathcal{D}}^l$ denotes the differential operators for the Glauber-Sudarshan distribution (6.38), which arise from a simple integration by parts of the differential operators for the Husimi-distribution:

$$\int P(\Omega) \mathcal{D}^l(\hat{A}) |\Omega\rangle \langle\Omega| d\mu(\Omega) = \int \tilde{\mathcal{D}}^l(\hat{A}) P(\Omega) |\Omega\rangle \langle\Omega| d\mu(\Omega). \quad (6.45)$$

A comparison of equation (6.41) and equation (6.44) shows an interesting correspondence and reveals the close connection between the differential operators and the Weyl-symbols of the operator \hat{B} . Note that a rather elegant way to formulate the relationship between operators and a family of s -parametrized functions on the corresponding classical phase space is provided by the Stratonovich-Weyl correspondence [63], where s denotes the operator ordering of the operator kernel. In this language, the mutual dependence of the phase space distributions (6.41) can be explained by the different operator ordering chosen for the integral kernel of the quasi phase space distribution. Here, the Q -function corresponds to normal operator ordering, as e.g. $\hat{E}_{jk} = \hat{a}_j^\dagger \hat{a}_k$ and the P -distribution results from anti-normal operator ordering $\hat{a}_k \hat{a}_j^\dagger$. This relation manifests itself again in the relation between the differential operators $\mathcal{D}^l(\hat{A})$ and $\tilde{\mathcal{D}}^l(\hat{A})$, which are connected by a partial integration (6.45).

As an example, we calculate the expectation value of the generalized angular momentum operators $\hat{E}_{jk} = \hat{a}_j^\dagger \hat{a}_k$ which span the $su(M)$ algebra in the Q -representation

using an integration by parts and the periodic boundary conditions. This provides the following result for the Q -function

$$\langle \hat{E}_{jk} \rangle = (N + M) \int x_k x_j^* Q(\mathbf{x}) d\mu(\mathbf{x}) - \delta_{jk}, \quad (6.46)$$

and the subsequent outcome for the P -function:

$$\langle \hat{E}_{jk} \rangle = N \int x_k x_j^* P(\mathbf{x}) d\mu(\mathbf{x}). \quad (6.47)$$

The differences are of course due to the operator ordering. For a coherent state $|\mathbf{x}_0\rangle$ with $P(\mathbf{x}) = \delta(\mathbf{x} - \mathbf{x}_0)$ we obtain

$$\langle \hat{E}_{jk} \rangle = N x_{k,0} x_{j,0}^*, \quad (6.48)$$

as expected.

6.3.3 Evolution equations

The time evolution of Q -function (6.39) follows from the formal time dependence of the density operator $\dot{\hat{\rho}} = -\frac{i}{\hbar}[\hat{H}, \hat{\rho}]$. With the help of the relation $\frac{\partial}{\partial t} Q(\Omega, t) = \text{tr}(\dot{\hat{\rho}} |\Omega\rangle \langle \Omega|)$, the properties of the trace and the hermiticity of the Hamiltonian one finds

$$\frac{\partial}{\partial t} Q(\Omega, t) = \frac{i}{\hbar} \left(\mathcal{D}^l(\hat{H}) - \mathcal{D}^l(\hat{H})^* \right) Q(\Omega, t), \quad (6.49)$$

independent of the specific structure of the dynamical group. In the following we will use rescaled units with $\hbar = 1$.

Starting from the definition of the differential operator corresponding to the generalized angular momentum operator \hat{E}_{jk} ,

$$\mathcal{D}^l(\hat{E}_{jk}) = x_k \frac{\partial}{\partial x_j} + x_k x_j^* \left(N - \frac{1}{2} (\mathbf{x} \nabla + \mathbf{x}^* \nabla^*) \right) \quad (6.50)$$

we first have to calculate the differential representation for the Hamiltonian $\mathcal{D}^l(\hat{H})$ and then to evaluate the imaginary part of the differential operator $\mathcal{D}^l(\hat{H})$.

For the determination of the imaginary part of differential operator for the Bose-Hubbard Hamiltonian (6.1) and later for the discussion of the the canonical structure of the resulting macroscopic dynamics (cf. section 7.2.2), it is most convenient to use an amplitude phase decomposition according to

$$x_1 = \sqrt{p_1}, \quad x_i = \sqrt{p_i} e^{-iq_i} \quad 2 \leq i \leq M. \quad (6.51)$$

In the case of the Bose-Hubbard model, the p_j directly refer to the relative occupation in the j -th well and q_j describes the relative phase between the j -th and the first well.

With a little bit of algebra one gets the exact phase space dynamics of the Bose-Hubbard model in terms of the Husimi-function:

$$\begin{aligned}
\frac{\partial Q}{\partial t}(\mathbf{p}, \mathbf{q}, t) = & \left\{ \sum_{k=2}^M (\epsilon_1 - \epsilon_k) \frac{\partial}{\partial q_k} + 2J \sqrt{p_2 p_1} \sin q_2 \frac{\partial}{\partial p_2} \right. \\
& + 2J \sum_{k=2}^{M-1} \sqrt{p_{k+1} p_k} \sin(q_k - q_{k+1}) \left(\frac{\partial}{\partial p_k} - \frac{\partial}{\partial p_{k+1}} \right) \\
& + J \sum_{k=1}^{M-1} \cos(q_{k+1} - q_k) \left(\sqrt{\frac{p_k}{p_{k+1}}} \frac{\partial}{\partial q_{k+1}} + \sqrt{\frac{p_{k+1}}{p_k}} \frac{\partial}{\partial q_k} \right) \\
& + UN \sum_{k=2}^M (p_1 - p_k) \frac{\partial}{\partial q_k} - U \sum_{k=2}^M p_k \frac{\partial^2}{\partial p_k \partial q_k} \\
& \left. + U \sum_{k,k'=2}^M (p_k - p_1) p_{k'} \frac{\partial^2}{\partial p_{k'} \partial q_k} \right\} Q(\mathbf{p}, \mathbf{q}, t), \tag{6.52}
\end{aligned}$$

with the definitions

$$q_1 \equiv 0, \quad \frac{\partial}{\partial q_1} \equiv - \sum_{k=2}^M \frac{\partial}{\partial q_k}. \tag{6.53}$$

This is the exact many-particle result without any approximations. Before we analyze this formula in the limit of large particle numbers, we will derive the analogous result for the P -function.

As the differential operators for the Glauber-Sudarshan distribution (6.38), denoted by \tilde{D} to avoid confusion, arise from a simple integration by parts of the differential operators for the Husimi-distribution (cf. equation (6.45)), we can easily derive the explicit expression for the differential operator of the generalized angular momentum operator :

$$\tilde{D}^l(\hat{E}_{jk}) = -x_k \frac{\partial}{\partial x_j} - \delta_{jk} + x_k x_j^* \left((N + M) + \frac{1}{2}(\mathbf{x}\nabla + \mathbf{x}^*\nabla^*) \right). \tag{6.54}$$

Here, we have used the same definitions as in equation (6.37). The origin of the minor changes compared to the case of the Q -function is clear: the additional factor M and the δ -symbol result from the different operator ordering and the sign is due to the integration by parts.

With these preliminary considerations, we can determine the time evolution of the P -function using the differential operators in an analogous way as for the Husimi-distribution:

$$\begin{aligned}
\dot{\hat{\rho}} &= \int \dot{P}(\Omega) |\Omega\rangle \langle \Omega| d\mu(\Omega) \\
&= i \int \left(\tilde{D}^l(\hat{H})^* - \tilde{D}^l(\hat{H}) \right) P(\Omega) |\Omega\rangle \langle \Omega| d\mu(\Omega). \tag{6.55}
\end{aligned}$$

Now we can calculate the exact dynamics of the P -function for the Bose-Hubbard model with M sites:

$$\begin{aligned}
\frac{\partial P}{\partial t}(\mathbf{p}, \mathbf{q}, t) = & \left\{ \sum_{k=2}^M (\epsilon_1 - \epsilon_k) \frac{\partial}{\partial q_k} + 2J \sqrt{p_2 p_1} \sin q_2 \frac{\partial}{\partial p_2} \right. \\
& + 2J \sum_{k=2}^{M-1} \sqrt{p_{k+1} p_k} \sin(q_k - q_{k+1}) \left(\frac{\partial}{\partial p_k} - \frac{\partial}{\partial p_{k+1}} \right) \\
& + J \sum_{k=1}^{M-1} \cos(q_{k+1} - q_k) \left(\sqrt{\frac{p_k}{p_{k+1}}} \frac{\partial}{\partial q_{k+1}} + \sqrt{\frac{p_{k+1}}{p_k}} \frac{\partial}{\partial q_k} \right) \\
& + U(N + M) \sum_{k=2}^M (p_1 - p_k) \frac{\partial}{\partial q_k} + U \sum_{k=2}^M p_k \frac{\partial^2}{\partial p_k \partial q_k} \\
& \left. - U \sum_{k,k'=2}^M (p_k - p_1) p_{k'} \frac{\partial^2}{\partial p_{k'} \partial q_k} \right\} P(\mathbf{p}, \mathbf{q}, t), \tag{6.56}
\end{aligned}$$

where we used rescaled units $\hbar = 1$ and the same definitions (6.53) as above.

A comparison with the result for the Husimi-distribution (6.52) shows that due to the operator ordering the interaction strength now varies with the particle number plus the number of sites, $U(N + M)$. Apart from this issue, the first order differential form is exactly the same. The second order contribution has apparently the same structure as above, but the sign has changed. In both cases the second order term vanishes in the macroscopic limit $N \rightarrow \infty$ with UN fixed as $\mathcal{O}(1/N)$ if the lattice size M is kept constant. A more detailed study of the macroscopic dynamics will be subject of section 7.2.2.

6.3.4 Numerical simulation using phase space ensembles

From a practical viewpoint, the simulation of the exact phase space dynamics (cf. equation (6.52) and equation (6.56)) is as complicated as the original problem. Still, the Liouville dynamics can be used for a quasi-classical simulation of the dynamics by an approximation based on phase space ensembles, which is comparable to numerical Monte Carlo methods (for an introduction to these methods see, e.g., [64]).

To this end, one computes the Husimi distribution Q of the initial many-body quantum state. Due to the properties of the Husimi-function this yields a positive probability distribution. Now one chooses an ensemble of starting points in phase space distributed according to this probability function $\rho_Q(p, q)$, where the dynamics of every point $(p_i(t), q_i(t))$ is given by the corresponding Gross-Pitaevskii equation. Thus, the evaluation of expectation values reduces to the calculation of classical ensemble averages:

$$\langle \hat{A} \rangle_t = \int A(p, q) \rho_Q(p, q, t) dp dq \approx \frac{1}{L} \sum_{i=1}^L A(p_i(t), q_i(t)). \tag{6.57}$$

This treatment allows for the approximate calculation of expectation values to all orders. Moreover, it links the depletion of the condensate to the dynamical stability of the GPE and provides a valuable tool for approximately studying the long time dynamics. Though, just like the case for the approximations discussed in section 8.4.4 neglecting the second order differential term can be construed as disregarding of quantum noise and thus the the uncertainty relation might not be satisfied.

Last but not least the simulation based on classical ensembles is much simpler to use and implement then both of the methods mentioned earlier, especially in the case of larger systems. This method will be especially beneficial in chapter 10, where it is used to analyze the many-body features in a generalized Landau-Zener setup.

Chapter 7

Relation to the general theory

In this chapter we highlight the connections between the general theory for quantum mean-field systems and the description of systems of ultracold atoms in optical lattices which is in the center of attention in the second part. In particular, we discuss the relation to the theory of mean-field dynamical semigroups developed in [12, 13] and apply the algorithm developed in chapter 5 to determine the first order corrections to the mean-field ground state energy to the Bose-Hubbard model. Since we are now concerned with a bosonic system, we have to restrict the analysis to the symmetric subspace.

Furthermore, we discuss several applications of the phase space approach presented in the preceding chapter. In detail, we will come back to the finite Quantum de Finetti theorem and its relation to the mean-field theory which we began to discuss in section 2.5. Here, we will be mainly concerned with the question of bounds on the error of the de Finetti approximation and especially the scaling behaviour of the error for large, but finite particle numbers. To this end, we will explicitly calculate bounds starting from the \mathcal{D} -algebraic representation introduced in chapter 6. In addition, we take a more general viewpoint to complement this approach and show that the generalized phase space representations not only allow for the derivation of another bound, but also to explicitly construct the states for which the bound is attained. Finally, in the last section of this chapter, we will derive and discuss bounds on the ground state energy for the Bose-Hubbard model, as well as their scaling behaviour with the inverse particle number, complementing the results from the general theory discussed in chapter 5.

7.1 The Bose-Hubbard model as a quantum mean-field system

In this section, we analyse the ground state problem for the Bose-Hubbard Hamiltonian in the language of symmetric operators and quantum mean-field systems. Note that the general theory was aimed at the description of quantum many-particle systems of indistinguishable particles and we have not yet commented on possible restriction to

the symmetric or anti-symmetric subspace. Still now we are concerned with a system consisting of bosonic atoms. This clearly needs some further considerations.

7.1.1 Formulation in symmetric operators

The general theory of quantum mean-field systems as summarized in theorem 11 is based on strictly symmetric operators. Obviously, the Bose-Hubbard model in the tight-binding or next-neighbour approximation,

$$\hat{H} = \sum_{i=1}^M \epsilon_i \hat{n}_i - J \sum_{i=1}^{M-1} \left(\hat{a}_i^\dagger \hat{a}_{i+1} + \hat{a}_{i+1}^\dagger \hat{a}_i \right) + \frac{U}{2} \sum_{i=1}^M (\hat{n}_i (\hat{n}_i - 1)), \quad (7.1)$$

is not invariant under an arbitrary permutation of sites. To analyze the symmetry properties under an arbitrary permutation of particles, it is most convenient to work with the generalized angular momentum operators $\hat{E}_{jk} = \hat{a}_j^\dagger \hat{a}_k$ satisfying

$$\left[\hat{E}_{jk}, \hat{E}_{mn} \right] = \hat{E}_{jn} \delta_{km} - \hat{E}_{mk} \delta_{nj} \quad (7.2)$$

with $j, k \in \{1, 2, \dots, M\}$, which we have already used to define the generalized $SU(M)$ -coherent states in section 6.1.2.

The operators \hat{E}_{jk} span the dynamical group and describe the hopping between the k -th and the j -th well. Yet, they are not single-particle operators, but collective operators on the many-particle Hilbert space $\mathcal{H}^{\otimes N}$ due to the indistinguishability of atoms,

$$\begin{aligned} \hat{E}_{jk} &= \sum_{\alpha=1}^N \underbrace{\mathbb{1} \otimes \dots \otimes \mathbb{1}}_{\alpha-1 \text{ times}} \otimes |j\rangle \langle k| \otimes \underbrace{\mathbb{1} \otimes \dots \otimes \mathbb{1}}_{N-\alpha \text{ times}} \\ &= \sum_{\alpha=1}^N |j\rangle \langle k|^{(\alpha)}, \end{aligned} \quad (7.3)$$

where $|j\rangle$ denotes the basis state of the single-particle Hilbert space localized at the j -th well. Note that the diagonal elements \hat{E}_{ii} are normalized as

$$\sum_{i=1}^M \hat{E}_{ii} = \sum_{i=1}^M \hat{n}_i = N. \quad (7.4)$$

Defining the single-particle transition operator from the k -th to the j -th well as $\hat{e}_{jk} = |j\rangle \langle k|$ allows us to write the rescaled generalized angular momentum operator as a symmetric operator of degree one,

$$\frac{1}{N} \hat{E}_{jk} = \text{sym}_N(\hat{e}_{jk}), \quad (7.5)$$

while the interaction term $\hat{n}_i(\hat{n}_i - 1)$ gives rise to a symmetric operator of degree 2,

$$\begin{aligned} \frac{1}{N(N-1)} \hat{E}_{ii}(\hat{E}_{ii} - 1) &= \frac{1}{N(N-1)} \sum_{\alpha, \beta=1}^N |i\rangle \langle i|^{(\alpha)} |i\rangle \langle i|^{(\beta)} - \sum_{\gamma=1}^N |i\rangle \langle i|^{(\gamma)} \\ &= \frac{1}{N(N-1)} \sum_{\alpha \neq \beta} |i\rangle \langle i|^{(\alpha)} |i\rangle \langle i|^{(\beta)} \\ &= \text{sym}_N(\hat{e}_{ii} \otimes \hat{e}_{ii}) \end{aligned} \quad (7.6)$$

With these preliminary considerations, we can rewrite the hamiltonian density $h_N = \hat{H}_N/N$ for the Bose-Hubbard Hamiltonian (7.1) as

$$\begin{aligned} h_N &= \frac{1}{N} \sum_{i=1}^M \epsilon_i \hat{E}_{ii} - \frac{J}{N} \sum_{i=1}^{M-1} (\hat{E}_{i,i+1} + \hat{E}_{i+1,i}) + \frac{g}{2N(N-1)} \sum_{i=1}^M (\hat{E}_{ii}(\hat{E}_{ii} - 1)) \\ &= \sum_{i=1}^M \epsilon_i \text{sym}_N(\hat{e}_{ii}) - J \sum_{i=1}^{M-1} \text{sym}_N(\hat{e}_{i,i+1} + \hat{e}_{i+1,i}) + \frac{g}{2} \sum_{i=1}^M \text{sym}_N(\hat{e}_{ii} \otimes \hat{e}_{ii}), \end{aligned} \quad (7.7)$$

where we have used the definition $g = U(N-1)$ for the macroscopic interaction strength. This notation clearly illustrates that the Bose-Hubbard Hamiltonian (7.1) is an example of a quantum mean-field system with pairwise interactions (cf. equation (2.4)) and once more underlines the condition for the mean-field limit, where we have to consider the limit of infinite particle numbers $N \rightarrow \infty$ under the constraint that the macroscopic interaction strength $g = U(N-1)$ is kept fixed, and not the microscopic interaction strength U . Since we need both the Hamiltonian and the hamiltonian density in this chapter, we use capital and small letters, \hat{H}_N and h_N , respectively.

7.1.2 The ground state problem

The $1/N$ fluctuations to the mean-field ground state of ultracold bosonic atoms are described by the celebrated Bogoliubov theory. This theory is commonly introduced in a framework where the total particle number is not considered to be a fixed number, which renders a thorough analysis of the mean-field limit $N \rightarrow \infty$ impossible. Number-conserving derivations exist, but even these are mostly based on heuristic arguments (see section 8.4.2 and [65]). In the following we show that the Bogoliubov Hamiltonian emerges as a fluctuation Hamiltonian in the framework introduced in chapter 5.

We start from the momentum representation of the Bose Hubbard model. To this end, we define the annihilation operator for an atom in momentum state p ,

$$\hat{a}_p := \frac{1}{\sqrt{M}} \sum_{\ell=1}^M e^{ip\ell} \hat{a}_\ell, \quad (7.8)$$

where $p \in \pi/M \times (-M, -M+2, -M+4, \dots, M-2)$ if M is even and $p \in \pi/M \times (-M+1, -M+3, -M+5, \dots, M-1)$ if M is odd. Assuming periodic boundary

conditions, the Bose Hubbard Hamiltonian reads

$$\hat{H} = \sum_p \epsilon_p \hat{a}_p^\dagger \hat{a}_p + \frac{U}{2M} \sum_{rs,pq} \delta_{r+s,p+q} \hat{a}_r^\dagger \hat{a}_s^\dagger \hat{a}_p \hat{a}_q \quad (7.9)$$

with the free particle energy $\epsilon_p = -2J \cos(p)$. The hamiltonian density for a system with N particles can then be written as

$$h_N = \text{sym}_N(h_2) \quad (7.10)$$

with the two-particle hamiltonian density

$$h_2 = \sum_p \frac{\epsilon_p}{2} (\hat{e}_{pp} \otimes \mathbb{1} + \mathbb{1} \otimes \hat{e}_{pp}) + \frac{g}{2M} \sum_{rspq} \delta_{r+s,p+q} \hat{e}_{rp} \otimes \hat{e}_{sq}. \quad (7.11)$$

Here and in the following \hat{e}_{rq} denotes the operator taking one atom from momentum state q to momentum state r , while \hat{e}_{rq} is the associated macroscopic fluctuation operator. One can easily see that the mean-field energy $\langle \rho^{\otimes 2}, h_2 \rangle$ assumes its minimum when all particles condense to the zero-momentum state, $\rho = |p=0\rangle \langle p=0|$.

Now if want to determine the ground state energy for N bosonic atoms, we must calculate the infimum of $\langle \rho_N, h_N \rangle$ over the set of *Bose symmetric* states. These satisfy the symmetry condition

$$\pi \rho = \rho \quad \text{and} \quad \rho \pi^\dagger = \rho \quad (7.12)$$

for any permutation π of two particles. Note that the set of Bose symmetric states is a proper subset of the permutation symmetric states. However, we can circumvent this restriction by a trick, enforcing Bose symmetry on the level of the Hamiltonian h_2 by applying the symmetrization operator $(\mathbb{1}_2 + \pi_{1,2})/2$. In particular, we will calculate the $1/N$ corrections to the mean-field ground state energy for the modified Hamiltonian

$$\begin{aligned} h'_2 &= \epsilon_0 \mathbb{1}_2 + \frac{1}{4} \sum_p (\epsilon_p - \epsilon_0) \left(\hat{e}_{pp} \otimes \mathbb{1} + \mathbb{1} \otimes \hat{e}_{pp} + \sum_\ell e_{p\ell} \otimes \hat{e}_{\ell p} + \hat{e}_{\ell p} \otimes e_{p\ell} \right) \\ &\quad + \frac{g}{2M} \sum_{rspq} \delta_{r+s,p+q} \hat{e}_{rp} \otimes \hat{e}_{sq}. \end{aligned} \quad (7.13)$$

Physically, this corresponds to the inclusion of the so-called exchange terms into h'_2 . Note that the interaction term in h_2 is already invariant under the permutation $\pi_{1,2}$. It is easily verified that h'_2 and the corresponding N -particle operator $h'_N = \text{sym}_N(h'_2)$ are equivalent to h_2 and h_N , respectively, when restricted to the Bose symmetric subspace. We now expand the two-particle Hamiltonian density h'_2 into fluctuation operators around the mean-field minimizer $\rho = |p=0\rangle \langle p=0|$ as described in chapter 5. For the kinetic energy term we need

$$\begin{aligned} \text{sym}_N \hat{e}_{pp} &= \rho(\hat{e}_{pp}) + \frac{1}{\sqrt{N}} \tilde{e}_{pp} \\ \sum_\ell \text{sym}_N(\hat{e}_{p\ell} \otimes \hat{e}_{\ell p}) &= \rho(\hat{e}_{p\ell}) \rho(\hat{e}_{\ell p}) + \frac{2}{\sqrt{N}} \delta_{p0} \tilde{e}_{00} \\ &\quad + \frac{1}{N} \sum_\ell \tilde{e}_{p\ell} \circ \tilde{e}_{\ell p} - \rho(\hat{e}_{p\ell} \circ \hat{e}_{\ell p}) + \rho(\hat{e}_{p\ell}) \rho(\hat{e}_{\ell p}). \end{aligned} \quad (7.14)$$

For the interaction term, we find the expansions

$$\begin{aligned} \text{sym}_N(\hat{e}_{rp} \otimes \hat{e}_{sq}) &= \delta_{r0}\delta_{p0}\delta_{s0}\delta_{q0} + \frac{1}{\sqrt{N}} (\delta_{r0}\delta_{p0}\tilde{e}_{sq} + \delta_{s0}\delta_{q0}\tilde{e}_{rp}) \\ &+ \frac{1}{N} \sum_{\ell} \tilde{e}_{rp} \circ \tilde{e}_{sq} - \rho(\hat{e}_{rp} \circ \hat{e}_{sq}) + \rho(\hat{e}_{rp})\rho(\hat{e}_{sq}). \end{aligned} \quad (7.15)$$

In these expressions, the \circ refers to the symmetric product of two operators as above. It is worth stopping here for a moment to investigate the fluctuation operators in more detail. We have shown that the macroscopic fluctuations obey canonical commutation relations

$$[\hat{e}_{ab}, \hat{e}_{cd}] = \rho([\hat{e}_{ab}, \hat{e}_{cd}]) \mathbb{1}. \quad (7.16)$$

However, the mean-field state ρ is such that most expectation values vanish exactly. In fact, the only non-vanishing commutators are given by

$$[\hat{e}_{0b}, \hat{e}_{a0}] = \delta_{ab}, \quad a, b \neq 0. \quad (7.17)$$

Hence, we can identify the fluctuation operator \hat{e}_{0b} with the annihilation operator of a bosonic field as it is common in Bogoliubov theory. As these operators are the only ones which contribute to the ground state energy of the Hamiltonian \hat{H} , we can basically neglect all other fluctuations. Indeed, we will only consider the 'bosonic' part of \hat{H} and drop all other terms in the following.

Collecting the results from equations (7.14) and (7.15), we thus have to retain only fluctuation operators with exactly one index that equals zero. Furthermore, we can exploit that $\rho(\hat{e}_{ab}) = \delta_{a0}\delta_{b0}$ for all a, b . We thus obtain the bosonic part of fluctuation Hamiltonian for the kinetic energy,

$$\begin{aligned} \hat{H}_{\text{kin}} &= \sum_{p \neq 0} \frac{\epsilon_p - \epsilon_0}{2} \hat{e}_{p0} \circ \hat{e}_{0p} + \sum_{\ell \neq 0} \frac{\epsilon_0 - \epsilon_0}{2} \hat{e}_{\ell 0} \circ \hat{e}_{0\ell} \\ &= \sum_{p \neq 0} \frac{\epsilon_p - \epsilon_0}{2} \hat{e}_{p0} \circ \hat{e}_{0p}. \end{aligned} \quad (7.18)$$

The scalar correction to the mean-field ground state is given by

$$\begin{aligned} \gamma_c(H_{\text{kin}}) &= \sum_{p, \ell} \frac{\epsilon_p - \epsilon_0}{2} (\rho(\hat{e}_{p\ell} \circ \hat{e}_{\ell p}) - \rho(\hat{e}_{p\ell})\rho(\hat{e}_{\ell p})) \\ &= \sum_p \frac{\epsilon_p - \epsilon_0}{4}. \end{aligned} \quad (7.19)$$

To evaluate the bosonic part of the interaction term we again make use of the fact that one of the indices r, p and p, q must equal zero and that we have the momentum conservation condition $r + s = p + q$. Thus we are left with the contributions

$$\hat{H}_{\text{int}} = \frac{g}{2M} \sum_{p \neq 0} (\hat{e}_{0,p} \circ \hat{e}_{p,0} + \hat{e}_{p,0} \circ \hat{e}_{0,p} + \hat{e}_{p,0} \circ \hat{e}_{-p,0} + \hat{e}_{0,p} \circ \hat{e}_{0,-p}) \quad (7.20)$$

and

$$\begin{aligned}\gamma_c(H_{\text{int}}) &= \frac{g}{2M} \sum_{rspq} \delta_{r+s,p+q} (\rho(\hat{e}_{rp} \circ \hat{e}_{sq}) - \rho(\hat{e}_{rp})\rho(\hat{e}_{sq})) \\ &= \frac{g(M-1)}{2M}.\end{aligned}\tag{7.21}$$

Finally, we use the commutator relations (7.17) to simplify our results. Notably, the resulting scalar terms are just canceled out by γ_c such that we finally get

$$\hat{H} - \gamma_c(H) = \sum_{p \neq 0} \left(\frac{\epsilon_p - \epsilon_0}{2} + \frac{g}{M} \right) \hat{e}_{p,0} \hat{e}_{0,p} + \frac{g}{2M} (\hat{e}_{p,0} \hat{e}_{-p,0} + \hat{e}_{0,p} \hat{e}_{0,-p}),\tag{7.22}$$

which is nothing but the well-known Bogoliubov Hamiltonian, (cf. equation (8.49)). More details on the heuristic derivation are given in section 8.4.1.

7.2 Mean-field dynamical semigroups

The second part of this thesis is devoted to the study of the dynamics of ultracold atoms in optical lattices, and especially the relation between the mean-field description and the exact many-particle dynamics. In this section, we give a brief introduction to the general theory of mean-field dynamical semigroups introduced in [12, 13]. As this illustrates the structure most clearly, we focus on hamiltonian systems and illustrate the consequences of the general theory for the special case of the Bose-Hubbard Hamiltonian (7.7). We have already seen in the preceding chapter that the dynamics can be described by a flow in quantum phase space, which turns out to be in perfect accordance with the predictions from the general theory for quantum mean-field systems. Yet the appearance of the symplectic phase space structure needs some further explanations. To this end, we will again need the differential calculus for state space function introduced in chapter 3. In addition, we will briefly comment on dissipative systems described by a master equation since these systems play a major role in the following chapters.

7.2.1 Hamiltonian flows

A quantum dynamical semigroup is defined as a family $(T_{t,N})_{N \in \mathbb{N}}$ of completely positive, identity preserving contractions

$$T_{t,N} : \mathcal{A}^N \rightarrow \mathcal{A}^N \quad \text{for } t \in \mathbb{R}_+ \quad \text{and } N \in \mathbb{N}.\tag{7.23}$$

In detail, we require that for each $N \in \mathbb{N}$, $T_{t,N}$ is a strongly continuous one-parameter semigroup on \mathcal{A}^N with generator G_N , that is $(T_{t,N} = e^{tG_N})_{t \geq 0}$.

In this section we restrict the discussion to hamiltonian systems, where the generator is given by a strictly symmetric hamiltonian density h_N as for example the Bose-Hubbard Hamiltonian (7.7). Hence the generator is given by

$$G_N = iN [h_N, \cdot]. \quad (7.24)$$

To establish an evolution in the mean-field limit, that means an automorphism $T_{t,\infty}$ on $\mathcal{S}(\mathcal{A})$,

$$T_{t,\infty}A_\infty = (T_{t,\cdot}A)_\infty, \quad (7.25)$$

we must assure that $T_{t,N}$ preserves the basic structure. Here and in the following, A refers to the sequence $N \mapsto A_N$ and not to a particular element A_N of the sequence. Therefore, we at most require the condition that $T_{t,N}$ maps approximately symmetric operators $X_N \in \tilde{\mathcal{Y}}$ to approximately symmetric operators $T_{t,N}X_N \in \tilde{\mathcal{Y}}$. A detailed analysis [12] shows, that we need an additional technical condition to cope with unbounded generators.

Theorem 25 (Limiting dynamics for quantum mean-field systems [12]). *For each $N \in \mathbb{N}$ let $(T_{t,N} = e^{tG_N})_{t \in \mathbb{R}}$ be a strongly continuous semigroup of automorphisms on \mathcal{A}^N . Then the following conditions are equivalent:*

1. *For each t , $T_{t,\cdot}$ is approximately symmetry preserving and the set of sequences A , such that $A_N \in \text{Dom}(G_N)$ and $\|G_N A_N\|$ is uniformly bounded is dense in $\tilde{\mathcal{Y}}$ in the seminorm (2.9).*
2. *The operator G_∞ defined by $G_\infty A_\infty = (G.A)_\infty$ on the domain*

$$\text{Dom}(G_\infty) = \{A_\infty \mid A_N \in \tilde{\mathcal{Y}} \quad \text{and} \quad G_N A_N \in \tilde{\mathcal{Y}}\} \quad (7.26)$$

is well defined, closed and generates a group automorphism on $\mathcal{C}(\mathcal{S}(\mathcal{A}))$.

If these conditions are satisfied, $T_{t,\infty} = e^{tG_\infty}$ is the mean-field limit of the sequence $T_{t,\cdot}$. Moreover, $T_{t,\infty}$ is implemented by a weak-continuous 2-sided flow $(F_t)_{t \in \mathbb{R}}$ on $\mathcal{S}(\mathcal{A})$, i.e. $\mathbb{R} \times \mathcal{S}(\mathcal{A}) \ni (t, \rho) \mapsto T_t \rho \in \mathcal{S}(\mathcal{A})$ is jointly continuous, $F_t \circ F_s = F_{t+s}$ for all $t, s \in \mathbb{R}$ and $T_{t,\infty} f = f \circ F_t$ for all $f \in \mathcal{C}(\mathcal{S}(\mathcal{A}))$ and all $t \in \mathbb{R}$.*

In the following discussion we restrict ourselves to strictly symmetric observables and especially to the evolution of linear functions on $\mathcal{S}(\mathcal{A})$, as e.g. $\rho(a)$. Note however, that one can establish a suitable condition which allows for the extension to a large subset of the approximately symmetric sequences (cf. condition 2.3 in [13]).

For hamiltonian systems, the generator of the limiting dynamics G_∞ can be determined by evaluating sequences of the form (7.24). In chapter 2 we have seen that for strictly symmetric sequences the commutator vanishes to leading order. However, now we are interested in the rescaled commutator. With the results from calculation (2.13) we can

directly conclude that for $A_N = \text{sym}_N(a_k), B_N = \text{sym}_N(B_\ell) \in \mathcal{Y}$ and for $N \geq k + \ell - 1$, the following relation holds

$$\begin{aligned} N[A_N, B_N] &= N \sum_{r=0}^{\min k, \ell} c_N(k, \ell, r) \text{sym}_N([A_k \otimes \mathbb{1}_{\ell-r}, \mathbb{1}_{k-r} \otimes B_\ell]) \\ &= k\ell \text{sym}_N([A_k \otimes \mathbb{1}_{\ell-1}, \mathbb{1}_{k-1} \otimes B_\ell]) + \mathcal{O}(N^{-1}). \end{aligned} \quad (7.27)$$

Hence, the rescaled commutator defines an approximately symmetric and therefore mean-field convergent sequence. Moreover, a comparison to the definition of the first order derivative (cf. equation (3.6)) shows that we can express the mean-field limit of the sequences in terms of derivatives,

$$\begin{aligned} \lim_{N \rightarrow \infty} \langle \rho^{\otimes N}, N[A_N, B_N] \rangle &= k\ell \langle \rho^{\otimes(k+\ell-1)}, [A_k \otimes \mathbb{1}_{\ell-1}, \mathbb{1}_{k-1} \otimes B_\ell] \rangle \\ &= \langle \rho, [\nabla_\rho A_\infty, \nabla_\rho B_\infty] \rangle. \end{aligned} \quad (7.28)$$

Note that due to the properties of the commutator this expression is independent of the convention to choose the representative of the equivalence class of derivatives.

The mean-field limit of the rescaled commutator defines a bilinear, skew-symmetric form on the set of differential functions $\mathcal{C}(\mathcal{S}(\mathcal{A}))$, which we can use to define a Poisson-like bracket,

$$\{A_\infty, B_\infty\} = i \langle \rho, [\nabla_\rho A_\infty, \nabla_\rho B_\infty] \rangle. \quad (7.29)$$

Still, in order to define a proper symplectic structure and hence a phase space structure, the bilinear form ought to be non-degenerate. This property clearly depends on the state ρ . We will come back to this point in the next section.

With this definition (7.29), we can associate to any differential function $A_\infty \in \mathcal{C}(\mathcal{S}(\mathcal{A}))$ the corresponding hamiltonian vector field induced by the mean-field limit of the Hamiltonian h_∞ by $A_\infty \mapsto \{h_\infty, A_\infty\}$. The integral curves of the vector field can be interpreted as the time evolution on $\mathcal{S}(\mathcal{A})$,

$$\frac{\partial}{\partial t} \langle \rho_t, a \rangle = i \langle \rho_t, [\nabla_\rho h_\infty, a] \rangle \quad (7.30)$$

for $a \in \mathcal{A}$. Here, we have used the fact that the gradient of a linear function $\rho(a)$ is proportional to a . Hence, the limiting generator of (7.24) is of the form

$$G_\infty f(\rho) = i \langle \rho_t, [\nabla_\rho h_\infty, \nabla_\rho f_\infty] \rangle. \quad (7.31)$$

Now we state the main theorem for quantum hamiltonian mean-field systems. In the next section, we will discuss the application of this theorem to the Bose-Hubbard Hamiltonian (7.7).

Theorem 26 (Mean-field limit of the dynamics for quantum hamiltonian systems [12, 13]). *Let H_N be a strictly symmetric self-adjoint sequence and set*

$$T_{t,N} A_N = e^{itNH_N} A_N e^{-itNH_N} \quad (7.32)$$

for all $N \in \mathbb{N}$ and $t \in \mathbb{R}$. Then

- $(T_{t,\cdot})$ has a mean-field limit $(T_{t,\infty})_{t \in \mathbb{R}}$ which is the group of automorphisms of $\mathcal{C}(\mathcal{S}(\mathcal{A}))$ generated by $\{\nabla_{\rho} h_{\infty}, \cdot\}$.
- $T_{t,\infty}$ is implemented by a flow F_t , the differential equation for $\rho_t = F_t \rho$ being $\langle \dot{\rho}_t, a \rangle = i \langle \rho_t, [\nabla_{\rho} h_{\infty}, a] \rangle$ for all $\rho_t \in \mathcal{S}(\mathcal{A})$ and $a \in \mathcal{A}$.

7.2.2 Limiting dynamics for the Bose-Hubbard Hamiltonian

With the general theory in mind, we can directly calculate the mean-field limit of the energy density of the Bose-Hubbard Hamiltonian (7.7):

$$h_{\infty}(\sigma) = \sum_{i=1}^M \epsilon_i \sigma(\hat{e}_{ii}) - J \sum_{i=1}^{M-1} \sigma(\hat{e}_{i i+1} + \hat{e}_{i+1 i}) + \frac{g}{2} \sum_{i=1}^M \sigma(\hat{e}_{ii} \otimes \hat{e}_{ii}). \quad (7.33)$$

Now theorem 26 states that the generator of the evolution in the limiting space is given by the first order derivative $\nabla_{\rho} h_{\infty}$,

$$\nabla_{\rho} h_{\infty} = \sum_{i=1}^M \epsilon_i \hat{e}_{ii} - J \sum_{i=1}^{M-1} (\hat{e}_{i i+1} + \hat{e}_{i+1 i}) + g \sum_{i=1}^M \hat{e}_{ii} \rho(\hat{e}_{ii}). \quad (7.34)$$

Note that we have already left out all terms which are simple multiples of the identity as these terms do not contribute to the commutator.

With these considerations the evolution equations for the single-particle operators $\hat{e}_{jk} \in \mathcal{A}$ in the Heisenberg picture are given by

$$\frac{d}{dt} \langle \rho_t, \hat{e}_{jk} \rangle = i \langle \rho_t, [\nabla_{\rho_t} h_{\infty}, \hat{e}_{jk}] \rangle. \quad (7.35)$$

Using the commutator relations $[\hat{e}_{jk}, \hat{e}_{\ell m}] = \delta_{k\ell} \hat{e}_{jm} - \delta_{mj} \hat{e}_{\ell k}$ and the abbreviation $\langle a \rangle = \rho(a)$ for the expectation value in the state $\rho \in \mathcal{S}(\mathcal{A})$, we obtain the following set of differential equations

$$\begin{aligned} i \frac{d}{dt} \langle \hat{e}_{jk} \rangle &= \langle [\hat{e}_{jk}, \nabla_{\rho_t} h_{\infty},] \rangle \\ &= \sum_{i=1}^M \epsilon_i \langle [\hat{e}_{jk}, \hat{e}_{ii}] \rangle - J \sum_{i=1}^{M-1} \langle [\hat{e}_{jk}, (\hat{e}_{i i+1} + \hat{e}_{i+1 i})] \rangle + g \sum_{i=1}^M \langle [\hat{e}_{jk}, \hat{e}_{ii}] \rangle \langle \hat{e}_{ii} \rangle \\ &= (\epsilon_k - \epsilon_j) \langle \hat{e}_{jk} \rangle - J (\langle \hat{e}_{j k+1} \rangle - \langle \hat{e}_{j-1 k} \rangle + \langle \hat{e}_{j k-1} \rangle - \langle \hat{e}_{j+1 k} \rangle) \\ &\quad + g (\langle \hat{e}_{jk} \rangle \langle \hat{e}_{kk} \rangle - \langle \hat{e}_{jk} \rangle \langle \hat{e}_{jj} \rangle). \end{aligned} \quad (7.36)$$

Hence, this treatment provides a rigorous justification for the heuristic argument that one can replace the expectation value of four-point functions, as e.g. $\hat{e}_{jk} \hat{e}_{kk}$ by a product of the expectation value of the two point functions \hat{e}_{jk} in the mean-field limit. This argument will be presented in more detail in section 8.4.1. Here, we just note that if we neglect the variances of the two-point functions in the exact equation (8.60) as proposed in the heuristic approach we recover exactly the above result.

By a simple calculation using the parameter transformation $\langle \hat{e}_{jk} \rangle = x_j^* x_k$, one can show that the result (7.36) is equivalent to the discrete Gross-Pitaevskii equation in its most common form,

$$i\dot{x}_j = \epsilon_j x_j - J(x_{j+1} + x_{j-1}) + g|x_j|^2 x_j, \quad (7.37)$$

provided that the mean-field state is pure. Still, one should keep in mind that the rigorous derivation presented in this section is based on number-conserving operators \hat{E}_{jk} , which avoids many conceptual problems, as will be argued in section 8.4.1.

Again using the decomposition into amplitude and phase (6.51), the dynamics described by the GPE (7.37) can be reformulated as canonical evolution equations

$$\dot{q}_i = \frac{\partial \mathcal{H}}{\partial p_i}, \quad \dot{p}_i = -\frac{\partial \mathcal{H}}{\partial q_i}, \quad (7.38)$$

with the corresponding Hamiltonian function

$$\mathcal{H}(\mathbf{p}, \mathbf{q}) = -2J \sum_{k=1}^{M-1} \sqrt{p_k p_{k+1}} \cos(q_{k+1} - q_k) + \frac{UN}{2} \sum_{k=1}^M p_k^2 + \sum_{k=1}^M \epsilon_k p_k, \quad (7.39)$$

where one should keep in mind that the parameters of the first well are not independent (cf. equation (6.31)).

A classical phase space distribution $\rho(\mathbf{p}, \mathbf{q}, t) d\mathbf{p} d\mathbf{q}$, with \mathbf{p}, \mathbf{q} being canonical conjugate variables, describes the probability that an ensemble of particles will be found in an infinitesimal phase space element $d\mathbf{p} d\mathbf{q}$. The dynamics according to the Hamiltonian function \mathcal{H} is given by the classical Liouville equation

$$\frac{d\rho}{dt} = \frac{\partial \rho}{\partial t} + \{\rho, \mathcal{H}\} = 0, \quad (7.40)$$

where $\{\cdot, \cdot\}$ denotes the classical Poisson bracket. Therefore the resulting evolution equations induced by the Hamiltonian function (7.39) are given by the hamiltonian flow

$$\begin{aligned} \frac{\partial \rho}{\partial t} &= \sum_{k=2}^M \frac{\partial \mathcal{H}}{\partial q_k} \frac{\partial \rho}{\partial p_k} - \sum_{k=2}^M \frac{\partial \mathcal{H}}{\partial p_k} \frac{\partial \rho}{\partial q_k} \\ &= \sum_{k=2}^M (\epsilon_1 - \epsilon_k) \frac{\partial}{\partial q_k} \rho + 2J \sqrt{p_2 p_1} \sin q_2 \frac{\partial \rho}{\partial p_2} \\ &\quad + 2J \sum_{k=2}^{M-1} \sqrt{p_{k+1} p_k} \sin(q_k - q_{k+1}) \left(\frac{\partial \rho}{\partial p_k} - \frac{\partial \rho}{\partial p_{k+1}} \right) \\ &\quad + J \sum_{k=1}^{M-1} \cos(q_{k+1} - q_k) \left(\sqrt{\frac{p_k}{p_{k+1}}} \frac{\partial \rho}{\partial q_{k+1}} + \sqrt{\frac{p_{k+1}}{p_k}} \frac{\partial \rho}{\partial q_k} \right) \\ &\quad + UN \sum_{k=2}^M (p_1 - p_k) \frac{\partial \rho}{\partial q_k}. \end{aligned} \quad (7.41)$$

Hence, with this particular choice of coordinates, we obtain a symplectic phase space structure. In the next section, we will see how we can put this argument on more solid grounds.

Still, before we proceed, we will discuss the connections between equation (7.41) and the exact evolution equations for the quantum phase space quasi-distributions (6.52) and (6.56) derived in chapter 6. The comparison shows that the exact phase space evolution equation consists of a first order differential equation plus a many-particle quantum correction of second order. This correction vanishes in the macroscopic limit $N \rightarrow \infty$ with g fixed. The first order terms can be thought of as the classical evolution since they are identical to the results of the Liouville equation for the hamiltonian function (7.41). Thus, in the noninteracting case this result coincides with the many-particle result – the Liouville equation is exact. In this case the GPE describes the evolution of the center or maximum of the phase space distribution. Thus, starting from the Liouville equation (7.40) and assuming a delta-distribution $\rho(p', q') = \delta(p' - p)\delta(q' - q)$, we get back to the GPE (7.37) in the form of canonical equations (7.41). This explains that the GPE is sometimes referred to as single-trajectory approach and demonstrates that it is obviously not possible to infer any details about higher-order moments from the GPE alone.

In contrast, the description in terms of a hamiltonian flow clearly goes beyond the area of validity of the GPE since there are no restrictions on the shape of the initial state, up to the usual ones set up by the uncertainty relation. As predicted by the general theory [12, 13], the leading term of the exact phase space dynamics (6.52) and (6.56) is exactly reproduced by the classical Liouville equation (7.41). In the macroscopic limit $N \rightarrow \infty$ with a fixed macroscopic interaction strength $g = U(N - 1)$, as well as for a fixed lattice size M , the next to leading order differential term vanishes as $\mathcal{O}(M/N)$ and is to first order in $1/N$ independent of the operator ordering. The choice of the operator ordering is closely related to the question of finite corrections to the quantum de Finetti theorem (cf. section 2.5 and especially corollary 14). This point will be taken up again in the following sections.

Note that the first order differential equation is obviously equivalent to an ordinary differential equation, whereas the full partial differential equations have a much more elaborate structure, as they belong to the class of pseudo-parabolic partial differential equations [66, 67] and thus cannot be easily treated, e.g. by stochastic differential equations [68].

The first order interaction term is responsible for a variation of the shape of the state, therefore an initially coherent state no longer stays coherent during the time evolution. This fact is usually denoted as the *break-down of mean-field* [69–71], indicating that the description by a single mean-field trajectory corresponding to the evolution of the center of the coherent state is no longer valid. Indeed this breakdown is resolved by using the Liouville approach, where we can take into account the variation of the shape of the initial state and therefore effects due to variation of the higher moments. Having in mind the general result it is directly obvious, that the assumption of a point distribution during the whole evolution is not correct. Instead, the general theory

predicts a hamiltonian flow in the mean-field limit in accordance with the exact result which we have derived in the preceding section using the \mathcal{D} -algebraic calculus.

The second order differential corrections to the classical Liouville equation decay with increasing particle number as $1/N$ in the macroscopic limit. These terms are responsible for many-particle effects as tunneling in quantum phase space and (self-)interference. It is interesting to note that both the Liouville equation and the whole equation without approximations conserve the normalization. These considerations demonstrate that the phase space approach presented in chapter 6 provides a suitable tool to explicitly calculate the explicit dynamics, as well as to determine the mean-field limit and quantify the deviations from the limiting dynamics.

7.2.3 Symplectic structure

For reasons of simplicity, we will restrict the following discussion to finite dimensional algebras $\mathcal{A} = \mathcal{M}_M$. For the Bose-Hubbard model, the dimension M is equivalent to the number of sites. As a direct consequence the state space $\mathcal{S}(\mathcal{A})$ is a finite dimensional manifold of dimension $M^2 - 1$. This allows us to use some concepts from differential geometry, which have already proven to be useful in the discussion of the differential calculus introduced in chapter 3. For a general introduction to the geometric aspects of hamiltonian mechanics and a physical motivation of the concepts of differential geometry, as e.g. 2-forms, we refer to the textbook [72]. For a detailed discussion of the ideas presented in this chapter, see [13]. In the following, we will closely follow this reasoning.

In chapter 3, we have identified the tangent space $T_p\mathcal{S}(\mathcal{A})$ of $\mathcal{S}(\mathcal{A})$ as

$$T_p\mathcal{S}(\mathcal{A}) = \{\phi \in \mathcal{A}^* \mid \phi = \phi^*, \quad \langle \phi, \mathbb{1} \rangle = 0\}, \quad (7.42)$$

which can be interpreted as the phase space containing all hamiltonian vector fields $\{h_\infty, \cdot\} = i\langle \rho, [\nabla_\rho h_\infty, \cdot]\rangle$. The cotangent space $T_p^*\mathcal{S}(\mathcal{A})$ is set of functions from $T_p\mathcal{S}(\mathcal{A})$ to \mathbb{R} . It contains the first order derivatives and is equivalent to the set of equivalence classes $[a] = a + \mathbb{R}\mathbb{1}$ with $a^* = a \in \mathcal{A}$.

In this language,

$$\sigma(a, b) = i\langle \rho, [b, a] \rangle \quad (7.43)$$

defines an antisymmetric bilinear form on $T_p^*\mathcal{S}(\mathcal{A}) \times T_p^*\mathcal{S}(\mathcal{A})$. Yet this is not a 2-form, as required for a hamiltonian system (see e.g. [72]), but a contravariant tensor of rank 2. Moreover, as a non-degenerate antisymmetric tensor can only exist in even dimensions it is in general degenerate and strongly depends on the choice of ρ . This can be directly seen from a simple example: For ρ being given by the maximally mixed state $\rho = \mathbb{1}_d/d$, the symplectic form vanishes identically for all $a, b \in \mathcal{A}$.

Thus, the null space at the point ρ defined as

$$\mathcal{N}_\rho = \{a \in T_p\mathcal{S}(\mathcal{A}) \mid \sigma(a, b) = 0 \quad \forall b \in T_p\mathcal{S}(\mathcal{A})\} \quad (7.44)$$

is in general a non-empty subset of $T_\rho\mathcal{S}(\mathcal{A})$. Obviously, the bilinear form σ is non-degenerate on the quotient space $T_\rho\mathcal{S}(\mathcal{A})/\mathcal{N}_\rho$. The problem is now to identify this space as the tangent space of some submanifold \mathcal{S} of $\mathcal{S}(\mathcal{A})$ through ρ . As this tangent space contains all the hamiltonian vector fields the hamiltonian flow is restricted to this submanifold. Hence we would obtain a symplectic manifold, which can be interpreted as the phase space.

To determine the submanifold \mathcal{S} we have to analyse the integral curves of the Hamiltonian vector field. Since the first order derivative of the mean-field limit of the Hamiltonian h_∞ (7.34) is an element of the single-particle space \mathcal{A} it defines an affine function of ρ . Thus, we can directly integrate

$$\frac{d}{dt}\langle\rho_t, a\rangle = \sigma(\nabla_\rho h_\infty, a) = \langle\rho_t, i[\nabla_\rho h_\infty, a]\rangle \quad (7.45)$$

to determine the flow

$$\langle\mathcal{F}_t\rho, a\rangle = \langle\rho_t, a\rangle = \langle\rho, e^{i\nabla_\rho h_\infty t} a e^{-i\nabla_\rho h_\infty t}\rangle \equiv \langle\rho, u a u^*\rangle, \quad (7.46)$$

where u is an element of the connected component G_0 of the identity of the unitary group of \mathcal{A} .

The elements of the subspace \mathcal{N}_ρ generate the fixed group G_ρ of ρ with

$$\langle\mathcal{F}_t\rho, a\rangle = \langle\rho, u a u^*\rangle = \langle\rho, a\rangle. \quad (7.47)$$

Since $a \in \mathcal{N}_\rho$ implies that $\sigma(a, b) = \langle\rho, [a, b]\rangle = 0$, this subset is equivalent to the centralizer of ρ , i.e. the set of all elements which commute with ρ .

Hence, we can define the submanifold \mathcal{S}_ρ to be given by the homogeneous space G_0/G_ρ . In [13] it is shown that indeed, on each such leaf \mathcal{S}_ρ we can obtain a suitable 2-form by inverting σ , which is closed. Therefore $(\mathcal{S}_\rho, \sigma-1)$ defines a proper symplectic phase space structure with the hamiltonian flow being generated by $\{h_\infty, \cdot\}$.

Here, we will not comment on the proof, but have a closer look at the structure of the phase space \mathcal{S}_ρ . For illustrative reasons, we restrict ourselves to the case $M = 2$, which we analyse in detail in chapter 9. In this case, the state space is equivalent to the set of normalized hermitian 2×2 matrices and hence equivalent to a 3-ball.

Let us denote the eigenvalues of the state ρ by ρ_1, ρ_2 . The tangent space at the identity G_0 contains the set of first order derivatives and is equivalent to the set of hermitian matrices \mathcal{M}_2 , thus $\dim G_0 = 2^2 = 4$. If we assume that $\rho_1 \neq \rho_2$, the centralizer contains only multiples of the identity. Therefore, the quotient space G_0/G_ρ is 2-dimensional and equivalent to a 2-sphere of constant radius. Furthermore, the orbits of the flow are given by the level lines of h_∞ . Some examples for such systems are depicted in figure 9.4. For the completely mixed state, $\rho_1 = \rho_2 = 1/2$, the centralizer is equivalent to \mathcal{M}_2 . Hence, the phase space G_0/G_ρ is simply given by the center of the Bloch sphere.

Note that while the above reasoning started from the mean-field dynamics and showed that it is possible to restrict the state space to a submanifold with a symplectic structure

which can be identified with the phase space one can also start the other way round: Using the phase space approach discussed in the preceding chapter, we define the phase space as the coset space (6.4) respective the parameter space of the coherent states. For the Glauber coherent states, the coset space is given by $H_4/U(1) \otimes U(1) \cong \mathbb{C}$. This is a complex space with an explicit diagonal metric. Hence, there is a symplectic structure [73]. With the parameter transformation $\alpha = 1/2(p+iq)$, the standard 2-form is given by $\omega = dp \wedge dq$, which induces the well known Poisson-bracket.

For the $SU(M)$ coherent states, the coset space (6.13) is given by $SU(M)/U(M-1)$. Hence for $SU(M)$ coherent states the phase space is isomorphic to a multi-dimensional sphere \mathcal{S}_{M-1} , which is again a complex space with an explicit metric. A straightforward, but quite lengthy computation shows that using a suitable parametrization (6.51), we indeed obtain the Poisson bracket (7.41). For more details, see [51, 55].

7.2.4 Some comments on dissipative systems

The general theory of dynamical mean-field semigroups [12] is not restricted to hamiltonian systems, but provides a description for arbitrary generators supposed their scaling properties are appropriate. In detail, we require G_N to be a sequence of bounded polynomial generators of degree g , that is a sequence of operators $(G_N)_{N \geq g}$ with $G_N \in \mathcal{B}(\mathcal{A}^{\otimes N})$ with

$$G_N = \frac{N}{g} \text{sym}_N(G_g) = \frac{1}{g(N-1)!} \sum_{\pi} \pi(G_g \otimes \text{id}_{N-g}) \pi^{-1}. \quad (7.48)$$

For this class of generators the limiting dynamics are given by a flow. This result can be even extended to approximately polynomial generators [12].

In the second part of this thesis, we are especially interested in the dynamics generated by the Lindblad master equation in second quantized form

$$\begin{aligned} \dot{\hat{\rho}} = & -i[\hat{H}, \hat{\rho}] - \frac{\kappa}{2} \sum_j^M (\hat{n}_j^2 \hat{\rho} + \hat{\rho} \hat{n}_j^2 - 2\hat{n}_j \hat{\rho} \hat{n}_j) \\ & - \frac{1}{2} \sum_j^M \gamma_{\text{atoms},j} \left(\hat{a}_j^\dagger \hat{a}_j \hat{\rho} + \hat{\rho} \hat{a}_j^\dagger \hat{a}_j - 2\hat{a}_j \hat{\rho} \hat{a}_j^\dagger \right), \end{aligned} \quad (7.49)$$

which will be introduced and motivated in detail in section 8.5.1. This approach takes into account two major effects, phase noise described by the term proportional to κ and localized loss processes with a site-dependent dissipation rate $\gamma_{\text{atoms},j}$. As the last term does not conserve the particle number it is not readily covered by the general approach. Still note that the resulting mean-field dynamics which are discussed extensively in the second part suggest that it might be possible to extend the rigorous results.

Hence, in this section we will restrict the analysis to the effects of phase noise, which is described by the following master equation

$$\frac{d}{dt} \rho = -\frac{\kappa}{2} \sum_{j=1}^M \hat{n}_j^2 \rho - \rho \hat{n}_j^2 - 2\hat{n}_j \rho \hat{n}_j. \quad (7.50)$$

Because of the appearance of quadratic terms in \hat{n}_j the scaling with the particle number is not obvious at first sight. To reveal the scaling properties more clearly, we calculate the resulting dynamics of an arbitrary single-particle operator, say $\hat{a}_j^\dagger \hat{a}_k$, in the Heisenberg picture

$$\begin{aligned}
\frac{d}{dt} \hat{a}_j^\dagger \hat{a}_k &= \mathcal{L} \hat{a}_j^\dagger \hat{a}_k \\
&= -\frac{\kappa}{2} \sum_{j=1}^M \hat{n}_j^2 \hat{a}_j^\dagger \hat{a}_k - \hat{a}_j^\dagger \hat{a}_k \hat{n}_j^2 - 2\hat{n}_j \hat{a}_j^\dagger \hat{a}_k \hat{n}_j \\
&= -\kappa(1 - \delta_{j,k}) \hat{a}_j^\dagger \hat{a}_k.
\end{aligned} \tag{7.51}$$

Thus it is evident that phase noise is just a single-particle effect, that degrades all coherences at a constant rate κ .

In the language of symmetrized operators, the master equation can be rewritten as

$$\frac{d}{dt} \rho_N = \mathcal{L}_N(\rho_N), \tag{7.52}$$

where the N -particle Liouvillian \mathcal{L}_N is obtained by symmetrizing the corresponding single-particle Liouvillian:

$$\begin{aligned}
\mathcal{L}_N &= N \text{sym}_N \mathcal{L}_1 \\
&= \sum_{a=1}^N \mathbb{1} \otimes \cdots \otimes \mathcal{L}_1^{(a)} \otimes \mathbb{1} \otimes \cdots \otimes \mathbb{1},
\end{aligned} \tag{7.53}$$

where the superscript (a) refers to the a -th particle. In the case of phase noise, the single-particle Liouvillian is given by

$$\mathcal{L}_1(\rho_1) = -\kappa \sum_{j=1}^M \frac{1}{M} \rho_1 - \hat{e}_{jj} \rho_1 \hat{e}_{jj}. \tag{7.54}$$

The dynamics generated by the phase noise Liouvillian \mathcal{L}_N is a rather simple example of an irreversible mean-field convergent dynamics. A general account of this topic is given in [12]. We will not go into details here and just note that the scaling factor $\sim N$ in equation (7.53) is essential. To illustrate this issue we give a simple example

by calculating the evolution equation for a symmetrized single-particle operator

$$\begin{aligned}
\frac{d}{dt} \text{sym}_N(\hat{e}_{jk}) &= N \text{sym}_N(\mathcal{L}_1) \text{sym}_N(\hat{e}_{jk}) \\
&= \frac{1}{N} \sum_{\substack{a \neq b \\ a, b=1}}^N \mathbb{1} \otimes \cdots \otimes \underbrace{\mathcal{L}_1^{(a)}(\mathbb{1})}_{=0} \otimes \mathbb{1} \otimes \cdots \otimes \hat{e}_{jk}^{(b)} \cdots \otimes \mathbb{1} \\
&\quad + \frac{1}{N} \sum_{a=1}^N \mathbb{1} \otimes \cdots \otimes \underbrace{\mathcal{L}_1(\hat{e}_{jk})^{(a)}}_{=-\kappa(1-\delta_{jk})\hat{e}_{jk}} \otimes \mathbb{1} \otimes \cdots \otimes \mathbb{1} \\
&= -\kappa(1 - \delta_{jk}) \frac{1}{N} \sum_{a=1}^N \mathbb{1} \otimes \cdots \otimes \hat{e}_{jk} \otimes \mathbb{1} \otimes \cdots \otimes \mathbb{1} \\
&= -\kappa(1 - \delta_{jk}) \text{sym}_N(\hat{e}_{jk}). \tag{7.55}
\end{aligned}$$

Hence, to leading order the time derivative vanishes and only the rescaling by N assures that one recovers a mean-field convergent expression. Furthermore, this calculation once more demonstrates the significance of the collision terms as all other terms vanish.

7.3 Applications of the phase space approach

We have already seen that the phase space approach provides an illustrative way to explicitly calculate the resulting hamiltonian flow including the first order corrections in $1/N$. However, the approach is not limited to dynamical questions, but has a wide range of possible applications. In particular, we will discuss two possible ways to derive a phase space version of the finite de Finetti theorem, which provide an illustrative insight in the relations of the de Finetti theorem to different phase space distributions and in particular to the purity of the state. Moreover, we obtain a nice corollary in the context of Renyi-Wehrl entropies. In the last section, a quite simple calculation illustrates that one can also use the phase space approach to determine bounds on the ground state energy and at least an interval for the $1/N$ corrections, even if these are not optimal.

7.3.1 A quantum de Finetti theorem starting from differential operators

In section 2.5 we have discussed the relation between finite quantum de Finetti theorems and mean-field systems. In this section, we show how we can use the \mathcal{D} -algebraic formalism introduced earlier to derive a similar bound to the one given in the de Finetti theorem, while in the next section, we analyse the relation of the theorem 14 to the generalized phase space distributions and the $SU(M)$ coherent states.

First of all, we paraphrase the problem addressed by the Quantum de Finetti theorem (14) in the language of second quantization:

Given a symmetric N -partite quantum state ρ_N , we consider the k -body reduced density matrix

$$\rho_k = \text{tr}_{N-k} \rho_N, \quad (7.56)$$

tracing out $N - k$ particles. In the language of creation and annihilation operators the reduced k -body density matrix is given by

$$\rho_k(j_1 j_2 \dots j_k; \ell_1 \ell_2 \dots \ell_k) = \frac{(N - k)!}{N!} \langle \hat{a}_{\ell_1}^\dagger \hat{a}_{\ell_2}^\dagger \dots \hat{a}_{j_1} \hat{a}_{j_2} \dots \rangle \quad (7.57)$$

These quantities are very important, for example the energy expectation value $\langle \hat{H} \rangle$ is completely determined by ρ_1 and ρ_2 if we have a Hamiltonian consisting of one-body terms and two-body interaction terms only. As is the case in the typical example of a quantum mean-field system with pairwise interactions (2.4) and in particular for the special example of the Bose-Hubbard Hamiltonian (7.1).

Now the quantum de Finetti theorem (14) promises that ρ_k can be approximated by a convex sum of product states

$$\rho_k \simeq \int \sigma^{\otimes k} d\mu(\sigma) \quad (7.58)$$

up to an error which vanishes as N^{-1} [11, 20–24].

Exact bounds have been derived for both, finite dimensional subsystems [29, 30], as well as infinite dimensional subsystems [31]. Here, we will prove a similar relation for the finite dimensional case using the \mathcal{D} -algebraic approach introduced in section 6.2 based on the $SU(M)$ coherent states (6.18). In the following, \mathbf{x} refers to the parametrization of $SU(M)$ coherent states in terms of the complex amplitudes $|\mathbf{x}\rangle = |x_1, x_2, \dots, x_M\rangle$ as defined in (6.28).

Theorem 27 (A quantum de Finetti theorem starting from differential operators). *Let ρ_N be a Bose-symmetric N -partite quantum state on the Hilbert space $(\mathbb{C}^M)^{\otimes N}$ that is $\pi\rho_N = \rho_N$ for arbitrary permutations $\pi \in S_N$. Then the reduced k -particle density matrix $\rho_k = \text{tr}_{N-k} \rho_N$ can be approximated by a convex combination of product states, respective $SU(M)$ coherent states*

$$\tilde{\rho}_k = \int d\mu(\mathbf{x}) S(\mathbf{x}) |\mathbf{x}\rangle \langle \mathbf{x}|, \quad (7.59)$$

where $S(\mathbf{x})$ is a probability density on $\mathcal{S}^{2(M-1)}$. The error of this approximation vanishes as N^{-1} ,

$$\|\rho_k - \tilde{\rho}_k\|_1 \leq \frac{k(M-1) + 2k^2}{N} + \mathcal{O}(N^{-2}), \quad (7.60)$$

where $\|\cdot\|_1$ denotes the trace norm.

Note that one particular choice for the probability distribution $S(\mathbf{x})$ is given by the Husimi function $Q(\mathbf{x}) = \langle \mathbf{x} | \rho_N | \mathbf{x} \rangle$, but that this is not necessarily optimal. For example if ρ_N is already a product state $|\mathbf{x}_0\rangle \langle \mathbf{x}_0|$, then the best choice is the point measure $\mathcal{S}(\mathbf{x}) = \delta(\mathbf{x} - \mathbf{x}_0)$, which is equivalent to the P -representation of the coherent state. Hence, this choice yields the exact result. However, the choice $Q_N(\mathbf{x})$ gives a measurable approximation for all possible quantum states ρ_N and also yields the upper bound for the error discussed earlier.

Proof. Here, we just sketch the basic idea and omit the technical parts wherever the explicit calculations are straightforward.

If we use the \mathcal{D} -algebraic calculus introduced in section 6.2, the expectation value needed to determine the k -body reduced density matrix

$$\begin{aligned} \rho_k(j_1 j_2 \dots j_k; \ell_1 \ell_2 \dots \ell_k) &= \frac{(N-k)!}{N!} \langle \hat{a}_{\ell_1}^\dagger \hat{a}_{\ell_2}^\dagger \dots \hat{a}_{j_1} \hat{a}_{j_2} \dots \rangle \\ &= \frac{(N-k)!}{N!} \int \mathcal{D}^\ell(\hat{E}_{\ell_1 j_1} \dots \hat{E}_{\ell_k j_k}) Q(\mathbf{x}) d\mu(\mathbf{x}) \end{aligned} \quad (7.61)$$

can be evaluated to next-to-leading order in terms of the Q -function. This involves a quite lengthy calculation, some commutation relations, lots of integration by parts, as well as tedious bookkeeping of indices. Therefore we only state the result:

$$\begin{aligned} \langle \hat{a}_{\ell_1}^\dagger \hat{a}_{\ell_2}^\dagger \dots \hat{a}_{j_1} \hat{a}_{j_2} \dots \rangle &= N^k \int x_{\ell_1}^* x_{\ell_2}^* \dots x_{j_1} x_{j_2} \dots Q(\mathbf{x}) d\mu(\mathbf{x}) \\ &+ N^{k-1} \left(kM + \frac{k(k-1)}{2} \right) \int x_{\ell_1}^* x_{\ell_2}^* \dots x_{j_1} x_{j_2} \dots Q(\mathbf{x}) d\mu(\mathbf{x}) \\ &- N^{k-1} \sum_{a,b=1}^k \delta_{\ell_b j_a} \int x_{\ell_1}^* \dots x_{\ell_{b-1}}^* x_{\ell_{b+1}}^* \dots x_{j_1} \dots x_{j_{a-1}} x_{j_{a+1}} \dots Q(\mathbf{x}) d\mu(\mathbf{x}) \\ &+ \mathcal{O}(N^{-2}). \end{aligned} \quad (7.62)$$

Note, that the order N^k does not contain any differentiation, while the term proportional to N^{k-1} does contain a single differentiation and so on. Removing this differentiation by an integration by parts yields the terms in the second and third line of equation (7.62). As we are only interested in the next-to-leading order, we will also expand the prefactor of equation (7.57) as

$$\begin{aligned} \frac{N^k(N-k)!}{N!} &= 1 + \frac{k(k-1)}{2N} + \mathcal{O}(N^{-2}) \\ \frac{N^{k-1}(N-k)!}{N!} &= \frac{1}{N} + \mathcal{O}(N^{-2}). \end{aligned} \quad (7.63)$$

In total, we find

$$\begin{aligned}
& \rho_k(j_1 j_2 \dots j_k ; \ell_1 \ell_2 \dots \ell_k) \\
&= \int x_{\ell_1}^* x_{\ell_2}^* \dots x_{j_1} x_{j_2} \dots Q(\mathbf{x}) d\mu(\mathbf{x}) \\
&\quad + \frac{kM + k(k-1)}{N} \int x_{\ell_1}^* x_{\ell_2}^* \dots x_{j_1} x_{j_2} \dots Q(\mathbf{x}) d\mu(\mathbf{x}) \\
&\quad - \frac{1}{N} \sum_{a,b=1}^k \delta_{\ell_b j_a} \int x_{\ell_1}^* \dots x_{\ell_{b-1}}^* x_{\ell_{b+1}}^* \dots x_{j_1} \dots x_{j_{a-1}} x_{j_{a+1}} \dots Q(\mathbf{x}) d\mu(\mathbf{x}) \\
&\quad + \mathcal{O}(N^{-2}).
\end{aligned} \tag{7.64}$$

In contrast, the matrix elements of the approximation $\tilde{\rho}_k$ with $S(\mathbf{x}) = Q_N(\mathbf{x})$ are simply given by

$$\tilde{\rho}_k(j_1 j_2 \dots j_k ; \ell_1 \ell_2 \dots \ell_k) = \int x_{\ell_1}^* x_{\ell_2}^* \dots x_{j_1} x_{j_2} \dots Q(\mathbf{x}) d\mu(\mathbf{x}), \tag{7.65}$$

such that the error in leading order given by the difference

$$E(j_1 j_2 \dots j_k ; \ell_1 \ell_2 \dots \ell_k) = \rho_k(j_1 j_2 \dots j_k ; \ell_1 \ell_2 \dots \ell_k) - \tilde{\rho}_k(j_1 j_2 \dots j_k ; \ell_1 \ell_2 \dots \ell_k).$$

Using the above result (7.64) and identifying once again the integrals with the reduced density matrices yields:

$$\begin{aligned}
E(j_1 \dots j_k ; \ell_1 \dots \ell_k) &= \frac{k(M-1) + k^2}{N} \rho_k(j_1 j_2 \dots j_k ; \ell_1 \ell_2 \dots \ell_k) \\
&\quad - \frac{1}{N} \sum_{a,b=1}^k \delta_{\ell_b j_a} \rho_{k-1}(j_1 j_2 \dots j_{a-1} j_{a+1} \dots ; \ell_1 \ell_2 \dots \ell_{b-1} \ell_{b+1} \dots) \\
&\quad + \mathcal{O}(N^{-2}).
\end{aligned} \tag{7.66}$$

Collecting all these elements, the error $E = \rho_k - \tilde{\rho}_k$ can be recast into matrix form

$$E = \frac{k(M-1)}{N} \rho_k + \frac{1}{N} \sum_{a,b=1}^N (\rho_k - \pi_{a,k}(\rho_{k-1} \otimes \mathbb{1})\pi_{b,k}) + \mathcal{O}(N^{-2}), \tag{7.67}$$

where $\pi_{a,k}$ denotes the permutation of particles a and k . This result can be checked by simply calculating the elements of E and using the Bose symmetry of the reduced density matrices ρ_{k-1} . Hence, starting from the trace norms of the reduced density matrices,

$$\begin{aligned}
\|\rho_k\|_1 &= 1 \\
\|\pi_{a,k}(\rho_{k-1} \otimes \mathbb{1})\pi_{b,k}\|_1 &= 1,
\end{aligned} \tag{7.68}$$

we can give an upper bound on the leading term of the error using the triangular inequality:

$$\|E\|_1 \leq \frac{k(M-1) + 2k^2}{N}. \tag{7.69}$$

□

7.3.2 A quantum de Finetti theorem in phase space

In the last section, we have seen how we can use the \mathcal{D} -algebraic formalism introduced in section 6.2 to explicitly calculate bounds on the de Finetti approximation. In this section, we present a more general approach to derive a Quantum de Finetti type theorem based on the concept of generalized phase space distributions for $SU(M)$ coherent states.

In section 6.3.1, we have introduced the P -representation of the N -particle state ρ_N ,

$$\rho_N = \int P_N(\mathbf{x}) |\mathbf{x}\rangle \langle \mathbf{x}|_N d\mu_N(\mathbf{x}), \quad (7.70)$$

where $d\mu_N(\mathbf{x})$ denotes for the invariant measure on the phase space corresponding to N particles. Moreover, the Q - or Husimi representation is defined as

$$Q_N(\mathbf{x}) = \langle \mathbf{x} | \rho_N | \mathbf{x} \rangle_N,$$

and is thus closely related to the P -distribution:

$$\begin{aligned} Q_N(\mathbf{x}) &= \langle \mathbf{x} |_N \int P_N(\mathbf{y}) |\mathbf{y}\rangle \langle \mathbf{y}|_N d\mu_N(\mathbf{y}) | \mathbf{x} \rangle_N \\ &= \int P_N(\mathbf{y}) |\langle \mathbf{y} | \mathbf{x} \rangle|^{2N} d\mu_N(\mathbf{y}). \end{aligned} \quad (7.71)$$

Here, $|\mathbf{x}\rangle_N$ denotes the $SU(M)$ -coherent states (6.18),

$$|\mathbf{x}\rangle_N = \frac{1}{\sqrt{N!}} \left(\sum_{k=1}^M x_k \hat{a}_k^\dagger \right)^N |0, 0, \dots, 0\rangle, \quad (7.72)$$

which are equivalent to the product states parametrized by the complex amplitudes (x_1, \dots, x_M) with $\sum_{i=1}^M x_i^* x_i = 1$. Due to this property, tracing out $N - k$ particles just results in a reduction of tensor factors,

$$|\mathbf{x}\rangle_N = |\mathbf{x}\rangle^{\otimes N} \quad \Rightarrow \quad \text{tr}_{N-k} |\mathbf{x}\rangle \langle \mathbf{x}|^{\otimes N} = |\mathbf{x}\rangle \langle \mathbf{x}|^{\otimes k}. \quad (7.73)$$

While the P -distribution is in general not positive definite, often singular and sometimes not even unique, the Q -function provides a positive definite and normalized functional, but does not give the right marginal distributions. Still, we can interpret it as a probability distribution on the set of product states and thus use it as a special choice of the measure for the approximation in the Quantum de Finetti theorem. This particular choice not necessarily gives the best approximation, but yields an upper bound on the error of the approximation.

In the following, we will be concerned with the evaluation of integrals on the finite dimensional phase space more than once. In this context, we are especially interested in the relationship between the reduced k -particle state $\rho_k := \text{tr}_{N-k} \rho_N$ and the full

N -particle state ρ_N , and therefore in the relations between different particle numbers. The size of the Hilbert space (cf. e.g. [74])

$$\dim \mathcal{H}_{M,N} = \frac{(M+N-1)!}{N!(M-1)!}, \quad (7.74)$$

depends on the number of particles N , as well as on the number of lattice sites M . This can be translated into a relation between the measures $d\mu_N(\mathbf{x})$ and $d\mu_{N+k}(\mathbf{x})$ linking the phase spaces corresponding to different particle numbers,

$$\begin{aligned} d\mu_N(\mathbf{x}) &= \frac{\dim \mathcal{H}_{M,N}}{\dim \mathcal{H}_{M,N+k}} d\mu_{N+k}(\mathbf{x}) \\ &= \frac{(M+N-1)!}{N!} \frac{(N+k)!}{(M+N+k-1)!} d\mu_{N+k}(\mathbf{x}). \end{aligned} \quad (7.75)$$

This result will turn out to be extremely useful in the following calculations. As a first application, we can use it to prove the relation,

$$\begin{aligned} \int |\mathbf{x}\rangle \langle \mathbf{x}|^{\otimes N+k} d\mu_N(\mathbf{x}) &= \frac{(M+N-1)!}{(M+N+k-1)!} \frac{(N+k)!}{N!} \int |\mathbf{x}\rangle \langle \mathbf{x}|^{\otimes N+k} d\mu_{N+k}(\mathbf{x}) \\ &= \frac{(M+N-1)!}{(M+N+k-1)!} \frac{(N+k)!}{N!} \mathbb{1}_{N+k}, \end{aligned} \quad (7.76)$$

where we have exploited the overcompleteness of the generalized coherent states

$$\int |\mathbf{x}\rangle \langle \mathbf{x}|^{\otimes N} d\mu_N(\mathbf{x}) = \mathbb{1}_N. \quad (7.77)$$

With these preliminary considerations, we can state the main result of this section:

Theorem 28 (A quantum de Finetti theorem based on generalized phase space distributions). *Let ρ_N be a Bose-symmetric N -partite quantum state on the Hilbert space $(\mathbb{C}^M)^{\otimes N}$. Then the reduced k -particle density matrix $\rho_k = \text{tr}_{N-k} \rho_N$ can be approximated by a convex combination of product states, that is $SU(M)$ coherent states*

$$\tilde{\rho}_k = \int d\mu(\mathbf{x}) S(\mathbf{x}) |\mathbf{x}\rangle \langle \mathbf{x}|, \quad (7.78)$$

where $S(\mathbf{x})$ is a probability density on $\mathcal{S}^{2(M-1)}$.

If we assume that $\text{tr}(\tilde{\rho}_k^2) \leq \text{tr}(\rho_k^2) \leq 1$, the error of the approximation is bounded as

$$\|\rho_k - \tilde{\rho}_k\|_2^2 \leq \frac{2k^2 M}{N}, \quad (7.79)$$

where $\|\cdot\|_2$ denotes the Frobenius norm which is defined as $\|A\|_2^2 = \text{tr}(A^\dagger A)$. In particular for the important case of the reduced single-particle density matrix, i.e. $k =$

1, and for the special choice $S(\mathbf{x}) = Q_N(\mathbf{x})$ of the measure on the set of product states $|\mathbf{x}\rangle_N$,

$$\tilde{\rho}_k = \int Q_N(\mathbf{x}) |\mathbf{x}\rangle \langle \mathbf{x}|^{\otimes k} d\mu_N(\mathbf{x}) \quad (7.80)$$

the bound is exactly given by

$$\|\rho_1 - \tilde{\rho}_1\|_2^2 = \text{tr}(\tilde{\rho}_1^2) - \frac{N-M}{N+M} \text{tr}(\rho_1^2) - \frac{2}{M+N}. \quad (7.81)$$

If we assume $\text{tr}(\tilde{\rho}_1^2) \leq \text{tr}(\rho_1^2) \leq 1$, this can be further simplified to:

$$\begin{aligned} \|\rho_1 - \tilde{\rho}_1\|_2^2 &\leq \frac{2M}{M+N} \text{tr}(\rho_k^2) - \frac{2}{M+N} \\ &\leq \frac{2(M-1)}{M+N}. \end{aligned} \quad (7.82)$$

Proof. As the 2-norm quantifying the error made by the approximation of ρ_k by the state $\tilde{\rho}_k$ is given by

$$\begin{aligned} \|\rho_k - \tilde{\rho}_k\|_2^2 &= \text{tr}((\rho_k - \tilde{\rho}_k)^\dagger (\rho_k - \tilde{\rho}_k)) \\ &= \text{tr}(\rho_k^2) + \text{tr}(\tilde{\rho}_k^2) - 2\text{tr}(\rho_k \tilde{\rho}_k), \end{aligned} \quad (7.83)$$

the proof of theorem 28 proceeds in two major steps. First we calculate the overlap $\text{tr}(\rho_k \tilde{\rho}_k)$ using the P -representation (7.70). In a second step, we then look for a good estimate of the overlap.

In the P -representation the corresponding reduced k -particle density matrix ρ_k of the full N -particle density matrix

$$\rho_N = \int P_N(\mathbf{x}) |\mathbf{x}\rangle \langle \mathbf{x}|^{\otimes N} d\mu_N(\mathbf{x}) \quad (7.84)$$

is due to the property (7.73) simply given by

$$\rho_k = \text{tr}_{N-k} \rho_N = \int P_N(\mathbf{x}) |\mathbf{x}\rangle \langle \mathbf{x}|^{\otimes k} d\mu_N(\mathbf{x}). \quad (7.85)$$

The approximation $\tilde{\rho}_k$ by the convex combination of product states distributed according to the Q -function expressed in terms of the P -distribution (7.71) reads:

$$\begin{aligned} \tilde{\rho}_k &= \int Q_N(\mathbf{x}) |\mathbf{x}\rangle \langle \mathbf{x}|^{\otimes k} d\mu_N(\mathbf{x}) \\ &= \int \int P_N(\mathbf{y}) |\langle \mathbf{x}|\mathbf{y}\rangle|^{2N} |\mathbf{x}\rangle \langle \mathbf{x}|^{\otimes k} d\mu_N(\mathbf{x}) d\mu_N(\mathbf{y}). \end{aligned} \quad (7.86)$$

Thus, the overlap between the exact state ρ_k and its approximation $\tilde{\rho}_k$ can be calculated as

$$\text{tr}(\rho_k \tilde{\rho}_k) = \int \int P_N(\mathbf{z}) P_N(\mathbf{y}) \int |\langle \mathbf{z}|\mathbf{x}\rangle|^{2k} \cdot |\langle \mathbf{y}|\mathbf{x}\rangle|^{2N} d\mu_N(\mathbf{x}) d\mu_N(\mathbf{y}) d\mu_N(\mathbf{z}). \quad (7.87)$$

Now the major difficulty is to find a suitable estimate for the integral (7.87). The technical considerations for establishing such a bound are summarized in the following lemma, which we will prove at the end of this section.

Lemma 29. *For arbitrary $k, N, M \in \mathbb{N}$ the following integral is bounded from below by*

$$\begin{aligned} & \int |\langle \mathbf{z} | \mathbf{x} \rangle|^{2k} \cdot |\langle \mathbf{y} | \mathbf{x} \rangle|^{2N} d\mu_N(\mathbf{x}) \\ & \geq \frac{(M + N - 1)!}{(M + N + k - 1)!} \frac{N!}{(N - k)!} |\mathbf{y} \cdot \mathbf{z}|^{2k}. \end{aligned}$$

Moreover, in the special case $k = 1$, one gets the exact result

$$\int |\langle \mathbf{z} | \mathbf{x} \rangle|^2 \cdot |\langle \mathbf{y} | \mathbf{x} \rangle|^{2N} d\mu_N(\mathbf{x}) = \frac{1}{M + N} (1 + N |\mathbf{y} \cdot \mathbf{z}|^2). \quad (7.88)$$

Now we can calculate a lower bound on the overlap between $\rho_k = \text{tr}_{N-k} \rho_N$ and the approximation $\tilde{\rho}_k$ (7.86) and thus give a proper estimate for the 2-norm of the difference of ρ_k and $\tilde{\rho}_k$ (7.83), which finally completes the proof of theorem 28.

Using lemma 29, the overlap $\text{tr}(\rho_k \tilde{\rho}_k)$ for arbitrary k can be estimated as

$$\begin{aligned} \text{tr}(\rho_k \tilde{\rho}_k) &= \int \int P_N(\mathbf{z}) P_N(\mathbf{y}) \int |\langle \mathbf{z} | \mathbf{x} \rangle|^{2k} \cdot |\langle \mathbf{y} | \mathbf{x} \rangle|^{2N} d\mu_N(\mathbf{x}) d\mu_N(\mathbf{y}) d\mu_N(\mathbf{z}). \quad (7.89) \\ &\geq \frac{(M + N - 1)!}{(M + N + k - 1)!} \frac{N!}{(N - k)!} \int \int P_N(\mathbf{z}) P_N(\mathbf{y}) |\langle \mathbf{y} | \mathbf{z} \rangle|^{2k} d\mu_N(\mathbf{z}) d\mu_N(\mathbf{y}). \end{aligned}$$

A closer analysis shows that the remaining integral exactly gives the trace of the squared density matrix,

$$\text{tr}(\rho_k^2) = \int \int P_N(\mathbf{z}) P_N(\mathbf{y}) |\langle \mathbf{y} | \mathbf{z} \rangle|^{2k} d\mu_N(\mathbf{z}) d\mu_N(\mathbf{y}), \quad (7.90)$$

which is a measure of the purity of the state. Therefore, we can rewrite the estimate as

$$\text{tr}(\rho_k \tilde{\rho}_k) \geq \frac{(M + N - 1)!}{(M + N + k - 1)!} \frac{N!}{(N - k)!} \text{tr}(\rho_k^2). \quad (7.91)$$

As expected from mean-field theory (or alternatively as promised by the theorem of Størmer [20], see e.g. section 2.5), this converges to one for a pure state, $\text{tr}(\rho_k^2) = 1$, in the macroscopic limit $N \rightarrow \infty$ with M, k fixed.

Now we have everything at hand to finally prove the theorem 28. For arbitrary k , the distance in the 2-norm between the reduced k -particle density ρ_k and the approximation $\tilde{\rho}_k$, respectively the error of the approximation can be estimated as (cf. equation (7.91)),

$$\begin{aligned} \|\rho_k - \tilde{\rho}_k\|_2^2 &= \text{tr}(\rho_k^2) + \text{tr}(\tilde{\rho}_k^2) - 2 \text{tr}(\rho_k \tilde{\rho}_k) \\ &\leq \text{tr}(\rho_k^2) + \text{tr}(\tilde{\rho}_k^2) - 2 \frac{(M + N - 1)!}{(M + N + k - 1)!} \frac{N!}{(N - k)!} \text{tr}(\rho_k^2). \quad (7.92) \end{aligned}$$

Assuming that $\text{tr}(\tilde{\rho}_k^2) \leq \text{tr}(\rho_k^2) \leq 1$, we finally get the promised bound on the error:

$$\begin{aligned} \|\rho_k - \tilde{\rho}_k\|_2^2 &\leq 2 \left(1 - \frac{(M+N-1)!}{(M+N+k-1)!} \frac{N!}{(N-k)!} \right) \text{tr}(\rho_k^2) \\ &\leq 2 \frac{k^2 M}{N}. \end{aligned} \quad (7.93)$$

For the special case $k = 1$, we don't even need an estimate, but get the exact result from lemma 29:

$$\begin{aligned} \text{tr}(\rho_1 \tilde{\rho}_1) &= \int \int P_N(\mathbf{z}) P_N(\mathbf{y}) \int |\langle \mathbf{z} | \mathbf{x} \rangle|^2 |\langle \mathbf{y} | \mathbf{x} \rangle|^{2N} d\mu_N(\mathbf{x}) d\mu_N(\mathbf{z}) d\mu_N(\mathbf{y}) \\ &= \frac{(M+N-1)!}{(M+N)!} \frac{N!}{(N-1)!} \frac{1}{N+1} \\ &\quad \cdot \int \int P_N(\mathbf{z}) P_N(\mathbf{y}) (1 + N |\mathbf{y} \cdot \mathbf{z}|^2) d\mu_N(\mathbf{z}) d\mu_N(\mathbf{y}) \\ &= \frac{1}{M+N} + \frac{N}{N+M} \text{tr}(\rho_1^2), \end{aligned} \quad (7.94)$$

where we used again the relation (7.90).

Thus, the 2-norm of the difference of ρ_k and $\tilde{\rho}_k$ (7.83) is given by

$$\begin{aligned} \|\rho_1 - \tilde{\rho}_1\|_2^2 &= \text{tr}(\rho_1^2) \left(1 - \frac{2N}{N+M} \right) + \text{tr}(\tilde{\rho}_1^2) - \frac{2}{M+N} \\ &= \text{tr}(\tilde{\rho}_1^2) - \frac{N-M}{M+N} \text{tr}(\rho_1^2) - \frac{2}{M+N}. \end{aligned} \quad (7.95)$$

Moreover, if we assume that $\text{tr}(\tilde{\rho}_1^2) \leq \text{tr}(\rho_1^2) \leq 1$, we get the following upper bound for the distance:

$$\begin{aligned} \|\rho_1 - \tilde{\rho}_1\|_2^2 &\leq \frac{2M}{N+M} \text{tr}(\rho_1^2) - \frac{2}{N+M} \\ &\leq \frac{2(M-1)}{N+M}. \end{aligned} \quad (7.96)$$

This finally proves the theorem. Note that this derivation does not only give the bound, but also yields by construction an explicitly expression for the state for which the bound is attained. \square

What remains to prove is the bound for the integral given lemma 29, which provided the estimate for the overlap.

Proof. To evaluate the central part of the integral 7.87, we introduce the definition

$$|\Psi\rangle = \frac{1}{(N+k)!} \sum_{\pi} \pi(|\mathbf{y}\rangle^{\otimes k} \otimes |\mathbf{z}\rangle^{\otimes N}), \quad (7.97)$$

where the sum is taken over all possible permutations π of the single-particle vectors $|\mathbf{y}\rangle$ and $|\mathbf{z}\rangle$ in the spirit of definition (2.6). Note that the vector $|\Psi\rangle$ is symmetric, but not normalized to one.

With the help of this definition, we can rewrite the central part of the integral (7.87), as follows:

$$\begin{aligned} & \int |\langle \mathbf{z} | \mathbf{x} \rangle|^{2k} \cdot |\langle \mathbf{y} | \mathbf{x} \rangle|^{2N} d\mu_N(\mathbf{x}) \\ &= \int |\langle \Psi | \mathbf{x} \rangle^{\otimes k} | \mathbf{x} \rangle^{\otimes N}|^2 d\mu_N(\mathbf{x}) \\ &= \langle \Psi | \int d\mu_N(\mathbf{x}) | \mathbf{x} \rangle \langle \mathbf{x} |^{\otimes N+k} | \Psi \rangle. \end{aligned}$$

Using the above result (7.76), we obtain

$$\begin{aligned} & \int |\langle \mathbf{z} | \mathbf{x} \rangle|^{2k} \cdot |\langle \mathbf{y} | \mathbf{x} \rangle|^{2N} d\mu_N(\mathbf{x}) \\ &= \frac{(M+N-1)!}{N!} \frac{(N+k)!}{(M+N+k-1)!} \langle \Psi | \Psi \rangle. \end{aligned} \quad (7.98)$$

Thus, we have reduced the problem to the calculation of the normalization $\langle \Psi | \Psi \rangle$ of the symmetric vector (7.97). Since this results again in the evaluation of the product of two symmetrized sums the combinatorics are completely analogous to the ones used in section 2.3. This can be seen most clearly for the simplest example $k=1$,

$$|\Psi\rangle = \frac{1}{N+1} \sum_{j=0}^N |\mathbf{y}\rangle^{\otimes j} |\mathbf{z}\rangle |\mathbf{y}\rangle^{\otimes N-j}, \quad (7.99)$$

where we get

$$\begin{aligned} \langle \Psi | \Psi \rangle &= \frac{1}{(N+1)^2} ((N+1) \langle \mathbf{y} | \mathbf{y} \rangle^N \langle \mathbf{z} | \mathbf{z} \rangle + N(N+1) \langle \mathbf{y} | \mathbf{y} \rangle^{N-1} \langle \mathbf{z} | \mathbf{y} \rangle \langle \mathbf{y} | \mathbf{z} \rangle) \\ &= \frac{1}{(N+1)} (1 + N |\mathbf{y} \cdot \mathbf{z}|^2). \end{aligned} \quad (7.100)$$

A comparison of the calculation to equation (2.11) clearly shows the analogies. Note that this also illustrates that the vector $|\Psi\rangle$ is not normalized for $\mathbf{y} \neq \mathbf{z}$.

For arbitrary k , we again can reorder the terms according to the number r of collision terms of $|\mathbf{y}\rangle$ and $|\mathbf{z}\rangle$. A similar calculation to the one presented in section 2.3 (see especially equation (2.13) et seqq.) yields the result:

$$\langle \Psi | \Psi \rangle = \sum_{r=0}^k c_{N+k}(k, k, r) |\mathbf{y} \cdot \mathbf{z}|^{2(k-r)}. \quad (7.101)$$

Analogously to the definition (2.14), the prefactor $c_{N+k}(k, k, r)$ is given by

$$\begin{aligned} c_{N+k}(k, k, r) &= \frac{k! k! N! N!}{(N+k)! r! (k-r)! (k-r)! (N-k+r)!} \\ &= \frac{N!}{(N+k)!} \frac{N!}{(N-k+r)!} r! \binom{k}{r}^2. \end{aligned} \quad (7.102)$$

as can be verified by simple combinatorics and careful counting.

Since only the terms with $r = 0$ contribute to leading order in $1/N$ (cf. equation (2.16)) and all summands are positive, we can approximate $\langle \Psi | \Psi \rangle$ as

$$\begin{aligned} \langle \Psi | \Psi \rangle &= \sum_{r=0}^k c_{N+k}(k, k, r) |\mathbf{y} \cdot \mathbf{z}|^{2(k-r)} \\ &\geq c_{N+k}(k, k, 0) |\mathbf{y} \cdot \mathbf{z}|^{2k} \\ &= \frac{N!^2}{(N+k)! (N-k)!} |\mathbf{y} \cdot \mathbf{z}|^{2k}. \end{aligned} \quad (7.103)$$

In summary we have found a lower bound for the central part of the integral (7.87):

$$\begin{aligned} &\int d\mu_N(\mathbf{x}) |\langle \mathbf{z} | \mathbf{x} \rangle|^{2k} \cdot |\langle \mathbf{y} | \mathbf{x} \rangle|^{2N} \\ &= \frac{(M+N-1)!}{N!} \frac{(N+k)!}{(M+N+k-1)!} \langle \Psi | \Psi \rangle \\ &\geq \frac{(M+N-1)!}{N!} \frac{(N+k)!}{(M+N+k-1)!} \frac{N!^2}{(N+k)! (N-k)!} |\mathbf{y} \cdot \mathbf{z}|^{2k} \\ &\geq \frac{(M+N-1)!}{(M+N+k-1)!} \frac{N!}{(N-k)!} |\mathbf{y} \cdot \mathbf{z}|^{2k}. \end{aligned} \quad (7.104)$$

This proves the lemma 29. □

7.3.3 Discussion of the bounds

Let us briefly compare our results on the error of the de Finetti approximation to the bounds obtained in the literature, in particular to the article by Christandl et al. [30]. Theorem 27 gives a comparable scaling for the error of the approximation to leading order, but includes an additional term $\sim k^2/N$ which is not present in [30]. Notably, our calculation is exact until the point where we have to invoke the triangle inequality. One might thus obtain a tighter bound if this step could be improved. On the other hand, theorem 28 is stated in terms of the Frobenius norm such that a comparison to the results of Christandl et al. is less straightforward. We note that the Frobenius is always smaller than the trace norm, $\|A\|_2 \leq \|A\|_1$, for all operators A . However, one observes that the bound for the Frobenius norm given in theorem 28 is weaker than the one derived for the trace norm – in particular it scales only as $N^{-1/2}$. Thus, there is surely room for improvement.

7.3.4 A note on quantum phase space entropies

Finally, we want to present another interesting application of the technical lemma 29 in the context of quantum phase space entropies. For the characterization of complex quantum states the generalized Renyi-Wehrl entropies $S_\rho^{(q)}$ have proven to be very useful. The generalized Renyi-Wehrl entropy is defined as

$$S_\rho^{(q)} := \frac{1}{1-q} \log W_\rho^{(q)}, \quad (7.105)$$

where $q > 0$ is the Renyi index and $W_\rho^{(q)}$ are the moments of the Husimi function:

$$W_\rho^{(q)} := \int d\mu(\mathbf{x}) Q_\rho(\mathbf{x})^q. \quad (7.106)$$

Note that the common von Neumann entropy is recovered in the limit $q \rightarrow 1$.

The following result establishes a connection between the second moment $W_\rho^{(2)}$ and the purity $\text{tr}(\rho_s^2)$ of the reduced density matrices $\rho_s = \text{tr}_{N-s} \rho_N$. Note that we use the index s instead the index k in order to avoid confusion later on. Hence, the corollary links the phase space distribution and the quantum entropies of the corresponding states. Moreover, it proves that the product states $\rho^{\otimes N}$ are the sole minimizers of the Renyi-Wehrl entropy $S_\rho^{(2)}$.

Corollary 30. *Given a Bose symmetric N -particle quantum state $\rho_N \in (\mathbb{C}^M)^{\otimes N}$. Then the second moment of its Husimi function is given by*

$$\begin{aligned} W_\rho^{(2)} &= \int d\mu_N(\mathbf{x}) \langle \mathbf{x}_N | \rho_N | \mathbf{x}_N \rangle^2 \\ &= \sum_{s=0}^N \frac{(N+M-1)! N!}{(2N+M-1)!} \binom{N}{s}^2 \text{tr}(\rho_s^2), \end{aligned} \quad (7.107)$$

where $\rho_s = \text{tr}_{N-s} \rho_N$ is the reduced s -particle density matrix. Furthermore, the second moment $W_\rho^{(2)}$ assumes its maximum and the Renyi-Wehrl entropy $S_\rho^{(2)}$ assumes its minimum if and only if ρ_N is a product state $\rho_N = \rho^{\otimes N}$.

Proof. We calculate the second moment explicitly starting from a decomposition of the Husimi function into the P -function:

$$W_\rho^{(2)} = \int d\mu_N(\mathbf{z}) \int d\mu_N(\mathbf{y}) P(\mathbf{z}) P(\mathbf{y}) \int d\mu_N(\mathbf{x}) |\mathbf{x} \cdot \mathbf{z}|^{2N} |\mathbf{x} \cdot \mathbf{y}|^{2N}. \quad (7.108)$$

The last integral can be evaluated as in lemma 29, setting $k = N$:

$$\begin{aligned} &\int d\mu_N(\mathbf{x}) |\mathbf{x} \cdot \mathbf{z}|^{2N} |\mathbf{x} \cdot \mathbf{y}|^{2N} \\ &= \sum_{r=0}^N \frac{(N+M-1)! (2N)!}{N! (2N+M-1)!} c_{2N}(N, N, r) |\mathbf{y} \cdot \mathbf{z}|^{2(N-r)}. \end{aligned} \quad (7.109)$$

Furthermore we use the relation

$$\begin{aligned}
& \int d\mu_N(\mathbf{z}) \int d\mu_N(\mathbf{y}) P(\mathbf{z}) P(\mathbf{y}) |\mathbf{y} \cdot \mathbf{z}|^{2(N-r)} \\
&= \text{tr} \left[\int d\mu_N(\mathbf{z}) |\mathbf{z}\rangle \langle \mathbf{z}|^{\otimes(N-r)} \times \int d\mu_N(\mathbf{y}) |\mathbf{y}\rangle \langle \mathbf{y}|^{\otimes(N-r)} \right] \\
&= \text{tr} (\rho_{N-r}^2).
\end{aligned} \tag{7.110}$$

For $r = N$ the integral equals one, such that we adopt the convention $\text{tr}(\rho_0^2) := 1$ in the following.

Inserting these two equations and the coefficients $c_{2N}(N, N, r)$ from equation (7.102) into the expression (7.108) for the second moment of the Husimi function finally yields the desired result:

$$W_\rho^{(2)} = \sum_{s=0}^N \frac{(N+M-1)!N!}{(2N+M-1)!} \binom{N}{s}^2 \text{tr}(\rho_s^2), \tag{7.111}$$

where we have set $s := N - r$.

Most importantly, all coefficients in the sum (7.111) are strictly positive. Thus, $W_\rho^{(2)}$ assumes its maximum if and only if

$$\text{tr}(\rho_s^2) = 1 \quad \forall s = 0, 1, \dots, N. \tag{7.112}$$

This is the case if and only if the original quantum state ρ_N is a product state

$$\rho_N = \rho^{\otimes N}. \tag{7.113}$$

As the Renyi-Wehrl entropy $S_\rho^{(2)}$ is strictly monotonously decreasing with $W_\rho^{(2)}$, the same condition holds for the minimum of $S_\rho^{(2)}$. This completes the proof. \square

While the fact that the product states are the sole minimizers of $S_\rho^{(q)}$ has been shown in a similar framework in [75], the illustrative connection to the purity of the reduced density matrices ρ_s was not addressed in this article.

7.3.5 The ground-state variational problem

In this section, we will discuss bounds for the ground state energy resulting from the Lieb-Berezin inequalities. These thermodynamic inequalities were independently proved by Lieb and Berezin in the context of quantum spin systems [76, 77] and provide upper and lower bounds for the quantum free energy in terms of classical free-energy functions based on $SU(2)$ coherent states. Later, their results were extended to quantum partition functions on arbitrary compact Lie groups by Simon [78].

In the following, the Q -representation of the Hamiltonian, that is the expectation value of the Hamiltonian \hat{H} in generalized coherent states $|\Omega\rangle$, will be denoted by

$$H_Q(\Omega) = \langle \Omega | \hat{H} | \Omega \rangle, \tag{7.114}$$

while the corresponding P -representation will be referred to as $H_P(\Omega)$, such that

$$\hat{H} = \int_X H_P(\Omega) |\Omega\rangle \langle \Omega| d\mu(\Omega). \quad (7.115)$$

In this language, the Lieb-Berezin inequalities are given by [51]

$$\int e^{-\beta H_Q(\Omega)} d\mu(\Omega) \leq \text{tr} e^{-\beta \hat{H}} \leq \int e^{-\beta H_P(\Omega)} d\mu(\Omega). \quad (7.116)$$

In the zero-temperature limit, the inequalities can be used to determine bounds for the ground-state energy:

Theorem 31 (Lieb-Berezin inequality for the ground state energy [51,79]). *The ground state energy E_G of a quantum system is bounded from below and above by*

$$\min_{\Omega} H_Q(\Omega) \geq E_G \geq \min_{\Omega} H_P(\Omega). \quad (7.117)$$

In the macroscopic limit $N \rightarrow \infty$ the difference between the bounds vanishes, $|H_Q(\Omega) - H_P(\Omega)| \rightarrow 0$.

For a detailed introduction to the general problem we refer to [78], while the connections to phase space functions are highlighted in [51]. Here, we will only present the basic idea and discuss its relation to the formalism based on the \mathcal{D} -algebra which we have introduced in section 6.2. Moreover, we will show how one can use the \mathcal{D} -algebraic formalism to explicitly evaluate these bounds for the ground state energy of the Bose-Hubbard Hamiltonian (7.1).

In general, the upper bound is rather easy to understand and to evaluate. By definition, the ground state ρ_G minimizes the energy functional $\langle E \rangle$, such that

$$\langle E \rangle = \text{tr}(\rho \hat{H}) \geq \text{tr}(\rho_G \hat{H}) := E_G \quad (7.118)$$

holds for every state ρ . Choosing in particular the $SU(M)$ coherent states (6.18) as trial states one finds

$$\min_{\Omega} \text{tr} \left(|\Omega\rangle \langle \Omega| \hat{H} \right) = \min_{\Omega} H_Q(\Omega) \geq E_G. \quad (7.119)$$

Due to the restriction of the trial states, this approach can only give an upper bound, but at least this bound can be evaluated much more easily than the general one, as the algebraic construction based on finite dimensional Lie groups provides a suitable parametrization of the coherent states. For the case of $SU(M)$ -coherent states $|\Omega\rangle = |\mathbf{x}\rangle$ (6.18), the evaluation of the left-hand side of equation (7.119) results in the calculation of the minimum of a function $H_Q : \mathcal{S}^{2(M-1)} \rightarrow \mathbb{R}$ only.

The lower bound H_P is much harder to compute in practice. Calculating the P -representation of a many-body Hamiltonian is in general a quite tedious task. In particular for $SU(M)$ -coherent states $|\Omega\rangle = |\mathbf{x}\rangle$ this involves the determination of integrals over $Y(\Omega) \langle \Omega| \hat{H} |\Omega\rangle$, where $Y(\Omega)$ are the higher dimensional spherical harmonic

functions on $\mathcal{S}^{2(M-1)}$ (for more details on spherical harmonics in higher dimensions, see e.g. [80]).

Instead, we can again make use of the \mathcal{D} -algebra representation introduced in section 6.2. In this representation the expectation value of the Hamiltonian \hat{H} is given by

$$\langle \hat{H} \rangle = \int \mathcal{D}^\ell(\hat{H}) Q(\Omega) d\mu(\Omega). \quad (7.120)$$

Using an integration by parts, we can remove all derivatives,

$$\langle \hat{H} \rangle = \int \tilde{H}(\Omega) Q(\Omega) d\mu(\Omega), \quad (7.121)$$

and finally obtain a function $\tilde{H}(\Omega)$ on the parameter space of the generalized coherent states instead of the differential operator $\mathcal{D}^\ell(\hat{H})$. The Q -function can be interpreted as a positive probability function, which is maximally localized in the case of a coherent state. Thus, the integration can be interpreted as an averaging procedure and we have

$$\langle \hat{H} \rangle \geq \min_{\Omega} \tilde{H}(\Omega), \quad (7.122)$$

where the equality sign holds in the macroscopic limit $N \rightarrow \infty$.

As an example, we calculate the variational bounds for the Bose-Hubbard Hamiltonian (7.1). For reasons of simplicity, we choose a lattice with M sites and periodic boundary conditions, such that

$$\hat{H} = -J \sum_i \left(\hat{a}_i^\dagger \hat{a}_{i+1} + \hat{a}_{i+1}^\dagger \hat{a}_i \right) + \frac{U}{2} \sum_j \hat{n}_j (\hat{n}_j - 1) \quad (7.123)$$

where we identify the lattice sites $i = 1$ and $i = M + 1$.

The expectation value of the Hamiltonian (7.123) in terms of $SU(M)$ coherent states is given by

$$\langle \Omega | \hat{H} | \Omega \rangle = -JN \sum_j (x_{j+1}^* x_j + x_j^* x_{j+1}) + \frac{1}{2} UN(N-1) \sum_j |x_j|^4. \quad (7.124)$$

The minimum of this expression is clearly attained for a spatially homogeneous distribution and phase, i.e. $|x_j|^2 = 1/M$. Thus, it immediately follows that

$$\sum_j |x_j|^4 = M \frac{1}{M^2} = \frac{1}{M} \quad \text{and} \quad \sum_j x_{j+1}^* x_j + x_j^* x_{j+1} = M \frac{2}{M} = 2, \quad (7.125)$$

such that we can determine the minimum of the functional (7.124) as

$$\min_{\Omega} \langle \Omega | \hat{H} | \Omega \rangle = N \left(-2J + \frac{U}{2} \frac{N-1}{M} \right). \quad (7.126)$$

Note that $(N - 1)/M \simeq N/M$ is approximately equal to the filling factor. Thus, we have found an upper bound for the ground state energy per particle, that is the energy density,

$$\frac{\langle E_G \rangle}{N} \leq -2J + \frac{U}{2} \frac{(N - 1)}{M}. \quad (7.127)$$

Keeping this result in mind, we come to the determination of a lower bound for the ground state energy of the Bose-Hubbard model (7.123). To this end we first calculate the expectation value of the Hamiltonian (7.123) in terms of the Q -function starting from the \mathcal{D} -algebra representation (6.36). A quite lengthy, but straightforward calculation based on an integration by parts allows us to determine the expectation values of the operators $\hat{a}_j^\dagger \hat{a}_k$ and $\hat{n}_j(\hat{n}_j - 1)$ as

$$\langle \hat{a}_j^\dagger \hat{a}_k \rangle = (N + M) \int x_j^* x_k Q(\mathbf{x}) d\mu(\mathbf{x}) \quad (7.128)$$

for $j \neq k$ and

$$\begin{aligned} \langle \hat{n}_j(\hat{n}_j - 1) \rangle &= (N^2 + N(2M + 1) + M(M + 1)) \int |x_j|^4 Q(\mathbf{x}) d\mu(\mathbf{x}) \\ &\quad - 4(N + M) \int |x_j|^2 Q(\mathbf{x}) d\mu(\mathbf{x}) - 2. \end{aligned} \quad (7.129)$$

Now we have to minimize the expectation value of the Hamiltonian (7.123) under the condition that Q represents a physical state, respecting the uncertainty condition. The maximally localized states are given by the $SU(M)$ coherent states, which converge towards a δ -distribution in the limit of infinite particle numbers. Thus, the approximation (7.122) yields a lower bound, which is attained in the macroscopic limit. Setting $x_j = 1/\sqrt{M}$ as above, we thus obtain for the minimum (7.122)

$$\begin{aligned} \min_{\mathbf{x}} \tilde{H}(\mathbf{x}) &= -2J(N + M) + \frac{U}{2} \frac{N^2 N(2M + 1) + M(M + 1)}{M} - 2U(N + M) - UM \\ &= -2J(N + M) + \frac{U}{2} \frac{N(N - 1)}{M} - U \frac{2MN + 7M^2 - 2N - M}{2M}. \end{aligned} \quad (7.130)$$

Summarizing our results, we have found the following bounds on the ground state energy E_G of the Bose-Hubbard Hamiltonian (7.123):

$$\begin{aligned} -2JN + \frac{U}{2} \frac{N(N - 1)}{M} &\geq E_G \\ &\geq -2J(N + M) + \frac{U}{2} \frac{N(N - 1)}{M} - U \frac{2MN + 7M^2 - 2N - M}{2M}. \end{aligned} \quad (7.131)$$

In other words, the possible values of the ground state energy are restricted to an interval with a width

$$\Delta E = -2JM + \frac{U}{2M} (2MN + 7M^2 - 2N - M). \quad (7.132)$$

Note that this result can be seen as a generalization of the results for the special case $M = 2$ treated in [76].

In the mean-field limit, i.e. in the limit of infinite particle numbers $N \rightarrow \infty$, but for a fixed macroscopic interaction strength $g = U(N - 1)$ and a fixed number of lattice sites M , we obtain for the energy density E_G/N

$$-2J + \frac{g}{2M} \geq \frac{E_G}{N} \geq -2J + \frac{g}{2M} - \mathcal{O}\left(\frac{1}{N}\right). \quad (7.133)$$

Thus, the energy per particle E_G/N of the interacting many-particle ground state converges towards

$$\frac{E_G}{N} \xrightarrow[g \text{ fixed}]{N \rightarrow \infty} -2J + \frac{g}{2M}, \quad (7.134)$$

which is exactly the energy which we would expect for a Bose-Einstein condensate (cf. equation (8.32) for the interaction part).

With these results on the ground state energy we leave the fundamental aspects of mean-field quantum systems. In the second part, we are concerned with several applications in the field of ultracold atoms.

Part II

Dynamics of Ultracold Atoms in Optical Lattices

Chapter 8

Ultracold atoms in optical lattices – models and methods

The physics of ultracold atoms in optical lattices has made an enormous progress in the last twenty years. They provide an excellent model system for a variety of fields such as nonlinear dynamics or condensed matter physics [81, 82]. Since the first experimental demonstration of Bose-Einstein condensation in a gas of alkaline atoms in 1995 these systems have turned out to be a genuine tool box to implement a wide range of many-body Hamiltonians featuring near perfect control and have inspired whole new fields of research. In this chapter we will discuss the basic definitions and physical concepts and introduce the models and methods used in the following chapters.

In the first section, we explain the phenomenon of Bose-Einstein condensation (BEC) in a system of non-interacting bosons. The second section gives a short review on experimental techniques from laser cooling to optical lattices and an account on current experiments with BECs. In section 8.3 we introduce the Bose-Hubbard Hamiltonian, a paradigmatic model for the study of ultracold, strongly interacting bosonic atoms and one possible realisation of the permutation symmetric systems discussed in the first part of this thesis. We have already seen that in the limit of large particle numbers these systems converge to a mean-field solution. In section 8.4 we comment on the resulting (discrete) Gross-Pitaevskii equation (GPE) and discuss possibilities for going beyond this approximation, which is strictly valid only in the limit of infinite particle numbers. Finally, in the last section, we extend these models to include noise and dissipation.

8.1 Bose-Einstein condensation

In 1924 Albert Einstein predicted a novel phase for an ideal Bose gas [83, 84], based on Satyendra Nath Bose's work on photon statistics [85]. Below a critical temperature, a dilute gas of non-interacting bosons condenses to the single-particle ground state of the system, such that a macroscopic occupation of this state arises. The result is a macroscopic matter wave exhibiting quantum phenomena on a large scale.

To illustrate this phase transition, we consider a gas of $N \gg 1$ non-interacting bosons in a large box of volume $V = L^3$. To keep the notation simple, we assume that the particles have no spin, $s = 0$. However, the extension to systems with spin is straightforward. In the following, we are interested in the thermodynamic limit, where the particle number N , as well as the volume L tend to infinity, $N, L \rightarrow \infty$, while the density $\rho = N/V$ is fixed.

To analyse the low-temperature limit of an ideal Bose gas, it is most convenient to work in the grand canonical framework with the grand canonical partition function

$$Z_G = \text{tr} e^{-\beta(\hat{H} - \mu\hat{N})}, \quad (8.1)$$

where $\beta = 1/k_B T$ denotes the inverse temperature and μ the chemical potential. The Hamiltonian for N non-interacting, non-relativistic particles is given by

$$\hat{H} = \sum_{i=1}^N \frac{\hat{p}_i^2}{2m}. \quad (8.2)$$

The single-particle energies are given by the eigenvalues $\epsilon_{\mathbf{p}} = (2\pi\hbar)^2 \mathbf{n}^2 / 2mL^2$ with $\mathbf{n} \in \mathbb{Z}^3$ due to the boundary condition.

Due to the restriction to the symmetric subspace of the total Hilbert space, the N -particle state is completely determined by the set of occupation numbers $n_{\mathbf{p}}$ of the energy eigenstates. The sum over all eigenstates gives the total particle number, $N = \sum_{\mathbf{p}} n_{\mathbf{p}}$, and the total energy is $E(\{n_{\mathbf{p}}\}) = \sum_{\mathbf{p}} n_{\mathbf{p}} \epsilon_{\mathbf{p}}$. As the grand canonical partition function (8.1) factorizes into the contributions from the single energy levels, Z_G can be determined as follows:

$$\begin{aligned} Z_G &= \sum_{N \geq 0} \sum_{\{n_{\mathbf{p}}\}} e^{-\beta(E(\{n_{\mathbf{p}}\}) - \mu N)} = \sum_{n_{\mathbf{p}}=0}^{\infty} e^{-\beta \sum_{\mathbf{p}} (\epsilon_{\mathbf{p}} - \mu) n_{\mathbf{p}}} \\ &= \prod_{\mathbf{p}} \sum_{n_{\mathbf{p}}} e^{-\beta(\epsilon_{\mathbf{p}} - \mu) n_{\mathbf{p}}} = \prod_{\mathbf{p}} \frac{1}{1 - e^{\beta(\epsilon_{\mathbf{p}} - \mu)}}. \end{aligned} \quad (8.3)$$

Now, all thermodynamic quantities can be deduced from the grand canonical potential,

$$\Phi \equiv -\beta^{-1} \log Z_G = \beta \sum_{\mathbf{p}} \log(1 - e^{-\beta(\epsilon_{\mathbf{p}} - \mu)}). \quad (8.4)$$

Note that, since the total energy is independent of the spin s , the extension to systems with spin just amounts to a multiplicative degeneracy factor $g = 2s + 1$ and not to a qualitatively different behaviour. In the last transformation of equation (8.3) we have used the geometric sum. To insure convergence, it is necessary that $\mu < \epsilon_{\mathbf{p}}$ for all \mathbf{p} . Since the ground state has zero energy $\epsilon_{\mathbf{p}} = 0$, the chemical potential μ thus must be negative.

The average particle number can be calculated from the grand canonical potential (8.4):

$$\langle \hat{N} \rangle = - \left(\frac{\partial \Phi}{\partial \mu} \right) = \sum_{\mathbf{p}} \frac{1}{1 - e^{\beta(\epsilon_{\mathbf{p}} - \mu)}}. \quad (8.5)$$

In the thermodynamic limit, the sum can be approximated by an integral $L^{-3} \sum_{\mathbf{p}} \rightarrow (2\pi\hbar)^{-3} \int_{\mathbb{R}^3}$, such that the density can be evaluated as

$$\rho \equiv \frac{\langle \hat{N} \rangle}{L^3} = \frac{g}{(2\pi\hbar)^3} \int_{\mathbb{R}^3} d^3p \frac{1}{1 - e^{\beta(\epsilon_{\mathbf{p}} - \mu)}}. \quad (8.6)$$

A closer analysis shows that this is a monotonically increasing function of $\mu \in [-\infty, 0]$, which assumes its maximum,

$$\rho_c(T) = g_{3/2}(1) \left(\frac{mk_B T}{2\pi\hbar^2} \right)^{2/3}, \quad (8.7)$$

for $\mu = 0$. This equation defines the critical density ρ_c , which still depends on the temperature T . For simplicity, we have used the generalized ζ -function

$$g_\nu(z) \equiv \frac{1}{\Gamma(\nu)} \int_0^\infty dx \frac{x^{\nu-1}}{e^x z^{-1} - 1} \quad \text{with} \quad \Gamma(\nu) \equiv \int_0^\infty dt e^{-t} t^{\nu-1} \quad (8.8)$$

instead of the full integral expression. In dependence of the fugacity $z = e^{\beta\mu} \in [0, 1]$, the function $g_{3/2}(z)$ assumes its maximum $g_{3/2}(1) \approx 2.612$ for $z = 1$, respective $\mu = 0$. Thus, we get the absurd result that for vanishing chemical potential, $\mu \rightarrow 0$, the density assumes its smallest value ρ_c . On the other hand, if we interpret equation (8.7) as an equation to determine the temperature, we get an expression for the critical temperature

$$T_c(\rho) = \frac{2\pi\hbar^2}{m} \left(\frac{\rho}{g_{3/2}(1)} \right)^{2/3}. \quad (8.9)$$

Below this critical temperature the density seems to be shrinking with decreasing temperature.

These obvious inconsistencies go back to the naive replacement of the sum by an integral. A more careful analysis shows, that the term with $\mathbf{p} = \mathbf{0}$ in equation (8.5) diverges in the limit of vanishing chemical potential $\mu \rightarrow 0$ and therefore has to be treated separately,

$$\begin{aligned} \langle \hat{N} \rangle &= N_{\mathbf{0}} + N_{\mathbf{p} \neq \mathbf{0}} \\ &= \frac{1}{e^{-\beta\mu} - 1} + \sum_{\mathbf{p} \neq \mathbf{0}} \frac{1}{1 - e^{\beta(\epsilon_{\mathbf{p}} - \mu)}}. \end{aligned} \quad (8.10)$$

The first term describes the number of particles N_0 in the single-particle ground state with $\mathbf{p} = \mathbf{0}$. Below the critical temperature T_c , the fraction of atoms $N_0/\langle \hat{N} \rangle$ in this state does not vanish in the thermodynamic limit (with ρ held fixed), but can be determined as

$$\lim_{N \rightarrow \infty} \frac{N_0}{\langle \hat{N} \rangle} = \begin{cases} 0 & T > T_c(\rho) \\ 1 - \left(\frac{T}{T_c(\rho)} \right)^{3/2} & T < T_c(\rho). \end{cases} \quad (8.11)$$

This macroscopic occupation of the single-particle ground state is called *Bose-Einstein condensation*. For a finite temperature below T_c one gets a mixture of the normal phase and a Bose-Einstein condensate, whereas one gets a fully condensed state for $T = 0$. For a fixed particle number the ground state wave function in the BEC phase is thus simply a product of single-particle wave functions in the lowest energy eigenstate.

A much more illustrative explanation of Bose-Einstein condensation can be given in terms of the thermal wavelength,

$$\lambda_{\text{thermal}} \equiv \sqrt{\frac{2\pi\hbar^2}{mkT}}. \quad (8.12)$$

If one compares this quantity to the critical density (8.7), one can paraphrase the condition for the onset of Bose-Einstein condensation as $\lambda_{\text{thermal}}^{-3} \propto g_{3/2}(1)\rho$. Thus, the phase transition to a macroscopic wave function takes place as soon as the thermal wavelength λ is of the order of the mean distance between the particles.

Note, that the derivation given was for a three-dimensional system. In a one- or two-dimensional volume the density (8.6) diverges, thus there is no Bose Einstein condensation in one and two dimensions in free space. This result is in accordance with the Mermin-Wagner theorem, which states the impossibility of long-range order in uniform one- or two-dimensional systems at a finite temperature T [86, 87]. The situation is different if the atoms are confined by an external potential. In this case it is possible to obtain a BEC also in one-dimensional systems [88, 89]. In two-dimensional systems a Berezinsky-Kosterlitz-Thouless transition [90–92], characterized by a huge, but finite correlation length occurs instead of a Bose-Einstein condensation.

Up to now, we were only concerned with non-interacting systems. As of yet there exists no general proof of Bose-Einstein condensation for interacting many-particle systems. There have, however, been many results in this direction. For a recent overview and a thorough introduction to the mathematical side of this problem, see [43]. Even at zero temperature it is not directly obvious how to generalize the concept of a macroscopic occupation of a single-particle state of an interacting system, since the eigenfunctions of the Hamiltonian no longer factorize into a product of single-particle states. To make the concept of Bose-Einstein condensation more precise, we introduce the reduced single-particle density matrix (SPDM). If the symmetric N -particle state is denoted by the wave function $\Psi(\mathbf{r}_1, \mathbf{r}_2, \dots, \mathbf{r}_N)$ the SPDM is defined as follows:

$$\rho_{\text{red}}(\mathbf{r}, \mathbf{r}', t) \equiv \int d\mathbf{r}_2 d\mathbf{r}_3 \dots d\mathbf{r}_N \Psi^*(\mathbf{r}, \mathbf{r}_2, \dots, \mathbf{r}_N) \Psi(\mathbf{r}', \mathbf{r}_2, \dots, \mathbf{r}_N). \quad (8.13)$$

By definition the SPDM is a hermitian operator, which can thus be decomposed into sets of eigenfunctions ψ_i and eigenvalues a_i ,

$$\rho_{\text{red}}(\mathbf{r}, \mathbf{r}', t) = \sum_{i=1}^{\infty} a_i \psi_i^*(\mathbf{r}, \mathbf{r}', t) \psi_i(\mathbf{r}, \mathbf{r}', t), \quad (8.14)$$

and is normalized, as $\text{tr } \rho_{\text{red}} = 1$. For a fully condensed state,

$$\Psi(\mathbf{r}_1, \mathbf{r}_2, \dots, \mathbf{r}_N) = \prod_{i=1}^N \psi_0(\mathbf{r}_i), \quad (8.15)$$

only one eigenvalue equals 1, while all the others are zero. The corresponding SPDM is thus simply given by $\rho_{\text{red}}(\mathbf{r}, \mathbf{r}', t) = \psi_0^*(\mathbf{r}, t)\psi_0(\mathbf{r}', t)$.

To turn the argument on its head, we can define Bose-Einstein condensation, respectively a macroscopic occupation as the appearance of an eigenvalue of the SPDM (8.13) which does not vanish the thermodynamic limit $N \rightarrow \infty$, but is of order unity $\mathcal{O}(1)$, whereas all others scale as $\mathcal{O}(1/N)$. This definition was first given in the context of liquid helium [93], where interactions play a dominant role and is now common standard (see, e.g., [94] and references therein). However, it is not restricted to a condensation in the ground state only, but can be extended to arbitrary states, including thermal states. Also, the system can condense to more than one state, as e.g. a set of hyperfine states instead of a single ground state. This is represented by an SPDM with more than one eigenvalue of the order of one and yields a so-called spinor BEC or a BEC consisting of various fragments.

Moreover, the SPDM can be used to characterize the system and quantify depletion during the dynamics, since the non-vanishing eigenvalue directly gives the fraction of condensed atoms. Therefore the SPDM will be frequently used in the following chapters.

8.2 Experimental overview

8.2.1 From laser cooling to the creation of a BEC

The first proposal for cooling atoms with light dates back to the advent of laser physics. This marked a major breakthrough in atomic physics with innumerable applications ranging from atomic clocks to precision spectroscopy. In 1997, Steven Chu, Claude Cohen-Tannoudji and William D. Phillips were awarded the Noble prize for their work on laser cooling of atoms and trapping techniques [95–97]. Here, we can only give a short introduction to two techniques frequently used for the creation of a BEC, namely Doppler cooling and evaporative cooling. A more detailed overview can be found in [98].

The basic principle of *Doppler cooling* relies on the Doppler effect due to the thermal motion of the atoms. The slight detuning of the electronic transition frequency depending on their direction relative to the near-resonant laser light is sufficient to influence the absorption rate of the photons. Thus, if the laser frequency lies just below the atomic transition frequency, only atoms travelling towards the beam strongly absorb photons. Since the scattered photons are re-emitted equally in all directions, this causes a net decrease of momentum due to the photon recoil and can thus be used to minimize the kinetic energy, and hence the temperature of the atoms. Together with optical pumping effects this allows for temperatures of a few hundreds micro-Kelvin.

When Doppler cooling is combined with *evaporative cooling* temperatures in the nano-Kelvin regime which are needed for Bose-Einstein condensation can be reached. In an evaporative cooling scheme the atoms are normally confined by a conservative trap using magnetic or optical dipole forces. If the trap depth is successively lowered, the

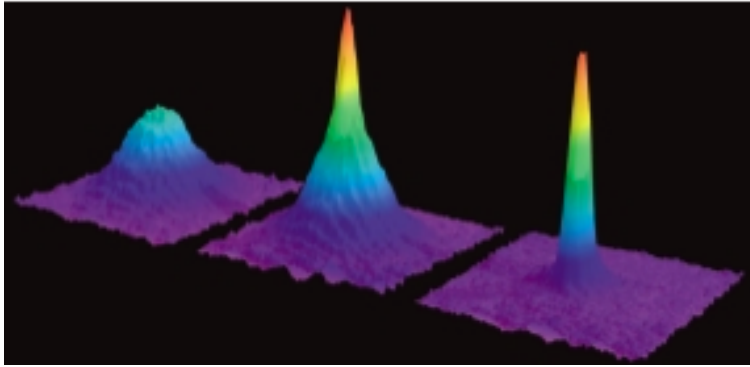


Figure 8.1: Bose-Einstein condensation (taken from the Nobel lecture of W. Ketterle [103]). Depicted is an absorption image vs. two spatial dimensions. The left picture shows an expanding cloud cooled to just above the transition point; middle: just after the appearance of the condensate; right: after further evaporative cooling an almost pure condensate is visible. The total number of atoms at the phase transition is about 7×10^5 , the temperature at the transition point is $2 \mu\text{K}$.

most energetic atoms can escape. In this kind of setup temperatures of few nano-Kelvin can be reached due to rethermalization processes, while the phase space density is still large enough to induce the phase transition to a BEC.

In 1938 a superfluid phase in liquid helium-4 was discovered, which can be partly explained as Bose-Einstein condensation. However, interactions play a dominant role and as we have discussed such an interpretation requires that the fundamental theory must be substantially modified. For a long time, it was an open problem if one could indeed realize a clean Bose-Einstein condensate, since in this temperature regime the stable phase would usually be a solid. To circumvent this problem the gas must be dilute enough to suppress three-body scattering events. In 1995, seventy years after the seminal work of Bose and Einstein, the first three independent experimental realizations of Bose-Einstein condensation in gases of alkaline atoms using ^{87}Rb , ^7Li and ^{23}Na were reported [99–101]. In 2001 Eric Cornell, Carl Wieman and Wolfgang Ketterle received the Nobel prize for their achievements [102, 103].

In figure 8.1 the momentum distribution of a BEC created in the group of Wolfgang Ketterle is shown. These images are created using a time-of-flight technique. The trapping potential is switched off, such that the atomic cloud can expand for a few milliseconds. By shining a resonant laser beam on the atomic cloud one can observe its shadow via a CCD camera. The result is a density profile of the momentum distribution. One clearly observes the macroscopic occupation of the $\mathbf{p} = \mathbf{0}$ state as discussed in the preceding section. For an in situ observation the required resolution is challenging. For ultracold atoms in optical lattices the resolution must be on the order of a hundreds of nanometers. This requires significant effort and has only been achieved recently [104, 105]. An introduction to different imaging techniques can be found e.g. in [106].

Today the physics of Bose-Einstein condensates is a whole new field of research in its own right. Bose-Einstein condensates of more than 13 different isotopes have been reported, including atomic hydrogen [107] and ^{52}Cr [108]. They are an ideal playground to study interference and correlations, superfluidity and the creation of vortices, the creation of solitons, as well as the behaviour of mixtures and spinor condensates (for a general overview see e.g. [109]). There are multiple suggestions for using BECs as quantum simulators for solid state systems (like the Bose-Hubbard model which will be introduced in the next section) or for relativistic problems, as for example black holes [110] or the *Zitterbewegung* of a Dirac particle, on which we will comment at the end of chapter 10. BECs have been employed as a quantum interface for light and matter, e.g. to slow down light [111] via electromagnetically induced transparency [112]. Nowadays the physics of Bose-Einstein condensation is no longer restricted to bosonic atoms: Ultracold fermions pair up to form molecular BECs [113–115], the condensation of magnons [116] and exciton-polaritons [117] offers the possibility for studying Bose-Einstein condensation at room temperature and the Bose-Einstein condensation of photons has only recently been reported [118, 119].

8.2.2 Trapping by light

Two laser beams in diametric opposition to each other form a standing light field, which induces an electric dipole moment in the atoms. The *ac Stark shift* is the energy shift $V_{\text{ac}}(\mathbf{r})$ of an atomic level due to the interaction between the induced dipole and the electric field [120, 121]:

$$V_{\text{ac}}(\mathbf{r}) = \frac{1}{2}\alpha(\omega)\langle\mathbf{E}^2(\mathbf{r}, t)\rangle, \quad (8.16)$$

where $\alpha(\omega)$ describes the specific dynamic polarizability of the atomic level under consideration and the time average $\langle\cdot\rangle$ has to be taken over one period of light. This energy shift may be regarded as an effective potential for the atoms, which gives rise to the dipole force

$$\mathbf{F}_{\text{dipole}} \equiv -\nabla V_{\text{ac}}(\mathbf{r}). \quad (8.17)$$

The detuning Δ of the light field is defined as the difference between the laser frequency ω and the frequency of an atomic transition: $\Delta = \omega - \omega_{\text{res}}$. Spontaneous emission can be neglected if the system is detuned far from resonance. If it is red-detuned, respective $\Delta < 0$, the induced dipole is in phase with the electric field. Therefore, the gradient of the potential energy points in the direction of the increasing field and the force is attractive, whereas it is repulsive for blue-detuned light, $\Delta > 0$.

Thus, the two opposed laser beams form a standing wave which leads to a periodic dipole potential

$$V_{\text{periodic}}(x) = V_0 \cos^2\left(\frac{2\pi x}{d}\right), \quad (8.18)$$

which is characterized by the lattice spacing $d = \lambda_{\text{laser}}/2$. A slight variation of the angle between the two beams gives the ability to influence the lattice spacing without

changing the wave length. The lattice depth is proportional to the ratio between the laser intensity and the saturation intensity of the atomic transition and is typically given in units of the recoil energy

$$E_{\text{recoil}} = \frac{\hbar^2 \pi^2}{2md^2}. \quad (8.19)$$

A combination of different beams allows various forms of potential. Moreover, by controlling the polarization one can even create state dependent potentials, which can be shifted relative to each other [122]. The special case of a bichromatic lattice, which can be implemented by superimposing two incoherent optical lattices (cf. e.g. [123, 124]), is analysed in section 10.3.

Ultracold atoms in a periodic potential allow the observation of many effects originally studied in condensed matter physics. Such as Bloch oscillations and Landau-Zener tunneling (cf. chapter 10), with almost perfect control over the lattice parameters. The significantly higher densities which can be reached with a BEC compared to ultracold atoms facilitate filling factors of more than one atom per site. Thus, interactions between the particles play a dominant role. They induce strong correlations and strongly influence the dynamics. Since the effective interaction strength is widely tunable using Feshbach resonances [109], this provides the opportunity to implement a wide range of many-body Hamiltonians, as e.g. the Bose-Hubbard model introduced in the next section.

8.3 The Bose-Hubbard model

In 1998 Jaksch *et al.* [125] proposed using a dilute gas of ultracold bosonic atoms in an optical lattice as a realisation of the Bose-Hubbard Hamiltonian, which was previously known from the theoretical description of Josephson junctions (cf. [126] and references therein). Unlike Josephson junctions in an optical lattice implementation of the Bose-Hubbard model all system parameters are easily accessed by a variation of the laser intensity and wave length in their proposal. Their idea and the famous realisation by Greiner *et al.* [127] showed that ultracold atoms provide ideal model systems for solid state physics. This attracted a great deal of attention in the quantum optics community and laid the foundations of a whole new field of research (cf. [82] and references therein).

In the following, we consider a dilute gas of ultracold bosons. In addition to the optical lattice $V_{\text{periodic}}(\mathbf{r})$, most experimental setups feature an optical or magnetic potential $V_{\text{trap}}(\mathbf{r})$ to confine the atoms. These trapping potentials, as well as any other specialized potentials are summarized in the external potential $V_{\text{ext}}(\mathbf{r})$, while the interaction potential between the particles is denoted as $V_{\text{int}}(\mathbf{r}, \mathbf{r}')$.

In second quantization this yields the Hamiltonian

$$\begin{aligned} \hat{H} = & \int d^3\mathbf{r} \hat{\Psi}^\dagger(\mathbf{r}) \left(\frac{\mathbf{p}^2}{2M} + V_{\text{periodic}}(\mathbf{r}) + V_{\text{ext}}(\mathbf{r}) \right) \hat{\Psi}(\mathbf{r}) \\ & + \frac{1}{2} \int d^3\mathbf{r} \int d^3\mathbf{r}' \hat{\Psi}^\dagger(\mathbf{r}) \hat{\Psi}^\dagger(\mathbf{r}') V_{\text{int}}(\mathbf{r}, \mathbf{r}') \hat{\Psi}(\mathbf{r}) \hat{\Psi}(\mathbf{r}'), \end{aligned} \quad (8.20)$$

with the field operators $\hat{\Psi}(\mathbf{r})$ and $\hat{\Psi}^\dagger(\mathbf{r})$ fulfilling the commutation relations

$$[\hat{\Psi}(\mathbf{r}), \hat{\Psi}^\dagger(\mathbf{r}')] = \delta^{(3)}(\mathbf{r} - \mathbf{r}'). \quad (8.21)$$

The interactions of the bosons $V_{\text{int}}(\mathbf{r}, \mathbf{r}')$ are mainly due to binary collisions. As all these scattering events take place at very low energies and momenta, it is sufficient to treat the scattering problem up to first order in the partial wave expansion. In this approximation, the scattering amplitude does not depend on the relative direction of the atoms, $V_{\text{int}}(|\mathbf{r} - \mathbf{r}'|)$. The s-wave scattering length a_s is defined as the limit of the scattering amplitude in the case of zero momentum and can be seen as a measure of the interaction strength (cf. [109]). If one is not interested in details of the scattering process, one can just as well replace the interaction potential by a delta-shaped model potential,

$$V_{\text{int}}(|\mathbf{r} - \mathbf{r}'|) = \frac{4\pi\hbar^2 a_s}{M_{\text{red}}} \delta(\mathbf{r} - \mathbf{r}'), \quad (8.22)$$

which is much easier to handle, but yields the same scattering length. Note, that this replacement is not correct for atoms featuring long-range interactions, such as the dipole-dipole interactions in ^{52}Cr [128].

The quantum dynamics in a deep optical lattice is now conveniently studied in the Wannier basis $w_n(\mathbf{r} - \mathbf{r}_i)$, which is defined as the Fourier transform of the Bloch basis [129]. Here, n labels the Bloch band, while i denotes the lattice site. The basis functions are exponentially localized in the minima \mathbf{r}_i of the periodic potential. If we decompose the field operators $\hat{\Psi}(\mathbf{r})$ into this basis

$$\hat{\Psi}(\mathbf{r}) = \sum_{n,i} w_n(\mathbf{r} - \mathbf{r}_i) \hat{a}_{n,i}, \quad (8.23)$$

the coefficients $\hat{a}_{n,i}$ can be determined as follows

$$\hat{a}_{n,i} = \int w_n^*(\mathbf{r} - \mathbf{r}_i) \hat{\Psi}(\mathbf{r}) d\mathbf{r} \quad (8.24)$$

and fulfill bosonic commutation relations. Their interpretation is evident: They destroy (or create) a boson in the state $w_n(\mathbf{r} - \mathbf{r}_i)$. Due to exponential localization, matrix elements of operators evaluated with two Wannier functions located at remote sites can be approximately neglected. This fact is commonly used for approximations and leads to an effective discretisation of the continuous system.

In the following, we restrict our analysis to the ground band $n = 0$. This *single-band approximation* is justified if the following conditions are fulfilled: The energetic difference

between the lowest and the higher energy bands is large compared to the thermal energy of the bosons, if there are no band crossings and the external fields are sufficiently weak. In this case, the band index can be considered as approximately conserved. In the *tight-binding or nearest neighbour approximation* we neglect the coupling between non-adjacent sites because of the exponential localisation of the Wannier functions.

Based on these assumptions, the continuous Hamiltonian (8.20) can be approximated by the discrete Bose-Hubbard Hamiltonian:

$$\hat{H} = \sum_{i=1}^M \epsilon_i \hat{n}_i - J \sum_{i=1}^{M-1} \left(\hat{a}_i^\dagger \hat{a}_{i+1} + \hat{a}_{i+1}^\dagger \hat{a}_i \right) + \frac{U}{2} \sum_{i=1}^M (\hat{n}_i (\hat{n}_i - 1)). \quad (8.25)$$

Here, we used the common definition $\hat{n}_i \equiv \hat{a}_i^\dagger \hat{a}_i$ and rescaled units such that $\hbar = 1$. The index i labels the M potential minima or sites and the parameter J describes the tunneling strength between neighbouring sites $|i - j| = 1$,

$$J_{ij} = - \int d^3 \mathbf{r} w^*(\mathbf{r} - \mathbf{r}_i) \left(-\frac{\hbar^2}{2M} \nabla^2 + V_{\text{periodic}}(\mathbf{r}) \right) w(\mathbf{r} - \mathbf{r}_j). \quad (8.26)$$

As the phase of the Wannier function is arbitrary, we can choose it such that J is real. Due to the tight-binding approximation, tunneling events between non-adjacent sites are negligible, just like interactions of bosons located at different sites, $i \neq j$, whereas the on-site interactions,

$$\begin{aligned} U_i &= \int \int d^3 \mathbf{r}' d^3 \mathbf{r} |w(\mathbf{r} - \mathbf{r}_i)|^2 V_{\text{int}}(|\mathbf{r} - \mathbf{r}'|) |w(\mathbf{r}' - \mathbf{r}_i)|^2 \\ &= \frac{4\pi a_s}{M_{\text{red}}} \int d^3 \mathbf{r} |w(\mathbf{r} - \mathbf{r}_i)|^4 \end{aligned} \quad (8.27)$$

play a crucial role for the dynamics. In the following, we assume a site-independent interaction strength $U_i \equiv U$. In addition, we have defined the local chemical potential as

$$\epsilon_i = \int d^3 \mathbf{r} V_{\text{ext}}(\mathbf{r}) |w(\mathbf{r} - \mathbf{r}_i)|^2. \quad (8.28)$$

Note, however, that this definition is only sensible if the variation of the external potential on the characteristic length of the optical lattice is small enough to be assumed to be constant over one lattice site.

In dependence of the parameter ratio, the Bose-Hubbard system undergoes a quantum phase transition from a superfluid phase for $J \gg U$, characterized by long range coherence and vanishing gap in the excitation spectrum, to the Mott phase for $U \gg J$, dominated by localization effects [130]. Especially the prediction [125] and the spectacular experimental realization [127] of the latter system attracted a lot of interest, since this shows that optical lattices can be seen as a kind of laboratory for strongly correlated many-body systems. Only recently this phase transition has been observed in an experiment with astonishing accuracy, being able to resolve single-sites as well as single atoms [104, 105].

One immediate consequence of the discretisation due to the tight-binding approximation is the reduction of the definition of the SPDM (8.13) is to the calculation of the matrix elements

$$\rho_{\text{red},ij} = \frac{1}{N} \langle \hat{a}_i^\dagger \hat{a}_j \rangle \quad (8.29)$$

with $i, j = 1, \dots, M$.

For an extended lattice the huge dimension of the N -particle Hilbert space \mathcal{H} ,

$$\dim \mathcal{H} = \frac{(M + N - 1)!}{N!(M - 1)!}, \quad (8.30)$$

precludes any attempt to solve the problem numerically exact for a realistic number of particles, while the interactions make analytic solutions a hard task, especially in the case where the interaction strength is of the order of the tunneling, $U \approx J$, such that perturbative approaches fail. Thus, approximations are of fundamental interest. In the next section, we will introduce the most common approximation, the (discrete) Gross-Pitaevskii equation (GPE) and discuss possibilities for going beyond this approximation.

8.4 The mean-field limit and beyond

Even if the Bose-Hubbard model (8.25), as well as the continuous problem (8.20) are inherently many-particle problems, the dynamics of the macroscopic wave function is remarkably well reproduced by the (discrete) Gross-Pitaevskii equation (GPE) if the systems undergoes Bose-Einstein condensation [131]. In this section, we will introduce the GPE and discuss possible ways to go beyond this approximation. To this end, we will follow the heuristic derivation of the GPE based on the work of Bogoliubov [132]. Note that a rigorous derivation of the mean-field dynamics based on the phase space description discussed in chapter 6, yields exactly the same hamiltonian function. Still, the rigorous treatment shows that the limiting dynamics is given by a phase space flow, in contrast to the heuristic description by Bogoliubov, where we consider only a single trajectory in phase space.

8.4.1 The time-independent Gross-Pitaevskii equation

To derive the time-independent Gross-Pitaevskii equation we start again with the full, second quantized, many-particle Hamiltonian (8.20), which we have discussed in the proceeding section. However, now we are interested in the limit of large particle numbers $N \rightarrow \infty$.

Under these conditions the energy of a fully condensed state (8.15) is given by

$$E = N \int d\mathbf{r} \left(\frac{\hbar^2}{2m} |\nabla \psi_0(\mathbf{r})|^2 + V_{\text{ext}}(\mathbf{r}) |\psi_0(\mathbf{r})|^2 + \frac{N-1}{2} U |\psi_0(\mathbf{r})|^4 \right). \quad (8.31)$$

For a uniform Bose gas confined to a volume V , the wave function of the ground state is $\psi_0 \propto 1/V^{1/2}$ and thus the expression for the energy reduces to

$$E = \frac{N(N-1)}{2V}U \approx \frac{UN^2}{2V} \quad \text{for } N \gg 1. \quad (8.32)$$

Motivated by the expression for the ground state energy of the condensate (8.31), we introduce the Gross-Pitaevskii energy functional [133–135]

$$\mathcal{E}_{\text{GP}}[\phi] = \int_{\mathbb{R}^3} d\mathbf{r} \left(\frac{\hbar^2}{2m} |\nabla\phi(\mathbf{r})|^2 + V_{\text{ext}}(\mathbf{r})|\phi(\mathbf{r})|^2 + \frac{U}{2}|\phi(\mathbf{r})|^4 \right), \quad (8.33)$$

with the condition

$$\int_{\mathbb{R}^3} d\mathbf{r} |\phi(\mathbf{r})|^2 = N. \quad (8.34)$$

Here, $|\phi(\mathbf{r})|^2$ describes the spatial density of particles. In the following, we will see that this normalization is much more convenient for the analysis of the scaling behaviour than a normalization to one. From now on we will assume a repulsive interaction, $U > 0$, to avoid technical difficulties. Moreover, this is the case for most isotopes used in experiments with ultracold atoms.

Minimizing the energy functional (8.33) with respect to the independent complex parameters ϕ and ϕ^* under the constraint of constant particle number N ,

$$\delta E - \mu \delta N = 0, \quad (8.35)$$

yields the variational equation

$$-\frac{\hbar^2}{2m}\nabla^2\phi(\mathbf{r}) + V_{\text{ext}}(\mathbf{r})\phi(\mathbf{r}) + \frac{U}{2}|\phi(\mathbf{r})|^2\phi(\mathbf{r}) = \mu\phi(\mathbf{r}). \quad (8.36)$$

This is the time-independent Gross-Pitaevskii equation (GPE), which has the form of a nonlinear Schrödinger equation taking into account the interactions by a mean-field potential. The eigenvalue of the GPE is the chemical potential μ , which was introduced as a Lagrange multiplier to ensure a constant number of particles N . Note that the chemical potential is no longer equivalent to the energy per particle as in the non-interacting case.

A rigorous analysis of the Gross-Pitaevskii functional [136] shows that there exists a unique, positive and continuously differentiable minimizer ϕ_{GP} , which depends only on the particle number N and the interaction strength U for a given external potential $V_{\text{ext}}(\mathbf{r})$. The corresponding energy is denoted by

$$E_{\text{GP}}(N, U) = \mathcal{E}_{\text{GP}}[\phi_{\text{GP}}] = \inf_{\int d\mathbf{r} |\phi(\mathbf{r})|^2 = N} \mathcal{E}_{\text{GP}}[\phi]. \quad (8.37)$$

To clarify the relationship between the ground state of the many-particle system and the Gross-Pitaevskii minimizer, we first consider two extremal cases. In the homogeneous case, the GPE (8.36) reduces to

$$\mu = U|\phi(\mathbf{r})|^2, \quad (8.38)$$

as one would have expected from the energy of the uniform state for a Bose gas (8.32) with $N \gg 0$ using the thermodynamic relation

$$\mu = \frac{\partial E}{\partial N}. \quad (8.39)$$

For a non-interacting system, the ground state is a BEC (8.15). In this case, the Gross-Pitaevskii minimizer is equivalent to the rescaled single-particle wave function: $\phi_{\text{GP}} = \sqrt{N}\psi_0$ and the Gross-Pitaevskii energy E_{GP} gives the correct ground state energy.

Thus, one would expect that one can establish a suitable limit, where the ground state energy E_0 and the GP energy coincide, $E_{\text{GP}} \approx E_0$ and the quantum mechanical ground state density

$$\rho_{\text{QM}}(\mathbf{r}) = N \int d\mathbf{r}_2 \dots d\mathbf{r}_N |\Psi(\mathbf{r}, \mathbf{r}_2, \dots, \mathbf{r}_N)|^2 \quad (8.40)$$

can be approximated by the Gross-Pitaevskii estimate $|\phi_{\text{GP}}(\mathbf{r})|^2$. A closer look at the scaling properties yields the following relations

$$E_{\text{GP}}(N, U) = N E_{\text{GP}}(1, UN) \quad \text{and} \quad \phi_{\text{GP}}^{N,U}(\mathbf{r}) = \sqrt{N} \phi_{\text{GP}}^{1,UN}(\mathbf{r}), \quad (8.41)$$

making the condition for the limit $N \rightarrow \infty$ more precise. And indeed, one can rigorously prove that in the limit $N \rightarrow \infty$ with a fixed macroscopic interaction strength $g \equiv UN$,

$$\lim_{N \rightarrow \infty} \frac{1}{N} E_0(N, U) = E_{\text{GP}}(1, g) \quad (8.42)$$

and

$$\lim_{N \rightarrow \infty} \frac{1}{N} \rho_{\text{QM}}^{(N,U)}(\mathbf{r}) = |\phi_{\text{GP}}^{1,g}(\mathbf{r})|^2 \quad (8.43)$$

converge in the weak L^1 -sense [136]. Thus, in the macroscopic limit $N \rightarrow \infty$, we get an effective single-particle problem. This limit can be interpreted in close analogy to the classical limit of quantum mechanics $\hbar \rightarrow 0$, since in a path integral formulation of the original problem (8.20) the saddle point equation is the GPE, thus giving the steepest descent approximation to the integral for $1/N \rightarrow 0$.

Note that the quantum mechanical density (8.40) is equivalent to the diagonal part of the rescaled SPDM (8.13),

$$\rho_{\text{QM}}(\mathbf{r}) = N \rho_{\text{red}}(\mathbf{r}, \mathbf{r}). \quad (8.44)$$

Thus it is not possible to make any predictions about Bose-Einstein condensation and deviations from a fully condensed state, as well as about coherence properties, based on results of the GPE alone. The implications of this fact will be discussed in the following chapters.

8.4.2 Bogoliubov theory

A major part of the results concerning Bose-Einstein condensates has its seeds in the ideas of Bogoliubov. Still his ansatz was not rigorous, but mainly a heuristic argument

based on a perturbative treatment of the low energy spectrum in the weakly-interacting case. Here we can give only a short introduction to set the basic ideas into a general context, a detailed discussion including mathematical details can be found in [43].

The basic setup we are looking at is again the same as in section 8.3, so we can directly start with the Hamiltonian (8.20). As above, we are concerned with the limit of infinite particle number $N \rightarrow \infty$, while the density remains constant. In addition, we assume periodic boundary conditions. To present the line of the argument most clearly without to many technical details, we omit the external potential $V_{\text{ext}}(\mathbf{r})$ and assume a local interaction potential $V_{\text{int}}(|\mathbf{r} - \mathbf{r}'|) = U\delta(\mathbf{r} - \mathbf{r}')$. Note, that the latter definition is in line with the assumptions which lead to the definition of the Bose-Hubbard Hamiltonian (8.3).

Thus, it is sensible to decompose the system into the Bloch modes with a discrete constant total momentum. To this end it is most convenient to introduce bosonic annihilation and creation operators

$$[\hat{a}_{\mathbf{p}}, \hat{a}_{\mathbf{p}'}^\dagger] = \delta_{\mathbf{p}, \mathbf{p}'} \quad \text{and} \quad [\hat{a}_{\mathbf{p}}, \hat{a}_{\mathbf{p}'}] = 0 = [\hat{a}_{\mathbf{p}}^\dagger, \hat{a}_{\mathbf{p}'}^\dagger], \quad (8.45)$$

such that the field operator $|\Psi\rangle$ in momentum representation is given by

$$|\Psi\rangle = \sum_{\mathbf{p}_1} \cdots \sum_{\mathbf{p}_N} \psi(\mathbf{p}_1, \dots, \mathbf{p}_N) \hat{a}_{\mathbf{p}_1}^\dagger \cdots \hat{a}_{\mathbf{p}_N}^\dagger |0\rangle, \quad (8.46)$$

with the vacuum state $|0\rangle$, defined as $\hat{a}_{\mathbf{p}}|0\rangle = 0$ for all \mathbf{p} , and the Fourier transform of the wave function $\psi(\mathbf{p}_1, \dots, \mathbf{p}_N)$. Under the aforesaid assumptions, the Hamiltonian (8.20) becomes

$$\hat{H} = \sum_{\mathbf{p}} \frac{p^2}{2m} \hat{a}_{\mathbf{p}}^\dagger \hat{a}_{\mathbf{p}} + \frac{U}{V} \sum_{\mathbf{p}, \mathbf{p}', \mathbf{q}} \hat{a}_{\mathbf{p}+\mathbf{q}}^\dagger \hat{a}_{\mathbf{p}'-\mathbf{q}}^\dagger \hat{a}_{\mathbf{p}'} \hat{a}_{\mathbf{p}}, \quad (8.47)$$

and the normalized, non-interacting ground state corresponding to zero energy is given by

$$|\Psi_0\rangle = (N!)^{1/2} \left(\hat{a}_{\mathbf{0}}^\dagger \right)^N |0\rangle, \quad (8.48)$$

such that all particles are condensed, $n_{\mathbf{p}} = \langle \hat{a}_{\mathbf{p}}^\dagger \hat{a}_{\mathbf{p}} \rangle = N\delta_{\mathbf{p}, \mathbf{0}}$.

This is the starting point for Bogoliubov's approximation: The condensation hypothesis acts on the assumption that for weak interactions the fraction of bosons condensed to the ground state n_0/N is of order one, while all the other excitations mainly come in pairs with opposite momentum. This can be motivated by a perturbative argument starting with a fully condensed state (8.48) and successively applying the Hamiltonian (8.47). A first application of the interaction term yields one pair of bosons with opposite momenta $\{\mathbf{p}, -\mathbf{p}\}$, while all the other $N - 2$ bosons remain in the ground state. A second application can either create a triplet $\{\mathbf{p}, \mathbf{p}', \mathbf{q}\}$, such that $\mathbf{p} + \mathbf{p}' + \mathbf{q} = \mathbf{0}$ or two pairs, $\{\mathbf{p}, -\mathbf{p}\}$ and $\{\mathbf{p}', -\mathbf{p}'\}$. However, the creation of two pairs is much more likely, since the relative probability is given by $(N - 2)(N - 3)/4$. If we keep only terms in the Hamiltonian (8.47), which result in pairs, we can get an upper bound to the ground state energy via diagonalization.

Bogoliubov even made a further simplification by neglecting all terms including quadratic pair operators on the grounds that these are expected to be small compared to the first two terms and by replacing the operator $\hat{a}_0^\dagger \hat{a}_0$ by its expectation value n_0 . For weak interactions one can assume that the condensate is essentially not depleted and thus, that n_0 is of the order of N . Approximating $N - 1$ by N finally yields the Hamiltonian

$$H_B = \frac{UN^2}{V} + \sum_{\mathbf{p} \neq 0} \left(\left(\frac{p^2}{2m} + \frac{UN}{V} \right) \hat{a}_{\mathbf{p}}^\dagger \hat{a}_{\mathbf{p}} + \frac{UN}{V} \left(\hat{a}_{\mathbf{p}} \hat{a}_{-\mathbf{p}} + \hat{a}_{\mathbf{p}}^\dagger \hat{a}_{-\mathbf{p}}^\dagger \right) \right). \quad (8.49)$$

Note that the first term just gives the mean-field approximation of the energy (8.32) for the uniform Bose gas as predicted by the Gross-Pitaevskii equation. Since we have neglected the quadratic terms, there is no reason why diagonalization should in general give an upper bound to the original problem. Nevertheless, the Bogoliubov theory has been successfully applied to study the excitation spectrum of a homogeneous gas at zero temperature, as well as the depletion of the condensate and the changes to the ground-state energy. Moreover, the approximation can be used to study inhomogeneous gases and can be extended to excitations at a finite temperature (cf. [109] and references therein). Yet, this treatment is basically linear response theory and thus clearly does not account for the backreaction of the excitations on the condensate.

8.4.3 The time-dependent Gross-Pitaevskii equation

To treat dynamical problems in the limit of infinite particle numbers it seems somehow natural to consider the time-dependent generalization of the Gross-Pitaevskii equation (8.36). There are several heuristic ways to motivate this equation starting directly from the many-body Hamiltonian (8.20) and assuming a macroscopic occupation of a single-particle state, which we will shortly present in the following. However, none of them is mathematically intangible and their use is mainly justified by pragmatic considerations, even though there are innumerable applications of the time-dependent GPE. One method for rigorously analysing the dynamics in the macroscopic limit is discussed in the chapter 6, where we comment also on its relation to the general theory of quantum mean-field systems.

In the Heisenberg picture, the equation of motion for the field operator $\hat{\Psi}$ is given by

$$i\hbar \frac{\partial}{\partial t} \hat{\Psi}(\mathbf{r}, t) = -\frac{\hbar^2}{2m} \Delta \hat{\Psi}(\mathbf{r}, t) + V_{\text{ext}}(\mathbf{r}) \hat{\Psi}(\mathbf{r}, t) + U \hat{\Psi}^\dagger(\mathbf{r}, t) \hat{\Psi}^2(\mathbf{r}, t). \quad (8.50)$$

To derive advantage of the macroscopic occupation of the single-particle state ψ_0 , one decomposes the field operator into contributions from the condensed state and deviations from this state $\delta\hat{\psi}(\mathbf{r}, t)$

$$\hat{\Psi}(\mathbf{r}, t) = \psi_0(\mathbf{r}, t) \hat{a}_0 + \delta\hat{\psi}(\mathbf{r}, t), \quad (8.51)$$

where \hat{a}_0 annihilates a boson in the condensate wave function:

$$\hat{a}_0 = \int d\mathbf{r} \psi_0^*(\mathbf{r}) \hat{\Psi}(\mathbf{r}, t). \quad (8.52)$$

If we substitute this ansatz into the equations of motion (8.50), this yields the exact equation

$$\begin{aligned}
i\hbar \left(\frac{\partial \psi_0}{\partial t} \hat{a}_0 + \frac{\partial}{\partial t} \delta \hat{\psi} \right) &= \left(-\frac{\hbar^2}{2m} \Delta \psi_0 + V_{\text{ext}}(\mathbf{r}) \psi_0 \right) \hat{a}_0 + U |\psi_0|^2 \psi_0 \hat{a}_0^\dagger \hat{a}_0^2 \\
&+ \left(-\frac{\hbar^2}{2m} \Delta + V_{\text{ext}}(\mathbf{r}) \right) \delta \hat{\psi} + U \left(2 |\psi_0|^2 \hat{a}_0^\dagger \hat{a}_0 \delta \hat{\psi} + \psi_0^2 \hat{a}_0^2 \delta \hat{\psi}^\dagger \right) \\
&+ U \left(\psi_0^* \hat{a}_0^\dagger \delta \hat{\psi}^2 + 2 \psi_0 \hat{a}_0 \delta \hat{\psi}^\dagger \delta \hat{\psi} + \delta \hat{\psi}^\dagger \delta \hat{\psi}^2 \right), \tag{8.53}
\end{aligned}$$

where we have already chosen an ordering according to the quantum fluctuation operator $\delta \hat{\psi}$. Now, the common folklore states that in the macroscopic limit, quantum fluctuations are small and can be neglected to leading order, such that all terms including powers of $\delta \hat{\psi}$ are omitted and $\hat{a}_0^\dagger \hat{a}_0$ can be replaced by the macroscopic expectation value N_0 . The next-to-leading order equations, which linearize the equations of motion for $\delta \hat{\psi}$ around the mean-field approximation given by the GPE, are normally referred to as Bogoliubov-de-Gennes equations and are used to describe low-energy excitations around the ground state (cf., e.g., [65, 137]).

Alternatively, one assumes the system to be in a Glauber coherent state with a fixed phase. In combination with the assumption of a macroscopic occupation of the single-particle state $N_0 \gg 0$, this suggests the replacement

$$\hat{a}_0 |N_0, \dots\rangle \approx \sqrt{N_0} |N_0 - 1, \dots\rangle \approx \sqrt{N_0} |N_0, \dots\rangle \quad \text{for } N_0 \gg 0. \tag{8.54}$$

Thus, if one divides equation (8.53) by $\sqrt{N_0}$ and takes the limit of a condensate with infinite particle number $N_0 \rightarrow \infty$, equation (8.53) reduces to the time-dependent Gross-Pitaevskii equation

$$i\hbar \frac{\partial}{\partial t} \psi_0(\mathbf{r}, t) = -\frac{\hbar^2}{2m} \Delta \psi_0(\mathbf{r}, t) + V_{\text{ext}}(\mathbf{r}) \psi_0(\mathbf{r}, t) + g |\psi_0(\mathbf{r}, t)|^2 \psi_0(\mathbf{r}, t), \tag{8.55}$$

where we again recover the macroscopic interaction strength $g = UN_0$, as in the time-independent case (8.36).

The most common way to infer the Gross-Pitaevskii equation is to replace the field operators in the Heisenberg equation of motion by its expectation values. For the Bose-Hubbard Hamiltonian (8.25) the corresponding Heisenberg equation of motion is given by

$$i \frac{d}{dt} \hat{a}_j = -J (\hat{a}_{j-1} + \hat{a}_{j+1}) + U \hat{a}_j^\dagger \hat{a}_j \hat{a}_j. \tag{8.56}$$

Substituting \hat{a}_j by its expectation value $\langle \hat{a}_j \rangle = \sqrt{N} x_j$ and truncating all correlations according to

$$\langle \hat{a}_j^\dagger \hat{a}_k \hat{a}_l \rangle \approx \langle \hat{a}_j^\dagger \rangle \langle \hat{a}_k \rangle \langle \hat{a}_l \rangle \tag{8.57}$$

yields the *discrete* Gross-Pitaevskii equation

$$i \dot{x}_j = \epsilon_j x_j - J (x_{j+1} + x_{j-1}) + UN |x_j|^2 x_j, \tag{8.58}$$

where the truncation (8.57) is again valid for a coherent state. However, an initially coherent state is readily depleted during the time-evolution

The assumption (8.54), respective the replacement (8.57), which leads to the Gross-Pitaevskii equation, is sometimes referred to as the Bogoliubov ansatz. Note, that even if this replacement of bosonic annihilation and creation operators by c-numbers seems to be crude, it can be made rigorous in certain cases [138]. However, the naive treatment presented here clearly faces some conceptual problems [65, 71, 94], where one major objection beyond the obvious mathematical ones is the problem to treat systems with fixed particle number. This being the scenario in experiments. In this case the expectation values $\langle \hat{a}_0 \rangle$ and $\langle \hat{a}_0^\dagger \rangle$ vanish for a BEC, such that its expectation value no longer yields a sensible parametrization. Even more confusing is the assumption of a Glauber coherent state in (8.54) or (8.57) is not at all compatible with a macroscopic occupation of a single-particle state. These problems are even more striking if one considers possible ways to go beyond this simple treatment, as we will see in the following section.

8.4.4 Dynamics beyond mean-field

Quantum fluctuations are completely neglected in the Bogoliubov approach for deriving the time-dependent GPE. To go beyond the Gross-Pitaevskii equation one has either to include the dynamics of the quantum fluctuations in equation (8.53) or equivalently add supplementary evolution equations for the normal $\hat{a}_k^\dagger \hat{a}_l$ and anomalous $\hat{a}_k \hat{a}_l$ two-point functions and truncate at a later stage as in equation (8.57). Depending if and to what extent anomalous terms are neglected, the resulting models are known as the Hartree-Fock-Bogoliubov (HFB), HFB-Popov or Griffin (see, e.g., [139] and references therein). However, all these methods face some characteristic difficulties which are direct consequences of the breaking of the $U(1)$ symmetry [140]. For instance, none of them conserves the total number of particles while, at the same time, allowing for particle exchange between the condensate and the remaining modes.

To avoid these conceptual problems, it is most convenient to use the two-point functions

$$\sigma_{jk} = \langle \hat{E}_{jk} \rangle = \langle \hat{a}_j^\dagger \hat{a}_k \rangle \quad (8.59)$$

given by the single-particle density function (8.29) instead of one-point functions $\langle \hat{a}_k \rangle$. In contrast to single annihilation and creation operators, these quantities are measurable and thus represent physically relevant observables. The expectation value of these operators for a BEC, given a product state with fixed particle number does not vanish, thus yielding a sensible parametrization for the bulk dynamics. Moreover, these quantities span the dynamical group of the Hamiltonian. This fact is essential for the quantum phase space description discussed in chapter 6.

The evolution equations of the two-point functions (8.59) for the Bose-Hubbard Hamiltonian (8.25) are given by

$$\begin{aligned} i\frac{d}{dt}\langle\hat{a}_j^\dagger\hat{a}_k\rangle &= (\epsilon_k - \epsilon_j)\langle\hat{a}_j^\dagger\hat{a}_k\rangle - J\langle\hat{a}_j^\dagger\hat{a}_{k+1} + \hat{a}_j^\dagger\hat{a}_{k-1} - \hat{a}_{j+1}^\dagger\hat{a}_k - \hat{a}_{j-1}^\dagger\hat{a}_k\rangle \\ &\quad + U\langle\hat{a}_j^\dagger\hat{a}_k\hat{a}_k^\dagger\hat{a}_k - \hat{a}_j^\dagger\hat{a}_j\hat{a}_j^\dagger\hat{a}_k\rangle. \end{aligned} \quad (8.60)$$

In terms of the SPDM and the covariances

$$\Delta_{jk\ell m} = \langle\hat{a}_j^\dagger\hat{a}_k\hat{a}_\ell^\dagger\hat{a}_m\rangle - \langle\hat{a}_j^\dagger\hat{a}_k\rangle\langle\hat{a}_\ell^\dagger\hat{a}_m\rangle \quad (8.61)$$

they can be rewritten as

$$\begin{aligned} i\frac{d}{dt}\sigma_{j,k} &= (\epsilon_k - \epsilon_j)\sigma_{j,k} - J(\sigma_{j,k+1} + \sigma_{j,k-1} - \sigma_{j+1,k} - \sigma_{j-1,k}) \\ &\quad + U(\sigma_{kk}\sigma_{jk} + \Delta_{jkkk} - \sigma_{jj}\sigma_{jk} - \Delta_{jjjk}). \end{aligned} \quad (8.62)$$

For a Bose-Einstein condensate with a macroscopic number of particles the variances scale only linearly with the particle number N , while the products $\sigma_{jk}\sigma_{\ell m}$ scale as N^2 . If one thus neglects the variances $\Delta_{jk\ell m}$ one recovers the discrete Gross-Pitaevskii equation (8.58) by the identification $\sigma_{j,k} = x_j^*x_k$. Note that here we have not assumed a Glauber coherent state but only a BEC at any stage of the approximation, in contrast to the approach based on one-point functions presented in the preceding section.

To describe quantum correlations and the depletion of the condensate, at least approximately, one has to calculate evolution equations for the four-point functions

$$\begin{aligned} i\frac{d}{dt}\langle\hat{a}_j^\dagger\hat{a}_m\hat{a}_k^\dagger\hat{a}_n\rangle &= (\epsilon_m + \epsilon_n - \epsilon_j - \epsilon_k)\langle\hat{a}_j^\dagger\hat{a}_m\hat{a}_k^\dagger\hat{a}_n\rangle \\ &\quad - J\langle\hat{a}_j^\dagger\hat{a}_m\hat{a}_k^\dagger\hat{a}_{n+1} + \hat{a}_j^\dagger\hat{a}_m\hat{a}_k^\dagger\hat{a}_{n-1} + \hat{a}_j^\dagger\hat{a}_{m+1}\hat{a}_k^\dagger\hat{a}_n + \hat{a}_j^\dagger\hat{a}_{m-1}\hat{a}_k^\dagger\hat{a}_n \\ &\quad - \hat{a}_{j+1}^\dagger\hat{a}_m\hat{a}_k^\dagger\hat{a}_n - \hat{a}_{j-1}^\dagger\hat{a}_{m+1}\hat{a}_k^\dagger\hat{a}_n - \hat{a}_j^\dagger\hat{a}_m\hat{a}_{k+1}^\dagger\hat{a}_n - \hat{a}_j^\dagger\hat{a}_m\hat{a}_{k-1}^\dagger\hat{a}_n\rangle \\ &\quad + U\langle\hat{a}_j^\dagger\hat{a}_m\hat{n}_m\hat{a}_k^\dagger\hat{a}_n + \hat{a}_j^\dagger\hat{a}_m\hat{a}_k^\dagger\hat{a}_n\hat{n}_n - \hat{n}_j\hat{a}_j^\dagger\hat{a}_m\hat{a}_k^\dagger\hat{a}_n - \hat{a}_j^\dagger\hat{a}_m\hat{n}_k\hat{a}_k^\dagger\hat{a}_n\rangle \end{aligned} \quad (8.63)$$

and neglect higher order variances in order to obtain a closed set of equations. Technically, this amounts to a truncation of six-point functions in the interaction term in (8.64) according to [140]

$$\begin{aligned} \langle\hat{a}_j^\dagger\hat{a}_m\hat{a}_k^\dagger\hat{a}_n\hat{a}_r^\dagger\hat{a}_s\rangle &\approx \langle\hat{a}_j^\dagger\hat{a}_m\hat{a}_k^\dagger\hat{a}_n\rangle\langle\hat{a}_r^\dagger\hat{a}_s\rangle + \langle\hat{a}_j^\dagger\hat{a}_m\hat{a}_r^\dagger\hat{a}_s\rangle\langle\hat{a}_k^\dagger\hat{a}_n\rangle \\ &\quad + \langle\hat{a}_k^\dagger\hat{a}_n\hat{a}_r^\dagger\hat{a}_s\rangle\langle\hat{a}_j^\dagger\hat{a}_m\rangle - 2\langle\hat{a}_j^\dagger\hat{a}_m\rangle\langle\hat{a}_k^\dagger\hat{a}_n\rangle\langle\hat{a}_r^\dagger\hat{a}_s\rangle. \end{aligned} \quad (8.64)$$

The coherent evolution of the variances is thus given by

$$\begin{aligned} i\frac{d}{dt}\Delta_{jmkn} &\approx (\epsilon_m + \epsilon_n - \epsilon_j - \epsilon_k)\Delta_{jmkn} \\ &\quad - J\left[\Delta_{j,m,k,n+1} + \Delta_{j,m,k,n-1} + \Delta_{j,m+1,k,n} + \Delta_{j,m-1,k,n} \right. \\ &\quad \left. - \Delta_{j,m,k+1,n} - \Delta_{j,m,k-1,n} - \Delta_{j+1,m,k,n} - \Delta_{j-1,m,k,n}\right] \\ &\quad + U\left[\Delta_{mmkn}\sigma_{jm} - \Delta_{jjkn}\sigma_{jm} + \Delta_{jmnn}\sigma_{kn} - \Delta_{jmkk}\sigma_{kn} \right. \\ &\quad \left. + \Delta_{jmkn}(\sigma_{mm} + \sigma_{nn} - \sigma_{kk} - \sigma_{jj})\right]. \end{aligned} \quad (8.65)$$

This approach based on the number conserving generators \hat{E}_{jk} of the $su(M)$ algebra was first introduced by James Anglin and Amichay Vardi [69, 141] and is commonly referred to as *Bogoliubov backreaction* (BBR). Several numerical examples shown in [140] suggest that the BBR method provides a better approximation to the many-particle dynamics than HFB and its varieties while being conceptually much simpler and avoiding the common problems of the Hartree-Fock-Bogoliubov approximation. But still, BBR is limited to the first two moments of the operators \hat{E}_{jk} . Higher order correlation functions are not defined at all. This is clearly different within the phase space description, which we have discussed in detail in the chapter 6.

8.5 Noise and dissipation in a trapped Bose-Einstein condensate

A major challenge for the effective control of quantum systems is to maintain coherence in the presence of decoherence effects and dissipation caused by the unavoidable coupling to the environment. Methods to attenuate phase noise for an open two-mode BEC were discussed in [142], and the effects of particle loss on the spin squeezing of such a system were analyzed in [143].

Recently, novel opportunities for engineering the dynamics of interacting many-body systems by controlling dissipation have received attention, in an attempt to take advantage of this inevitable problem. It has been shown that dissipative processes can be tailored to prepare arbitrary pure states for quantum computation and strongly correlated states of ultracold atoms [144, 145] or even, in principle, to implement a universal set of quantum gates [146]. A recent experiment has even proven that inelastic collisions may inhibit particle losses and induce strong correlations in a quasi one-dimensional gas of ultracold atoms [147, 148].

In chapter 9 we will give a detailed analysis of the effects of phase noise and dissipation on a Bose-Einstein condensate in a double-well trap. There, we will see that the phase coherence of a weakly-interacting condensate as well as the response to an external driving show a pronounced stochastic resonance effect: Both quantities assume a maximum for a finite value of the loss rate matching the intrinsic time scales of the system and can thus be effectively tuned by controlled dissipation. Similar effects have been found in spin chains, where the entanglement assumes an maximum for a finite amount of thermal noise [149]. Even stronger effects are observed when dissipation acts concurrently with strong inter-particle interactions, as we will explain in section 9.3.3. In this case, dissipation can be used to restore the purity of the condensate almost completely and increase the phase coherence significantly. These effects are not restricted to the case of two modes, but are also present in extended lattices. In chapter 11 we will analyse the effects of phase noise and particle loss on the dynamics of a Bose-Einstein condensate in optical lattices and show how localized particle dissipation can lead to surprising dynamical effects, such as an effective suppression of decay and

an inhibition of tunneling, a restoration of coherence and creation of stable nonlinear structures, such as discrete breathers and dark solitons.

Such localized loss effects in an optical lattice require single-site addressability, which implies a resolution on the order of the laser wavelength. Such a challenging optical resolution of a few hundred nanometers has only been recently achieved by advanced imaging techniques [104, 105]. Up to now, the best spatial resolution of about 150 nm could be achieved using a technique based on scanning electron microscopy [150], where atoms are removed from the lattice via a focused electron beam.

In the following, we will give a short overview over the theoretical description of phase noise and particle dissipation for ultracold bosons in an optical lattice. We also introduce the Monte Carlo wave function method [151–153], a method for simulating the dynamics of a master equation by a wave function evolution including a stochastic element.

8.5.1 Master equation

Even though current experiments with Bose-Einstein condensates reach temperatures of less than 10^{-6} Kelvin, heating processes e.g. due to collisions, incoherent scattering and spontaneous emission of light or laser fluctuations leading to phase noise and amplitude noise on the lattice potential, are inevitable. Two recent, but independent approaches taking into account these processes lead to the same generic form of the master equation, while in both cases the coherent part of the dynamics are described by the Bose-Hubbard Hamiltonian (8.25).

A first model for noise and dissipation in a deep trapping potential has been derived by James Anglin [154] and later extended by Janne Ruostekoski and Dan F. Walls [155]. They consider a dilute gas of bosons in a deep trap, respectively in a double-well trap (cf. section 9.1), where only one mode in each well is significantly populated, whereas all higher, unbound modes contribute to the heat bath. The dynamics are then given by the master equation

$$\begin{aligned} \dot{\hat{\rho}} = & -i[\hat{H}, \hat{\rho}] - \frac{\kappa}{2} \sum_{j=1,2} (\hat{n}_j^2 \hat{\rho} + \hat{\rho} \hat{n}_j^2 - 2\hat{n}_j \hat{\rho} \hat{n}_j) \\ & - \frac{\gamma_{\text{atoms}}}{2} \sum_{j=1,2;\pm} \left(\hat{C}_{j\pm}^\dagger \hat{C}_{j\pm} \hat{\rho} + \hat{\rho} \hat{C}_{j\pm}^\dagger \hat{C}_{j\pm} - 2\hat{C}_{j\pm} \hat{\rho} \hat{C}_{j\pm}^\dagger \right) \end{aligned} \quad (8.66)$$

with the Lindblad operators

$$\begin{aligned} \hat{C}_{j+} &= \hat{a}_j^\dagger \quad \text{and} \\ \hat{C}_{j-} &= e^{\beta/2(\epsilon_j - \mu + U\hat{n}_j)} \hat{a}_j, \end{aligned} \quad (8.67)$$

describing growth and depletion of the condensate.

Let us briefly discuss the effects of the noise and dissipation terms. The second term $\sim \kappa$ in (8.66) describes phase noise due to elastic collisions with the background gas atoms.

It is usually the dominating contribution, effectively heating the system, but leaving the total particle number invariant. If only phase noise is present, the system relaxes to an equilibrium state where all coherences are lost and all Dicke states $|n_1, N - n_1\rangle \sim \hat{a}_1^{\dagger n_1} \hat{a}_2^{\dagger N - n_1} |0, 0\rangle$ are equally populated

$$\langle n_1, N - n_1 | \hat{\rho} | n'_1, N - n'_1 \rangle = \frac{1}{N + 1} \delta_{n_1, n'_1}, \quad (8.68)$$

as long as $J \neq 0$ [59, 156]. This corresponds to a thermal state of infinite temperature, respectively a completely mixed state.

The remaining terms $\sim \gamma_{\text{atoms}}$ in the master equation (8.66) describe amplitude noise, that is the growth and depletion of the condensate due to inelastic collisions with the background gas. In contrast to phase noise, amplitude noise can heat *and* cool the system. Note that the system will relax to the proper thermal state with a density operator $\hat{\rho} \propto \exp(-\beta(\hat{H} - \mu\hat{n}))$ only if both amplitude and phase noise are present.

In current experiments intrinsic amplitude noise is usually extremely weak in comparison to phase noise [155], if it is not introduced artificially as for example by forced evaporative cooling during the preparation of the BEC. For example, phase noise damps Josephson oscillations on a timescale of a few hundred milliseconds in the experiments, while less than 10% of the atoms are lost during a 30 s experiment [157–159]. Thus, the effects of intrinsic amplitude noise can be neglected to a good approximation.

In the same manner, one could argue, that perturbations caused by the background gas could be prevented to a large extent by a careful cooling process and a lower pressure. Yet, elastic collisions are not the only source of phase noise in current experiments. The dominant heating mechanism, especially in the case of red-detuned lattices, is expected to be incoherent scattering of laser light (cf., e.g., [160]). A detailed study of the decoherence of many-body states due to spontaneous emission is given in [161], where the dominant processes in a system described by a single-band Bose-Hubbard Hamiltonian (8.25) are described by the master equation

$$\dot{\hat{\rho}} = -i[\hat{H}, \hat{\rho}] - \frac{\kappa}{2} \sum_j^M (\hat{n}_j^2 \hat{\rho} + \hat{\rho} \hat{n}_j^2 - 2\hat{n}_j \hat{\rho} \hat{n}_j). \quad (8.69)$$

Non-trivial effects of dissipation such as the stochastic resonance discussed in chapter 9 or the creation of stable nonlinear structures addressed in chapter 11 require localized, controlled loss processes. Such a strong and tunable source of dissipation can be implemented artificially by shining a resonant laser beam using a high resolution objective with single-site addressability [104, 105] or by a focused electron beam [150], that removes atoms with the site-dependent rates $\gamma_{\text{atoms},j}$. In magnetic trapping potentials, this can also be achieved by a forced rf-transition to an untrapped magnetic substate [162].

The master equation description of forced, localized particle loss, is well established [59] and routinely used in the context of photon fields. In the following chapters we will

thus consider the dynamics generated by the master equation

$$\begin{aligned} \dot{\hat{\rho}} = & -i[\hat{H}, \hat{\rho}] - \frac{\kappa}{2} \sum_{j=1,2} (\hat{n}_j^2 \hat{\rho} + \hat{\rho} \hat{n}_j^2 - 2\hat{n}_j \hat{\rho} \hat{n}_j) \\ & - \frac{1}{2} \sum_{j=1,2} \gamma_{\text{atoms},j} \left(\hat{a}_j^\dagger \hat{a}_j \hat{\rho} + \hat{\rho} \hat{a}_j^\dagger \hat{a}_j - 2\hat{a}_j \hat{\rho} \hat{a}_j^\dagger \right), \end{aligned} \quad (8.70)$$

including thus both phase noise and particle dissipation.

8.5.2 Monte Carlo wave function method

Quantum theory is usually used to describe ensembles, and can not be adapted to the description of single realisations without further explanation. This is especially true in the case of a system subject to dissipation caused by the irreversible coupling to the environment, which usually has far too many degrees of freedom to monitor them all at a time. In this case the common knowledge is to describe the evolution of the microsystem by a master equation, tracing out the reservoir states and resulting in an effective description by density matrices, which are nothing else than ensemble descriptions.

Some advanced techniques in quantum optics – including ion traps, cavities and optical lattices – allow experimental observations and manipulations of single particles, which feature quantum jumps. These jumps are due to a sudden increase of knowledge, since e.g. a photon is detected or not, and lead to a conditional time evolution. Even if there is no real measurement taking place, one could imagine a series of repeated *gedanken measurements* with random results, which determine the state of system and bring about the irreversibility of the dynamics. In the context of quantum optics several methods for treating single realizations via a conditional dynamics of wave functions have been developed. These are variously described as Quantum Jump, Monte Carlo Wave function (MCWF) or the Quantum Trajectory method. For a comprehensive review of these methods and a careful discussion of their interrelationships see e.g. [163]. Beneath their descriptive appeal, these methods provide an extremely useful computational tool, since the number of equations which need to be solved simultaneously scales linearly with the number of states and not quadratically, as it is the case for density matrices.

Here we will follow the argument presented in [151] to introduce the general idea behind the Quantum Jump approach. For further details see also [152, 153].

To keep both the notation and the physics simple, we use the generic example of a two-level atom coupled simultaneously to a classical laser field, together with a quantized electromagnetic field inducing spontaneous emission. The two states of the atom are labeled $|g\rangle$ for the ground state and $|e\rangle$ for the excited state, while the laser field is chosen to be monochromatic,

$$E(t) = E_0 \cos(\omega_L t). \quad (8.71)$$

In the rotating wave approximation, the interaction Hamiltonian of the atom and the laser in terms of the raising $\hat{S}^+ = |e\rangle\langle g|$ and lowering operators $\hat{S}^- = |g\rangle\langle e|$ is given by

$$\hat{H}_0 = -\Delta\hat{S}^+\hat{S}^- + \frac{\Omega}{2}(\hat{S}^+ + \hat{S}^-). \quad (8.72)$$

Here, $\Delta = \omega_L - \omega_{\text{res}}$ denotes the detuning of the laser with respect to the atomic transition and $\Omega = -dE_0$ is the Rabi frequency, defined as the atomic dipole moment d times the electric field of the laser. Note that we again use rescaled variables such that $\hbar = 1$.

At time t , the total state of the composed atom-laser system and the quantized electromagnetic field in the vacuum state $|0\rangle$ is given by

$$\begin{aligned} |\Psi(t)\rangle &= |\phi(t)\rangle \otimes |0\rangle \\ &= (\alpha|g\rangle + \beta|e\rangle) \otimes |0\rangle. \end{aligned} \quad (8.73)$$

One time step further, at $t + dt$, one photon may have been emitted spontaneously. To ensure that it is at most one, we choose dt to be much smaller than all other timescales involved,

$$dt \ll \Gamma^{-1}, \Omega^{-1}, \Delta^{-1}, \quad (8.74)$$

where Γ denotes the rate of spontaneous emission. Within a perturbative treatment of the problem, commonly known as Wigner-Weisskopf approach [164], we can now calculate the wave function at time $t + dt$ as

$$|\Psi(t + dt)\rangle = (\alpha'(t)|g\rangle + \beta'|e\rangle) \otimes |0\rangle + |g\rangle \otimes \sum_{\mathbf{k}, \epsilon} c_{\mathbf{k}, \epsilon} |\mathbf{k}, \epsilon\rangle. \quad (8.75)$$

Since we restrict the analysis to very short timescales dt , the probability of a re-excitation after the spontaneous emission can be neglected. Thus it is sufficient to consider only the case where the quantized field contains a single excitation, with a probability amplitude $c_{\mathbf{k}, \epsilon}$ in the respective mode, while the atom is still in the ground state and not yet re-excited.

The square of the norm of the second summand is equal to the probability for a spontaneous emission during the interval dt :

$$dp = \Gamma dt |\alpha|^2 = \Gamma dt \langle \phi(t) | \hat{S}^+ \hat{S}^- | \phi(t) \rangle, \quad (8.76)$$

and the total norm is preserved, $\langle \Psi(t) | \Psi(t) \rangle = 1$. The coefficients α', β' can be determined from the evolution of the atomic state $|\phi(t)\rangle$ during dt under the action of the non-hermitian Hamiltonian

$$\hat{H} = \hat{H}_0 - \frac{i}{2}\Gamma\hat{S}^+\hat{S}^-, \quad (8.77)$$

which reduces the amplitude of the excited state by a factor $1 - \Gamma dt/2$.

If we now perform a perfect *gedanken measurement* on the atom, we get two possible, but random results: With a probability dp , cf. equation (8.76), we detect a photon and destroy it. Thus, the conditional wave function reads

$$|\Psi(t + dt)\rangle = |g\rangle \otimes |0\rangle. \quad (8.78)$$

In the case of no detection, we get a modification of the initial wave function as well,

$$\begin{aligned} |\Psi(t + dt)\rangle &= (1 - dp)^{-1/2} (\alpha' |g\rangle + \beta' |e\rangle) \otimes |0\rangle \\ &= (1 - dp)^{-1/2} \left(1 - idt\hat{H}\right) |\phi(t)\rangle \otimes |0\rangle, \end{aligned} \quad (8.79)$$

where the prefactor $\mu = (1 - dp)^{-1/2}$ is a result of the renormalization after the projection onto the subspace.

In both cases, the structure of the total wave function remains the same as in equation (8.73). To determine the random time evolution of the atom, one has to repeat this procedure and consider the averaged result. This method is known as the Monte Carlo Wave function approach, as presented in [151]. The result $\overline{\sigma(t)}$, which we obtain by averaging over the different outcomes $\sigma(t) = |\phi(t)\rangle \langle\phi(t)|$ is equivalent to the result obtained from the master equation. This can be seen directly by an expansion in terms of dt

$$\begin{aligned} \overline{\sigma(t + dt)} &= \overline{|\phi(t)\rangle \langle\phi(t)|} \\ &= (1 - dp)\mu^2 - \left(1 - idt\hat{H}\right) |\phi(t)\rangle \langle\phi(t)| \left(1 + idt\hat{H}^\dagger\right) + dp |g\rangle \langle g| \\ &\approx \sigma(t) + idt \left(\hat{H}\sigma(t) - \sigma(t)\hat{H}^\dagger\right) + \Gamma dt \hat{S}^- \sigma(t) \hat{S}^+ \end{aligned} \quad (8.80)$$

Taking the average over the random outcomes $|\phi(t)\rangle$ all starting from the initial value $|\phi(0)\rangle$ yields

$$\frac{d\bar{\sigma}}{dt} = i \left[\bar{\sigma}, \hat{H}_0\right] + \frac{\Gamma}{2} \left(\hat{S}^+ \hat{S}^- \bar{\sigma} + \bar{\sigma} \hat{S}^+ \hat{S}^- \right) + \Gamma \hat{S}^- \bar{\sigma} \hat{S}^+, \quad (8.81)$$

which is equivalent to the master equation describing an atom subject to spontaneous emission [165, 166].

The MCWF method turns out to be not only a valuable computing method, but also provides a vivid illustration of the random nature of the quantum evolution. To adapt this method to the dissipative processes discussed in the previous section, two major differences have to be considered: Firstly, we are not considering one single atom, but a whole cloud of ultracold bosons, and secondly, we are not interested in the internal dynamics between atomic levels, but in localized particle loss processes. Thus, the wave function we are considering is an element of the symmetrized Fock space of N particles and the quantum jumps, respective the loss events, reduce the particle number one by one. Keeping in mind these differences, the basic structure remains the same: Calculating the conditional dynamics for the different possible outcomes by an effective non-hermitian evolution interrupted by quantum jumps and averaging over the random results allows for the simulation of the exact dynamics of about 100-200 atoms in a double- or triple-well trap. This will be especially beneficial in chapter 9 and in chapter 11, where we study dynamics in extended lattices.

Chapter 9

Dynamics of an open two-mode Bose-Einstein condensate

9.1 Ultracold atoms in a double-well trap

Ultracold atoms confined in a double-well trap are an extremely popular model system that can be realized in various experimental settings, e.g. by superimposing an optical lattice with an optical dipole trap [157–159], in a bichromatic optical lattice [124, 167], or on an atom chip [168]. The unitary part of the dynamics is described by the Bose-Hubbard Hamiltonian (8.25) restricted to two modes,

$$\hat{H} = -J \left(\hat{a}_1^\dagger \hat{a}_2 + \hat{a}_2^\dagger \hat{a}_1 \right) + \epsilon_1 \hat{n}_1 + \epsilon_2 \hat{n}_2 + \frac{U}{2} \left(\hat{a}_1^{\dagger 2} \hat{a}_1^2 + \hat{a}_2^{\dagger 2} \hat{a}_2^2 \right), \quad (9.1)$$

where \hat{a}_j and \hat{a}_j^\dagger are the bosonic annihilation and creation operators in mode $j \in \{1, 2\}$ and $\hat{n}_j = \hat{a}_j^\dagger \hat{a}_j$ is the corresponding number operator. J is the tunneling matrix element, ϵ_i denotes the on-site energies and U gives the interaction strength of two particles in the same well. As in the general case discussed earlier, we set $\hbar = 1$, thus measuring all energies in frequency units. Even if the model (9.1) seems simplistic it can describe the fundamental phenomena of two weakly coupled BECs in more general setups [169] and features complex dynamics as e.g. Landau-Zener transitions between different Bloch bands [170, 171], which will be discussed in more detail in chapter 10.

In this chapter, we will study the dynamics of a Bose-Einstein condensate (BEC) in a double-well trap including the effects of localized particle loss and phase noise. The basic setup under consideration including a potentially asymmetric particle loss is depicted in figure 9.1. The corresponding master equation description has been introduced in section 8.5.1:

$$\begin{aligned} \dot{\hat{\rho}} = & -i[\hat{H}, \hat{\rho}] - \frac{\kappa}{2} \sum_{j=1,2} \left(\hat{n}_j^2 \hat{\rho} + \hat{\rho} \hat{n}_j^2 - 2\hat{n}_j \hat{\rho} \hat{n}_j \right) \\ & - \frac{1}{2} \sum_{j=1,2} \gamma_{\text{atoms},j} \left(\hat{a}_j^\dagger \hat{a}_j \hat{\rho} + \hat{\rho} \hat{a}_j^\dagger \hat{a}_j - 2\hat{a}_j \hat{\rho} \hat{a}_j^\dagger \right). \end{aligned} \quad (9.2)$$

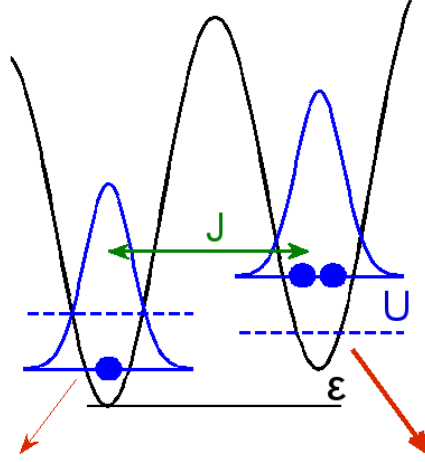


Figure 9.1: The two-mode system with (possibly) asymmetric loss rates

as discussed there, $\gamma_{\text{atoms},j}$ denotes the loss rate at the j -th lattice site and κ measures the strength of phase noise. In this section, we will focus on the coherent dynamics and especially on the dynamics in the mean-field limit. A detailed analysis of the effects of dissipation and phase noise on the dynamics will be the main subject of the subsequent sections.

In the following, the common transformation using the collective operators

$$\begin{aligned}\hat{L}_x &= \frac{1}{2} (\hat{a}_1^\dagger \hat{a}_2 + \hat{a}_2^\dagger \hat{a}_1), & \hat{L}_y &= \frac{i}{2} (\hat{a}_1^\dagger \hat{a}_2 - \hat{a}_2^\dagger \hat{a}_1), \\ \hat{L}_z &= \frac{1}{2} (\hat{a}_2^\dagger \hat{a}_2 - \hat{a}_1^\dagger \hat{a}_1),\end{aligned}\quad (9.3)$$

will turn out to be extremely useful, not only for illustrative reasons. With these definitions the Hamiltonian (9.1) can be rewritten as

$$\hat{H} = -2J\hat{L}_x + 2\epsilon\hat{L}_z + U\hat{L}_z^2 \quad (9.4)$$

up to a constant term with ϵ being defined as the difference between the on-site energies, $2\epsilon = \epsilon_1 - \epsilon_2$. Thus, the dynamical group is spanned by an angular momentum algebra $su(2)$,

$$[L_i, L_j] = \epsilon_{ijk} L_k, \quad (9.5)$$

with rotational quantum number $N/2$ [52, 141, 172, 173].

In chapter 6 we have seen how one can generalize the concept of coherent states based on the respective dynamical group. The generalization of the concept of the translation operator to the $su(2)$ algebra yields a rotation operator (cf. section 6.1.2). Thus, the

Bloch coherent states $|\theta, \phi\rangle$ can be defined as

$$\begin{aligned}
|\theta, \phi\rangle &= \hat{R}(\theta, \phi) |N, 0\rangle & (9.6) \\
&= e^{-i\theta(\hat{J}_x \sin \phi - \hat{J}_y \cos \phi)} |N, 0\rangle \\
&= \sum_{n_1+n_2=N} \binom{N}{n_2}^{\frac{1}{2}} \cos\left(\frac{\theta}{2}\right)^{n_1} \sin\left(\frac{\theta}{2}\right)^{n_2} e^{-in_2\phi} |n_1, n_2\rangle \\
&= \frac{1}{\sqrt{N!}} \left(\cos\left(\frac{\theta}{2}\right) a_1^\dagger + \sin\left(\frac{\theta}{2}\right) e^{-i\phi} a_2^\dagger \right)^N |0, 0\rangle, & (9.7)
\end{aligned}$$

where the last line illustrates the equivalence of $SU(2)$ coherent states to product states.

The group of rotations $\hat{R}(\theta, \phi)$ and equivalently the parameter space of coherent states can be described by two angles $0 \leq \theta \leq \pi, 0 \leq \phi < 2\pi$ and is thus isomorphic to a sphere \mathcal{S}^2 . This parametrization is often referred to as Bloch representation.

The expectation value of the angular momentum operators in Bloch coherent states (9.6) yields the (rescaled) Bloch vector

$$\mathbf{s} = \frac{\langle \theta, \phi | \hat{\mathbf{L}} | \theta, \phi \rangle}{N} = \frac{1}{2} \begin{pmatrix} \sin \theta \cos \phi \\ \sin \theta \sin \phi \\ -\cos \theta \end{pmatrix}. \quad (9.8)$$

The z -component of the Bloch vector \mathbf{s} is equivalent to the population imbalance of the two modes, while the polar angle represents the relative phase. Since this variable is cyclic and not defined if all particles are in a single well (respectively at the poles), the topology of the phase space is clearly that of a sphere. Note that, while considering systems with particle loss and thus a time-dependent particle number $N(t)$, it could also be beneficial to study the dynamics of the expectation values without rescaling, which will be denoted by $\ell(t) = \langle \theta, \phi | \hat{\mathbf{L}} | \theta, \phi \rangle$.

In section 7.2.2 we have seen that an amplitude phase transformation reveals the canonical structure of the macroscopic dynamics most clearly. Using the parametrization in terms of the relative population of the second mode, $p = \sin(\theta/2)^2$, and the relative phase between the modes $q = \phi$ the Bloch vector is given by

$$\mathbf{s} = \begin{pmatrix} \sqrt{p(1-p)} \cos(q) \\ \sqrt{p(1-p)} \sin(q) \\ p - 1/2 \end{pmatrix}. \quad (9.9)$$

In this parametrization the resulting Hamiltonian flow (cf. section 7.2.2) for the two-mode Bose-Hubbard model (9.1) is governed by the Hamiltonian function

$$\mathcal{H}(p, q) = -2J\sqrt{p(1-p)} \cos(q) + \frac{g}{4}(2p-1)^2 + \epsilon(2p-1) \quad (9.10)$$

and the dynamics is given by the canonical equations

$$\dot{q} = \frac{\partial \mathcal{H}}{\partial p} \quad \text{and} \quad \dot{p} = -\frac{\partial \mathcal{H}}{\partial q}. \quad (9.11)$$

As defined earlier $g = UN$ denotes the macroscopic interaction strength.

The resulting equations are equivalent to the discrete Gross-Pitaevskii equation

$$i \frac{d}{dt} \begin{pmatrix} x_1 \\ x_2 \end{pmatrix} = \begin{pmatrix} \epsilon + g|x_2|^2 & -J \\ -J & -\epsilon + g|x_2|^2 \end{pmatrix} \begin{pmatrix} x_1 \\ x_2 \end{pmatrix}, \quad (9.12)$$

which we have discussed in section 8.4.3. This can be easily verified by an identification of $x_1 = \sqrt{1-p}$ and $x_2 = \sqrt{p} \exp(-iq)$ and a neglect of the global phase (cf. equation (8.58)). The connection to the description in terms of the Bloch vector \mathbf{s} is given by

$$\mathbf{s} = \frac{1}{2} \begin{pmatrix} x_1^* x_2 + x_2^* x_1 \\ i(x_1^* x_2 - x_2^* x_1) \\ x_2^* x_2 - x_1^* x_1 \end{pmatrix}. \quad (9.13)$$

Thus, the evolution equations for the coherent mean-field dynamics of the Bloch vector read

$$\begin{aligned} \dot{s}_x &= -2\epsilon s_y - 2U s_y s_z, \\ \dot{s}_y &= 2J s_z + 2\epsilon s_x + 2U s_x s_z, \\ \dot{s}_z &= -2J s_y. \end{aligned} \quad (9.14)$$

The corresponding dynamics is depicted in figure 9.4 (a) and (d). Since the normalization of the Bloch vector $|\mathbf{s}|^2 = 1/2$, respective the total particle number N , is a conserved quantity, the mean-field dynamics is restricted to the surface of the Bloch sphere. The fixed points of the dynamics are identical to the critical points of the Hamiltonian function (9.10). In the linear case, cf. figure 9.4 (a), one recovers simple Rabi or Josephson oscillations. This changes drastically for an increasing interaction strength U , as is shown in figure 9.4 (d). If the interaction strength exceeds a critical value, $g = 2J$, one of the elliptic fixed points bifurcates into two novel elliptic and one hyperbolic fixed point. Due to the population imbalance at the fixed points, this is known as a self-trapping effect [172–174] and can be directly observed in current experiments [157].

Figure 9.2 shows an in-situ observation of the tunneling dynamics in a double-well trap by the group of Markus Oberthaler at the university of Heidelberg [157, 175]. One clearly observes the differences between Josephson oscillations (left) and the dynamics in the self-trapping regime (right), where only a minor fraction of the atoms tunnels between the wells, while the major part remains in the left well.

Note that the bifurcation of fixed points can be readily explained by topological considerations, since the Euler characteristic χ_{Euler} of the domain of a Hamiltonian function $\mathcal{H}(p, q)$ (9.10) is a topological invariant [176].

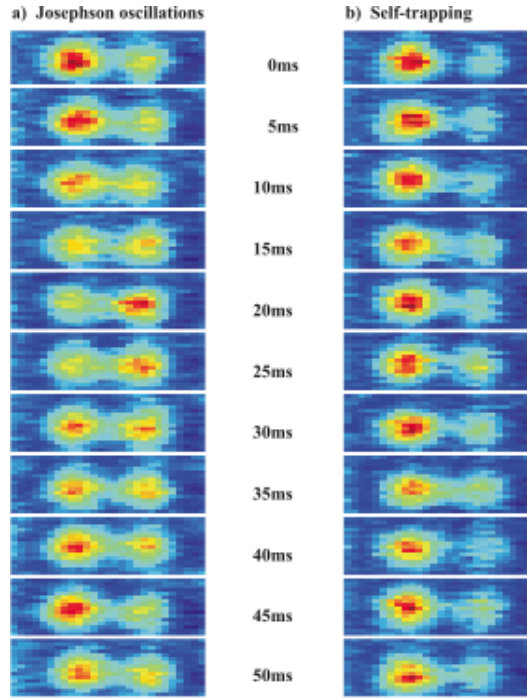


Figure 9.2: Observation of the macroscopic tunneling dynamics between two weakly linked BECs in a symmetric double well potential by the group of Markus Oberthaler at the university of Heidelberg (taken from the Dissertation of Michael Albiez [175]). Shown are absorption images of the atomic cloud after a variable evolution time in the subcritical, $g = UN < 2J$, and in the supercritical regime, $g > 2J$.

9.2 Dissipative mean-field dynamics

In the preceding section we have shortly commented on the coherent dynamics of ultra-cold atoms in a double-well trap. In this section, we are interested in the macroscopic dynamics of the atomic cloud, which is well described within a mean-field approximation, now including the effects of particle loss and dissipation.

9.2.1 Relation to the non-hermitian Gross-Pitaevskii equation

Starting from the master equation (9.2), we can calculate the evolution equations for the expectation values of the angular momentum operators (9.3),

$$\dot{\ell}_j = \text{tr}(\hat{L}_j \dot{\hat{\rho}}) \quad (9.15)$$

with $j = x, y, z$, as well as the expectation value of the total particle number $n = \langle \hat{n}_1 + \hat{n}_2 \rangle$:

$$\begin{aligned}\dot{\ell}_x &= -2\epsilon\ell_y - 2U(\ell_y\ell_z + \Delta_{yz}) - T_2^{-1}\ell_x, \\ \dot{\ell}_y &= 2J\ell_z + 2\epsilon\ell_x + 2U(\ell_x\ell_z + \Delta_{xz}) - T_2^{-1}\ell_y, \\ \dot{\ell}_z &= -2J\ell_y - T_1^{-1}\ell_z - T_1^{-1}f_a n/2, \\ \dot{n} &= -T_1^{-1}n - 2T_1^{-1}f_a\ell_z.\end{aligned}\tag{9.16}$$

Note that here and in the following the initial particle number is denoted by n_0 , whereas the time-dependent expectation value of the particle number is denoted by $n(t)$ to avoid confusion between the two quantities. A comparison to the coherent dynamics shows that equation (9.16) still includes the covariances

$$\Delta_{jk} = \langle \hat{L}_j \hat{L}_k + \hat{L}_k \hat{L}_j \rangle / 2 - \langle \hat{L}_j \rangle \langle \hat{L}_k \rangle,\tag{9.17}$$

which are neglected in the mean-field limit. This approximation is valid in the macroscopic limit, since the covariances vanish as $1/n$ if we assume the many-particle quantum state to be close to a pure BEC. The possibility to go beyond this approximation by truncating at a later stage and consider higher moments at least approximately will be addressed in chapter 11.

Moreover, the dynamics is fundamentally altered by dissipation, where we differentiate between two effects: The transversal T_2^{-1} and longitudinal T_1^{-1} damping rates are defined as follows

$$T_1^{-1} = (\gamma_{\text{atoms},1} + \gamma_{\text{atoms},2})/2 \quad \text{and} \quad T_2^{-1} = \kappa + T_1^{-1}\tag{9.18}$$

and the asymmetry factor of the loss rates is given by $f_a = (\gamma_{\text{atoms},2} - \gamma_{\text{atoms},1})/(\gamma_{\text{atoms},1} + \gamma_{\text{atoms},2})$. While the longitudinal damping rate T_1^{-1} describes the relaxation of the population imbalance, the transversal damping rate T_2^{-1} gives the rate at which the coherence between the two wells is suppressed.

In the non-interacting case $U = 0$, the equations of motion (9.16) resemble the Bloch equations in nuclear magnetic resonance (NMR) [177], except for the fact that the 'equilibrium' value of the population imbalance ℓ_z is given by $-f_a n/2$ and therefore depends on the decreasing expectation value of the total particle number n . The longitudinal relaxation is now associated with particle loss. In the interacting case, the dynamics is substantially altered compared to the NMR setup.

The major effect of phase noise is a reduction of the phase coherence between the two wells. In the Bloch picture this is reflected by the fact that the normalization of the Bloch vector $|\boldsymbol{\ell}|$ is no longer conserved. If only phase noise is present, an initially coherent state converges rapidly to a fully mixed state $\boldsymbol{\ell} = \mathbf{0}$, while the particle number $n(t)$ remains constant.

In the absence of phase noise the dynamics can be further simplified. In this case the particle number coincides with the magnitude of the Bloch vector $\sqrt{\ell_x^2 + \ell_y^2 + \ell_z^2} =$

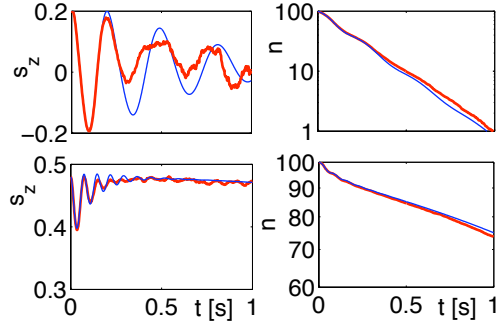


Figure 9.3: Comparison of the mean-field approximation (thin blue line) with the full many-particle dynamics calculated with the MCWF method (thick red line) for $J = 10 \text{ s}^{-1}$, $U = 1 \text{ s}^{-1}$, $\kappa = 3 \text{ s}^{-1}$ and for asymmetric particle loss $\gamma_{\text{atoms},1} = 0$ and $\gamma_{\text{atoms},2} = 5 \text{ s}^{-1}$. The initial state was assumed to be a pure BEC (that means a product state) with $\mathbf{s} = (0.46, 0, 0.2)$ (a) and $\mathbf{s} = (0.14, 0, 0.48)$ (b), respectively, and $n = 100$ particles.

$n(t)/2$, which we can use to reformulate the mean-field dynamics by an effective non-hermitian Gross-Pitaevskii equation

$$i \frac{d}{dt} \begin{pmatrix} \psi_1 \\ \psi_2 \end{pmatrix} = \begin{pmatrix} \tilde{\epsilon}_1 + U|\psi_1|^2 & -J \\ -J & \tilde{\epsilon}_2 + U|\psi_2|^2 \end{pmatrix} \begin{pmatrix} \psi_1 \\ \psi_2 \end{pmatrix} \quad (9.19)$$

now with complex on-site energies $\tilde{\epsilon}_j = \epsilon_j - i\gamma_{\text{atoms},j}/2$. Contrary to equation (9.12), we have chosen (ψ_1, ψ_2) not to be normalized to one, but to the particle number $n(t) = |\psi_1|^2 + |\psi_2|^2$, such that in this effective description a loss of particles is represented by a loss of normalization. The relation to the Bloch picture is given by the identification

$$\begin{aligned} \ell_x &= \frac{1}{2}(\psi_1^* \psi_2 + \psi_2^* \psi_1), & \ell_y &= \frac{1}{2i}(\psi_2^* \psi_1 - \psi_1^* \psi_2), \\ \ell_z &= \frac{1}{2}(|\psi_2|^2 - |\psi_1|^2). \end{aligned} \quad (9.20)$$

Note that the effective macroscopic interaction strength $g = Un(t)$ is now time-dependent.

An extension of this derivation to an arbitrary number of modes is straightforward, as we will see in chapter 11. Similar non-hermitian mean-field systems have been introduced phenomenologically to analyse resonances, transport and localization effects [178–183].

In the following, we depict the rescaled variables $s_j = \ell_j/n$, thus renormalizing to separate the decay of the particle number $n(t)$ from the internal dynamics.

Figure 9.3 shows a first comparison of the mean-field approximation including phase noise and dissipation to the full many-particle quantum dynamics calculated with the Monte Carlo wave function (MCWF) method, introduced in section 8.5.2. The trajectory in figure 9.3 (a) was started at $\mathbf{s} = (0.46, 0, 0.2)$ with a moderate population

imbalance, thus performing Josephson oscillations [157]. The amplitude is damped because of the phase noise, while the oscillation period increases as the effective macroscopic interaction strength $g(t) = Un(t)$ decreases. The decay of the particle number $n(t)$ is also strongly modulated by the oscillations of the population imbalance. The trajectory in figure 9.3 (b) was started at $\mathbf{s} = (0.14, 0, 0.48)$ in the self-trapping region. The residual oscillations are rapidly damped out and the system relaxes to a quasi-steady state on the shown time scale. The particle number decreases slowly and non-exponentially, since the condensate is mostly localized in the non-decaying potential well, cf. also [179]. All these features of the dynamics are well reproduced by the mean-field description, and the decay of the particle number is accurately predicted. Strong deviations are only expected in the vicinity of unstable fixed points of the mean-field dynamics. These fixed points will be analysed in more detail in next section.

9.2.2 Analysis of fixed points

We now consider the dynamics for a fixed value of the macroscopic interaction strength $g = Un = \text{const.}$ in the special case $\gamma_{\text{atoms},1} =: \gamma$ and $\gamma_{\text{atoms},2} = 0$. To explore the genuine effects of particle loss, phase noise is neglected ($\kappa = 0$) in the following.

Even though the restriction to a fixed interaction constant seems to be artificial, it reveals the effects of the particle loss on the structure of the mean-field phase space and especially the character of the fixed points most clearly. Moreover, the dynamics under a fixed interaction constant correspond to the periods of constant particle number between two loss processes in the quantum jumps picture, as introduced in section 8.5.2. Therefore this treatment provides a well-suited description of the short- as well as the long-time behaviour. Note that the more general case $\gamma_{\text{atoms},1} \neq 0$ and $\gamma_{\text{atoms},2} \neq 0$ does not lead to a fundamentally different dynamical behaviour since only the difference of the decay rates influences the internal dynamics. However, the expectation value of the particle number $n(t)$ and thereby also the effective interaction strength $g(t)$ decrease faster.

The resulting dynamics of the Bloch vector is illustrated in figure 9.4. The upper row (a-c) shows the phase space for the linear case, $U = 0$, where the mean-field approximation is exact. For comparison, the loss-free case is depicted in (a), showing the famous Josephson oscillations discussed earlier. An analysis of the fixed points for the dissipative dynamics shows the emergence of two regimes depending on the amplitude of the loss rate: For weak losses, $|\gamma| \leq 2J$, the fixed points are given by

$$\mathbf{s}_{\pm}^{\text{Josephson}} = \begin{pmatrix} \pm \left[\frac{1}{4} - \left(\frac{\gamma}{4J} \right)^2 \right]^{\frac{1}{2}} \\ -\frac{\gamma}{4J} \\ 0 \end{pmatrix}. \quad (9.21)$$

While the fixed points remain elliptic and the population is still equally distributed, the fixed points are no longer symmetric, since the relative phase between them decreases (b). This behaviour can be qualitatively understood within the analogy to

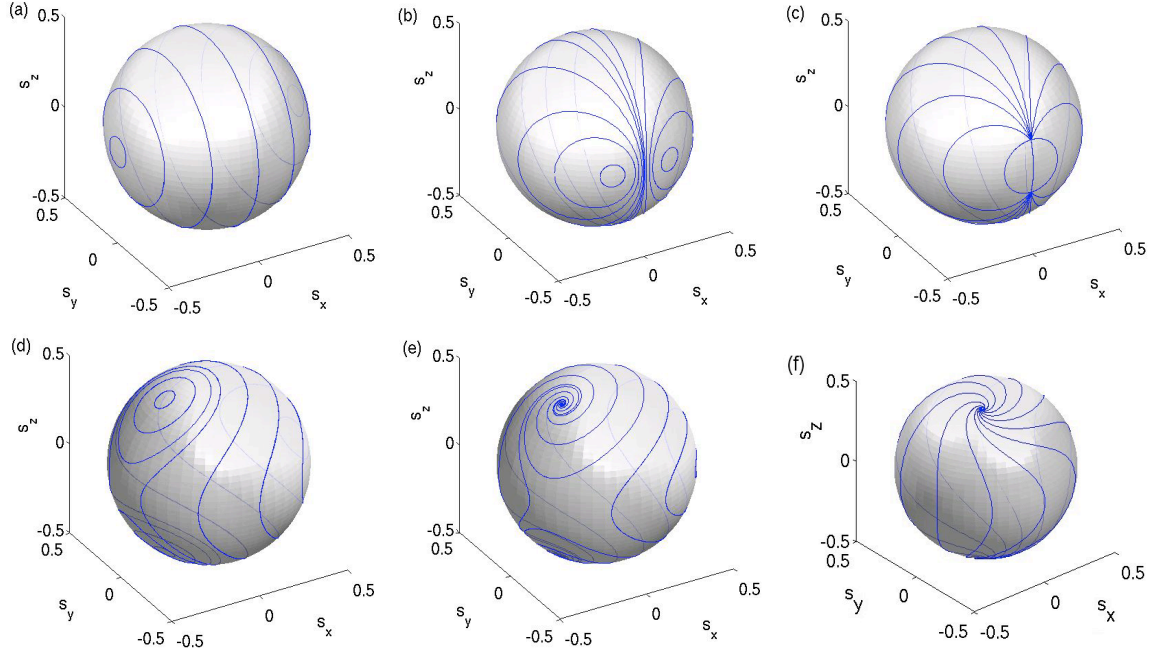


Figure 9.4: Mean-field dynamics for the non-interacting case $g = 0$ (upper row) and for a fixed interaction strength $g = 4 \text{ s}^{-1}$ (lower row) in dependence of the decay rate ($\gamma = 0$ for (a) and (d), $\gamma = 1.9 \text{ s}^{-1}$ for (b), $\gamma = 2.1 \text{ s}^{-1}$ for (c), $\gamma = 1 \text{ s}^{-1}$ for (e) and $\gamma = 4 \text{ s}^{-1}$ for (f)) – for all figures holds $J = 1 \text{ s}^{-1}$ and $\epsilon = 0$.

Josephson junctions: The weak decay induces an asymmetry between the wells leading to a continuous particle stream to the first well. At the fixed points this effect is compensated by the Josephson current $I_J \propto J s_y$ requiring $s_y \neq 0$.

For stronger decay rates, $|\gamma| \geq 2J$, the two fixed points are given by

$$\mathbf{s}_{\pm}^{\text{Decay}} = \begin{pmatrix} 0 \\ -\frac{J}{\gamma} \\ \pm \left[\frac{1}{4} - \left(\frac{J^2}{\gamma^2} \right)^{\frac{1}{2}} \right] \end{pmatrix}. \quad (9.22)$$

Above the critical value $|\gamma| = 2J$ the character of the two fixed points changes abruptly from elliptic into an attractive and a repulsive one as shown in figure 9.4 (c). The maximal Josephson current is no longer sufficient to compensate the current induced by the decay leading to a population excess in the non-decaying site. This explains the population imbalance in the fixed points which increases with ascending decay rates.

In the strongly interacting case without dissipation one observes the splitting of one of the elliptic fixed points into two novel elliptic and one hyperbolic fixed point, as discussed at the beginning of this chapter. However, the critical interaction strength for the occurrence of this bifurcation is lowered in the presence of dissipation to $g_{\text{crit}}^2 = U^2 n^2 \geq 4J^2 - \gamma^2$. In the subcritical regime for $\gamma < 2J$ and $U^2 n^2 \leq 4J^2 - \gamma^2$, we find oscillations around the same fixed points \mathbf{s}_{\pm}^J as in the non-interacting, but

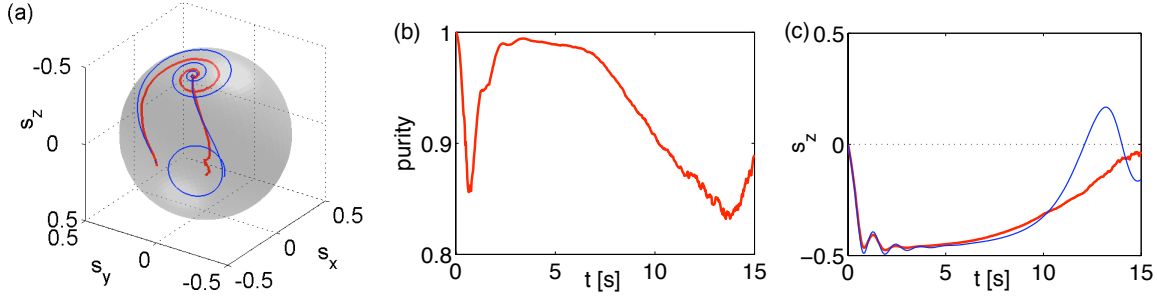


Figure 9.5: Comparison of the many-particle dynamics (thick red line) to the mean-field approximation (thin blues line) for an initially pure BEC with $\mathbf{s} = (-0.5, 0, 0)$ and $n(0) = 200$ particles: Dynamics of the Bloch vector \mathbf{s} (a), evolution of the purity (9.24) of the BEC (b) and evolution of the population imbalance s_z (c). The system initially relaxes to a non-linear quasi-steady state with a purity of almost one, which is then lost as $n(t)$ decreases. Parameters are chosen as $J = 1 \text{ s}^{-1}$, $Un(0) = 10 \text{ s}^{-1}$, $T_1 = 1 \text{ s}$ and $f_a = 1$.

dissipative case (9.21). However, these are now distorted (not shown in the figure). In the supercritical regime $g = Un > \sqrt{4J^2 + \gamma^2}$ and for a weak decay $\gamma < 2J$ one rediscovers a generalized self-trapping effect. As a result of the dissipative process, one elliptic fixed point now bifurcates into an attractive and a repulsive fixed point (by contrast to the two elliptic ones) and one hyperbolic one (cf. figure 9.4 (e)). The novel fixed points are located at:

$$\mathbf{s}_{\pm}^{\pi} = \frac{1}{\gamma^2 + g^2} \begin{pmatrix} -gJ \\ -\gamma J \\ \pm \sqrt{(\gamma^2 + g^2)(\frac{\gamma^2 + g^2}{4} - J^2)} \end{pmatrix}. \quad (9.23)$$

For stronger decay rates, $\gamma \geq 2J$, the hyperbolic and the elliptic fixed point s_{\pm}^J (9.21) meet and annihilate themselves as illustrated in figure 9.4 (f). Their disappearance is accompanied by the complete disintegration of periodic orbits.

9.2.3 Metastable dynamics

Let us finally discuss the implication of this phase space structure. We especially focus on the emergence of the attractive fixed point since it is stable and therefore strongly influences the many-body quantum dynamics. Figure 9.5 shows the dynamics of the rescaled Bloch vector \mathbf{s} comparing results of a MCWF simulation (solid red line) to the mean-field approximation (thin blue line). The given parameters correspond to the situations illustrated in figure 9.4 (b) or (e), respectively, depending on the value of the macroscopic interaction strength $g(t) = Un(t)$. The Bloch vector first relaxes to the attractive fixed point illustrated in figure 9.4 (e). The contraction of the mean-field trajectories to the attractive fixed point manifests itself by a convergence towards a

pure BEC, being the state of tightest localization in phase space. This is illustrated in figure 9.5 (b) where we have plotted the purity

$$p = 2 \operatorname{tr}(\hat{\rho}_{\text{red}}^2) - 1 \quad (9.24)$$

of the reduced single-particle density matrix [69, 94, 141]

$$\hat{\rho}_{\text{red}} = \frac{1}{N} \begin{pmatrix} \langle \hat{a}_1^\dagger \hat{a}_1 \rangle & \langle \hat{a}_1^\dagger \hat{a}_2 \rangle \\ \langle \hat{a}_2^\dagger \hat{a}_1 \rangle & \langle \hat{a}_2^\dagger \hat{a}_2 \rangle \end{pmatrix}. \quad (9.25)$$

Note, that the definition of the purity (9.24) is chosen such that a pure BEC, corresponding to a product state, is characterized by $p = 1$ and a completely mixed state yields $p = 0$, according to the common usage of this term in experimental physics. One can easily show that the purity is related to the Bloch vector \mathbf{s} by $p = |\mathbf{s}|^2 = |\boldsymbol{\ell}|^2/n^2$.

Figure 9.5 shows that the attractive fixed point is lost as $g(t) = Un(t)$ decreases, and thus the Bloch vector departs again and the purity starts to decrease again. This behaviour is very well predicted by the mean-field approximation already for the relatively small atom number assumed in the simulation. The mean-field trajectory then converges to the limit cycle shown in figure 9.4 (b). However, as the atoms are so rapidly lost nearly no particles remain to follow the limit cycle predicted by mean-field theory. This transition effect between different fixed points is closely related to the quantum state diffusion in and out of a metastable state, which can be observed in optical bistability (see, e.g., [184]). Note however, that the system considered here irretrievably departs from the metastable self-trapping state because the fixed point is lost as $n(t)$ decreases.

9.3 Dissipation induced coherence and stochastic resonance

Stochastic resonance (SR) is a strongly surprising, yet very general effect in nonlinear dynamical systems. Against our naive understanding, the response of a system to an external driving can be facilitated if an appropriate amount of noise is added. In fact, the maximum of the response – the stochastic resonance – is found if the timescale of the noise matches an intrinsic time scale of the system. The effect was first described for strongly damped classical systems such as the overdamped particle in a driven double well trap. In this case the noise is strong enough to induce transitions between the wells, whereas it is still weak enough not to randomize the dynamics completely. The particle will then hop to and fro almost deterministically if the average transition time between the wells due to the noise equals half of the driving period [185]. By now, a stochastic resonance has been shown in a variety of systems, an overview can be found in the review articles [186–189]. In addition to numerous examples in classical dynamics, stochastic resonance has also been found in a variety of quantum systems (see, e.g., [189–195]).

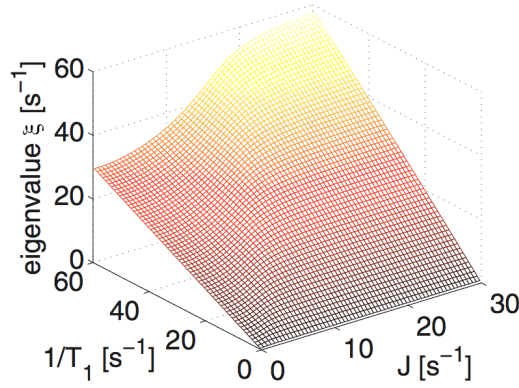


Figure 9.6: Decay rate ξ of the quasi-steady-state (9.27) as a function of the tunneling rate J and the dissipation rate T_1^{-1} for $\kappa = 5 \text{ s}^{-1}$ and $U = \epsilon = 0$.

In the following, we will show that a finite amount of dissipation induces a maximum of the coherence of a two-mode BEC, which can be understood as a stochastic resonance effect. In this discussion we have to distinguish between two different kinds of coherence, which will both be considered in the following. First of all we consider the phase coherence between the two wells, which is measured by the average *contrast* in interference experiments as described in [157–159] and given by

$$\alpha(t) = \frac{2|\langle \hat{a}_1^\dagger \hat{a}_2 \rangle|}{\langle \hat{n}_1 + \hat{n}_2 \rangle} = \frac{\sqrt{\ell_x(t)^2 + \ell_y(t)^2}}{n(t)}. \quad (9.26)$$

Secondly, we will analyze how close the many-particle quantum state is to a pure Bose-Einstein condensate. This property is quantified by the purity $p = 2 \text{tr}(\hat{\rho}_{\text{red}}^2) - 1$ of the reduced single-particle density matrix (9.25), with $p = 1$ indicating a pure BEC, as discussed earlier.

9.3.1 Dissipation induced coherence in a weakly-interacting Bose-Einstein condensate

In this section, we show that a proper amount of dissipation can indeed increase the phase coherence (9.26) of a two-mode BEC similar to the stochastic resonance effect. For simplicity, we start with the linear case $U = 0$, where the mean-field equations of motion for the expectation values (9.16) are exact. As already mentioned, the linear equations resemble the Bloch equations for driven nuclear spins in the rotating wave approximation [177], which are known to show a pronounced stochastic resonance effect [196]: The amplitude of forced oscillations of the spins given by ℓ_y assumes a maximum for a finite value of the relaxation rates T_1^{-1} and T_2^{-1} , provided that these two rates are coupled. For the two-mode BEC considered here this is automatically the case as given by equation (9.18). Thus we also expect a maximum of the steady state value of the phase coherence (9.26) for a finite value of T_1^{-1} .

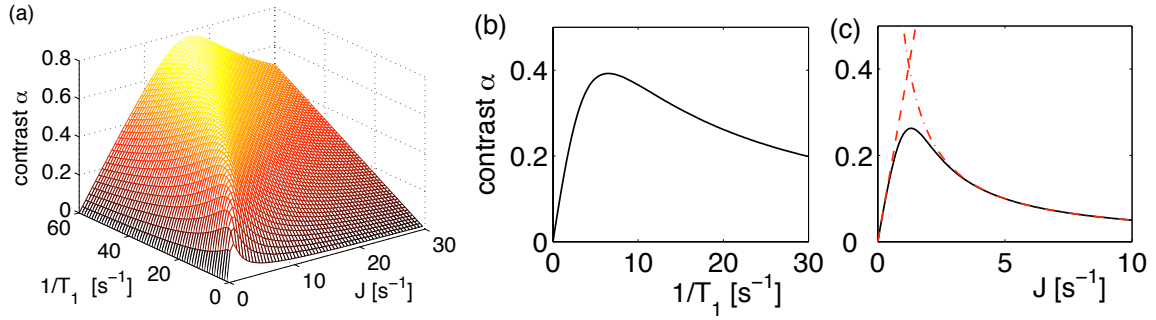


Figure 9.7: Contrast α of the quasi-steady state (9.27) as a function of the tunneling rate J and the dissipation rate T_1^{-1} (a) for $\kappa = 5 \text{ s}^{-1}$ and $U = \epsilon = 0$ and (b) for a fixed value of the tunneling rate $J = 2 \text{ s}^{-1}$ and (c) a fixed value of the dissipation rate $T_1^{-1} = 2 \text{ s}^{-1}$. The dash-dotted red lines represent the approximations (9.32) for small and large values of J , respectively.

Let us now determine the steady state value of the contrast (9.26) which quantifies the phase coherence of the two wells, as a function of the system parameters and the relaxation rates. Obviously, the only steady state in the strict sense is given by $\ell = \mathbf{0}$ and $n = 0$, corresponding to a completely empty trap. However, the system rapidly relaxes to a quasi-steady state where the internal dynamics is completely frozen out and all components of the Bloch vector and the particle number decay at the same rate:

$$\ell(t) = \ell_0 e^{-\xi t}, \quad n(t) = n_0 e^{-\xi t}. \quad (9.27)$$

Substituting this ansatz into the equations of motion (9.16), the quasi-steady state is determined by the eigenvalue equation

$$\mathbf{M} \begin{pmatrix} \ell_{x0} \\ \ell_{y0} \\ \ell_{z0} \\ n_0 \end{pmatrix} = \xi \begin{pmatrix} \ell_{x0} \\ \ell_{y0} \\ \ell_{z0} \\ n_0 \end{pmatrix} \quad (9.28)$$

with the matrix

$$\mathbf{M} = \begin{pmatrix} T_2^{-1} & 2\epsilon & 0 & 0 \\ -2\epsilon & T_2^{-1} & -2J & 0 \\ 0 & 2J & T_1^{-1} & f_a T_1^{-1} \\ 0 & 0 & f_a T_1^{-1} & T_1^{-1} \end{pmatrix}, \quad (9.29)$$

which is readily solved numerically.

Figure 9.6 depicts the smallest real eigenvalue ξ corresponding to the most stable quasi-steady-state as a function of J and T_1^{-1} for the noninteracting case and $\epsilon = 0$. It determines the basic time scale of the system and is essentially proportional to the dissipation rate T^{-1} .

Figure 9.7 shows the resulting values of the contrast α as a function of the dissipation rate T_1^{-1} and the tunneling rate J for $U = \epsilon = 0$ and $\kappa = 5 \text{ s}^{-1}$. For a fixed value of one of the parameters, say J , one observes a typical SR-like maximum of the contrast for a finite value of the dissipation rate T_1^{-1} as shown in part (b) of the figure. In particular, the contrast is maximal if the time scales of the tunneling and the dissipation are matched according to

$$4J^2 \approx f_a^2 T_1^{-2} + f_a \kappa T_1^{-1}. \quad (9.30)$$

Furthermore, the contrast $\alpha(J)$ shows a similar maximum for a finite value of the tunneling rate J when the dissipation rate is fixed as shown in figure 9.7 (c). Contrary to our intuition this shows that an increase of the coupling of two modes can indeed *reduce* their phase coherence.

In the special case $\epsilon = 0$, illustrated in figure 9.7, one can solve the eigenvalue equation (9.28) exactly. In this case one has $\ell_x = 0$ and the contrast α is related to the eigenvalue ξ by

$$\alpha = \frac{2J(T_1^{-1} - \xi)}{f_a T_1^{-1}(T_2^{-1} - \xi)}. \quad (9.31)$$

Evaluating the roots of the characteristic polynomial to determine ξ leads to an algebraic equation of third order which can be solved analytically. The resulting expressions are quite lengthy, but the limits for small and large values of the tunneling rate are readily obtained as

$$\begin{aligned} \alpha &\approx \frac{2J}{T_2^{-1} - (1 - f_a)T_1^{-1}} && \text{for } J \ll T_1^{-1} \\ \alpha &\approx \frac{f_a T_1^{-1}}{2J} && \text{for } J \gg T_1^{-1}. \end{aligned} \quad (9.32)$$

These approximations are plotted as dashed red lines in figure 9.7 (c). Their intersection given by (9.30) gives a very good approximation for the position of the SR-like maximum of the contrast $\alpha(J)$.

An important experimental issue is the question whether the quasi-steady state is reached fast enough, such that the typical SR-like curve of the contrast as shown in figure 9.7 can be observed, while still enough atoms are left in the trap. To answer this question, we integrate the equations of motion (9.16) starting from a pure BEC with $\ell(0)/n(0) = (\sqrt{3}/4, 0, 1/4)$ and $n(0) = 100$ particles. Figure 9.8 (a) shows the relaxation of the contrast for $J = 4 \text{ s}^{-1}$ and $T_1 = 1 \text{ s}$. The steady state value is nearly reached after $t = 1 \text{ s}$, when still 40% of the atoms are left in the trap. Figure 9.8 (b) shows the development of the contrast $\alpha(J)$ in time. It is observed that the characteristic SR-like maximum is already well developed after 1 second, where roughly half of the atoms are lost. Thus one can conclude that the SR-like maximum of the contrast should be observable in ongoing experiments.

The stochastic resonance effect introduced earlier is robust and generally not altered by changes of the system parameters or in the presence of weak inter-particle interactions. For instance, a change of the bias ϵ of the on-site energies of the two wells preserves the general shape of $\alpha(T_1^{-1}, J)$ shown in figure 9.7, and especially the existence of a

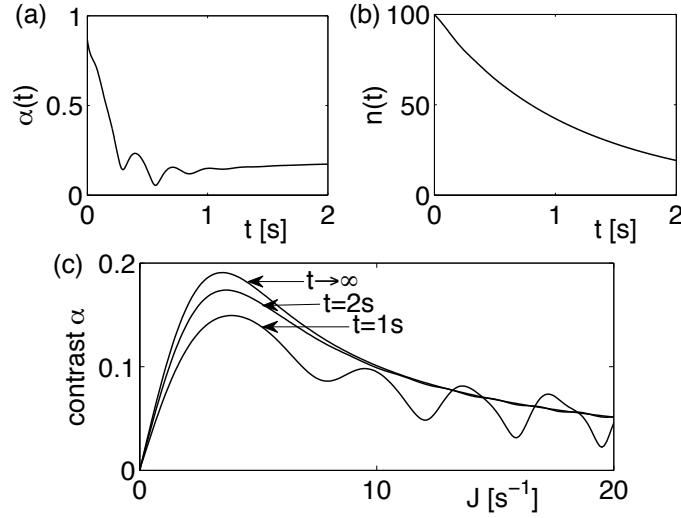


Figure 9.8: Relaxation to the quasi-steady state for $\kappa = 5 \text{ s}^{-1}$, $T_1^{-1} = 1 \text{ s}^{-1}$, $\epsilon = 10 \text{ s}^{-1}$ and $U = 0$. (a) Relaxation of the contrast $\alpha(t)$ for $J = 4 \text{ s}^{-1}$. (b) Decay of the particle number $n(t)$ for $J = 4 \text{ s}^{-1}$. (c) Development of the SR-maximum of the contrast $\alpha(J)$.

pronounced SR-like maximum. At most, the function $\alpha(T_1^{-1}, J)$ is stretched, shifting the position of the SR-like maximum. This shift is illustrated in figure 9.9 (a) where we have plotted the contrast as a function of J for the dissipation rate $T_1^{-1} = 2 \text{ s}^{-1}$ and different values of ϵ . Thus, this effect provides a useful tool to shift the maximum to values of J , which are easier accessible in ongoing experiments.

Similarly, the position of the maximum of the coherence $\alpha(J)$ is shifted in the presence of weak inter-particle interactions. An interacting BEC will usually not show a simple exponential decay of the form (9.27) because the instantaneous decay rate depends on the effective interaction strength $Un(t)$, which also decreases [179, 197, 198]. However, the discussion of quasi-steady states and instantaneous decay rates is still useful if the decay is weak. In this case the system can follow the quasi-steady states adiabatically and the decay of the population is given by

$$\begin{aligned} \frac{dn(t)}{dt} &= -\xi(n(t))n(t) \quad \text{and} \\ \frac{d\ell(t)}{dt} &= -\xi(n(t))\ell(t) \end{aligned} \quad (9.33)$$

in good approximation. Substituting this ansatz into the equations of motion (9.16) yields four coupled nonlinear algebraic equations, which can be disentangled with a little algebra. For a given number of particles n , the instantaneous decay rate ξ is obtained by solving the fourth order algebraic equation

$$\begin{aligned} [(\xi - T_2^{-1})^2 + (Un)^2(\xi - T_1^{-1})^2] [(\xi - T_1^{-1})^2 - f_a^2 T_1^{-2}] \\ + 4J^2 f_a^2 T_1^{-2} (\xi - T_1^{-1})(\xi - T_2^{-1}) = 0. \end{aligned} \quad (9.34)$$

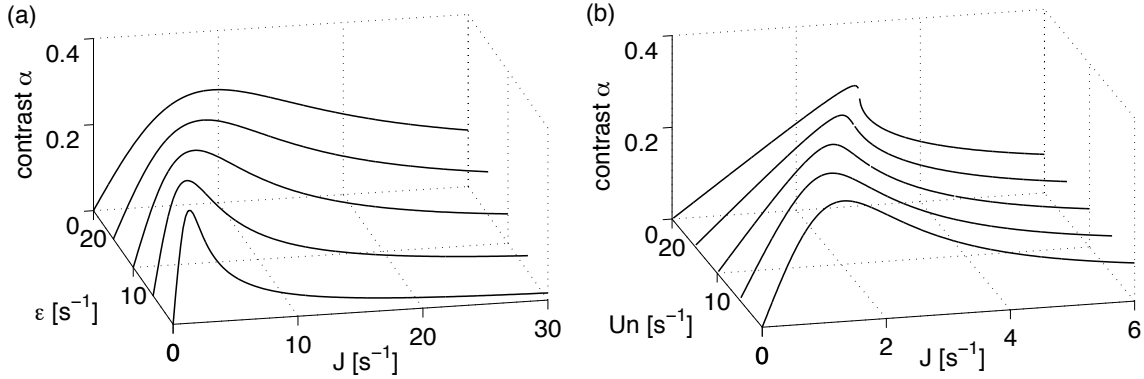


Figure 9.9: Steady state values of the contrast α as a function of the tunneling rate, for $U = 0$ and different values of the energy bias ϵ (a), and as a function of the effective interaction strength $g = Un$ for $\epsilon = 0$ (b). The remaining parameters are $\kappa = 5 \text{ s}^{-1}$ and $T_1^{-1} = 2 \text{ s}^{-1}$.

The Bloch vector for the corresponding quasi-steady state is then given by

$$\begin{aligned}
 \ell_{x0} &= \frac{\xi - T_1^{-1} (\xi - T_1^{-1})^2 - f_a^2 T_1^{-2}}{\xi - T_2^{-1} \frac{4J f_a^2 T_1^{-2}}{4J f_a^2 T_1^{-2}}} U n^2, \\
 \ell_{y0} &= \frac{(\xi - T_1^{-1})^2 - f_a^2 T_1^{-2}}{4J f_a T_1^{-1}} n, \\
 \ell_{z0} &= \frac{\xi - T_1^{-1}}{2f_a T_1^{-1}} n.
 \end{aligned} \tag{9.35}$$

The fourth order equation (9.34) yields four solutions for the decay rate ξ . Discarding unphysical values, one finds either one or three quasi-steady states. The effects of the appearance of novel nonlinear stationary states on the dynamics is reminiscent of the bifurcation of fixed points discussed in section 9.1 and will be analysed in more detail in chapter 10 in the context of Landau-Zener tunneling.

The resulting contrast $\alpha(J)$ in a quasi-steady state is shown in figure 9.9 (b) for different values of the effective interaction constant $g = Un$. One observes that the position of the SR-like maximum of the contrast is shifted to larger values of the tunneling rate, while the height remains unchanged. Furthermore the shape of the stochastic resonance curve $\alpha(J)$ is altered, becoming flatter for $J < J_{\max}$ and steeper for $J > J_{\max}$. For even larger values of the interaction constant Un one finds a bifurcation into three distinct quasi-steady states as introduced earlier. This case will be discussed in detail below (cf. section 9.3.3).

The reasons for the occurrence of an SR-like maximum of the contrast in terms of the underlying many-particle dynamics are illustrated in figure 9.10. To obtain these results we have simulated the dynamics generated by the Master equation (8.70) using the Monte Carlo wave function (MCWF) method averaging over 100 quantum trajectories. For a given particle number n , the probabilities P to obtain the population imbalance

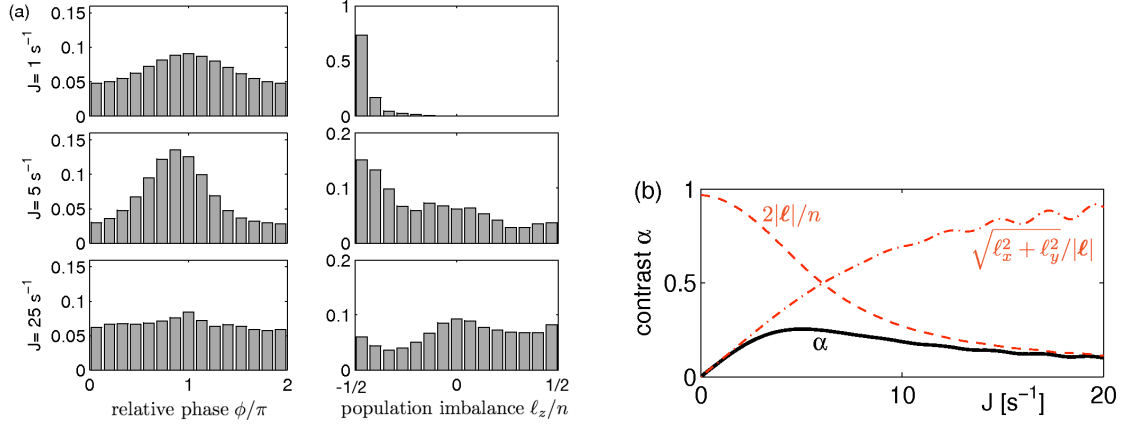


Figure 9.10: (a) Histogram of the probabilities to measure the relative phase ϕ and the relative population imbalance ℓ_z in a single experimental run after $t = 1.5 \text{ s}$ obtained from a MCWF simulation of the many-body dynamics. The initial state was chosen to be a pure BEC (equivalent to a product state) with $\ell_z = n/4$ and $n(0) = 100$ particles and the remaining parameters are $\kappa = 5 \text{ s}^{-1}$, $T_1 = 0.5 \text{ s}$, $\epsilon = 10 \text{ s}^{-1}$, $U = 0.1 \text{ s}^{-1}$. (b) Average contrast $\alpha = 2\sqrt{\ell_x^2 + \ell_y^2}/n$ (solid black line) after $t = 1.5 \text{ s}$ compared to $\sqrt{\ell_x^2 + \ell_y^2}/|\ell|$ and $2|\ell|/n$ (dashed red lines).

ℓ_z and the relative phase ϕ in a projective measurement are thereby given by

$$\begin{aligned} P(\ell_z) &= \text{tr}(|\ell_z\rangle\langle\ell_z| \hat{\rho}) \quad \text{and} \\ P(\phi) &= \text{tr}(|\phi\rangle\langle\phi| \hat{\rho}), \end{aligned} \quad (9.36)$$

where the \hat{L}_z eigenstates

$$\begin{aligned} |\ell_z\rangle &= |n/2 - \ell_z, n/2 + \ell_z\rangle \quad \text{with} \\ \ell_z &= -n/2, -n/2 + 1, \dots, n/2 \end{aligned} \quad (9.37)$$

and the phase eigenstates

$$\begin{aligned} |\phi\rangle &:= \frac{1}{\sqrt{n+1}} \sum_{\ell_z=-n/2}^{+n/2} e^{i\phi\ell_z} |\ell_z\rangle \quad \text{with} \\ \phi &= 0, 2\pi \frac{1}{n+1}, \dots, 2\pi \frac{n}{n+1} \end{aligned} \quad (9.38)$$

each form a complete basis.

Part (a) of figure 9.10 shows a histogram of the probabilities to observe the relative population imbalance ℓ_z/n and the relative phase ϕ in a single experimental run for three different values of the tunneling rate J after the system has relaxed to the quasi-steady state. With increasing J , the atoms are distributed more equally between the two wells so that the single shot contrast increases. Within the mean-field description

this is reflected by an increase of $\sqrt{\ell_x^2 + \ell_y^2}/|\ell|$ at the expense of $|\ell_z|/|\ell|$ (cf. part (b) of the figure). However, this effect also makes the system more vulnerable to phase noise so that the relative phase of the two modes becomes more and more random and $|\ell|/n$ decreases. The average contrast (9.26) then assumes a maximum for intermediate values of J as shown in part (b) of the figure.

9.3.2 Stochastic resonance of a driven Bose-Einstein condensate

So far we have demonstrated a stochastic resonance of the contrast for a BEC in a static double-well trap with biased particle losses. In the following we will show that the system's response to a weak external driving also assumes a maximum for a finite dissipation rate – an effect which is conceptually closer to the common interpretation of stochastic resonance. From a mathematical viewpoint, however, one can rather relate the *undriven* case discussed earlier to the stochastic resonance effect in nuclear magnetic resonance [196]. In fact, the Bloch equations for the magnetization have constant coefficients in the rotating wave approximation, and should thus be compared to the undriven equations of motion (9.16).

Let us consider the response of the system to a weak sinusoidal driving of the tunneling rate

$$J(t) = J_0 + J_1 \cos(\omega t) \quad (9.39)$$

at the resonance frequency $\omega = \sqrt{J_0^2 + \epsilon^2}$, while the amplitude of the driving is small and fixed as $J_1/J_0 = 10\%$. A variation of J can be realized in a quite simple way in an optical setup [157–159], where the tunneling barrier between the two wells is given by an optical lattice formed by two counter-propagating laser beams. A variation of the intensity of the laser beams then directly results in a variation of the tunneling rate J . Figure 9.11 shows the resulting dynamics for $T_1 = 0.5$ s and three different values of J_0 and $U = 0$. After a short transient period, the relative population imbalance $\ell_z(t)/n(t)$ oscillates approximately sinusoidally. One clearly observes that the response, respective the amplitude of the forced oscillations, assumes a maximum for intermediate values of J_0 matching the external time scale of the dissipation given by T_1^{-1} .

For a detailed quantitative analysis of this stochastic resonance effect, we evaluate the amplitude of the oscillation based on a linear response argument for $U = 0$. In the following, we will use a complex notation for notational convenience, while only the real part is physically significant. The equations of motion (9.16) are then rewritten in matrix form as

$$\frac{d}{dt} \begin{pmatrix} \ell \\ n \end{pmatrix} = (\mathbf{M}_0 + \mathbf{M}_1 e^{i\omega t}) \begin{pmatrix} \ell \\ n \end{pmatrix}. \quad (9.40)$$

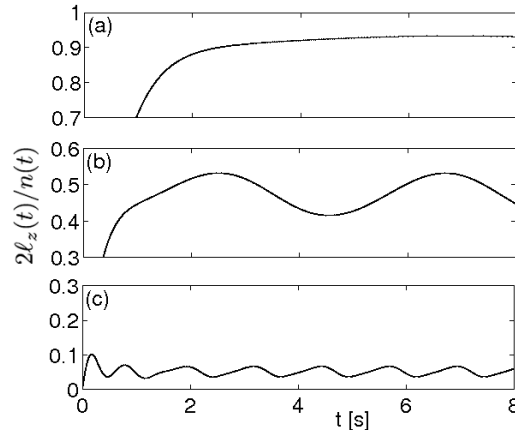


Figure 9.11: Dynamics of the relative population imbalance $\ell_z(t)/n(t)$ in a weakly driven double well trap for three different values of the tunneling rate: $J_0 = 0.5 \text{ s}^{-1}$ (a), $J_0 = 1.5 \text{ s}^{-1}$ (b) and $J_0 = 5 \text{ s}^{-1}$ (c). The amplitude of the forced oscillations assumes a maximum for intermediate values of J_0 as shown in part (b). The remaining parameters are $T_1^{-1} = 2 \text{ s}^{-1}$, $U = 0$, $\epsilon = 0$, $\kappa = 5 \text{ s}^{-1}$ and $J_1/J_0 = 10\%$. Please note the different scalings.

The matrices M_0 and M_1 are defined by

$$\mathbf{M}_0 = \begin{pmatrix} T_2^{-1} & 2\epsilon_0 & 0 & 0 \\ -2\epsilon_0 & T_2^{-1} & -2J_0 & 0 \\ 0 & 2J_0 & T_1^{-1} & f_a T_1^{-1} \\ 0 & 0 & f_a T_1^{-1} & T_1^{-1} \end{pmatrix} \quad (9.41)$$

and

$$\mathbf{M}_1 = \begin{pmatrix} 0 & 0 & 0 & 0 \\ 0 & 0 & -2J_1 & 0 \\ 0 & 2J_1 & 0 & 0 \\ 0 & 0 & 0 & 0 \end{pmatrix}. \quad (9.42)$$

As before we consider the dynamics after all transient oscillations have died out, assuming that $\ell(t)$ as well as $n(t)$ decay exponentially at the same rate. However, we now also have an oscillating contribution so that we make the ansatz

$$\begin{aligned} \ell(t) &= (\ell_0 + \ell_1 e^{i\omega t}) e^{-\xi t}, \\ n(t) &= (n_0 + n_1 e^{i\omega t}) e^{-\xi t}. \end{aligned} \quad (9.43)$$

The amplitude of the oscillations, respective the system response, is thus directly given by ℓ_1/n_0 . Substituting this ansatz in the equations of motion and dividing by $e^{-\xi t}$

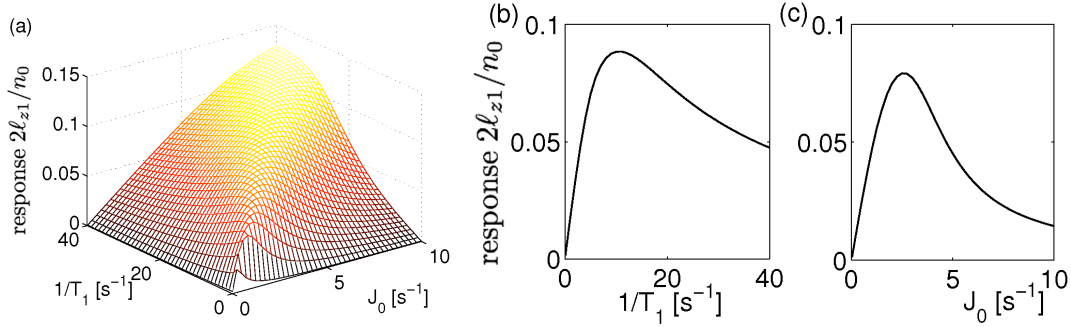


Figure 9.12: (a) Response (amplitude of the oscillations of $\ell_z(t)/n(t)$) of a weakly driven double well trap vs. T_1^{-1} and J_0 calculated within linear response theory. (b) For a fixed value of the tunneling rate $J_0 = 2.5 s^{-1}$. (c) For a fixed value of the dissipation rate $T_1^{-1} = 2 s^{-1}$. The remaining parameters are $U = 0$, $\epsilon = 0$, $\kappa = 5 s^{-1}$ and $J_1/J_0 = 10\%$.

yields

$$\begin{aligned}
 & -\xi \begin{pmatrix} \ell_0 \\ n_0 \end{pmatrix} + (i\omega - \xi) \begin{pmatrix} \ell_1 \\ n_1 \end{pmatrix} e^{i\omega t} \\
 & = [\mathbf{M}_0 + \mathbf{M}_1 e^{i\omega t}] \times \left[\begin{pmatrix} \ell_0 \\ n_0 \end{pmatrix} + \begin{pmatrix} \ell_1 \\ n_1 \end{pmatrix} e^{i\omega t} \right].
 \end{aligned} \tag{9.44}$$

Neglecting the higher order terms $\sim e^{2i\omega t}$ in a linear response approximation and dividing equation (9.44) in the time-dependent and the time-independent parts yields the equations

$$[-\mathbf{M}_0 + (i\omega - \xi)\mathbb{1}] \begin{pmatrix} \ell_1 \\ n_1 \end{pmatrix} = \mathbf{M}_1 \begin{pmatrix} \ell_0 \\ n_0 \end{pmatrix} \tag{9.45}$$

and (9.28), which determine ℓ_1 and n_1 . The resulting values of the system response are shown in figure 9.12. One observes the characteristic signatures of a stochastic resonance: If one of the two parameters J_0 and T_1 is fixed, the response assumes a maximum for a finite value of the remaining parameter as shown in part (b) and (c) of the figure. Part (a) shows that this maximum is assumed if the external (T_1^{-1}) and the internal (J_0) timescale are matched similar to the undriven case illustrated in figure 9.7.

A different situation arises if the energy bias is driven instead of the tunneling rate J such that

$$\epsilon(t) = \epsilon_1 \cos(\omega t). \tag{9.46}$$

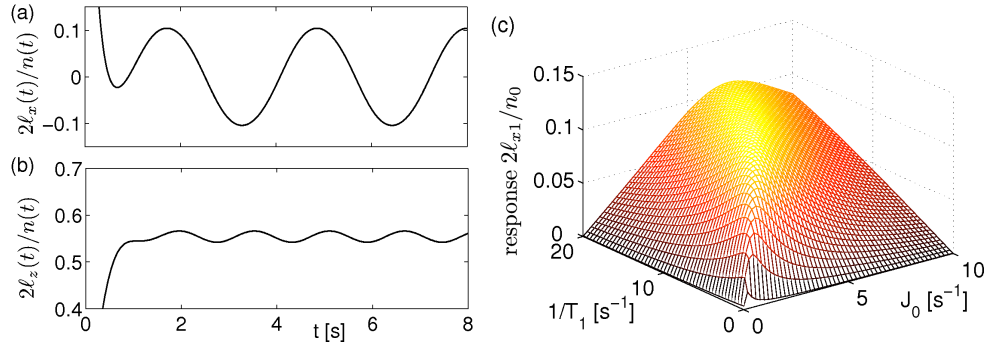


Figure 9.13: Dynamics of the coherence $\ell_x(t)/n(t)$ (a) and the relative population imbalance $\ell_z(t)/n(t)$ (b) for a double well trap with a driven energy bias ϵ for $J_0 = 2 \text{ s}^{-1}$ and $T_1^{-1} = 4 \text{ s}^{-1}$. (c) Response (amplitude of the oscillations of $\ell_x(t)/n(t)$) vs. T_1^{-1} and J_0 calculated within linear response theory. The remaining parameters are $U = 0$, $\epsilon_1 = 1 \text{ s}^{-1}$, $\kappa = 5 \text{ s}^{-1}$.

As in the case of a driven tunneling strength, we can evaluate the amplitude of the forced oscillations within the linear response theory, however with

$$\mathbf{M}_1 = \begin{pmatrix} 0 & -2\epsilon_1 & 0 & 0 \\ 2\epsilon_1 & 0 & 0 & 0 \\ 0 & 0 & 0 & 0 \\ 0 & 0 & 0 & 0 \end{pmatrix}. \quad (9.47)$$

Solving the equations (9.45) and (9.28) then yields $\ell_{1y} = \ell_{1z} = 0$. Remarkably, a driving of the energy bias does not affect the population imbalance in leading order. Only the first component of the Bloch vector ℓ_x , and thus also the contrast α is strongly affected.

This is illustrated in figure 9.13 (a) and (b) where the relative population imbalance $\ell_z(t)/n(t)$ and the first component of the Bloch vector $\ell_x(t)/n(t)$ are plotted for $J_0 = 2 \text{ s}^{-1}$, $T_1^{-1} = 4 \text{ s}^{-1}$ and $\epsilon_1 = 1 \text{ s}^{-1}$. The coherence oscillates strongly at the fundamental frequency ω , while the population imbalance oscillates only with a tiny amplitude at the second harmonic frequency 2ω . The oscillation amplitude of the coherence then again shows the familiar SR-like dependence on the parameters J_0 and T_1 as illustrated in figure 9.13 (c).

9.3.3 Dissipation induced coherence in a strongly-interacting Bose-Einstein condensate

Let us finally discuss the case of strong interactions, which is experimentally most relevant and theoretically most profound. An example for the dynamics of a strongly-interacting BEC is shown in figure 9.14 (a) for an initially pure BEC with $\ell_z = n/4$, calculated both with the MCWF method and within the mean-field approximation (9.16).

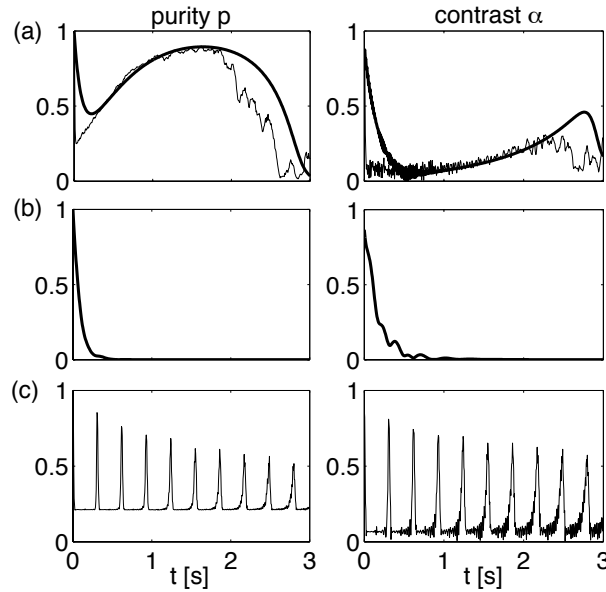


Figure 9.14: (a) Time evolution of the purity p and the contrast α for $J = U = 10 \text{ s}^{-1}$, $\epsilon = 0$, $T_1 = 0.5 \text{ s}$. (b) Time evolution without interactions ($U = 0$) and (c) without dissipation ($T_1^{-1} = T_2^{-1} = 0$) for comparison. The occasional revivals are artifacts of the small particle number. The initial state is a pure BEC with $\ell_z = n/4$ and $n(0) = 100$ particles. The results of a MCWF simulation averaged over 100 runs are plotted as a thin solid line in (a) and (c), while the mean-field results are plotted as a thick line in (a) and (b). Note that the mean-field approximation is exact in case (b), whereas it breaks down in case (c) and is thus not shown.

One observes that the purity p and the contrast α first drop rapidly due to the phase noise and, more importantly, due to the interactions. This is an effect well-known from the non-dissipative system and can be attributed to a dynamical instability. However, a surprising effect is found at intermediate times: The purity p is restored almost completely and the contrast α is slightly increasing.

Most interestingly, the observed values of the purity and the coherence are much larger than in the cases where one of the two effects – interactions and dissipation – is missing. The time evolution for these two cases are also shown in figure 9.14. In the case of no interactions both purity and coherence rapidly drop to values of almost zero and do not revive. This case has been discussed in detail in section 9.3.1. In the interacting case without dissipation one observes regular revivals, which are artifacts of the small particle number in the simulation and become less pronounced with increasing particle number. Apart from these occasional revivals, however, the purity and the coherence relax to values which are much smaller than in the interacting *and* dissipative case.

The effects which lead to this surprising re-purification of a strongly-interacting BEC by particle dissipation can be understood within the phase space picture introduced in section 9.2.2 and illustrated in figure 9.4. Parts (a) and (d) of the figure 9.4 show the phase space structure without dissipation and $Un = 0$ and $Un = 4J$, respectively. One

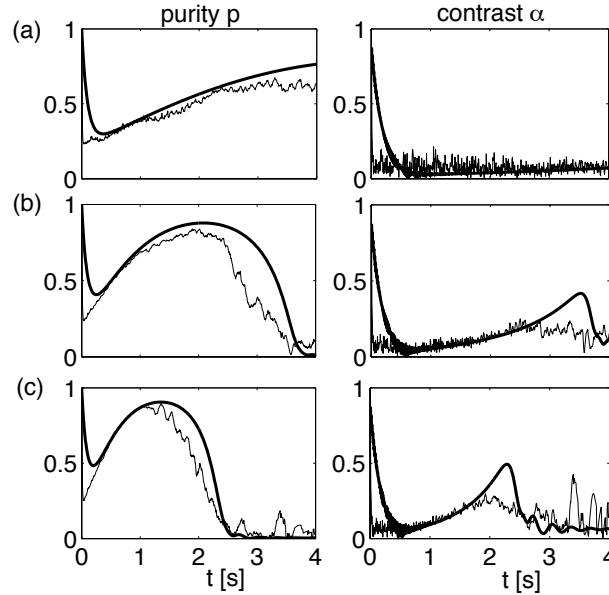


Figure 9.15: Time evolution of the purity p and the contrast α for $J = U = 10 \text{ s}^{-1}$, $\epsilon = 0$ and $T_1^{-1} = 0.5 \text{ s}^{-1}$ (a), $T_1^{-1} = 1.5 \text{ s}^{-1}$ (b) and $T_1^{-1} = 2.5 \text{ s}^{-1}$ (c). The initial state is a pure BEC with $\ell_z = n/4$ and $n(0) = 100$ particles. The results of a MCWF simulation averaged over 100 runs are plotted as a thin solid line, while the mean-field results are plotted as a thick line.

observes the familiar self-trapping bifurcation of the fixed points for $Un > 2J$ [69,173]. The phase space structure is significantly altered in the presence of particle loss as shown in parts (b), (c), (e) and (f), with the most important consequence being the occurrence of an attractive and a repulsive fixed point instead of the elliptic fixed points in the dissipation-free case.

In the course of time the dissipative, interacting system will thus relax to the attractive stationary state, as illustrated in figure 9.4 (e). A many-particle quantum state can now be represented by a quasi-distribution function on this classical phase space (cf. section 6.3.1). In this picture, a pure BEC is represented by a maximally localized distribution function and the loss of purity corresponds to a broadening or distortion. The existence of an attractive fixed point clearly leads to the recontraction of the phase space distribution function and thus to a re-purification of the many-particle quantum state as observed in figure 9.14 (a).

However, we have already seen in section 9.2.2 that this nonlinear stationary state exists only as long as the particle number exceeds a critical value given by

$$U^2 n^2 \gtrsim 4J^2 - f_a^2 T_1^{-2}. \quad (9.48)$$

This was at the origin of the metastable behaviour discussed in section 9.2.3. Here, we observe a similar effect: As particles are slowly lost from the trap, the particle number eventually falls below the critical value. For this reason the attractive fixed point vanishes and the purity drops to the values expected for the linear case $U = 0$. Since

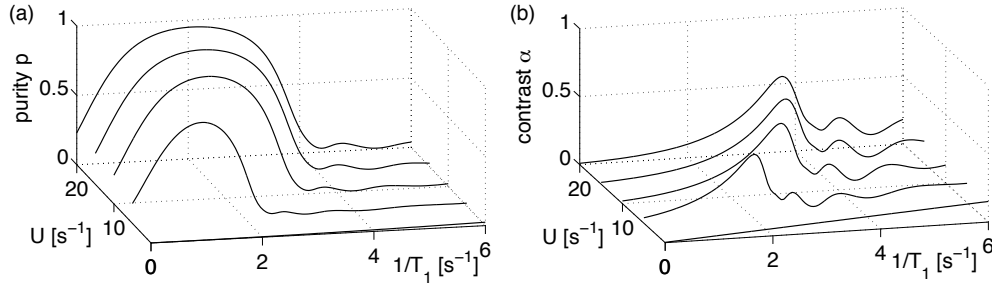


Figure 9.16: Purity p (a) and contrast α (b) after $t = 2$ s as a function of the dissipation rate T_1^{-1} for different values of the interaction strength Un calculated within the mean-field approximation. The remaining parameters are chosen as in figure 9.14 (a).

the attractive fixed point tends towards the equator maximizing $\ell_x/|\ell|$, the contrast assumes a maximum just before the disappearance of the attractive fixed point, while the purity is still large. In figure 9.14 (a) this happens after approx. 2.5 seconds.

The surprising effect of the re-purification of a BEC is extremely robust – it is present as long as the condition (9.48) is satisfied. A variation of the system parameters does not destroy or significantly weaken the effect, it only changes the time scales of this relaxation process. Figure 9.15 compares the time evolution of the purity and the contrast for three different values of the particle loss rate T_1^{-1} . With increasing losses, the nonlinear stationary state is reached much faster, but is also lost earlier. One can thus maximize the purity or the contrast at a given point of time by engineering the loss rate. This effect is further illustrated in Figure 9.16, where the purity and the contrast after 2 seconds of propagation are shown in dependence of the loss rate T_1^{-1} . Both curves assume a maximum for a certain finite value of T_1^{-1} .

9.4 Conclusion

In this chapter, we have discussed the dynamics of a Bose-Einstein condensate in a double-well trap subject to phase noise and particle loss. Starting from the full many-body dynamics described by a master equation the mean-field limit has been derived resulting in an effective non-hermitian (discrete) Gross-Pitaevskii equation and a detailed analysis of its fixed points has been presented. The structure of the phase space reflects the metastable behaviour of the many-body system, which is at the origin of a repurification of the state mediated by the dissipation. This manifestation of a stochastic resonance effect in a many-body system was analysed in three different settings: The phase coherence of a weakly-interacting condensate, experimentally measured via the contrast in an interference experiment, assumes a maximum for a finite value of the dissipation rate matching the intrinsic time scales of the system. In the same manner, the response to an external driving assumes a maximum for a finite value of the dissipation rate. Most interestingly for strong inter-particle interactions acting in concurrence with dissipation, the purity of the condensate is almost completely restored and the phase coherence can be significantly increased.

Chapter 10

Landau-Zener transitions and Bloch oscillations in optical lattices

In this chapter we discuss the dynamics of Bose-Einstein condensates (BECs) in an optical lattice under the influence of an additional static or a periodic force. Contrary to our intuition, a weak external field inhibits quantum transport in a periodic potential and leads to a periodic motion instead. These so-called Bloch oscillations [199] have been observed in a variety of systems, from electrons in semiconductor superlattices [200–203] to light in photonic materials [204–208]. A realization by ultracold atoms in optical potentials [209–211] provides not only near-perfect control and an astonishing accuracy, but also the possibility to observe the dynamics in-situ [81]. In an optical lattice the accelerating force can be either implemented by a chirp of the difference between the lattice beams [211], by magnetic gradient fields [212] or directly by the gravitational force in a vertical lattice setup [213]. In vertical setups Bloch oscillations can even be used for high precision measurements of the gravitational acceleration [214]. However, if the external field is so strong that the atoms can no longer adiabatically follow the lowest energy band, transitions to higher Bloch bands can occur at the edge of the Brillouin zone, such that directed transport becomes possible again. Such nonadiabatic transitions at avoided level crossings are generally referred to as Landau-Zener tunneling.

In the standard Landau-Zener scenario, the dynamics is restricted to two levels with a constant coupling J , whose energy difference varies linearly in time, $\epsilon(t) = \alpha t$. Of particular interest is the Landau-Zener tunneling probability between the two adiabatic states which is found to be

$$P_{\text{LZ}} = e^{-\pi J^2/\alpha}, \quad (10.1)$$

independent of the initially occupied level. Due to its generality, this result has been applied to numerous problems in various contexts like, e.g., spin-flip processes in nano-scale systems [215], molecular collisions [216], quantum-dot arrays [217], dissipative systems [218, 219] or quantum information processing tasks [220–223], to name but a few examples.

The Landau-Zener scenario was one of the first major problems addressed within time-dependant quantum theory. While the single-particle case was solved independently by Landau, Zener, Majorana and Stückelberg already in 1932 [224–227], the generalization of the results to interacting many-particle systems remains an open question up to today, and even the mean-field dynamics is not yet fully understood. The non-linear self-interaction fundamentally alters the dynamics, leading to a breakdown of adiabaticity due to the bifurcation of nonlinear stationary states [170, 171, 228–232]. The many-particle Landau-Zener problem is of fundamental interest not only from the theoretical but also from the experimental point of view and has in recent years attracted a lot of interest, especially in the context of the dynamics of Bose-Einstein condensates (BECs) in optical lattices [233–237]. In a tilted or accelerated optical lattice successive Landau-Zener tunneling at the Brillouin zone edge lead to a pulsed coherent output of atoms, called coherent droplets [210].

In this chapter, we will give a detailed analysis of the dynamics of an interacting Bose-Einstein condensate in tilted and driven optical (super-)lattices, including both Bloch oscillations and Landau-Zener tunneling. The effective nonlinearity due to the interactions between the particles leads to a dynamical instability, which results in rapid depletion going far beyond the mean-field regime. Thus, we will especially focus on the relation between the full many-particle problem and the mean-field approximation.

This chapter is divided into two parts. In the first section, we analyze the influence of the interactions between the particles onto the transition for the illustrative case of a driven double-well potential. The extension of this system to a chain of driven double-wells has only recently been studied experimentally [238, 239]. In the first section of this part, we will review the basic features of non-linear Landau-Zener tunneling and study the breakdown of adiabaticity due to the nonlinearity in more detail. In section 10.1.2, we will show that the phase space techniques presented in chapter 6, are not only an extremely useful tool to depict the dynamics, but can also be used to simulate the evolution including the depletion of the condensate, which plays a dominant role, as well as squeezing effects occurring during the transition (cf. section 10.1.3). In particular, going beyond the usual mean-field limit resolves the formerly imputed incommutability between adiabatic and semiclassical limits [170, 229, 230]. This subject will be addressed in section 10.1.5. Moreover, in section 10.1.6 we study the influence of phase noise and propose a Landau-Zener sweep as a sensitive, yet readily implementable probe for decoherence, since this has a significant effect on the transition rate for slow parameter variations.

In the second part of this chapter we turn to extended systems and study the dynamics of a Bose-Einstein condensate in a tilted (and driven) bichromatic optical lattice, which is ideally suited to study the coherent superposition of Bloch oscillations and Landau-Zener tunneling. The main objective of this part is the influence of the interactions onto the coherent dynamics of the macroscopic matter wave, and how this effective nonlinearity can lead to instabilities of the condensate. In section 10.3.1, we calculate the nonlinear Bloch bands and analyze their dynamical stability. Based on these results, we provide a thorough analysis for four different dynamical settings in a

bichromatic lattice. In section 10.3.2, we will study nonlinear Landau-Zener tunneling in a bichromatic lattice. The depletion of the condensate will be addressed in section 10.3.3. In section 10.3.4 the coherent interplay between Bloch oscillations and Zener tunneling and in section 10.3.5 the coupling of Bloch bands by a periodic driving is explored. The chapter closes with a short conclusion and an outlook.

10.1 Interacting BEC in a time-varying double-well trap

To get a feel for the influence of the interactions onto a Landau-Zener transition and the conceptual differences between the single- and many-particle problem, we consider the dynamics of the double-well model system (9.1), which has been introduced in chapter 9. As presumed in the standard Landau-Zener setting, we choose a linear time variation of the energy difference between the wells, $\epsilon(t) = \alpha t$, and assume a constant coupling J . The resulting description by a Bose-Hubbard type Hamiltonian thus reads

$$\begin{aligned}\hat{H} &= \epsilon(t) \left(\hat{a}_2^\dagger \hat{a}_2 - \hat{a}_1^\dagger \hat{a}_1 \right) - J \left(\hat{a}_1^\dagger \hat{a}_2 + \hat{a}_2^\dagger \hat{a}_1 \right) + \frac{U}{2} (\hat{n}_1(\hat{n}_1 - 1) + \hat{n}_2(\hat{n}_2 - 1)) \\ &= 2\epsilon(t)\hat{L}_z - 2J\hat{L}_x + U\hat{L}_z^2.\end{aligned}\quad (10.2)$$

As in the preceding chapters, we will set $\hbar = J = 1$ in all numerical examples, thus measuring time in units of the tunneling time \hbar/J .

Initially, the two modes are energetically well separated and the ground state of the Bose-Hubbard Hamiltonian (10.2) is

$$|\Psi(t \rightarrow -\infty)\rangle = (N!)^{-1/2} (\hat{a}_1^\dagger)^N |0\rangle, \quad (10.3)$$

thus we assume that initially all particles are localized in the first well, corresponding to a fully condensed state. The many-particle Landau-Zener transition probability for the population is then given by

$$P_{\text{LZ}}^{\text{mp}} := \frac{\langle \hat{n}_1(t \rightarrow +\infty) \rangle}{\langle \hat{n}_1(t \rightarrow -\infty) \rangle}. \quad (10.4)$$

In the following, the many-particle quantum state is denoted by a capital Ψ , while we use $\mathbf{x} = (x_1, x_2)$ for the components of the mean-field state vector in close connection to the parametrization introduced in section 9.1 (cf. equation (9.13)). To distinguish the transition probabilities we use the superscripts mp and mf for the many-particle and mean-field quantities, respectively.

In the mean-field approximation (cf. section 9.1, and especially equation (9.12)), the time evolution is given by the discrete Gross-Pitaevskii equation [172, 173]:

$$i \frac{d}{dt} \begin{pmatrix} x_1 \\ x_2 \end{pmatrix} = \begin{pmatrix} \alpha t + g|x_1|^2 & -J \\ -J & -\alpha t + g|x_2|^2 \end{pmatrix} \begin{pmatrix} x_1 \\ x_2 \end{pmatrix}, \quad (10.5)$$

where $g = UN$ is the macroscopic interaction strength and \mathbf{x} is normalized to one, $|x_1|^2 + |x_2|^2 = 1$. In this setting, the Landau-Zener tunneling probability in the level $j = 1, 2$ is defined as

$$P_{\text{LZ}}^{\text{mf}} := \frac{|x_j(t \rightarrow +\infty)|^2}{|x_j(t \rightarrow -\infty)|^2}. \quad (10.6)$$

As for the many-particle problem (10.3), we assume that all particles are initially localized in one of the modes, that means $x_1(t \rightarrow -\infty) = 1$.

In chapter 6 we have introduced the generalized phase space representation of Bose-Hubbard type systems and discussed the relation between the (single-trajectory) mean-field approximation, respective the GPE (10.5), and the Hamiltonian flow, which allows to go beyond expectation values and take also the higher moments and their time evolution into account at least approximately (cf. especially section 6.3.4, as well as section 7.2.2 for the numerical implementation). Here, we just review the basic definitions, which we will need in the following sections, for the two-mode case.

Starting from the Husimi or Q -Function, which is defined as the projection onto the set of Bloch coherent states (9.6)

$$Q(\theta, \phi, t) = |\langle \theta, \phi | \Psi(t) \rangle|^2, \quad (10.7)$$

one can calculate the exact dynamics as

$$\begin{aligned} \frac{\partial}{\partial t} Q(\theta, \phi) = & \left\{ 2\epsilon(t) \frac{\partial}{\partial \phi} + 2J \left(\sin \phi \frac{\partial}{\partial \theta} - \cos \phi \cot \theta \frac{\partial}{\partial \phi} \right) \right. \\ & \left. - g \cos \theta \frac{\partial}{\partial \phi} + \frac{g}{N} \sin \theta \frac{\partial^2}{\partial \phi \partial \theta} \right\} Q(\theta, \phi). \end{aligned} \quad (10.8)$$

The evolution equations thus consist of a classical Liouvillian phase space flow, which is equivalent to the discrete Gross-Pitaevskii equation (10.5) in the appropriate parametrization (cf. section 7.2.2), and a quantum correction term which vanishes as $1/N$. Hence, the truncated dynamics provides a semiclassical approximation of the phase space flow, which allows to calculate the dynamics of the higher moments of the quantum state approximately: The initial state is mapped to its Husimi function, which is then propagated according to a classical Liouville equation omitting the quantum corrections in equation (10.8). Equivalently one can consider an ensemble of classical phase space trajectories whose starting points are distributed according to the initial Husimi function (cf. section 6.3.4). This method is referred to as ensemble simulation in the following. Section 6.3.2 comments on the evaluation of expectation values by an integration over quasi-probability densities. In particular, the expectation value of the generalized angular momentum operators (9.3) can be calculated as

$$\langle \hat{\mathbf{L}} \rangle = (N + 2) \int \mathbf{s}(\theta, \phi) Q(\theta, \phi) \sin \theta d\theta d\phi, \quad (10.9)$$

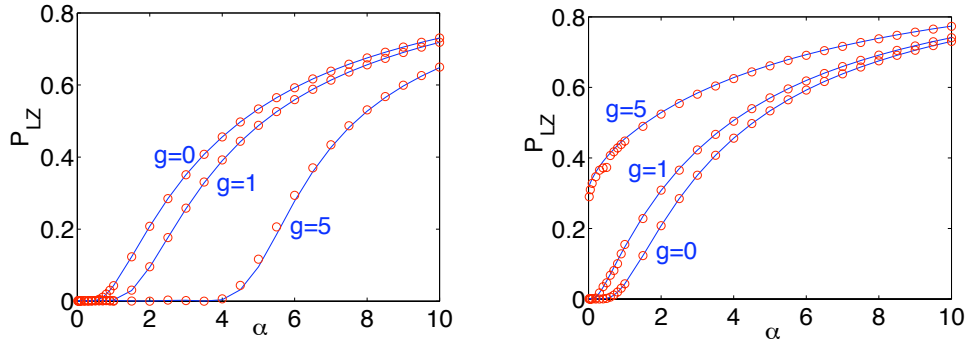


Figure 10.1: Landau-Zener tunneling probability in the lower level (left) and the upper level (right) for $J = 1$ and $g = 0, 1, 5$. Mean-field results $P_{LZ}^{\text{mf}}(\alpha)$ are plotted as solid blue lines, many-particle results $P_{LZ}^{\text{mp}}(\alpha)$ for $N = 50$ particles as red circles.

thus the eigenvalues of the reduced single-particle density matrix (SPDM, cf. equation (9.25)),

$$\rho = \begin{pmatrix} 1/2 - \langle \hat{L}_z \rangle / N & \langle \hat{L}_x \rangle / N - i \langle \hat{L}_y \rangle / N \\ \langle \hat{L}_x \rangle / N + i \langle \hat{L}_y \rangle / N & 1/2 + \langle \hat{L}_z \rangle / N \end{pmatrix}, \quad (10.10)$$

are no longer restricted to $\{0, 1\}$, as it is the case in the mean-field approximation. This allows to study the consequences of dynamical instabilities, which will be at the focus of the following sections. Moreover, this approach allows to investigate the dynamics of different initial states, since it is not restricted to product states alone.

10.1.1 Nonlinear Landau-Zener tunneling

The linear Landau-Zener tunneling probability is strongly affected by the nonlinear self-interaction, where the most striking feature is the breakdown of adiabaticity, that is the non-vanishing transition probability in the adiabatic limit $\alpha \rightarrow 0$ for a large enough interaction strength. Numerical results illustrating this behaviour are shown in figure 10.1.

The solid lines show the mean-field Landau-Zener tunneling probability (10.6) in dependence of the parameter velocity α for different values of the interaction strength g . Note, that for this calculation the common (single-trajectory) mean-field approximation has been used. However, there are no visible differences to the phase-space ensemble simulation for the actual parameters. The open circles represent the corresponding many-particle results. In the linear case $g = 0$, one recovers the result (10.1) for the Landau-Zener tunneling probability. For a slow parameter variation, the state can adiabatically follow the instantaneous eigenstates and thus most particles tunnel coherently to the other well. For a faster sweep, this coherent tunneling effect is strongly disturbed such that the Landau-Zener transition probability no longer vanishes. This effect is present in the transition probability in the upper and the lower level.

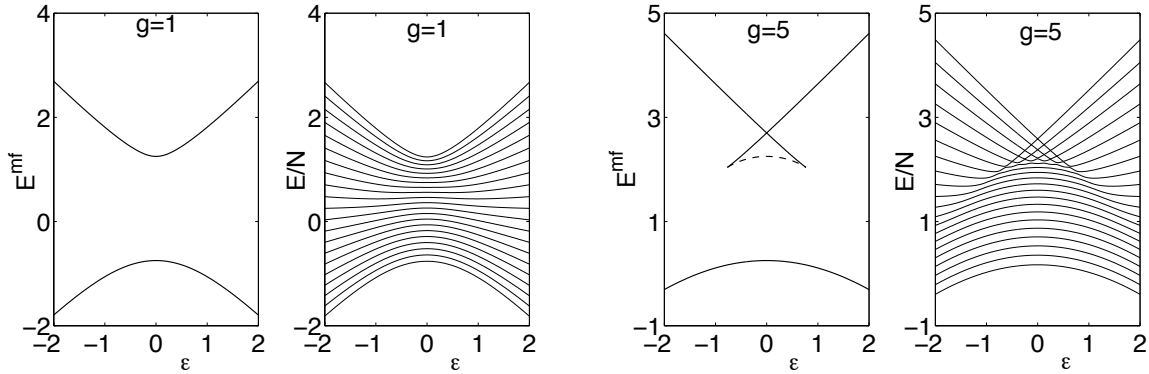


Figure 10.2: Energy of the mean-field stationary states (10.11) in comparison to the eigenenergies of the two-mode Bose-Hubbard model (9.1) in dependence of the offset ϵ for $J = 1$ and $g = 1$ (left) and $g = 5$ (right) and $N = 20$ particles.

In the nonlinear case, the tunneling probability becomes strongly asymmetric: it increases as g increases in the upper level, while it decreases in the lower level. To understand this effect, it is useful to consider the total energy of the mean-field system. Figure 10.2 shows the eigenenergies of the Hamiltonian (10.2) in dependence of the difference of the on-site energies $\epsilon = \epsilon_1 - \epsilon_2$ in comparison to the total energies of the ‘nonlinear eigenstates’, i.e. the stationary states of the mean-field dynamics (10.5),

$$E^{\text{mf}} = \epsilon(|x_2|^2 - |x_1|^2) - J(x_1^*x_2 + x_2^*x_1) + \frac{g}{2}(|x_1|^4 + |x_2|^4). \quad (10.11)$$

Compared to the non-interacting case $g = 0$, the left-hand side of figure 10.2 shows that the upper level is sharpened, while the lower level is flattened for small interactions $0 < g < 2J$. This flattening suppresses the tunneling probability from the lower level to the upper level, leading to a decreased Landau-Zener probability in the adiabatic regime. On the other hand, the sharpening of the upper level makes it more difficult to follow the adiabatic eigenstates, which results in an increased Landau-Zener probability for the upper level, as can be seen on the right-hand side of figure 10.1.

Most remarkably, the tunneling probability in the upper level does not even vanish in the adiabatic limit $\alpha \rightarrow 0$ for $g > 2J$, as expected from the linear case. Thus adiabaticity breaks down in the strongly interacting case.

To explore the origin of this breakdown of adiabaticity we compare again the eigenstates of the many-particle system to the stationary states of the mean-field system. For $g > 2J$ the mean-field eigenenergies show a swallow’s tail structure in the upper level, reflecting the occurrence of a bifurcation of one of the steady states into three new ones, one of them hyperbolically unstable (dashed line) and two elliptically stable (solid lines). This so called self-trapping effect has been discussed in detail in section 9.1. The system can adiabatically follow the steady states as long as these are elliptically stable. This is possible only until the end of the swallow’s tail where the elliptic fixed point vanishes in an inverse bifurcation with the hyperbolic fixed point [228, 229]. Then the dynamics becomes unstable and adiabaticity is lost even for very small values of α .

The swallow's tail in the mean-field energy corresponds to a caustic of the many-particle eigenenergy curves in the limit $N \rightarrow \infty$, which are bounded by the mean-field energies from below and above. Within this caustic we find a series of quasi-degenerate avoided crossings of the many-particle levels. The level splitting at these crossings tends to zero exponentially fast in the mean-field limit $N \rightarrow \infty$ with $g = UN$ fixed [171, 240]. Thus the system will show a complete diabatic time evolution at these quasi-crossings even for very small values of α . Outside the swallow's tail one finds common avoided crossings, where the system evolves adiabatically for small values of α .

Note, however, that the breakdown of adiabaticity is only approximate for the many-particle system. It is known that for a symmetric tridiagonal Hamiltonian, such as the one we are considering (9.1) with $J \neq 0$, the level spacings in the spectrum may be exponentially small but nevertheless is always non-zero [241]. Thus adiabaticity can be restored when the parameter velocity α is decreased well below the square of the residual level splitting Δ [240, 242]:

$$\alpha \stackrel{!}{\ll} \Delta^2 \quad \text{with} \quad \Delta \propto N \exp(-\eta N), \quad (10.12)$$

where η is a proportionality constant which depends of the system parameters. However, the adiabaticity condition on the velocity becomes exponentially difficult to fulfill for large particle numbers. Thus the breakdown of adiabaticity is also present in the full many-particle system for any realistic set of parameters. The same dynamics is found for attractive nonlinearities, $g < 0$, only the roles of the upper and lower level are exchanged.

10.1.2 Landau-Zener tunneling in phase-space

Further insight into the dynamics of nonlinear Landau-Zener tunneling can be gained within the phase space picture introduced in chapter 6, and briefly reviewed at the beginning of this chapter.

According to the remarks in the previous section, the system will undergo a series of diabatic transitions up to the end of the swallow's tail and evolve adiabatically afterwards. To verify these claims, we compare the actual many-particle quantum state $|\Psi(t)\rangle$ to the instantaneous eigenstate in figure 10.3 at four points in time during a Landau-Zener passage. To visualize the quantum states, we use the Husimi distribution $Q(\theta, \phi, t)$ in polar representation (9.8) as defined in section 9.1. The right-hand side of figure 10.3 illustrates the series of diabatic/adiabatic transitions and the specific instantaneous eigenstates shown in upper panels of the figure. One observes a good agreement between the dynamical state and the instantaneous eigenstates, during the transition as well as afterwards. However, the crossover from diabatic to adiabatic transitions is not absolutely sharp. The final state contains small contributions from other instantaneous eigenstates.

To characterize the many-particle quantum state during the Landau-Zener transition, we have plotted the eigenvalues of the single-particle density matrix (10.10) on the

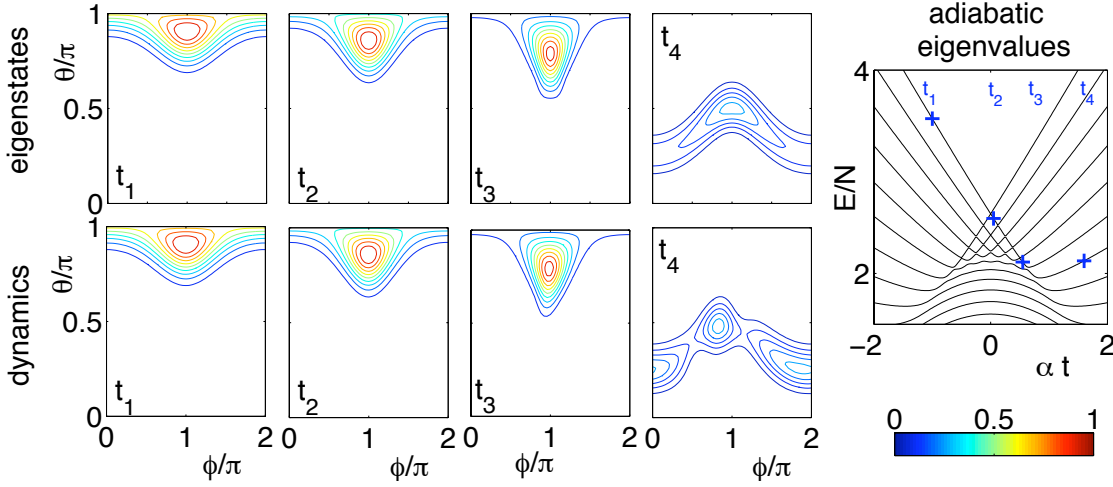


Figure 10.3: Dynamics of the many-particle Landau-Zener transition for $J = 1$, $g = 5$, $N = 20$ and $\alpha = 0.1$. The upper figures show a contour plot of the Husimi distribution of the instantaneous eigenstates marked in the level scheme on the right at times $t_j = -10, 0.5, 5.5, 16$. The lower figures show the Husimi distribution of the dynamical quantum state $|\Psi(t)\rangle$ at the same times.

left-hand side of figure 10.4. One eigenvalue remains equal to unity, while the other one vanishes, indicating a fully coherent state until the crossover from diabatic to adiabatic transitions. Then we observe an oscillation of the SPDM eigenvalues: The contributions of the different many-particle eigenstates de- and rephase periodically giving rise to a beat signal which is genuinely quantum. The oscillation of the coherence is mirrored in the evolution of the uncertainties of the angular momentum operators $\Delta\hat{L}_x$ and $\Delta\hat{L}_y$ shown on the right-hand side of figure 10.4. The uncertainties are strongly enhanced when the coherence is (partly) lost. This behaviour can be intuitively explained in terms of the dynamics of the Husimi distribution. The centre of mass of the Husimi function oscillates rapidly in the ϕ -direction, leading to oscillations of the expectation values $\langle\hat{L}_x\rangle$ and $\langle\hat{L}_y\rangle$. Furthermore the distribution breathes in the ϕ -direction at a slower timescale, leading to the oscillations of the width $\Delta\hat{L}_x$ and $\Delta\hat{L}_y$ and the periodic revivals of the coherence. The oscillations of the expectation values die out at the times when the Husimi function is spread nearly uniformly in the ϕ -direction, that is at the times where the coherence is minimal. In contrast, the Husimi distribution is well localized in the θ -direction for long times and the corresponding uncertainty $\Delta\hat{L}_z$ remains small. The population difference $\langle\hat{L}_z\rangle$ is thus well described by the simple Bogoliubov mean-field approximation. Many-particle and mean-field results for the Landau-Zener tunneling rate show an excellent agreement (cf. figure 10.1), because they depend only on the population difference and not on the coherence.

The evolution of the coherence and the uncertainties $\Delta\hat{L}_x$ and $\Delta\hat{L}_y$ certainly goes beyond the Bogoliubov mean-field approximation, but most of the effects can be taken into account by the semi-classical phase space approach. Figure 10.6 shows the dynamics of the many-particle Landau-Zener scenario in quantum phase space in comparison

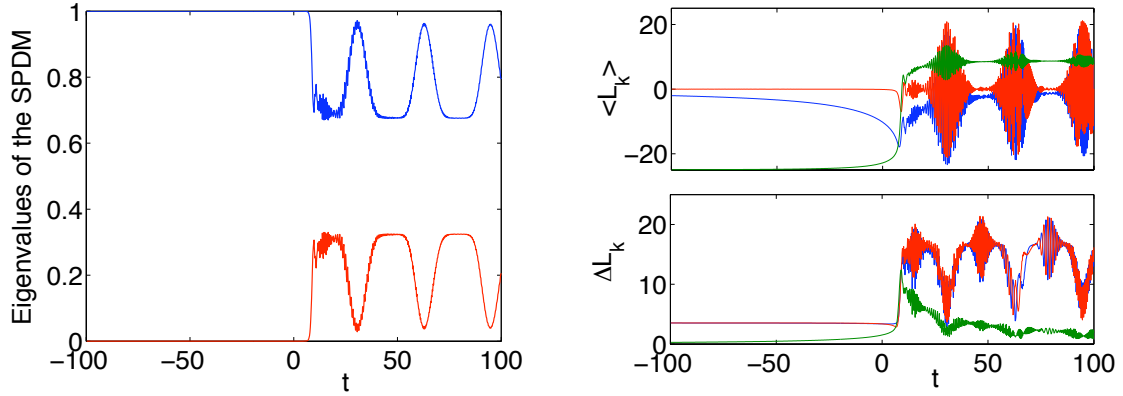


Figure 10.4: Dynamics of the many-particle Landau-Zener transition for $g = 5$, $N = 50$ and $\alpha = 0.1$. The left figure shows the eigenvalues of the SPDM (10.10). The expectation values $\langle \hat{L}_k \rangle$ and widths $\Delta \hat{L}_k$ of the angular momentum operators (9.3) for $k = x$ (blue), $k = y$ (red) and $k = z$ (green) are plotted on the right-hand side. The onset of the oscillatory dynamics corresponds to the cusp of the swallow-tail structure in the mean-field representation (cf. figure 10.2).

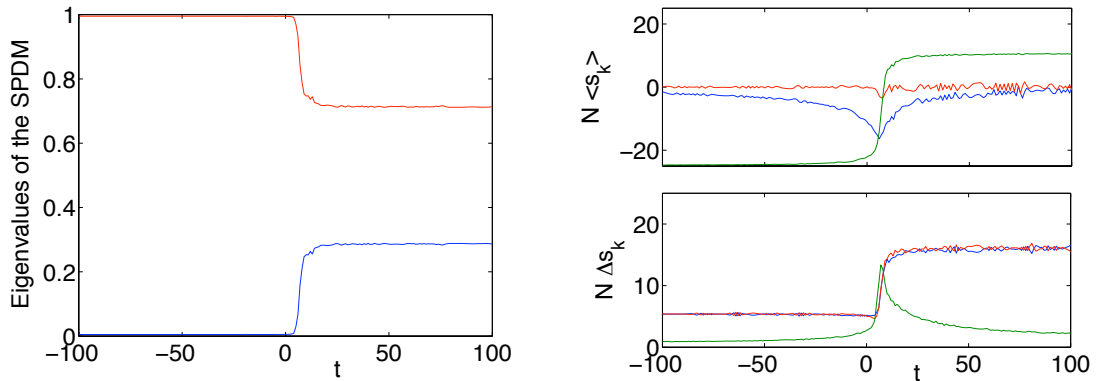


Figure 10.5: Semiclassical simulation of the many-particle Landau-Zener transition for $J = 1$, $g = 5$, $N = 50$ and $\alpha = 0.1$. The left figure shows the eigenvalues of the ensemble approximation for the SPDM $\rho_{kl} = \langle \psi_k^* \psi_l \rangle_{\text{cl}}$. The ensemble expectation values $N \langle s_k \rangle_{\text{cl}}$ and the standard deviation $N \Delta s_k$ of the Bloch vector (9.8) for $k = x$ (blue), $k = y$ (red) and $k = z$ (green) are plotted on the right-hand side.

to the dynamics of a classical phase space ensemble. The expectation values and variances of the Bloch vector $\hat{\mathbf{L}}$ (9.8) calculated from such an ensemble simulation are plotted in figure 10.5. It is observed, that the spreading of the Husimi distribution in the direction of the relative phase ϕ and the loss of coherence are well reproduced by the classical ensemble. However, the quantum beat oscillations of the coherence are of course not present in the classical distributions as shown in figure 10.5. The expectation value and the fluctuations of the classical Bloch vector \mathbf{s} as defined in equation (9.8) show a similar effect. The global dynamics of the angular momentum operator

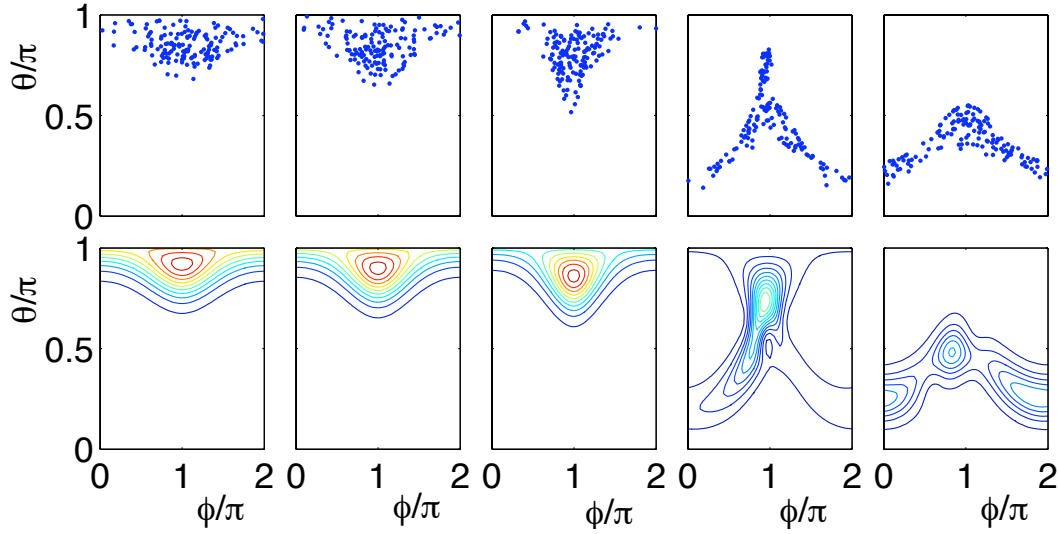


Figure 10.6: The many-particle Landau-Zener scenario in phase space. The dynamics of an ensemble of 150 classical trajectories (upper panels) is compared to the evolution of the Husimi distribution (lower panels) at times $t = -16, -8, 0, 8, 16$ (from left to right). Parameters are chosen as in figure 10.3.

$\hat{\mathbf{L}}$ plotted in figure 10.4 is well reproduced, whereas all the quantum beats are absent. These are genuine many-particle quantum effects.

10.1.3 Number squeezing during the transition

The previous results show that the many-particle quantum state after a nonlinear Landau-Zener sweep is far from being a pure BEC. In particular it has been claimed that the final state is strongly number squeezed in comparison to a pure BEC with the same atomic density distribution [243]. The figures 10.4 and 10.5 show the evolution of the expectation values and variances of $\hat{\mathbf{L}}$, comparing many-particle results to a phase space approximation. One observes that the number fluctuations ΔL_z^2 are strongly increased during the sweep, but relax to a smaller value again afterwards. This evolution is well described within the semiclassical phase space picture. A further quantitative analysis of number squeezing during a Landau-Zener sweep is provided in figure 10.7, comparing exact results (red) to an ensemble simulation (green). For a pure BEC with a given atomic distribution, number fluctuations are given by $\Delta L_{z,\text{ref}}^2 = \langle \hat{n}_1 \rangle \langle \hat{n}_2 \rangle / N$. Thus one can define the parameter

$$\xi_N^2 = \frac{\Delta L_z^2}{\Delta L_{z,\text{ref}}^2} = \frac{N \Delta L_z^2}{\langle \hat{n}_1 \rangle \langle \hat{n}_2 \rangle}, \quad (10.13)$$

which measures the suppression of number fluctuations in comparison to a pure BEC. Figure 10.7 (a) shows the value of ξ_N^2 during a slow Landau-Zener sweep with $\alpha = 0.1$. Indeed, ξ_N^2 drops well below one for long times indicating number squeezing. Again, this feature is well reproduced by a phase space simulation (green). The final value of ξ_N^2 after the sweep is shown in Figure 10.7 (b) as a function of the parameter velocity

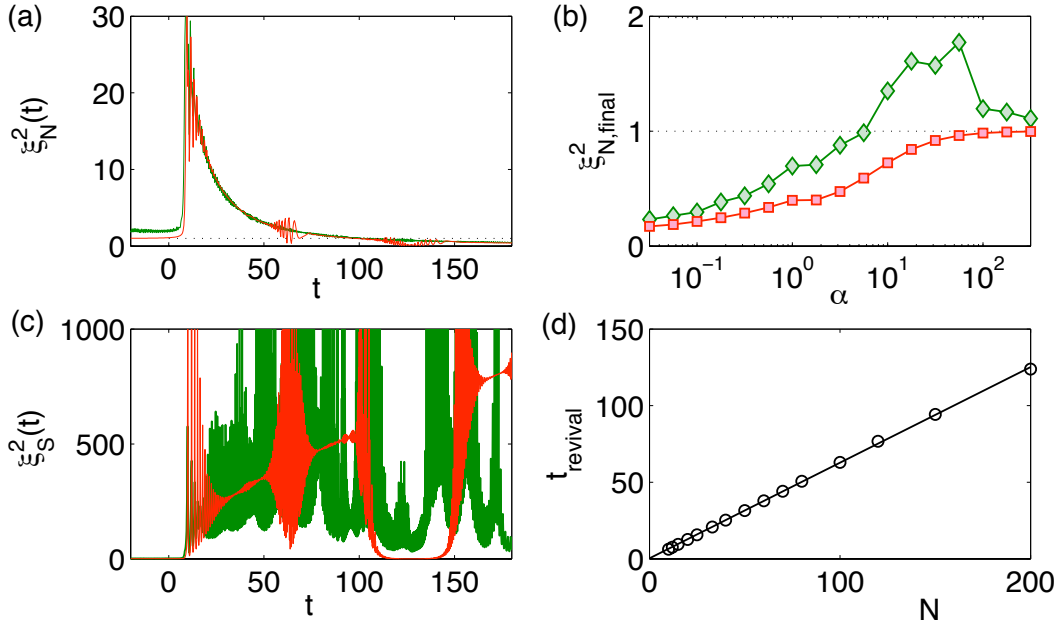


Figure 10.7: Number squeezing during a Landau-Zener sweep. Many-particle results (red) are compared to an ensemble simulation (green). (a) Evolution of the relative squeezing parameter ξ_N^2 for a slow sweep with $\alpha = 0.1$. (b) Final value of ξ_N^2 (10.13) after the sweep as a function of the parameter velocity α . (c) Evolution of the spectroscopic squeezing parameter ξ_S^2 (10.14) for a slow sweep with $\alpha = 0.1$. (d) Dependence of the revival time of the occurrence of a squeezed state on the particle number N . The remaining parameters are $J = 1$, $g = -5$ and $N = 200$ particles.

α . Number squeezing with $\xi_N^2 < 1$ is observed for small values of α in the regime of the breakdown of adiabaticity, e.g. for a large interaction strength, $2J < g$. The phase space simulation overestimates the variances and thus also ξ_N^2 , but gives the correct overall behaviour. For a fast sweep, ξ_N^2 tends to one as the state remains approximately coherent.

However, an application of number squeezing in quantum metrology requires a reduction of number fluctuations as well as a large phase coherence. Thus, a quantum state is defined to be *spectroscopically squeezed* if and only if

$$\xi_S^2 := N \frac{\Delta \hat{L}_z^2}{\langle \hat{L}_x \rangle^2 + \langle \hat{L}_y \rangle^2} < 1. \quad (10.14)$$

Spectroscopic squeezing indicates multipartite entanglement of the trapped atoms [244, 245]. The evolution of the squeezing parameter ξ_S^2 during a slow Landau-Zener sweep with $\alpha = 0.1$ is plotted in figure 10.7 (c). While the number fluctuations $\Delta \hat{L}_z^2$ assume a small constant value after the sweep, the phase coherence $\langle \hat{L}_x \rangle^2 + \langle \hat{L}_y \rangle^2$ strongly oscillates due to the periodic de- and rephasing of the many-particle eigenstates (cf. figure 10.4). True spin squeezing with $\xi_S^2 < 1$ is present only temporarily in the periods of maximum phase coherence. The timescale of the occurrence of these minima depends

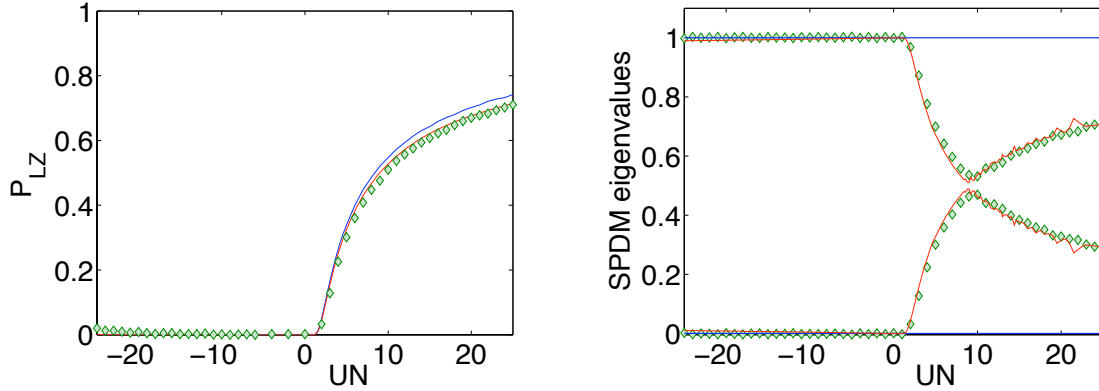


Figure 10.8: Left panel: Landau-Zener tunneling probability as a function of the interaction strength UN for a slow parameter variation $\alpha = 0.1$ and $J = 1$, $N = 50$. Right panel: Eigenvalues of the SPDM for $t \rightarrow +\infty$. The exact many-particle results (red line) are compared to a phase space ensemble simulation (green diamonds) and the single-trajectory mean-field results (blue line).

linearly on the particle number N , as shown in figure 10.7 (d). For macroscopic particle numbers it takes very long before the states rephase such that $\xi_S^2 < 1$ is observed. Moreover these revivals are extremely sensitive to phase noise. Thus, it is doubtful that for realistic particle numbers Landau-Zener sweeps may be useful to generate squeezed states in a controlled way. Finally we note that the revivals of the phase coherence are not described by the phase space picture. Even small fluctuations in the phase coherence lead to large errors. Therefore the phase space approximation cannot account for the short periods where true spin squeezing $\xi_S^2 < 1$ is observed.

10.1.4 Influence of interactions onto the Landau-Zener transition probability

Let us finally investigate the global dependence of the Landau-Zener tunneling rate on the interaction strength $g = UN$ in more detail. To this end we calculate the quantum and the classical tunneling rates given by equations (10.4) and (10.6), respectively, as well as the eigenvalues of the SPDM (9.25). We consider an initial state that is localized in the upper level for $t \rightarrow -\infty$ so that adiabaticity breaks down for a repulsive nonlinearity $g > 2J$. As discussed earlier, a change of the sign of the interaction strength g corresponds to an interchange of the two modes. For an attractive nonlinearity, adiabaticity breaks down in the lower level instead. Thus we obtain a global picture of the dynamics either by calculating the tunneling rate in the upper and the lower level for $g > 0$, or by calculating the tunneling rate in the upper level alone for $g > 0$ and $g < 0$. In the following we choose the latter option.

Figure 10.8 shows the results for $J = 1$ and $\alpha = 0.1$, where the linear system evolves completely adiabatically. The left-hand side shows the many-particle and mean-field Landau-Zener tunneling probabilities as defined in equation (10.4) and (10.6), respec-

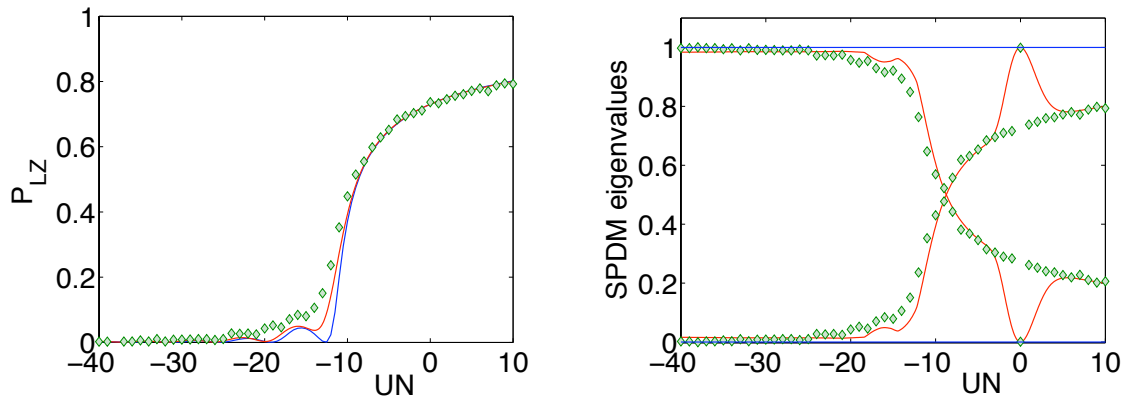


Figure 10.9: Left panel: Landau-Zener tunneling probability as a function of the interaction strength $g = UN$ for a fast parameter sweep $\alpha = 10$ and $J = 1$, $N = 50$. Right panel: Eigenvalues of the SPDM for $t \rightarrow +\infty$. The exact many-particle results (red line) are compared to a phase space ensemble simulation (green diamonds) and the single-trajectory mean-field results (blue line).

tively. The right-hand side shows the eigenvalues of the SPDM (9.25) for $t \rightarrow +\infty$. Note, however, that the eigenvalues of the SPDM oscillate for $t > 0$ as shown in figure 10.4, indicating a periodic loss and revival of coherence. Figure 10.8 shows the eigenvalues of the SPDM for large times, omitting the temporal revivals explicitly. As expected, adiabaticity breaks down as soon as $g > 2J$ and the Landau-Zener tunneling rate increases with g . In the adiabatic regime, one eigenvalue of the SPDM is close to one, indicating a fully coherent state. Coherence is lost when the adiabaticity breaks down and particles are scattered out of the condensate mode.

Figure 10.9 shows the results for a fast sweep $\alpha = 10$ for $J = 1$. In the linear case, equation (10.1) predicts a Landau-Zener tunneling rate of $P_{LZ} = 0.7304$. Surprisingly, the basic structure of the numerical results is very similar to the adiabatic case shown in figure 10.8. The curves are shifted, but the general progression remains the same. This is understood as follows. As argued earlier, an attractive nonlinearity flattens the upper level so that Landau-Zener tunneling is decreased. The current example shows that this effect is so strong that the tunneling process is completely suppressed so that $P_{LZ} \rightarrow 0$ for large negative values of g . On the contrary, a repulsive nonlinearity leads to an increase of P_{LZ} . The transition between an effectively adiabatic and non-adiabatic dynamics occurs at $g = 2J$ for a slow parameter variation $\alpha \rightarrow 0$. For a fast sweep, P_{LZ} is non-zero in the linear case $g = 0$. However, a strong attractive nonlinearity can flatten the level so much that adiabaticity is restored again. Thus one can always enforce an adiabatic transition, but the necessary interaction strength $|g|$ increases monotonically with α . This behaviour is also reflected in the coherence properties of the final state shown on the right-hand side of figure 10.8 and 10.9.

One astonishing feature observed in the figures 10.8 and 10.9 is the excellent agreement of the Landau-Zener tunneling rate P_{LZ} and the eigenvalues of the SPDM. Deviations are only found around $g = 0$ in figure 10.9. This can be understood by a loss of the

coherence between the two modes for long times, that is

$$\langle \hat{a}_1^\dagger \hat{a}_2 \rangle \rightarrow 0 \quad \text{for } t \rightarrow +\infty, \quad (10.15)$$

if we do not take into account the temporal revivals illustrated in figure 10.4. This happens either if the atoms are not in a coherent state any longer or if all atoms are localized in one of the modes. In any case we can rewrite the reduced SPDM as

$$\rho(t \rightarrow +\infty) \approx \begin{pmatrix} \langle \hat{n}_1(t \rightarrow +\infty) \rangle & 0 \\ 0 & \langle \hat{n}_2(t \rightarrow +\infty) \rangle \end{pmatrix} = \begin{pmatrix} 1 - P_{\text{LZ}} & 0 \\ 0 & P_{\text{LZ}} \end{pmatrix}. \quad (10.16)$$

So the eigenvalues of the SPDM are directly given by the Landau-Zener tunneling rate if the two modes are not coherent. For strong nonlinearities g this is always the case and so the left- and the right-hand sides of the figures 10.8 and 10.9 show an excellent agreement except for a small region around $g = 0$ in figure 10.9. In the non-interacting case ($g = 0$) the dynamics of all atoms is identical and the condensate will be fully coherent at all times. Thus the leading eigenvalue of the SPDM is always equal to one independent of the Landau-Zener tunneling rate, such that the approximation (10.16) is no longer valid in the non-interacting case.

10.1.5 Semiclassical and adiabatic limit

Having discussed various aspects of the mean-field many-particle correspondence in the previous sections, we now investigate the convergence to the mean-field limit quantitatively. The left-hand side of figure 10.10 compares the mean-field Landau-Zener tunneling probability $P_{\text{LZ}}(\alpha)$ (10.6) to the corresponding many-particle results (10.4) for different particle numbers and $g = -5$. While the many-particle dynamics usually converges rapidly to the mean-field limit, the occurrence of a dynamical instability for $|g| > 2J$ leads to a breakdown of adiabaticity for small values of α . In this parameter region the convergence to the many-particle limit is logarithmically slow. This is further illustrated in figure 10.10 on the right-hand side, where the Landau Zener tunneling probability $P_{\text{LZ}}^{\text{mp}}$ is plotted as a function of the inverse particle number $1/N$. Another observation from the numerical data presented in figure 10.10 is that a simple mean-field description gives qualitatively wrong results in the adiabatic limit of small α . As already discussed in section 10.1.1, the many-particle Landau-Zener tunneling probability $P_{\text{LZ}}^{\text{mp}}(\alpha)$ will always tend to zero for $\alpha \rightarrow 0$ since the level splittings in the many-particle spectrum may become small, but are always non-zero for finite N . Its mean-field counterpart $P_{\text{LZ}}^{\text{mf}}(\alpha)$, however, is always affected by the appearance of the dynamical instability which destroys adiabaticity also for infinitesimally small values of α . Consequently, the Landau-Zener tunneling probability is believed to be non-zero even in this limit. This difference led to the claim that the adiabatic limit $\alpha \rightarrow 0$ and the semiclassical limit $1/N \rightarrow 0$ do *not* commute [240]. However, this claim is true only for arguments based on expectation values assuming a pure condensate at all times, which is obviously no longer true in the present case.

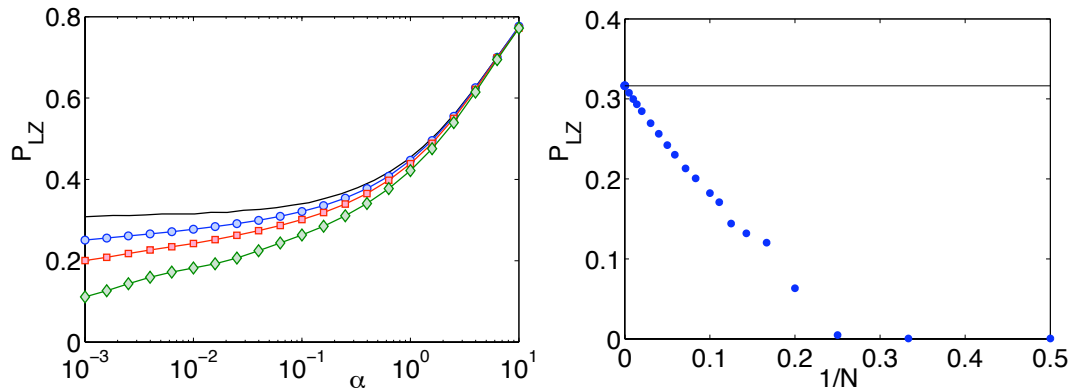


Figure 10.10: Left panel: Landau-Zener tunneling probability P_{LZ} as a function of α for $g = -5$. Single-trajectory mean-field results (solid black line) are compared to exact many-particle results for $N = 10$ (green diamonds), $N = 20$ (red squares) and $N = 40$ (blue circles) particles. The lines are drawn to guide the eye. Right panel: Slow convergence to the mean-field limit in the adiabatic regime. The Landau-Zener tunneling probability P_{LZ} is plotted as a function of the inverse particle number for $\alpha = 0.01$ and $g = -5$. The black line corresponds to the single-trajectory mean-field results which are approached in the limit $1/N \rightarrow 0$.

As discussed in the previous section, the proper semiclassical limit of the quantum dynamics is a phase space flow rather than a single phase space trajectory. This description is valid also if the classical dynamics is unstable and the many-particle quantum state deviates from a pure condensate. The left-hand side of figure 10.11 shows the Landau-Zener tunneling probability $P_{LZ}^{\text{ens}}(\alpha)$ for different particle numbers calculated from the propagation of a semiclassical phase space ensemble. It is observed that the many-particle results (cf. figure 10.10) can be reproduced to a very good approximation even for small values of α . Thus there is no incommutability of the adiabatic and semiclassical limits if the latter is interpreted correctly. Also the slow convergence to the single-trajectory limit is well described by the semiclassical phase space approach. The right-hand side of figure 10.11 shows P_{LZ}^{ens} as a function of the inverse particle number $1/N$ for $\alpha = 0.01$ which is well in the adiabatic regime. Significant differences to the many-particle results (cf. figure 10.10) are observed only for very small particle numbers, $N \lesssim 10$.

10.1.6 Influence of phase noise

We finally want to approach the question how an interaction with the environment affects the transition from quantum-many body to the classical mean-field dynamics. To this end we consider the Landau-Zener problem subject to phase noise, which is the dominant influence of the environment provided that the two condensate modes are held in sufficiently deep trapping potentials (cf. section 8.5.1). The many-particle

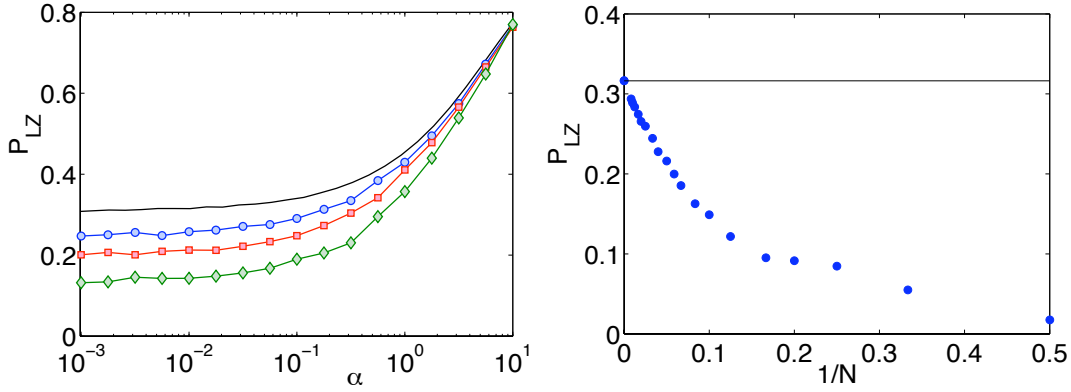


Figure 10.11: Left panel: Landau-Zener tunneling probability P_{LZ}^{ens} as a function of α calculated from a semi-classical ensemble simulation for $g = -5$ and $N = 10$ (green diamonds), $N = 20$ (red squares) and $N = 40$ (blue circles) particles. The lines are drawn to guide the eye. The black line corresponds to the single-trajectory mean-field results which are approached in the limit $1/N \rightarrow 0$. Right panel: The Landau-Zener tunneling probability P_{LZ}^{ens} as a function of the inverse particle number calculated from a semi-classical ensemble simulation for $\alpha = 0.01$ and $g = -5$.

dynamics is then given by the master equation

$$\frac{d}{dt}\hat{\rho} = -i[\hat{H}, \hat{\rho}] - \frac{\kappa}{2} \sum_{j=1,2} (\hat{n}_j^2 \hat{\rho} + \hat{\rho} \hat{n}_j^2 - 2\hat{n}_j \hat{\rho} \hat{n}_j). \quad (10.17)$$

Phase noise leads to transversal relaxation degrading the coherences s_x and s_y of the two condensate modes. Note that the magnitude of the Bloch vector $|\mathbf{s}|$ is no longer conserved because of this effect.

The resulting Landau-Zener tunneling probabilities are plotted in figure 10.12 as a function of α for different values of the noise strength κ . It is observed that phase noise has an important effect only for small values of α , where it drives the system to a completely mixed state with equal population in both wells such that $P_{LZ} = 1/2$. On the contrary, almost no consequences are observed for fast parameter sweeps. In this case, the tunneling time during which the atoms are delocalized is so short that phase noise cannot affect the dynamics. The transition to the incoherent regime occurs when the time scale of the noise κ^{-1} is smaller than the tunneling time which is roughly given by α^{-1} . Therefore the sweep is incoherent such that $P_{LZ} = 1/2$ if

$$\alpha \lesssim \kappa, \quad (10.18)$$

while the interaction strength g has a minor effect only.

Comparing mean-field and many-particle results, significant differences are observed for very small values of α and $g = -5$ in the non-dissipative case $\kappa = 0$, which has been discussed in detail in section 10.1.3. In addition we note that already a small amount of phase noise is sufficient to remove these differences. For $\alpha \rightarrow 0$ and $\kappa \neq 0$

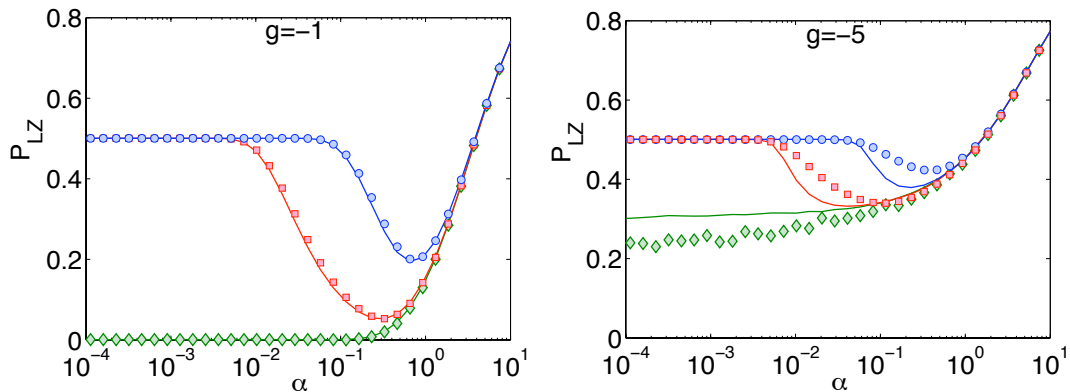


Figure 10.12: Landau-Zener tunneling probability $P_{LZ}(\alpha)$ in the presence of phase noise for $g = -1$ (left) and $g = -5$ (right). The strength of the phase noise is chosen as $\kappa = 0$ (green diamonds), $\kappa = 0.01$ (red squares) and $\kappa = 0.1$ (blue circles). Mean-field results (solid lines) are compared to many-particle results $N = 40$ particles (symbols).

the mean-field approximation (10.5) correctly predicts the transition to a completely mixed state with $P_{LZ} = 1/2$. Furthermore, significant differences are observed for $g = -5$ and intermediate values of α . In this case the many-particle quantum state is no longer a pure BEC but rather strongly number squeezed as discussed earlier. This state is more easily driven to a completely mixed state by phase noise than a pure BEC, a process which certainly cannot be described by the simple single-trajectory mean-field approximation.

Finally, these results suggest that Landau-Zener sweeps may actually be used as a probe of decoherence in systems of ultracold atoms (cf. also [218]). A measurement of the transition point to the incoherent regime where $P_{LZ} = 1/2$ gives an accurate quantitative estimate of the noise strength κ with a fairly simple experiment.

10.2 Bloch oscillations

In the subsequent sections we will be concerned with the dynamics of ultracold atoms in a tilted optical (super-)lattice. As is known from solid state physics, the single-particle dynamics in such a periodic one-dimensional potential under the influence of an additional static field features a periodic motion, the Bloch oscillations. In this section, we explain the basic principles of the dynamics of Bloch oscillations in the context of ultracold bosons in an optical potential. For reasons of simplicity, we neglect the interactions between the atoms and consider a single Bloch band only. This allows an analytic treatment in the tight-binding approximation, which will be presented in this section following the presentation in [246]. In the subsequent sections, we will then analyze the dynamics in a bichromatic lattice, where the Bloch band splits up in two minibands and the atoms can undergo Landau-Zener transitions between them, including the effects of inter-particle interactions.

Under the assumption that the dynamics is restricted to the lowest energy band in each of the potential minima, the dynamics of a dilute gas of ultracold atoms in an optical lattice subject to an additional static force is given by the Bose-Hubbard type Hamiltonian

$$H = -J \sum_{j=1}^{M-1} \left(\hat{a}_{j+1}^\dagger \hat{a}_j + \hat{a}_j^\dagger \hat{a}_{j+1} \right) + F \sum_{j=1}^M j \hat{a}_j^\dagger \hat{a}_j. \quad (10.19)$$

Here, F denotes the difference of the strength of the static field at two neighbouring lattice sites and J is the tunneling matrix element, as introduced in section 8.3.

A transformation of the problem, using a representation in terms of creation and annihilation operators of Bloch waves with quasi-momentum $-\frac{\pi}{2} \leq q \leq \frac{\pi}{2}$

$$\hat{a}_q = \sqrt{\frac{1}{2\pi}} \sum_{j=-\infty}^{\infty} e^{ijq} \hat{a}_j, \quad (10.20)$$

instead of creation operators in the Wannier basis (8.24) localized at the j -th lattice site

$$\hat{a}_j = \frac{1}{\sqrt{2\pi}} \int e^{-ijq} \hat{a}_q dq, \quad (10.21)$$

reduces the computational effort significantly. In this basis, the Hamiltonian (10.19) is diagonal and reads

$$\hat{H}(q) = -2J \cos(q) \hat{a}_q^\dagger \hat{a}_q + iF \hat{a}_q^\dagger \frac{\partial}{\partial q} \hat{a}_q. \quad (10.22)$$

The eigenstates of this Hamiltonian are the so-called Wannier stark states, which are given by

$$\begin{aligned} w_m(q) &= \frac{1}{\sqrt{2\pi}} e^{-imq + \frac{2J}{F} \sin(q)} \quad \text{with} \quad m \in \mathbb{Z} \\ &= w_m(q + 2\pi) \end{aligned} \quad (10.23)$$

in the Bloch wave basis. These states correspond to the eigenenergies $E_m = mF$. This is often referred to as the Wannier-Stark ladder [247–249].

With a little bit of algebra, we obtain the time evolution operator

$$\begin{aligned} \hat{U} &= \sum_m \int \int w_m(q) e^{-iE_m t} w_m^*(q') \hat{a}_q^\dagger \hat{a}_{q'} dq' dq \\ &= \frac{1}{2\pi} \int \int e^{-i2J/F(\sin(q) - \sin(q'))} \sum_m e^{-im(q - q' + Ft)} \hat{a}_q^\dagger \hat{a}_{q'} dq' dq \\ &= \int \int e^{-i2J/F(\sin(q) - \sin(q'))} \delta(q - q' + Ft) \hat{a}_q^\dagger \hat{a}_{q'} dq' dq \end{aligned} \quad (10.24)$$

The quasi-momentum depends linearly on the time

$$q(t) = q(0) - Ft, \quad (10.25)$$

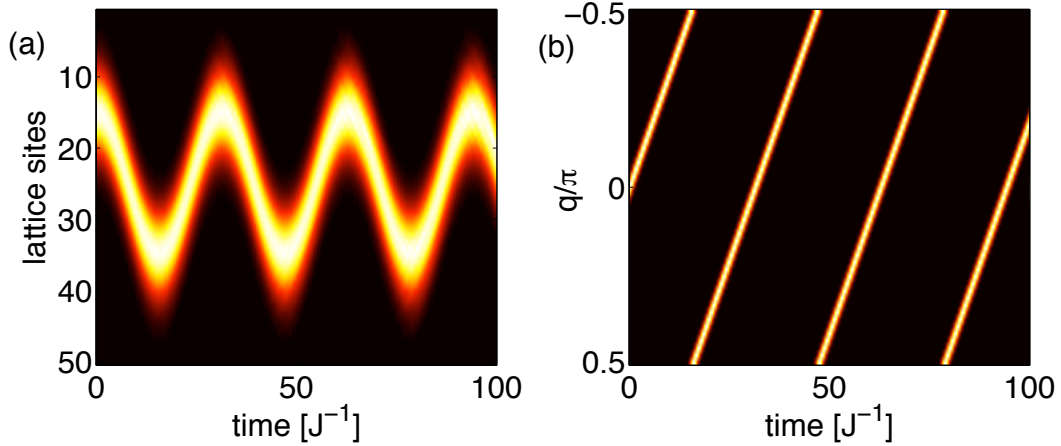


Figure 10.13: Bloch oscillations in real (a) and momentum space (b). Shown is the time evolution of the particle density $|\psi|^2$ in dependence of the lattice sites, respective the quasi momentum q . We assume that the initial state is a pure BEC (10.30) in the ground Bloch band with $q = 0$ weighted by a Gaussian envelope (10.45) with $\sigma = 4$ and $n_0 = 15$. The parameters are $J = 1$ and $F = 0.2$.

such that the dynamics is periodic with an oscillation period

$$T_{\text{Bloch}} = \frac{2\pi}{F}. \quad (10.26)$$

The dynamics can be compared to a classical particle which is accelerated at a constant rate until it reaches the edge of the Brillouin zone, where it is Bragg-reflected. This result is also known as the acceleration theorem [250].

A Fourier transformation yields the time evolution operator in the Wannier basis

$$\hat{U} = \sum_{j,k} \mathcal{J}_{j-k} \left(\frac{4J}{F} \sin\left(\frac{Ft}{2}\right) \right) e^{i(j-k)(\pi-Ft)/2 - ikFt} \hat{a}_j^\dagger \hat{a}_k, \quad (10.27)$$

where we used the integral representation of the Bessel function \mathcal{J}_{j-k} [251]. Using this representation, it is straightforward to calculate the dynamics of a wave packet or of expectation values.

In figure 10.13 one example of Bloch oscillations in an extended lattice of 50 lattice sites is shown. Depicted is the particle density $|\psi|^2$ in real (a) and momentum space (b). The initial state is chosen to be a pure BEC distributed over the lattice sites according to a Gaussian distribution. One clearly observes the periodic motion in real space and the linear dependence of the quasi momentum on time, as well as the Bragg-reflections at the edge of the Brillouin zone.

10.3 Interacting BEC in a bichromatic lattice

As we have seen in the preceding section, Bloch oscillations of ultracold atoms in optical lattices occur if the atoms are accelerated by a weak external field until they are Bragg reflected at the edge of the Brillouin zone leading to a periodic motion. Though for stronger fields a directed motion is re-introduced by repeated Landau-Zener transitions to higher Bloch bands. Since the band gap between the excited bands decreases more and more the atoms are irretrievably lost due to tunneling to higher bands on a short time scale [210, 235].

For a bichromatic lattice, each Bloch band split up into two minibands, whereas all higher bands are energetically well separated. Here, the external field induces also Landau-Zener tunneling [236], but the atoms are confined to the two lowest bands. Thus, the dynamics of a BEC in a tilted bichromatic optical lattice is governed by an interplay of the intraband dynamics and the transitions between the two minibands. On longer timescale repeated Landau-Zener tunneling takes place, which leads to a complex dynamics due to the interference effects of atoms in the two minibands [232, 252, 253]. This makes bichromatic lattices a perfect model system to study nonlinear Bloch-Zener tunneling.

Moreover, these effects can be used as a coherent beam splitter for atomic matter waves. Therefore the coherent superposition of Bloch oscillations and Landau-Zener tunneling between two minibands provides a natural realization of a matter wave Mach-Zehnder interferometer [232, 252] and thus enable a variety of possible applications in matter wave interferometry and quantum metrology [253].

Here, we will consider ultracold atoms in a bichromatic optical lattice with an alternating depth of the lattice wells. The many-body dynamics is described by the Bose-Hubbard type Hamiltonian

$$\begin{aligned}
 H = & -J \sum_{n=1}^{M-1} \left(\hat{a}_{n+1}^\dagger \hat{a}_n + \hat{a}_n^\dagger \hat{a}_{n+1} \right) + \frac{U}{2} \sum_{n=1}^M \hat{a}_n^{\dagger 2} \hat{a}_n^2 \\
 & + \sum_{n=1}^M \left(\frac{\delta}{2} (-1)^n + Fn \right) \hat{a}_n^\dagger \hat{a}_n, \tag{10.28}
 \end{aligned}$$

where \hat{a}_n and \hat{a}_n^\dagger are the bosonic annihilation and creation operators, respectively. As discussed in section 8.3 the parameter J is defined as the tunneling rate between the wells and U is the interaction strength. Moreover, F denotes the strength of the static external field which accelerates the atoms and the parameter $\delta \geq 0$ is the difference of the on-site energies between adjacent wells.

The corresponding mean-field dynamics is then given by a generalization of the GPE (8.58) [81]

$$i\dot{x}_n = -J(x_{n+1} + x_{n-1}) + \left[\frac{(-1)^n \delta}{2} + Fn + UN|x_n|^2 \right] x_n. \tag{10.29}$$

Bichromatic lattices have been implemented by superimposing two incoherent optical lattices [123, 124], or by combining optical potentials based on virtual two-photon and

four-photon processes [236, 253–256]. These superlattices allow to engineer the Bloch band structure of the system by tuning few experimental parameters, e.g. the tunneling rate can be controlled to a large extent by tuning the lattice parameters and the difference of the on-site energies between adjacent wells, $\delta \geq 0$, is directly proportional to the intensity of the double-periodic optical lattice [254].

One of the main objectives of this section is a careful analysis of how the interactions affect the coherent dynamics of a BEC in a bichromatic lattice and how they possibly lead to instabilities of the condensate. In the following we thus assume that the system is initially prepared as a pure BEC with N particles:

$$|\Psi(0)\rangle = \frac{1}{\sqrt{N!}} \left(\sum_n \psi_n \hat{a}_n^\dagger \right)^N |0\rangle. \quad (10.30)$$

Dynamical instabilities lead to a depletion of the condensate such that the mean-field approximation is no longer applicable. To simulate the dynamics beyond mean-field we use the Bogoliubov backreaction (BBR) method introduced in section 8.4.4 which also gives a quantitative prediction for the depletion of the condensate [69, 140, 141]. In particular the nature of the many-body quantum state is indicated by the reduced single-particle density matrix (SPDM)

$$\sigma_{j,m} = \frac{1}{N} \langle \hat{a}_j^\dagger \hat{a}_m \rangle, \quad (10.31)$$

as introduced in section 8.3. The leading eigenvalue of this matrix, λ_0 , gives the fraction of atoms in the condensate mode. Consequently, the non-condensed fraction is given by $1 - \lambda_0$, cf. section 9.2.3.

10.3.1 Stability of Bloch bands

Bloch states for the bichromatic lattice are the simultaneous eigenstates of the field-free Hamiltonian and a translation over *two* lattice sites. The dynamics of a BEC in a bichromatic lattice can be understood to a large extent from the properties of linear and non-linear Bloch states. In this section, we thus give a detailed analysis of the Bloch states and their stability properties.

In the simplest case of a single atom, where interactions are obviously irrelevant, the Bloch bands are easily calculated as [252]

$$E_\alpha(q) = \frac{(-1)^{\alpha+1}}{2} \sqrt{\delta^2 + 16J^2 \cos^2(q)}, \quad (10.32)$$

where $\alpha = 0, 1$ labels the two minibands and $q \in [-\pi/2, +\pi/2]$ denotes the quasimomentum. The band gap between the two minibands is directly given by the parameter δ . The corresponding Bloch states are given by $|\chi_{\alpha,q}\rangle = \hat{b}_{\alpha,q}^\dagger |0\rangle$, where

$$\begin{aligned} \hat{b}_{0,q} &= \frac{1}{\sqrt{N_q}} \sum_n u_q e^{i(2n+1)q} \hat{a}_{2n} + v_q e^{i(2n+2)q} \hat{a}_{2n+1} \\ \hat{b}_{1,q} &= \frac{1}{\sqrt{N_q}} \sum_n v_q e^{i2nq} \hat{a}_{2n} - u_q e^{i(2n+1)q} \hat{a}_{2n+1} \end{aligned} \quad (10.33)$$

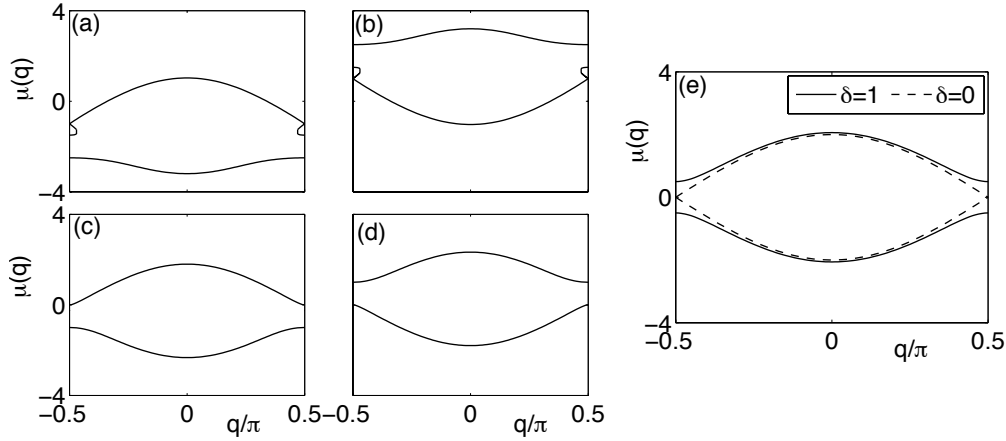


Figure 10.14: Nonlinear Bloch bands in a bichromatic optical lattice with $\delta = 1$ and $F = 0$ for different values of the interaction strength: $g = -2$ (a), $g = +2$ (b), $g = -0.5$ (c) and $g = +0.5$ (d). (e) Comparison of the linear Bloch bands ($g = 0$) in a bichromatic lattice $\delta = 1$ (solid line) and for $\delta = 0$ (dashed line) corresponding to a simple lattice.

and

$$\begin{aligned} u_q &= 4J \cos(q) \\ v_q &= \delta + \sqrt{\delta^2 + 16J^2 \cos^2(q)}, \end{aligned}$$

$N_q = \pi(u_q^2 + v_q^2)$ being a normalization constant.

In the mean-field approximation one can also analytically calculate the 'nonlinear' Bloch states, which are defined as stationary states of the discrete nonlinear Schrödinger equation (DNLSE)

$$\mu \phi_n = -J(\phi_{n+1} + \phi_{n-1}) + UN|\phi_n|^2 \phi + (-1)^n \frac{\delta}{2} \phi_n, \quad (10.34)$$

respecting the translation symmetry $\phi_{n+2} = e^{2iq} \phi_n$. Making the ansatz

$$\phi_n \sim \begin{cases} u_q e^{iqn} & n \text{ even} \\ v_q e^{iqn} & n \text{ odd}, \end{cases} \quad (10.35)$$

one finds that the coefficients u_q, v_q are determined by the two-mode DNLSE

$$\begin{pmatrix} \delta/2 + g|u_q|^2 & -2J \cos(q) \\ -2J \cos(q) & -\delta/2 + g|v_q|^2 \end{pmatrix} \begin{pmatrix} u_q \\ v_q \end{pmatrix} = \mu \begin{pmatrix} u_q \\ v_q \end{pmatrix}. \quad (10.36)$$

Using the normalization $|u_q|^2 + |v_q|^2 = 1$, the effective coupling constant is given by $g = 2U\rho$, where ρ is the average particle density.

Examples of nonlinear Bloch bands are shown in figure 10.14. One observes that the bands become strongly asymmetric – the ground band is sharpened and the excited

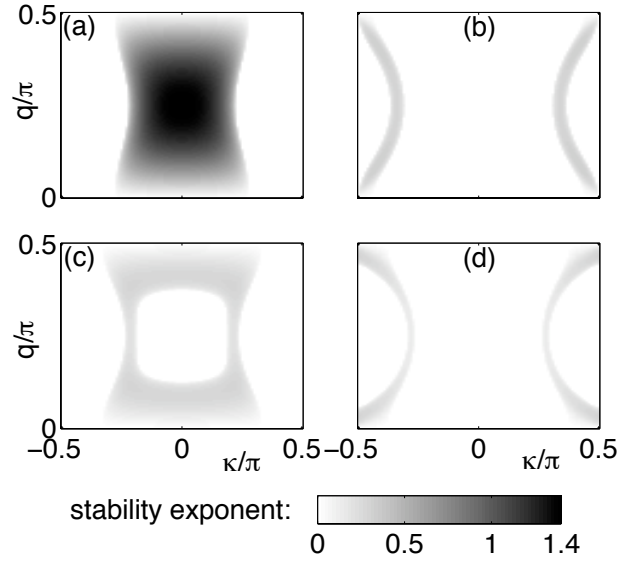


Figure 10.15: Stability map for a nonlinear Bloch state with quasimomentum q in the ground band for $\delta = 1$ and for different values of the interaction strength: $g = -2$ (a), $g = +2$ (b), $g = -0.5$ (c) and $g = +0.5$ (d). The gray scale map shows the stability exponent, i.e. the growth rate of a perturbation with quasimomentum q . Dynamical instability leads to a depletion of the condensate if the stability exponent is non-zero for at least one value of q .

band is flattened for a repulsive nonlinearity $g > 0$ and vice versa for an attractive nonlinearity $g < 0$. For strong nonlinearities novel stationary states appear at the band edge $q = \pm\pi/2$, forming the so-called looped Bloch bands [230, 257]. A quantitative analysis shows that DNLSE (10.36) admits four solutions if [229]

$$g^{2/3} > \delta^{2/3} + |2J \cos(q)|^{2/3}. \quad (10.37)$$

Thus the critical nonlinearity for the existence of looped levels is directly linked to the band gap δ . The deformation of the Bloch bands has significant consequences for the dynamics which will be discussed in detail in section 10.3.2. An adiabatic dynamics is hindered by a sharpening of the levels and becomes completely impossible as soon as the loops form.

The nonlinear Bloch states calculated in equation (10.35) are stationary states of the DNLSE (10.29). However, they can become dynamically unstable due to the nonlinear interaction term, which also indicates a rapid depletion of the BEC. To determine the stability properties of a Bloch state (10.35), we add a small perturbation with quasimomentum \tilde{q} :

$$\begin{aligned} \psi_n(t) = & e^{-i\mu t} \phi_n \\ & + \begin{cases} e^{i(qn-\mu t)}(\xi_{0,q}e^{i\tilde{q}n} + \zeta_{0,q}^*e^{-i\tilde{q}n}) & n \text{ even} \\ e^{i(qn-\mu t)}(\xi_{1,q}e^{i\tilde{q}n} + \zeta_{1,q}^*e^{-i\tilde{q}n}) & n \text{ odd} \end{cases} \end{aligned} \quad (10.38)$$

and analyze the consequences for the energy and the dynamics of the condensate. If every perturbation increases the total energy given by the Gross-Pitaevskii energy functional

$$E = -J \sum_n \psi_{n+1}^* \psi_n + \psi_n^* \psi_{n+1} + \frac{UN}{2} \sum_n |\psi_n|^4 + \frac{\delta}{2} \sum_n (-1)^2 |\psi_n|^2, \quad (10.39)$$

then the Bloch state represents a local energy minimum and thus a stable superflow. Otherwise a perturbation may lower the energy and the Bloch state suffers a Landau instability. Here, we are more concerned with the dynamical instability of a Bloch state, which occurs if a perturbation grows exponentially, as this indicates a rapid depletion of the condensate mode [52, 53, 137, 258]. Note that dynamical instability always indicates energetical instability, but not vice versa [230].

To determine the energetical stability we substitute the ansatz (10.38) into the Gross-Pitaevskii energy functional (10.39) and expand it up to second order in the perturbation. The variation of the energy is then given by

$$\delta E = \int d\tilde{q} \Xi_q^\dagger L_{\text{en}}(q, \tilde{q}) \Xi_q \quad (10.40)$$

with the matrix

$$L_{\text{en}}(q, \tilde{q}) = \begin{pmatrix} H(q + \tilde{q}) & gV \\ gV^* & H(q - \tilde{q}) \end{pmatrix}. \quad (10.41)$$

Here we have introduced the abbreviations

$$H(k) = \begin{pmatrix} \frac{\delta}{2} + 2g|u|^2 - \mu & -2J \cos(k) \\ -2J \cos(k) & -\frac{\delta}{2} + 2g|v|^2 - \mu \end{pmatrix}, \\ V = \begin{pmatrix} u^2 & 0 \\ 0 & v^2 \end{pmatrix} \quad \text{and} \\ \Xi_q = (\xi_{0,q}, \xi_{1,q}, \zeta_{0,q}, \zeta_{1,q})^T. \quad (10.42)$$

The Bloch state represents a stable energy minimum if δE is positive for any perturbation, i.e. if the matrix $L_{\text{en}}(q, \tilde{q})$ is positive definite for every perturbation \tilde{q} .

The dynamical stability properties are found by substituting the ansatz (10.38) into the DNLSE (10.29). In first order, the perturbation evolves according to the Bogoliubov-de Gennes equation (cf. section 8.4.3)

$$i \frac{d}{dt} \Xi_q = L_{\text{BdG}}(q, \tilde{q}) \Xi_q \quad (10.43)$$

with

$$L_{\text{BdG}}(q, \tilde{q}) = \sigma_z L_{\text{en}}(q, \tilde{q}) = \begin{pmatrix} H(q + \tilde{q}) & gV \\ -gV^* & -H(q - \tilde{q}) \end{pmatrix}. \quad (10.44)$$

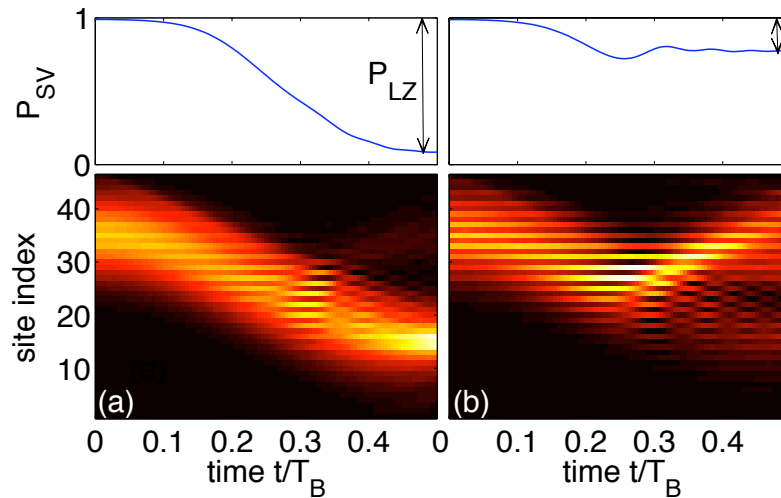


Figure 10.16: Many-particle Landau-Zener tunneling between two minibands for two different values of the band gap, $\delta = 0.2$ (a) and $\delta = 1$ (b). The dynamics has been calculated with the BBR method for the parameters $J = 1$, $F = 0.2$, $UN = 2$ and $N = 100$ particles. The upper panels show the survival probability (10.46) in the upper half of the lattice.

A dynamical instability occurs if a perturbation grows exponentially, that means if there is any \tilde{q} for which the eigenvalues of the matrix $L_{\text{BdG}}(q, \tilde{q})$ are not purely real.

The dynamical stability for the Bloch states in the ground band is depicted in figure 10.15 for the same parameters as in figure 10.14. A grey scale map shows the stability exponent, that means the maximum imaginary part of the eigenvalues of the Bogoliubov-de Gennes matrix $L_{\text{BdG}}(q, \tilde{q})$ in dependence of q and \tilde{q} . This imaginary part indicates the growth rate of a perturbation with wavenumber \tilde{q} and thus also the depletion rate of the condensate. A Bloch state with quasimomentum q is dynamically stable only if the growth rate is zero for all values of \tilde{q} . One observes that two different kinds of dynamical instability exist in a bichromatic lattice. In the attractive case $g < 0$, the Bloch states in the center of the Brillouin zone become strongly unstable already for a quite modest nonlinearity. Thus we face the surprising conclusion that an attractive interaction on the one hand flattens the ground band and thus facilitates an adiabatic evolution, but on the other hand leads to instability. In contrast, a strong repulsive nonlinearity is required to introduce a weak dynamic instability at the edge of the Brillouin zone, which is associated with the occurrence of looped Bloch bands. Thus one can infer that a significant depletion takes place only for a much stronger interaction than in the attractive case and that it sets in at the edge of the Brillouin zone around $q = \pi/2$.

10.3.2 Nonlinear Zener tunneling

To begin with, we explore the basic features of the dynamics in a tilted bichromatic lattice – Bloch oscillations and Landau-Zener tunneling – for the weakly interacting

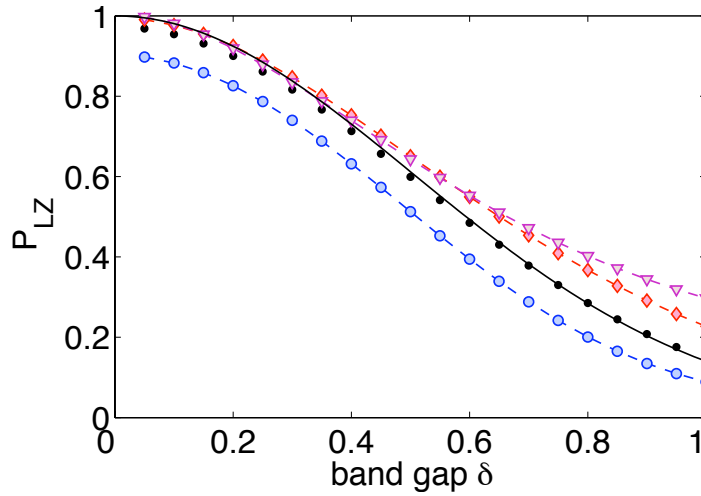


Figure 10.17: Landau-Zener tunneling probability P_{LZ} between two minibands as a function of the band gap δ for $UN = -2$ (\circ), $UN = 0$ (\cdot), $UN = +2$ (\diamond) and $UN = +4$ (∇) and $N = 100$ particles. The solid line shows the analytic approximation (10.47) for the linear case. Dashed lines are plotted to guide the eye.

case. We assume that the initial state is a pure BEC (10.30) in the ground Bloch band with $q = 0$ weighted by a Gaussian envelope

$$\psi_n(0) \sim \phi_n \exp(-(n - n_0)^2/4\sigma^2) \quad (10.45)$$

with a width of $\sigma = 5$ sites centered around the site $n_0 = 35$. In the forthcoming examples we choose the total particle number to be $N = 100$ located in a lattice with $M = 46$ sites and $F = 0.2$, unless otherwise stated. A weak nonlinearity induces a reversible dephasing, which damps Bloch oscillations [212, 258, 259], and, of course, alters the Landau-Zener tunneling rate between the two minibands.

Figure 10.16 shows two examples of the many-body dynamics starting from the initial state (10.30) for a weak repulsive interaction, $UN = 2$, and two different values of the band gap δ . The figures show the evolution of the density $\langle \hat{n}_j(t) \rangle$, $j = 1, \dots, M$ in false color. Here and in the following, we take the Bloch time $T_B = 2\pi/F$ of the single-periodic lattice ($\delta = 0$) as the reference time scale. One observes that the BEC is first accelerated by the external field F until it reaches the edge of the Brillouin zone at $T = T_B/4$. If the band gap δ is large (cf. figure 10.16 (b)), the BEC matter wave stays in the ground miniband and performs Bloch oscillations with a period of $T_B/2$. In contrast, the matter wave tunnels to the excited miniband if the gap is small and performs Bloch oscillations with the full period T_B (figure 10.16 (a)). At time $t = T_B/2$ it is located at the turning point of the Bloch oscillations. For intermediate values of the band gap, only a fraction of the condensate tunnels to the excited miniband and the wavepacket splits.

For a further quantitative analysis of the Landau-Zener tunneling rate we estimate the survival probability in the ground miniband by the number of atoms remaining in the

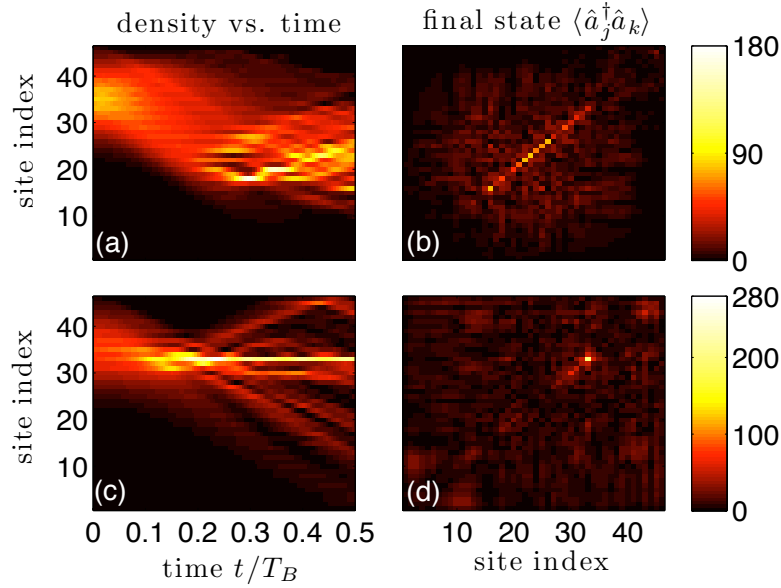


Figure 10.18: Unstable dynamics in a tilted bichromatic optical lattice for a strong repulsive interaction $UN = +20$ (a,b) as well as a strong attractive interaction $UN = -10$ (c,d). The left panels (a,c) show the evolution of the density and the right-panels (b,d) show the magnitude of the scaled SPDM $N|\sigma_{j,k}| = |\langle \hat{a}_j^\dagger \hat{a}_k \rangle|$ at $t = T_B/2$ in a colormap plot. The remaining parameters are $\delta = 0.2$ and $N = 1000$.

upper half of the lattice:

$$P_{\text{SV}}(t) = \frac{1}{N} \sum_{j=24}^{46} \langle \hat{n}_j(t) \rangle. \quad (10.46)$$

Hence, the Landau-Zener tunneling probability to the excited band is given by $P_{\text{LZ}} := 1 - P_{\text{SV}}(T_B/2)$. The time dependence of the survival probability (10.46) is shown in the upper panels of figure 10.16 together with P_{LZ} .

Figure 10.17 shows the Landau-Zener tunneling probability P_{LZ} in dependence of the band gap δ for different values of the interaction strength UN . In the linear case $UN = 0$ one can approximate the avoided crossing of the two minibands at the edge of the Brillouin zone by an effective two-level model, which yields the following approximation for the Landau-Zener probability [252]:

$$P_{\text{LZ}}^{(0)} \approx \exp\left(-\frac{\pi\delta^2}{8JF}\right). \quad (10.47)$$

This approximation shows an excellent agreement with the numerical results shown in figure 10.17. In the weakly nonlinear case one observes an increase of the Landau-Zener tunneling rate P_{LZ} for a repulsive nonlinearity $U > 0$ and a decrease for an attractive nonlinearity $U < 0$, which has also been demonstrated experimentally [233]. This effect can be understood from the structure of the nonlinear Bloch states introduced in equation (10.35). With increasing interaction strength, the nonlinear Bloch bands

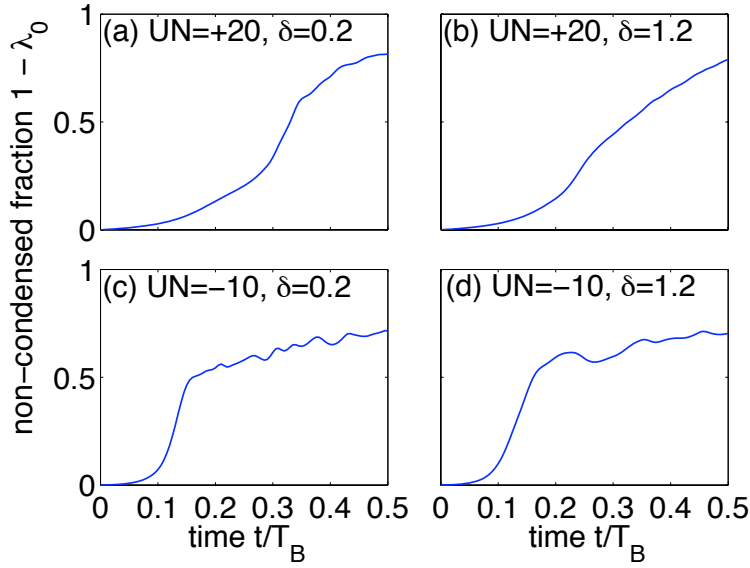


Figure 10.19: Depletion of the condensate during nonlinear Landau-Zener tunneling. Temporal growth of the non-condensed fraction $1 - \lambda_0$ for a strong repulsive interaction $UN = +20$ (a,b) and an attractive interaction $UN = -10$ (c,d). The remaining parameters are $\delta = 0.2$ (a,c) and $\delta = 1.2$ (b,d), respectively, and $N = 1000$.

$\mu(q)$ become strongly asymmetric as shown in figure 10.14. For $UN < 0$, the ground band is flattened so that adiabaticity is facilitated and P_{LZ} decreases, while the excited band is sharpened. The inverse effect is found for $UN > 0$ such that P_{LZ} increases. If the nonlinearity UN exceeds a critical value, a Bloch state at the edge of a band bifurcates to a looped structure, which prevents an adiabatic evolution even for very small values of the field strength F .

10.3.3 Depletion of the condensate

In the preceding chapters we have seen that strong inter-atomic interactions alter the dynamics of the BEC completely. This effect is present in bichromatic lattices, too. Examples are shown in figure 10.18 for a repulsive (a,b) and an attractive (c,d) interaction, respectively. One observes that the familiar Bloch oscillation pattern is significantly disturbed, especially in the case of attractive interactions. In the repulsive case, the atoms are distributed over several lattice sites, but the phase coherence between these sites is lost almost completely. This is indicated by a strong suppression of the non-diagonal parts of the SPDM (10.31) as shown in figure 10.18 (b). A strong attractive nonlinearity leads to a collapse of the condensate. Figure 10.18 (c) shows that the atoms are strongly focused to a single lattice site at $t \approx 0.15 T_B$. Afterwards, a fraction of the atoms explodes from the focus and the condensate mode is rapidly depleted.

To further analyze the different mechanisms of instability due to repulsive and attractive interactions we calculate how the condensate is depleted. Figure 10.19 shows the

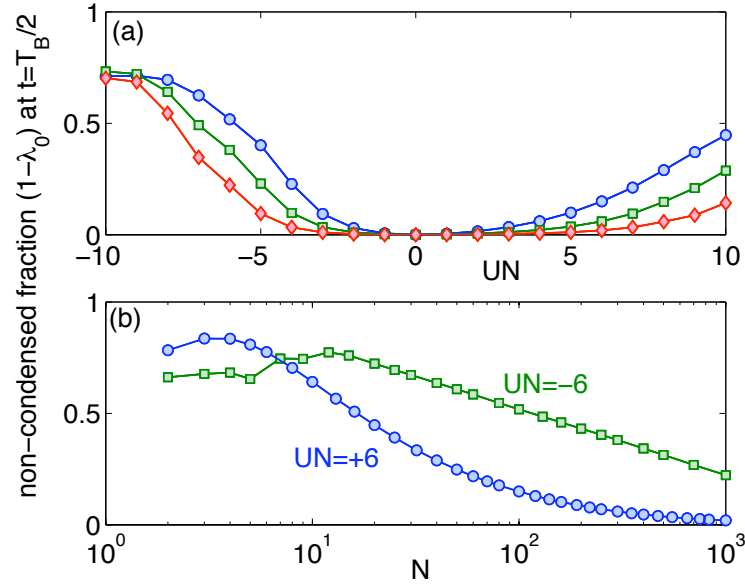


Figure 10.20: The non-condensed fraction $1 - \lambda_0$ at time $t = T_B/2$ as a function of (a) the interaction strength UN for $N = 100$ (\circ), $N = 300$, (\square) and $N = 1000$ (\diamond) and (b) as a function of the particle number N for a fixed interaction strength $UN = +6$ (\circ) and $UN = -6$ (\square). Solid lines are drawn to guide the eye.

time evolution of the non-condensed fraction $1 - \lambda_0$ for a strong repulsive ($UN = +20$) and a strong attractive nonlinearity ($UN = -10$), respectively. In the attractive case, instability sets in much earlier and takes place on a very short time scale. This difference can be explained by the results of a linear stability analysis as discussed in section 10.3.1. In the repulsive case the onset of dynamical instability can be associated with the emergence of looped Bloch bands. The condensate becomes dynamically unstable at the edge of the Brillouin zone where the loops emerge. In contrast, already modest attractive interactions lead to a dynamic instability at the center of the Brillouin zone (cf. figure 10.15) such that the depletion of the condensate sets in immediately.

A quantitative analysis of the depletion of the condensate is provided in figure 10.20, where we have plotted the non-condensed fraction at $t = T_B/2$ as a function of the interaction strength UN in (a) and the particle number N for a fixed value of the interaction strength $UN = \pm 6$ in (b). Figure 10.20 (a) clearly shows the qualitative difference between an attractive and a repulsive interaction. In the first case, one observes a rapid increase of the non-condensed fraction when the interaction strength exceeds the critical value for the onset of a dynamical instability. For a repulsive interaction, however, the dynamics is rather stable so that the non-condensed fraction remains small for all values of $|UN| < 10$ shown in the figure. The non-condensed fraction decreases with the particle number and tends to zero in the mean-field limit $N \rightarrow \infty$. However, the speed of convergence depends crucially on the stability of the dynamics as shown in figure 10.20 (b). In the repulsive case, $UN = +6$, the dynamics is stable and thus convergence is fast. The non-condensed fraction decreases rapidly

with increasing particle number such that the mean-field description by the DNLS is valid already for quite small values of the particle number. In contrast, the convergence is logarithmically slow for $UN = -6$ due to the dynamical instability.

10.3.4 Bloch-Zener oscillations

On a longer timescale, the dynamics of a BEC in a tilted optical lattice is governed by the interference of Bloch oscillations and Zener tunneling between the Bloch bands. Figure 10.21 (b) shows an example of the dynamics of the atomic density for $\delta = 0.5$. The condensate wave packet is coherently split by Landau-Zener tunneling between the two minibands at $t = T_B/4$ and recombined again at $t = 3T_B/4$, thus realizing an effective matter wave Mach-Zehnder interferometer. The splitting ratio of this interferometer, which is given by the Landau-Zener tunneling rate (10.47), is easily tunable by changing the band gap δ .

For very small and for very large values of δ , the condensate occupies only one miniband – it remains in the ground band for large δ and tunnels completely to the other miniband for small δ as shown in figure 10.21 (c). In both cases the condensate shows simple Bloch oscillations and returns back to its initial state at $t = T_B$. For intermediate values of δ , the condensate is split into two parts at $t = T_B/4$. The further dynamics and especially the occupation of the two minibands is governed by the interference of the two possible paths. For the given parameters, about one half of the population is still localized in the excited miniband at $t = T_B = 2\pi/F$. In this parameter range, the dynamics is very sensitive even to small nonlinearities as shown in figure 10.21 (d). The survival probability at $t = T_B$ differs significantly for $UN = -1$ and $UN = +1$, although the nonlinearity is still comparatively weak.

For the given interaction strength $|U| \leq 1$, the splitting and also the recombination of the condensate is fully coherent; the fraction of non-condensed atoms is less than 0.4% at $t = 2T_B$ as shown in figure 10.21 (a). A significant depletion of the condensate is observed only for stronger nonlinearities; for instance the non-condensed fraction at $t = 2T_B$ exceeds 10% for $UN \gtrsim 5$.

This example demonstrates that Landau-Zener tunneling and Bloch-Zener oscillations are versatile tools in quantum metrology. These tools can be used, for instance, to directly measure the band structure of a bichromatic potential as demonstrated in [253]. This is a unique feature of bichromatic optical lattices. In a simple periodic potential, a matter wave will be accelerated further towards $-\infty$ after it has escaped from the ground band, such that no interference can be observed.

10.3.5 Coupling of bands by a periodic driving

Previously, we have discussed the effects of Zener tunneling between the two minibands induced by the external field F . A coupling of the bands can also be introduced in the field free case by a periodic driving of the system parameters. This has the advantage

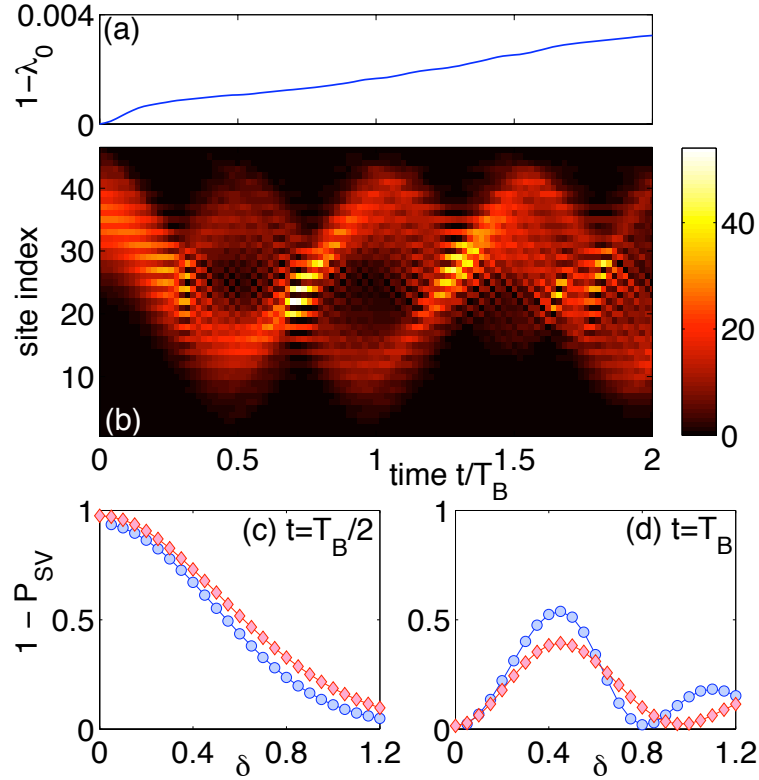


Figure 10.21: Bloch-Zener oscillations of a BEC with $N = 300$ atoms in a tilted bichromatic lattice. (a) Non-condensed fraction $1 - \lambda_0$ for $\delta = 0.5$ and $UN = 1$. (b) Atomic density in real space for $\delta = 0.5$ and $UN = 1$. (c,d) Survival probability (10.46) in the upper half of the lattice after $t = T_B/2$ (c) and $t = T_B$ (d), respectively, for $UN = -1$ (\circ) and $UN = +1$ (\diamond).

that the quasi momentum q is conserved such that a different regime of the dynamics can be explored.

Here we consider a BEC initially prepared in the ground miniband with a well defined quasimomentum q . The strength of the double-periodic optical lattice is varied in time to realize a harmonic driving of the energy offset

$$\delta(t) = \delta_0 + \delta_1 \cos(\omega t). \quad (10.48)$$

This driving induces transitions between the two minibands if the frequency is chosen to be resonant with the band gap, $\omega = E_1(q, \delta_0) - E_0(q, \delta_0)$. In the following example we set $\delta_0 = 0.4$, $\delta_1 = 0.2$ and $U = 0$. The initial state is assumed to be pure BEC (10.30) with momentum $q = 0.1\pi$, weighted by a Gaussian envelope (cf. equation (10.45)) with $\sigma = 10$. The resulting dynamics is shown in figure 10.22 in real (left) and momentum space (right). One clearly observes the transitions between the two minibands, while the quasimomentum of the BEC is conserved (panel (b)). A further quantitative analysis of this effect is provided in panel (d), where the occupation of the two minibands $p_{0,1}$ is plotted. The oscillation between the bands has remarkable

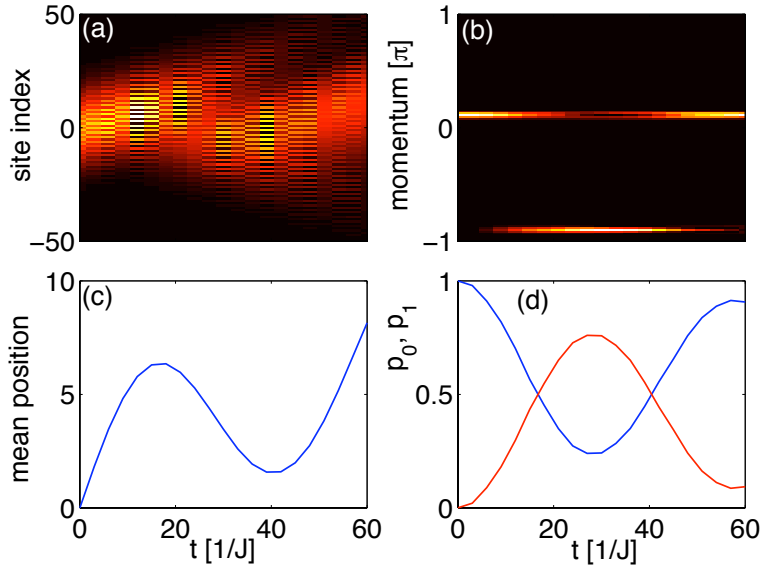


Figure 10.22: Quantum dynamics of BEC in a bichromatic lattice with periodic driving $\delta(t)$ and $F = 0$. (a,b) Atomic density in real and momentum space, respectively. (c) Position expectation value $\sum_j j \langle \hat{n}_j \rangle / N$. (d) Occupation of the two minibands p_0 (blue) and p_1 (red).

consequences for the real-space dynamics of the BEC shown on the left-hand side of the figure. As the two minibands have opposite curvature, a transition between the bands reverses the group velocity of the matter wave. This leads to an oscillatory motion of the mean position, which can be understood as a quantum analogue of the *Zitterbewegung* of a Dirac spinor. This relativistic effect results from the interference of particle and anti-particle contributions moving to opposite directions. In the discussed quantum simulator, the two minibands thus play the role of particle and anti-particle contributions, respectively. Similar effects were recently predicted for optical waveguide arrays [260, 261].

10.4 Concluding remarks

In the first part of this chapter we have presented an analysis of nonlinear Landau-Zener tunneling between two modes in quantum phase space. It was shown that adiabaticity breaks down if the interaction strength $g = UN$ exceeds the critical value $g_c = 2J$ – the Landau-Zener tunneling probability does not vanish even for an extremely slow variation of the system parameter. This phenomenon can be understood by the disappearance of adiabatic eigenstates in an inverse bifurcation in the mean-field approximation. Within the full many-particle description, the breakdown of adiabaticity results from the occurrence of diabatic avoided crossings, where the level separation vanishes exponentially with the number of particles.

The correspondence of the quantum dynamics and the ‘classical’ mean-field approximation has been discussed in detail in section 10.1.2. The many-particle and the mean-field Landau-Zener tunneling probability show an excellent agreement, because quantum fluctuations of the populations are small. In contrast, there is no fixed phase relation between the two modes, which certainly goes beyond the simple Bogoliubov mean-field theory. An improved classical approximation using phase space ensembles can describe the depletion of the condensate mode and the loss of phase coherence as well as number squeezing ξ_N^2 of the final state. Yet temporal revivals of this coherence are genuine many-particle effects and cannot be described classically. Thus, the spectroscopically relevant squeezing parameter ξ_S^2 is not reproduced by the ensemble simulation, as shown in section 10.1.3. However, the timescale for the occurrence of these revivals and accordingly of the spectroscopical squeezing increases linearly with the particle number. For realistic setups, this is way to long compared to decoherence and phase noise rates. Before the system reaches the squeezed state, nearly all coherences are already lost.

In section 10.1.5, we have studied how the dynamics depends on the number of particles N and compare our results to the discrete Gross-Pitaevskii equation that describes the dynamics in the limit $N \rightarrow \infty$. We show that the contradiction between the mean-field prediction and the exact many-particle transition rate in the adiabatic regime is no longer present in the phase space approach, and must therefore be considered as an artifact of the single-trajectory description. However, to reproduce true quantum features such as quantum beats semiclassically, a more refined treatment is necessary. Furthermore, we show in section 10.1.6 that already the presence of a small amount of phase noise is sufficient to introduce enough decoherence to make the system ‘classical’, so that the many-particle dynamics is well reproduced with a simple single-trajectory mean-field approach. Finally we have argued that a measurement of the transition to an incoherent Landau-Zener sweep could be used as a sensitive probe of decoherence.

In the second part of this chapter, we have discussed the dynamics of a Bose-Einstein condensate in a bichromatic optical lattice. In such a lattice, the ground Bloch band splits up into two minibands with a controllable band gap. And, since the higher bands are energetically well separated, the atoms are mainly confined to these bands. Hence, bichromatic lattices are ideally suited to study the complex quantum dynamics resulting from the interplay of the intraband dynamics and Landau-Zener transition between the minibands.

The basic dynamics of a BEC in an optical lattice can be inferred from the band structure of the system. Within the tight-binding approximation, one can readily calculate the linear as well as the nonlinear Bloch states. In particular, this treatment yields an explicit expression for the critical interaction strength for the occurrence of looped Bloch bands, which leads to a breakdown of adiabatic motion. The stability properties of the Bloch states have been analyzed in detail in section 10.3.1 by the Bogoliubov-de Gennes approach.

The dynamics of a BEC in an extended lattice was simulated using the Bogoliubov backreaction method which also provides a quantitative estimate for the depletion of

the condensate. The Landau-Zener tunneling of a BEC between minibands in a tilted or accelerated bichromatic lattice has been investigated in detail in section 10.3.2. For weak interactions, the condensate remains essentially intact, whereas the Landau-Zener tunneling process is strongly affected. Repulsive interactions increase the tunneling rate in particular in the 'adiabatic regime' of large band gaps, while attractive interactions suppress Zener tunneling. Strong interactions cause a dynamical instability and thus a rapid depletion of the condensate mode. However, the mechanism of dynamical instability is significantly different: In the repulsive case, instability sets in at the edge of the Brillouin zone and is intimately related to the occurrence of looped Bloch bands. A condensate with attractive interactions is unstable already in the center of the Brillouin zone, leading to a collapse and finally to the destruction of the condensate, cf. section 10.3.3.

On longer timescales, the interplay of Bloch oscillations and Landau-Zener tunneling leads to a complex dynamics due to the interference of the contributions in the two minibands studied in section 10.3.4. A quantitative analysis of this effect has been given, which also shows the applicability of Bloch-Zener oscillations in matter wave interferometry. A remarkable dynamics is also observed in section 10.3.5, where the transitions between the bands are not induced by a static external field, but by a periodic driving which leaves the quasimomentum unchanged. Because of the different curvature of the minibands, the matter waves in the two minibands move into opposite directions. The interference of the two contributions then leads to a dynamics which is comparable to the *Zitterbewegung* of a Dirac spinor.

The results presented in this chapter can also be used to understand the dynamics in more complicated systems. Only recently, a system of pairwise tunnel-coupled one-dimensional Bose liquids has been studied experimentally [238, 239] with focus on the influence of the inter-particle interactions. Just as in single two-mode system, adiabaticity breaks down and the Landau-Zener transition probability is strongly affected by the effective nonlinearity. Moreover, one finds the same quantitative dependence of the tunneling rate on the starting wells, respective the sign of the interaction strength as we have discussed in section 10.1.4. As discussed in the second part of this chapter depletion due to the interactions plays a dominant role, which implications on thermalization and non-equilibrium dynamics.

Chapter 11

Decay of a Bose-Einstein condensate in an optical lattice

Decoherence and dissipation, caused by the irreversible coupling of a quantum system to its environment, represent a major obstacle for the long-time coherent control of quantum states. However, in the last years it has been realized that dissipation can be extremely useful if it is controlled accurately. Recent experiments have shown that strong correlations can be induced by two-body losses in ultracold quantum gases [147, 148]. Three-body losses can be tailored to generate effective three-body interactions [262] and to prepare strongly correlated states for quantum simulations of color superfluidity [263], quantum hall physics [264] or d-wave pairing [265]. Even more, dissipation can be used as a universal tool in quantum state preparation [144, 145], entanglement generation [266] and quantum information processing [146].

These concepts of controlling quantum dynamics and transport are particularly important for experiments with ultracold atoms in optical lattices, where it is possible to optically address the quantum system with single-site resolution [105, 267]. An even higher spatial resolution has been realized with a focused electron beam, removing atoms one by one from the lattice [150, 268].

In chapter 9 we have analyzed the dynamics of a Bose-Einstein condensate (BEC) in a double-well trap subject to phase noise and particle loss. We have seen that an asymmetric loss can be used to restore the purity of the condensate almost completely and increase the phase coherence significantly. In this chapter we consider a Bose-Einstein condensate in an extended, but finite lattice. So far, most studies of the dynamical effects of localized particle loss and phase noise have only been concerned with nonlinear effects, discussing the possibility to induce nonlinear structures such as bright breathers [181, 269], dark solitons [270] or ratchets [271]. All these studies were based on a mean-field approximation, where the loss was introduced heuristically as an imaginary potential.

In this chapter we investigate the possibility to control the macroscopic dynamics of a Bose condensed state in a Bose-Hubbard chain using localized dissipation in the mean-field limit *and beyond*. To this end, we use the BBR approximation introduced

in section 8.4.4, taking into account higher-order moments explicitly. The validity of both approximations is tested by a comparison to numerically exact simulations of the many-body quantum dynamics for small systems using the Monte-Carlo wave function method (cf. section 8.5.2).

To be able to analyze the deviations from mean-field results properly it is necessary to focus on an intermediate regime, where a mean-field approximation still provides a good description of the system, though quantum effects are no longer negligible. This is the case for intermediate filling factors.

This chapter is organized as follows: Starting from the master equation introduced in section 8.5.1, we discuss the mean-field limit and generalize the BBR method (cf. section 8.4.4) to the dissipative case. In this section, we will also see that the mean-field treatment of loss by an imaginary potential is only valid in the absence of phase noise. In the second section, we test the BBR approach by a comparison to the full many-body dynamics for a double well trap with loss from a single site, a system for which we have discussed the mean-field dynamics in great detail already in chapter 9. Unlike the mean-field approximations, the BBR results are able to reproduce the repurification predicted by the exact simulation. Beside the obvious loss of particles, strongly biased loss rates inhibit quantum tunneling between the respective sites. This effect is spotlighted in section 11.2.

After this illustrative preface, we go on to larger lattices. In section 11.3, we analyze how boundary dissipation induces localization and can be used to purify a BEC. In section 11.4, we consider localized loss from a single lattice site, which creates a vacancy and leads to a fragmentation of the condensate. Remarkably, strong dissipation can suppress the decay of the condensate and a coherent dark soliton can be generated by properly engineering the dynamics. These novel opportunities to control the quantum dynamics will be addressed in section 11.5. Note that all techniques presented there can be directly applied in ongoing experiments [150, 268].

In the last section, a short outlook on possible future research directions is given.

11.1 Dissipative mean-field dynamics and beyond

As in the preceding chapters, the coherent part of the dynamics of ultracold atoms in optical lattices is described by the Bose-Hubbard Hamiltonian

$$\hat{H} = -J \sum_j \left(\hat{a}_{j+1}^\dagger \hat{a}_j + \hat{a}_j^\dagger \hat{a}_{j+1} \right) + \frac{U}{2} \sum_j \hat{a}_j^\dagger \hat{a}_j^\dagger \hat{a}_j \hat{a}_j, \quad (11.1)$$

introduced in section 8.3. In the presence of dissipation, the dynamics is given by a master equation in Lindblad form [165],

$$\dot{\hat{\rho}} = -i[\hat{H}, \hat{\rho}] + \mathcal{L}\hat{\rho}. \quad (11.2)$$

Here, we are especially interested in the effects of localized particle loss, which can be implemented by an electron beam [150, 268] or by a strongly focused resonant blast

laser. Furthermore, phase noise is always present in experiments, which degrades the phase coherence between adjacent wells and heats the sample [158, 159]. In section 8.5.1 we have argued that these two processes are described by the Liouvillians [154, 155, 165]

$$\begin{aligned}\mathcal{L}\hat{\rho} &= \mathcal{L}_{\text{loss}}\hat{\rho} + \mathcal{L}_{\text{phase}}\hat{\rho} \\ &= -\frac{1}{2}\sum_j \gamma_j \left(\hat{a}_j^\dagger \hat{a}_j \hat{\rho} + \hat{\rho} \hat{a}_j^\dagger \hat{a}_j - 2\hat{a}_j \hat{\rho} \hat{a}_j^\dagger \right) \\ &\quad -\frac{\kappa}{2}\sum_j \hat{n}_j^2 \hat{\rho} + \hat{\rho} \hat{n}_j^2 - 2\hat{n}_j \hat{\rho} \hat{n}_j,\end{aligned}\tag{11.3}$$

where γ_j denotes the loss rate at site j and κ is the strength of the phase noise.

To derive the mean-field approximation, we start from the single particle reduced density matrix (SPDM) $\sigma_{jk} = \langle \hat{a}_j^\dagger \hat{a}_k \rangle = \text{tr}(\hat{a}_j^\dagger \hat{a}_k \hat{\rho})$, as defined in (8.29). The equations of motion for σ_{jk} are obtained from the master equation (11.2), as follows

$$\begin{aligned}i\frac{d}{dt}\sigma_{j,k} &= \text{tr}\left(\hat{a}_j^\dagger \hat{a}_k [\hat{H}, \hat{\rho}] + i\hat{a}_j^\dagger \hat{a}_k \mathcal{L}\hat{\rho}\right) \\ &= -J(\sigma_{j,k+1} + \sigma_{j,k-1} - \sigma_{j+1,k} - \sigma_{j-1,k}) \\ &\quad + U(\sigma_{kk}\sigma_{jk} + \Delta_{jkkk} - \sigma_{jj}\sigma_{jk} - \Delta_{jjjk}) \\ &\quad - i\frac{\gamma_j + \gamma_k}{2}\sigma_{j,k} - i\kappa(1 - \delta_{j,k})\sigma_{j,k},\end{aligned}\tag{11.4}$$

where we have defined the covariances $\Delta_{jklm} = \langle \hat{a}_j^\dagger \hat{a}_k \hat{a}_l^\dagger \hat{a}_m \rangle - \langle \hat{a}_j^\dagger \hat{a}_k \rangle \langle \hat{a}_l^\dagger \hat{a}_m \rangle$. In the mean-field limit $N \rightarrow \infty$ with $g = UN$ fixed, one neglects the variances Δ_{jklm} in equation (11.4) to obtain a closed set of evolution equations:

$$\begin{aligned}i\frac{d}{dt}\sigma_{j,k} &= -J(\sigma_{j,k+1} + \sigma_{j,k-1} - \sigma_{j+1,k} - \sigma_{j-1,k}) \\ &\quad + U(\sigma_{kk}\sigma_{jk} - \sigma_{jj}\sigma_{jk}) - i\frac{\gamma_j + \gamma_k}{2}\sigma_{j,k} - i\kappa(1 - \delta_{j,k})\sigma_{j,k}.\end{aligned}\tag{11.5}$$

If phase noise can be neglected, respective $\kappa = 0$, the equations of motion (11.5) are equivalent to the non-hermitian discrete nonlinear Schrödinger equation

$$i\frac{d}{dt}\psi_k = -J(\psi_{k+1} + \psi_{k-1}) + U|\psi_k|^2\psi_k - i\frac{\gamma_k}{2}\psi_k\tag{11.6}$$

by the identification $\sigma_{j,k} = \psi_j^* \psi_k$. This argument provides a proper link between the many body-dynamics and the non-hermitian Schrödinger equation, which has previously been applied only heuristically [181, 269, 270]. In contrast, if only phase noise is present, all coherences, i.e. the non-diagonal elements of the SPDM decay at a constant rate κ . Thus it is no longer possible to map the mean-field equations to a nonlinear Schrödinger equation.

The mean-field approximation assumes a pure BEC and is strictly valid only in the limit $N \rightarrow \infty$. To describe many-body effects such as quantum correlations and the depletion of the condensate for large, but finite particle numbers, one has to take into

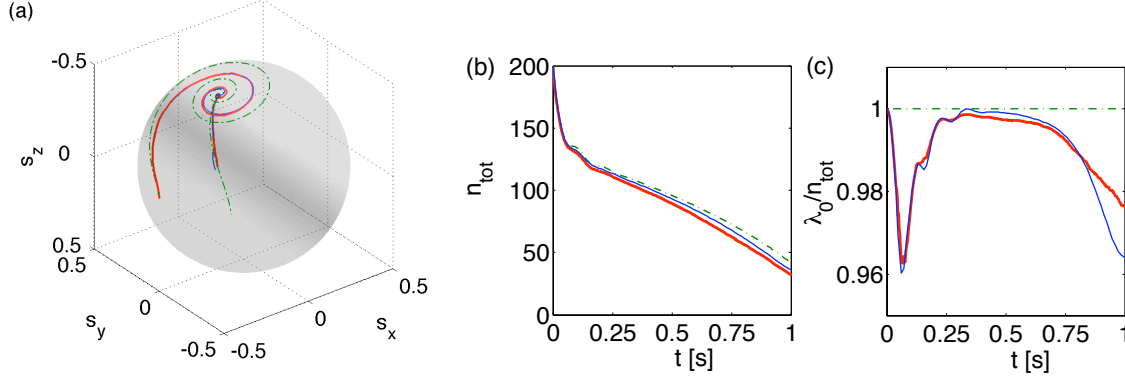


Figure 11.1: Dynamics of a BEC in a leaky double-well trap: (a) Trajectory of the Bloch vector $\mathbf{s}(t)$, (b) total particle number $\langle \hat{n}_{\text{tot}}(t) \rangle$ and (c) condensate fraction λ_0/n_{tot} , comparing the exact results (thick red line) to the mean-field (green dash-dotted line) and the BBR approximation (solid blue line). Atoms are lost from the right well only at a rate $\gamma_2 = 20 \text{ s}^{-1}$. The initial state is assumed to be a pure condensate of 200 particles and $\mathbf{s} = (-1/2, 0, 0)$. The remaining parameters are $J = 10 \text{ s}^{-1}$ and $U = 0.5 \text{ s}^{-1}$, $\kappa = 0$.

account the variances Δ_{jmnk} explicitly. One possibility to do so at least approximately is the BBR approach introduced in section 8.4.4.

Obviously the interaction Hamiltonian leads to higher-order correlation functions. To obtain a closed set of evolution equations, these functions ought to be truncated according to

$$\begin{aligned} \langle \hat{a}_j^\dagger \hat{a}_m \hat{a}_k^\dagger \hat{a}_n \hat{a}_r^\dagger \hat{a}_s \rangle &\approx \langle \hat{a}_j^\dagger \hat{a}_m \hat{a}_k^\dagger \hat{a}_n \rangle \langle \hat{a}_r^\dagger \hat{a}_s \rangle + \langle \hat{a}_j^\dagger \hat{a}_m \hat{a}_r^\dagger \hat{a}_s \rangle \langle \hat{a}_k^\dagger \hat{a}_n \rangle \\ &+ \langle \hat{a}_k^\dagger \hat{a}_n \hat{a}_r^\dagger \hat{a}_s \rangle \langle \hat{a}_j^\dagger \hat{a}_m \rangle - 2 \langle \hat{a}_j^\dagger \hat{a}_m \rangle \langle \hat{a}_k^\dagger \hat{a}_n \rangle \langle \hat{a}_r^\dagger \hat{a}_s \rangle. \end{aligned} \quad (11.7)$$

While the coherent part of the evolution of the variances is given by [69, 140]

$$\begin{aligned} i \frac{d}{dt} \Delta_{jmnk} &= (\epsilon_m + \epsilon_n - \epsilon_j - \epsilon_k) \Delta_{jmnk} \\ &- J \left[\Delta_{j,m,k,n+1} + \Delta_{j,m,k,n-1} + \Delta_{j,m+1,k,n} + \Delta_{j,m-1,k,n} \right. \\ &\quad \left. - \Delta_{j,m,k+1,n} - \Delta_{j,m,k-1,n} - \Delta_{j+1,m,k,n} - \Delta_{j-1,m,k,n} \right] \\ &+ U \left[\Delta_{mmkn} \sigma_{jm} - \Delta_{jjkn} \sigma_{jm} + \Delta_{jmn} \sigma_{kn} - \Delta_{jmk} \sigma_{kn} \right. \\ &\quad \left. + \Delta_{jmnk} (\sigma_{mm} + \sigma_{nn} - \sigma_{kk} - \sigma_{jj}) \right], \end{aligned} \quad (11.8)$$

particle loss and phase noise affect the dynamics of the variances as follows

$$\begin{aligned} \frac{d}{dt} \Delta_{jmnk} &= -\frac{\gamma_j + \gamma_m + \gamma_k + \gamma_n}{2} \Delta_{jmnk} + \delta_{mk} \gamma_m \sigma_{jm} \\ &- \kappa (\delta_{mn} + \delta_{jk} - \delta_{jn} - 2\delta_{km}) (\Delta_{jmnk} + \sigma_{jm} \sigma_{kn}) \\ &- \kappa (2 - \delta_{jm} - \delta_{kn}) \Delta_{jmnk}. \end{aligned} \quad (11.9)$$

The BBR method is especially useful if the many-body state is close to, but not exactly equal to a pure BEC, since it includes higher order moments at least approximately. In particular, it accurately predicts the onset of the depletion of the condensate mode. The number of particles in this mode is given by the leading eigenvalue λ_0 of the SPDM $\sigma_{j,k}$, whereas the total number of atoms is given by the trace of $\sigma_{j,k}$ [69, 94]:

$$n_{\text{tot}}(t) = \text{tr } \sigma_{j,k}. \quad (11.10)$$

Thus, the time-dependent condensate fraction is given by λ_0/n_{tot} .

The BBR approach has been extensively tested for closed systems in [140]. Therefore, we only briefly comment on the performance of this method in the presence of dissipation. To get a first idea of the scope of the mean-field approximation and the BBR approach for a BEC in an optical lattice with particle loss, we consider the same setup as we have discussed in great detail in chapter 9.2.3 and especially in figure 9.5. There we have analysed the mean-field dynamics of an interacting Bose-Einstein condensate in a double-well trap with strongly biased loss rates. Figure 11.1 shows an example of the dynamics in the Josephson regime, now comparing not only the exact many-particle results calculated with the Monte-Carlo wave function method with the mean-field approximation (11.5), but also the results of the BBR method, as given by equations (11.4), (11.8) and (11.9). The initial state has been chosen to be a pure Bose-Einstein condensate

$$|\Psi\rangle = \frac{1}{\sqrt{N!}} \left(\sum_j \psi_j \hat{a}_j^\dagger \right)^N |0\rangle, \quad (11.11)$$

with equal population distribution between the two wells, $\psi_2 = -\psi_1 = 1/\sqrt{2}$. Figure 11.1 (a) shows the microscopic dynamics of the BEC in terms of the Bloch vector $\mathbf{s} = \langle \hat{\mathbf{L}} \rangle / \langle \hat{n}_{\text{tot}} \rangle$. Figure 11.1 (b) and (c) show the dynamics of the total particle number $\langle \hat{n}_{\text{tot}} \rangle$ and the condensate fraction, respectively. While the decay of the total particle number is already well described by the simple mean-field approximation, one observes significant deviations from the exact results for the Bloch vector $\mathbf{s}(t)$. The mean-field approximation overestimates the oscillations of the components of $\mathbf{s}(t)$, as it cannot take into account the decoherence of the BEC. In contrast one observes almost no differences between the BBR and the exact results.

The most important advantage of the BBR method is that it accurately predicts the depletion and repurification of the condensate mode. Figure 11.1 (c) shows the condensate fraction, which is defined as the leading eigenvalue of the SPDM λ_0 rescaled by the total particle number n_{tot} . The simple mean-field approximation (11.5) always assumes a pure condensate, respective $\lambda_0/n_{\text{tot}} = 1$, while the BBR results show a very good agreement with the exact results. Significant differences from the exact results are visible only for very long times. However, at this time the particle number has already dropped to approx. 20 particles, so that it is not surprising to find deviations from mean-field and BBR predictions.

The dependence of the quality of the BBR approximation on the strength of dissipation is further analyzed in figure 11.2. Figure 11.2 shows two examples for the

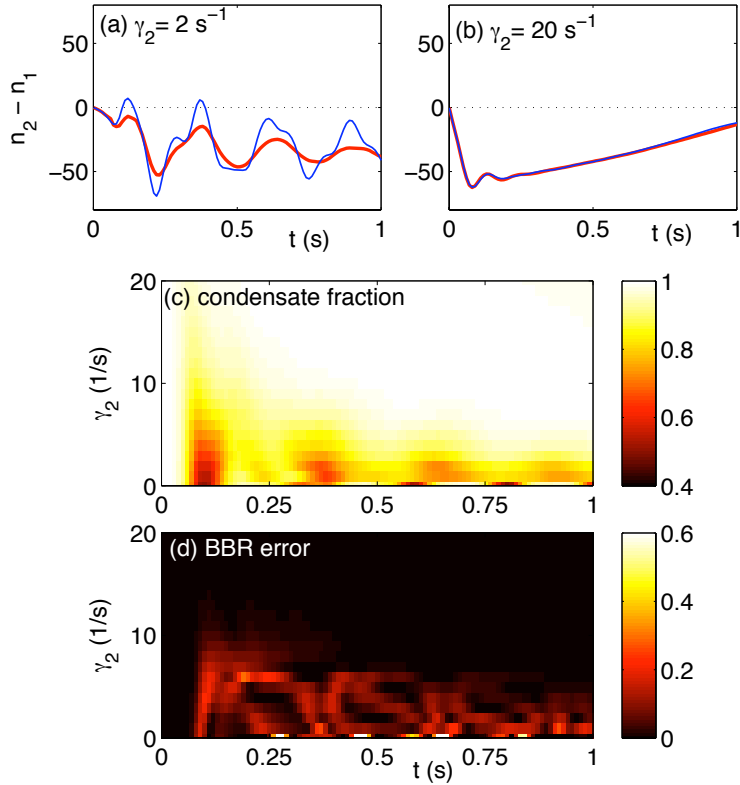


Figure 11.2: Numerical test of the BBR methods for a leaky double-well trap with loss in the second well. (a) and (b) Dynamics of the population imbalance $\langle \hat{n}_2 - \hat{n}_1 \rangle$ for two different values of the loss rate, comparing the BBR approximation (solid blue line) to numerically exact results (thick red line). (c) Condensate fraction λ_0/n_{tot} as a function of time and the loss rate γ_2 . (d) Trace distance (11.12) between the exact rescaled SPDM $\sigma(t)/n(t)$ and the respective BBR approximation. In all cases the initial state is assumed to be a pure BEC with with equal population and a phase difference of π between the two modes. The remaining parameters are $J = 10 \text{ s}^{-1}$, $\kappa = 0$, $U = 0.5 \text{ s}^{-1}$ and $n(0) = 200$ atoms.

dynamics of the population imbalance in a leaky double-well trap, comparing the BBR approximation (solid blue line) and numerically exact results (thick red line) for two different dissipation rates. The initial state is assumed to be a pure BEC with equal population and a phase difference of π between the two modes. In the case of strong dissipation, the BBR approximation predicts the correct evolution of the population imbalance $\langle \hat{n}_2 - \hat{n}_1 \rangle$ with an astonishing precision. In contrast, significant differences are observed for weak losses. This means that the presence of particle loss actually improves the performance of the BBR method, as the dissipation drives the many-body quantum state towards a pure BEC. This is confirmed by the numerical results for the condensate fraction λ_0/n_{tot} plotted in figure 11.1 (c). A significant depletion of the condensate is only observed for small values of the loss rate γ_2 .

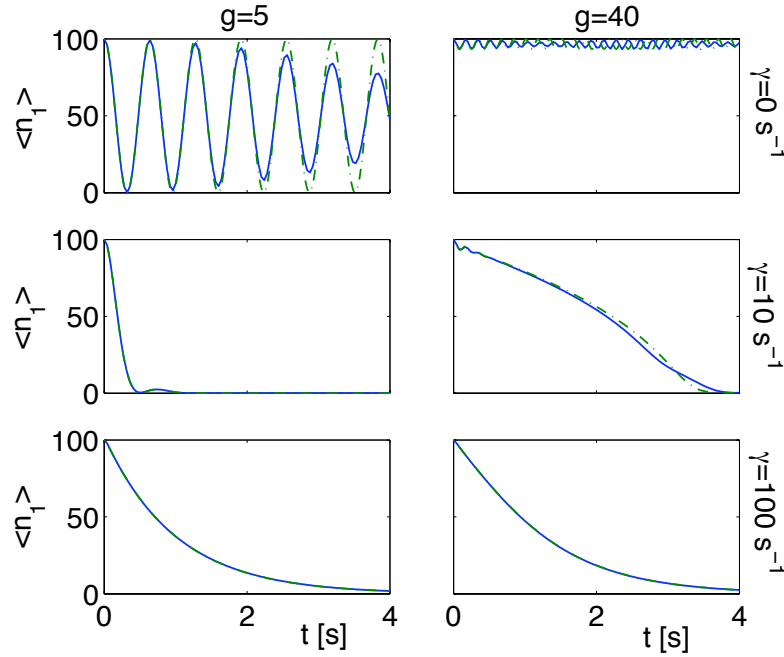


Figure 11.3: Inhibition of quantum tunneling by particle loss of a BEC initially prepared in the first well. In the lossless case (upper panels) one observes fast Rabi oscillations between the two wells for $g < 2J$ (left) and nonlinear self-trapping for $g > 2J$ (right). Strong losses in the second well ($\gamma_2 = 100 \text{ s}^{-1}$, lowest panels) slow down the quantum tunneling significantly. The remaining parameters are $J = 5 \text{ s}^{-1}$ and $N = 100$. Mean-field results are plotted as dash-dotted lines and BBR results as solid lines.

For a further quantitative analysis we compare exact and BBR results for the rescaled SPDM $\sigma(t)/n(t)$. Figure 11.2 (d) shows the trace distance of the exact matrix and the matrix obtained by the BBR method,

$$d := \frac{1}{2} \text{tr} (|\sigma_{\text{BBR}}/n_{\text{BBR}} - \sigma_{\text{ex}}/n_{\text{ex}}|), \quad (11.12)$$

as a function of time for different values of γ_2 . For sufficiently large dissipation, one observes that the distance approximately vanishes for all times. In this regime the quantum dynamics is faithfully reproduced by the BBR approximation.

11.2 Inhibition of quantum tunneling

The most obvious effect of particle dissipation as described by the Liouvillian (11.3) is the loss of atoms from the lattice. A less obvious, but nevertheless important effect is that dissipation actually inhibits quantum tunneling to and from a leaky lattice site as illustrated in figure 11.3. As in the preceding chapters, we use the two-mode case with decay from the second well as an illustrative model. In the examples shown in in

figure 11.3 all atoms are initially localized in mode 1, while particle loss occurs from mode 2 with a rate γ_2 . In the unitary case ($\gamma_2 = 0$), depicted in the upper panels, one observes the familiar Rabi and self-trapping oscillations, depending on the interaction strength $g = Un(t=0)$ [157, 173, 272]. For strong losses ($\gamma_2 = 100\text{s}^{-1}$) the dynamics effectively slows down, as can be seen in the lowest panels. Tunneling to the second mode is much slower than in the Rabi regime, where atoms tunnel back and fro with a period J^{-1} . In the strongly interacting case, the effects of particle loss are much more diverse. As observed on the right-hand side of figure 11.3, the self-trapping of atoms in mode 1 is effectively destroyed by the dissipation.

The inhibition of quantum tunneling to a leaky lattice site can be understood by a simple analogy to wave optics: A large mismatch of the index of reflection leads to an almost complete reflection of a light wave from a surface. This is true for real index of refraction just as well as for an imaginary index describing an absorbing material such as a metal. Similarly, a strong difference of the on-site potential, real or imaginary, prevents tunneling of the atoms to the respective lattice site. Another interpretation has been given in [273] in term of the quantum Zeno effect. The decay of atoms can be viewed as a continuous measurement of the quantum state of the leaky lattice site. This measurement causes a Zeno effect in that it prevents tunneling to the observed site.

To understand this phenomenon more quantitatively, consider first the non-interacting case $U = 0$, for which the equations of motion can be solved analytically. For $\gamma < \gamma_c = 4J$, the dynamics of the populations is exactly given by

$$\begin{aligned} n_1(t) &= n_0 e^{-\gamma t/2} \left[\cos(\omega t) + \frac{\gamma}{4\omega} \sin(\omega t) \right]^2, \\ n_2(t) &= n_0 e^{-\gamma t/2} \frac{J^2}{\omega^2} \sin^2(\omega t), \end{aligned} \quad (11.13)$$

with the frequency $\omega = (J^2 - \gamma^2/16)^{1/2}$. One can see that the frequency decreases with the decay rate for small values of γ . For $\gamma > \gamma_c$ the frequency becomes imaginary, such that the Rabi oscillations are suppressed completely. Notably, for the critical decay rate, $\gamma_c = 4J$, the population of the second well is always zero, $n_2(t) \equiv 0$. In this case every atom that tunnels to the second well is immediately lost from the lattice. For strong interactions, the dynamics becomes more involved, and a quantum state can be localized due to the dissipation as well as due to nonlinear self-trapping. We shall explore the resulting dynamics in section 11.4 in more detail.

11.3 Boundary dissipation

In this section we show that coherent discrete breathers are formed and stabilized dynamically in a lattice with boundary dissipation. To test the mean-field and the BBR approximation, we first consider the dynamics in small systems for which numerically exact solutions of the many-particle dynamics are still possible.

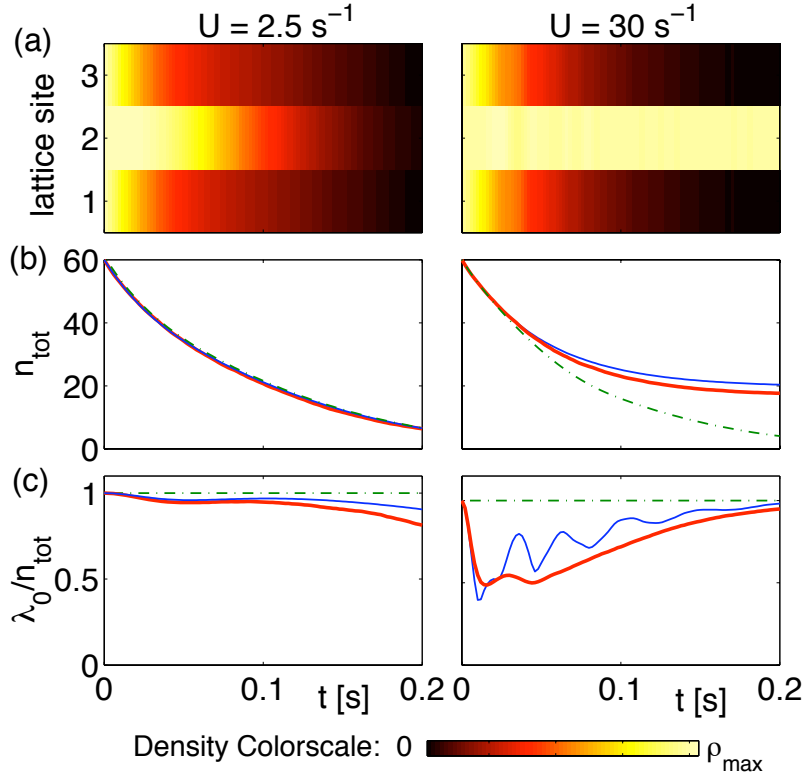


Figure 11.4: Dynamics of a BEC in a triple-well trap with boundary dissipation in dependence of the interaction strength: (a) atomic density $\langle \hat{n}_j(t) \rangle$, (b) total particle number and (c) the condensate fraction λ_0/n_{tot} for $J = 5 \text{ s}^{-1}$, $\gamma = 20 \text{ s}^{-1}$, $\kappa = 0$ and $n(0) = 60$ atoms for $U = 2.5 \text{ s}^{-1}$ (left), respective $U = 30 \text{ s}^{-1}$ (right). Mean-field (— · —) and BBR (—) results are compared to numerically exact simulations with the quantum jump method averaging over 200 trajectories (thick red line).

To get a first intuition, we analyse the decay of an initially pure, homogeneous BEC in a triple-well trap with boundary dissipation. Figure 11.4 shows the evolution of the atomic density and the total particle number, and the purity of the BEC for weak (left side) and strong (right side) interactions, respectively. In both cases, the population at the boundary rapidly decays from the lattice. For longer times, however, the dynamics is significantly different. If interactions are weak ($U = 2.5 \text{ s}^{-1}$), the population at the central lattice site tunnels to the boundary, where it decays. The tunneling is slightly slowed down by the dissipation as discussed in section 11.2, but the decay rate is not strong enough to suppress the tunneling completely. This is remarkably different in the case of strong interactions $U = 30 \text{ s}^{-1}$, for which the population at the central site is remarkably stable. The total atom number rapidly drops to about one third of its initial value, where it approximately saturates for the observed span of time. This counterintuitive localization phenomenon in the presence of repulsive atomic interaction is a consequence of the dynamical formation of a discrete breather centered in the middle of the triple well trap. Generally, a discrete breather is a spatially localized and stable (or at least long-lived) excitation in a periodic discrete system

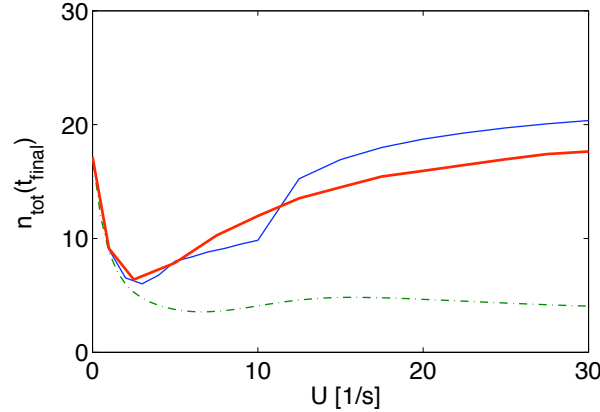


Figure 11.5: Formation of a discrete breather in a triple-well lattice with boundary dissipation. Total particle number after a fixed propagation time $t_{\text{final}} = 0.2$ s as a function of the interaction strength U . The remaining parameters are chosen according to figure 11.4. As above mean-field ($-\cdot-$) and BBR ($-$) results are compared to numerically exact simulations with a quantum jump method averaging over 200 trajectories (thick red line).

[274–276]. Discrete breathers arise intrinsically from the combination of nonlinearity and the discreteness of the system. In the presence of boundary dissipation, these excitations become attractively stable such that the quantum state of the atoms will converge to a BEC with a breather-like density for a wide class of initial states. Once the breather has formed in the triple well trap, it remains stable even when the dissipation is turned off.

The crucial role of strong interactions is further illustrated in figure 11.5, where the residual atom number after a fixed propagation time $t_{\text{final}} = 0.2$ s is plotted as a function of the interaction strength U . The particle number increases for large values of U to $n_{\text{tot}}(t_{\text{final}}) \approx 20$ due to the breather formation. For strong interactions a simple mean-field approximation fails. It strongly underestimates the residual particle number as it predicts that discrete breather are formed only for stronger losses. In contrast, the BBR results agree well with the many-particle simulation even for large values of U . We thus conclude that quantum fluctuations facilitate the formation of repulsively bound structures.

As expected, a mean-field approach cannot account for genuine many-body features of the dynamics. This is illustrated in figure 11.4 (c), which shows the evolution of the condensate fraction λ_0/n_{tot} . In the beginning, interactions lead to a rapid depletion of the condensate. On a longer time scale, however, dissipation restores the coherence and drives the atoms to a pure BEC localized at the central lattice site, which can be seen as another manifestation of the stochastic resonance effect discussed in chapter 9. The BBR approach faithfully reproduces the depletion and re-purification but additionally predicts unphysical temporal revivals. This example thus demonstrates the strength but also the limitations of this method.

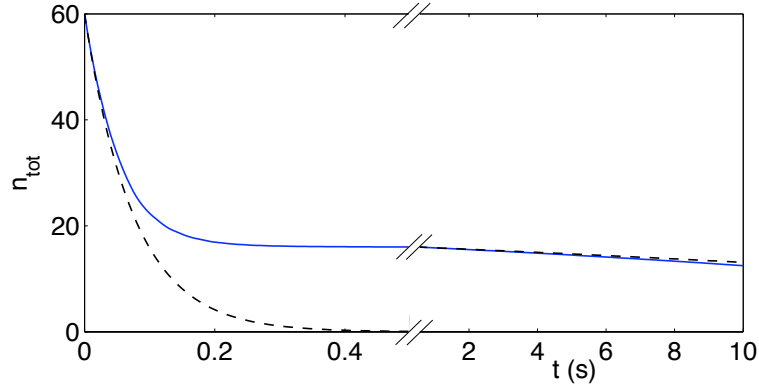


Figure 11.6: Decay of a discrete breather state for $J = 5 \text{ s}^{-1}$, $\gamma = 20 \text{ s}^{-1}$, $\kappa = 0$ and $U = 15 \text{ s}^{-1}$. Numerical results calculated with the BBR method (—) are compared to the analytic estimates (11.14) and (11.15), respectively (— —).

The decay dynamics of the discrete breather state is further analyzed in figure 11.6. The total atom number $n_{\text{tot}}(t)$ decreases rapidly until the discrete breather is formed around $t \approx 0.2 \text{ s}$. Afterwards the decay is much slower and clearly non-exponential. In both regimes, one can calculate the evolution of $n_{\text{tot}}(t)$ approximately, starting from the relation $\dot{n}_{\text{tot}} = -\gamma(n_1 + n_3)$. Initially, all sites are filled homogeneously, $n_1 = n_3 = n_{\text{tot}}/3$, such that the total particle number decays as

$$n_{\text{tot}}(t) \approx n_{\text{tot}}(0)e^{-2\gamma/3t}. \quad (11.14)$$

When the discrete breather is formed, the population of the outer wells is given by $n_1 = n_3 = J^2/(U^2 n_{\text{tot}})$ in first order perturbation theory. The atom number then decays as

$$n_{\text{tot}}(t) \approx \sqrt{n_{\text{db}}^2 - 4t\gamma J^2/U^2}, \quad (11.15)$$

where n_{db} is the number of atoms bound in the discrete breather state. In figure 11.6 both approximations are compared to the BBR simulation results, assuming a breather with $n_{\text{db}} = 16$ atoms. One observes an excellent agreement in the both regimes, that is an exponential decay for very short times ($t \lesssim 0.1 \text{ s}$) and an algebraic decay when the discrete breather is formed. The transition between the linear and nonlinear decay takes place at $t \approx 0.2 \text{ s}$. A deviation from the algebraic decay (11.15) for the discrete breather is observed only for very long times when the atom number is very small such that the simple perturbative estimate for $n_{1,3}$ is no longer valid.

11.4 Localized loss

Recent experiments with ultracold atoms have demonstrated an enormous progress in spatial addressability using specialized optical imaging systems [105, 267] or a focused electron beam [150, 268]. Especially the latter experiment allows to manipulate a Bose-Einstein condensate in an optical lattice dissipatively with single-site resolution.

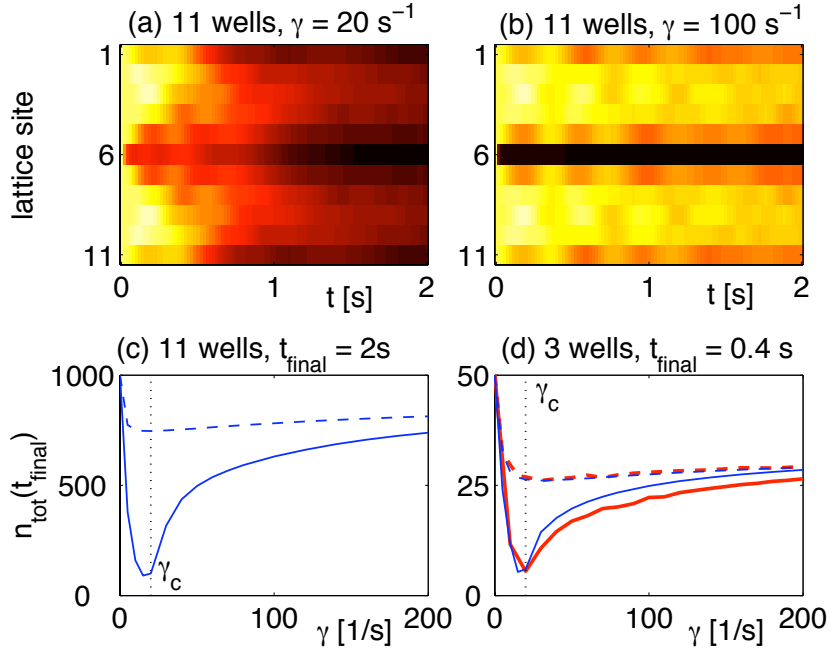


Figure 11.7: Formation of vacancies by localized loss at the central lattice site. (a,b) Evolution of the atomic density $\langle \hat{n}_j(t) \rangle$ (color scale as in figure 11.4). (c,d) Final value of the total particle number after a fixed propagation time t_{final} as a function of the loss rate γ , without (solid lines) and with strong phase noise (dashed lines, $\kappa = 50 \text{ s}^{-1}$). The remaining parameters are $J = 5 \text{ s}^{-1}$, $U = 0.2 \text{ s}^{-1}$ and $n(0) = 1000$ particles (a-c) and $U = 2 \text{ s}^{-1}$ and $n(0) = 50$ particles (d). The dynamics has been simulated with the BBR (thin blue lines) and the quantum jump method (thick red lines).

In the following, we study the quantum dynamics in a finite lattice of 11 sites with closed boundary conditions and loss occurring from the central site only, which leads to a quite different decay scenario as in the case of boundary dissipation studied earlier.

A remarkable feature of the quantum dynamics is illustrated in figure 11.7, showing the results of a BBR simulation for an initially pure homogeneous BEC. For a modest loss rate $\gamma = 20 \text{ s}^{-1}$, cf. figure 11.7 (a), atoms tunnel to the central site where they are dissipated with a rate γ , such that the BEC decays almost homogeneously. In contrast, stronger losses ($\gamma = 100 \text{ s}^{-1}$) depicted in (b) lead to a formation of a stable vacancy. The central site is rapidly depleted, but the atoms in the remaining wells are mostly unaffected. Thus one faces the paradoxical situation that an increase of the loss rate can suppress the decay of the BEC. Two effects contribute to this counterintuitive behavior: (i) The absorbing potential suppresses tunneling to the leaky lattice site, as discussed in section 11.2. (ii) A dark breather stabilizes the vacancy and prevents the flow of atoms to the central site. This nonlinear structure remains stable also if the dissipation is reduced or switched off afterwards (cf. also [274, 276, 277]).

The suppressed decay of the BEC is further illustrated in figure 11.7 (c), where the residual atom number after a fixed propagation time is plotted as a function of the loss rate γ . First, the number of remaining atoms decreases with the loss rate, as

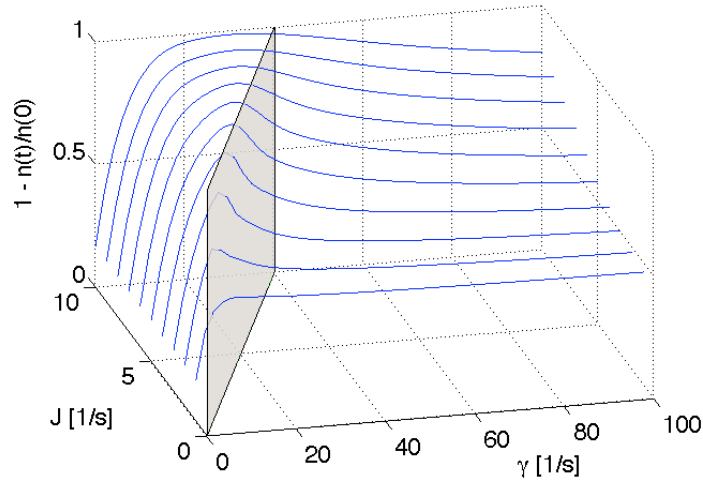


Figure 11.8: Decay of a BEC in a lattice with 11 wells and particle loss from the central site. Shown is the fraction of particles decaying from the lattice after a fixed propagation time t_{final} as a function of the loss rate γ and the tunneling rate J calculated with the BBR method (blue solid line). The shaded plane indicates the critical decay rate $\gamma_c(J) = 4J$. The remaining parameters are $g(0) = 200 \text{ s}^{-1}$, $n(0) = 1000$ and $t_{\text{final}} = 10/J$.

one would naively expect. However, for higher loss rates the inhibition of quantum tunneling becomes more and more important. The atoms can no longer tunnel to the leaky lattice site and remain in the lattice. Thus, the fraction of lost atoms decreases again and assumes a maximum for a finite loss rate γ_c .

Since a comparison of the BBR result to an exact calculation with a maintainable effort is only possible for smaller lattices, figure 11.7 (d) shows the respective results for a triple-well trap with loss from the central site. A comparison of the BBR approximation to a numerically exact many-particle simulation features a good agreement for all values of γ . Moreover, one can see that phase noise suppresses decay as it effectively decouples the lattice sites. Thus, only the atoms initially loaded at the leaky lattice site decay as $e^{-\gamma t}$, while the other atoms remain at their initial positions. With increasing loss rate γ , the number of atoms lost from the trap approaches $\approx n(0)/M$ with M being the number of lattice sites as shown in figure 11.7 (c,d) independent of the amount of phase noise κ .

A comparison of figure 11.7 (c) and (d) shows another interesting feature: An important quantity for the breather formation and stability is the effective nonlinearity of the system $\lambda = Un_{\text{tot}}(t)/2J$, which, due to particle loss, is time-dependent. Strikingly, though λ depends on the interaction strength U (which is different in figure 11.7 (c) and (d) by one order of magnitude), the fairly good estimate γ_c is to first order independent of U .

In the following, we will have a closer look at dependence on the tunneling rate J of the extremum at γ_c and show that the extremum is reminiscent of the quantum stochastic resonance discussed in chapter 9. In figure 11.8 the fraction of atoms which decay from

the lattice during a fixed propagation time $t_{\text{prop}} = 10/J$ is given as a function of the loss rate γ and the tunneling rate J . As seen in the preceding example, the coherent output of the system, that is the number of lost atoms, assumes a well-pronounced maximum for a finite loss rate. However, one clearly sees that this maximum depends on the tunneling rate.

The position of the maximum, respective γ_c can be estimated by determining a lower bound for γ for the dynamical breather formation. As a single (both bright and dark) breather exhibits a pronounced population imbalance between the central site and the neighbouring sites, we estimate γ_c by matching the timescales of dissipation $\tau_D = 2/\gamma$ and tunneling τ_J , that is $\tau_D = \tau_J$. For smaller values of γ , atoms can tunnel away from the leaky lattice site again before they are lost, while for larger values of γ a population imbalance can form. When the timescales of dissipation and tunneling are matched, $\tau_D = \tau_J$, all atoms tunneling to the central site are dissipated. Note that the factor $1/2$ in $\tau_J = 1/(2J)$ accounts for atoms tunneling from two sites to the leaky site. This estimate leads to a critical loss rate $\gamma = 4J$, which we identify with γ_c defined in section 11.2. Indeed, the increase of the position of the maximum with the tunneling rate J is well described by a linear dependence $\gamma_c = 4J$ as illustrated in figure 11.8. Likewise, we find good agreement of our qualitative estimate for γ_c (dotted vertical lines in figure 11.7 (c)) with the dip in the total particle number.

11.5 Engineering quantum states by dissipation

The previous reasoning suggests to use dissipation as a tool to coherently engineer the quantum state of a BEC in an optical lattice. Moreover mean-field theory predicts that dissipation can be used to efficiently create a coherent dark soliton [270].

In this section, we will analyze the possibilities to generate dark solitons beyond nonlinear theory and especially focus on the coherence properties of the generated structures. In addition, we give a short outlook on the possibilities to control a BEC by a dynamic loss event.

In figure 11.9 we consider the setup discussed in section 11.4, a cloud of ultracold atoms in an lattice with loss from the central site. The results of a BBR and a quantum jump simulation of the many-body dynamics reveal the limitations of the phase coherence of a soliton generated by local dissipation. This is depicted in figure 11.9. The upper panels (a,b) show the rescaled eigenvalues λ_m/n_{tot} of the SPDM. One observes that there are two macroscopic eigenvalues approaching $1/2$, while all remaining eigenvalues vanish approximately. This proves that the dissipation generates a fragmented BEC consisting of two incoherent parts rather than a single BEC with a solitonic wavefunction. The BBR simulations correctly describe the fragmentation of the condensate, but predict temporal revivals of the coherence which must be considered as artifacts of the approximation. Experimentally, one can test the coherence by the interference of the

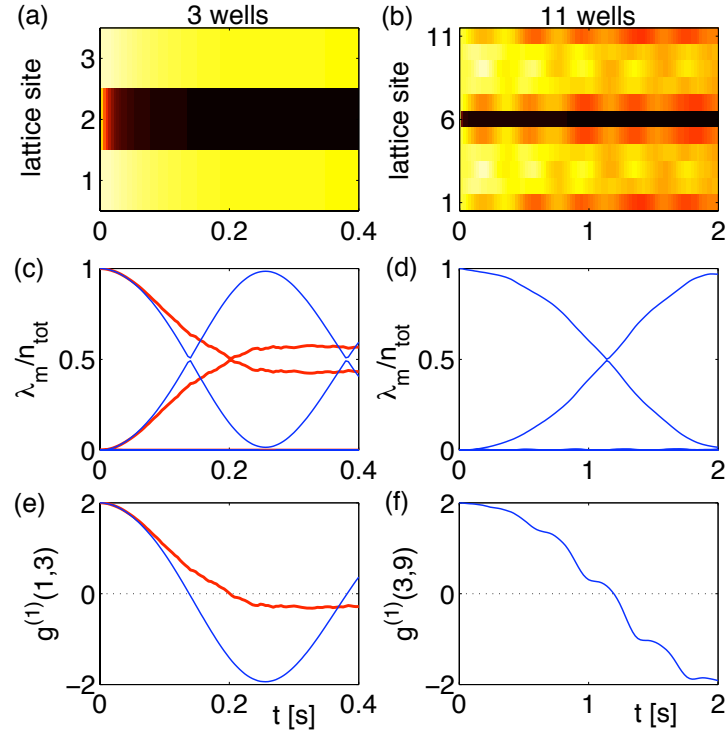


Figure 11.9: Coherence of a vacancy generated by loss from the central site in a lattice consisting of three wells (left) and 11 wells (right): (a,b) Atomic density, (c,d) rescaled eigenvalues λ_m/n_{tot} of the SPDM and (e,f) phase coherence $g^{(1)}$ between the two BEC fragments. Parameters are the same as in figure 11.7 with $\gamma = 100\text{s}^{-1}$ and $\kappa = 0$. Results of a quantum jump simulation are plotted as thick red lines, BBR results as thin blue lines.

two fragments in a time-of-flight measurement. Figure 11.9 (e,f) shows the coherence

$$g^{(1)}(\ell, m) = \frac{\langle \hat{a}_\ell^\dagger \hat{a}_m + a_m^\dagger \hat{a}_\ell \rangle}{\sqrt{\langle \hat{n}_\ell \rangle \langle \hat{n}_m \rangle}} \quad (11.16)$$

between the wells $\ell, m = 1, 3$ (left) and $\ell, m = 3, 9$ (right), respectively. One clearly observes the breakdown of phase coherence between the two condensate fragments.

To overcome the loss of coherence, one can, however, engineer the many-body dynamics. Figure 11.10 illustrates the generation of dark solitons comparing three different strategies. If the dissipation is switched off after the generation of a vacancy at $t = 0.1\text{ s}$, the condensate remains pure for long times. However, the vacancy is not stable but decays into two dark solitons traveling outwards [270], where they are reflected at the boundaries. The effects of a phase imprinting, which is an established experimental method (cf. e. g. [278]), are shown in figure 11.10 (b). A local potential is applied to the lower half of the lattice for $t < 0.1\text{ s}$ imprinting a phase difference of π . Again coherence is preserved but the generated solitons travel outwards. A coherent and stable dark soliton can be engineered by combining both methods, as shown in figure 11.10

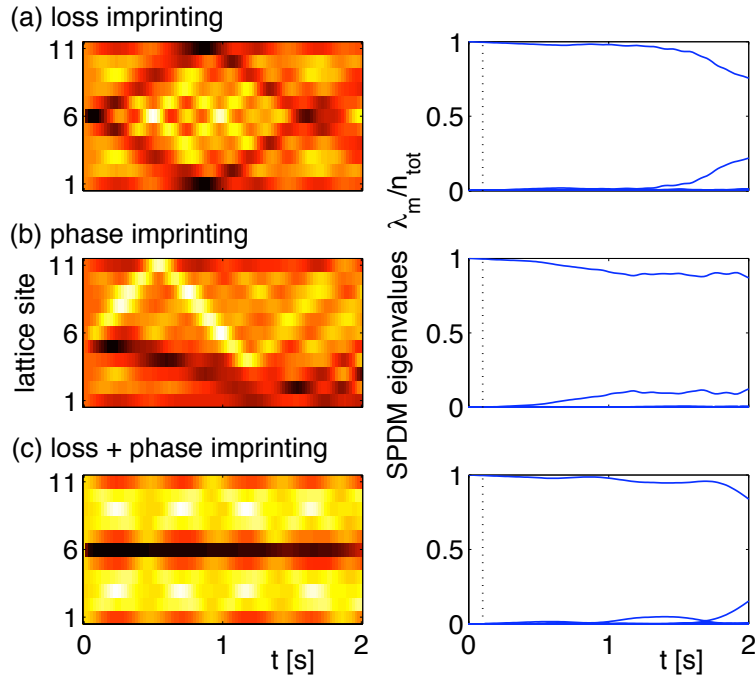


Figure 11.10: Generation of dark solitons using loss imprinting at a rate $\gamma = 100 \text{ s}^{-1}$ at the central site (a,c) and phase imprinting in the lower half of the lattice (b,c), both for times $t < 0.1 \text{ s}$ only. Shown are the atomic density (left, color scale as in figure 11.4) and the rescaled eigenvalues of the SPDM (right) calculated with the BBR method. Parameters are $J = 5 \text{ s}^{-1}$, $U = 0.1 \text{ s}^{-1}$, $\kappa = 0$ and $n(0) = 1000$ particles.

(c). The generated dark soliton stays at its initial position and remains coherent over a long time.

Another surprising effect is that loss can actually exert a drag on the atoms if it is scanned through the lattice. This can be used to compress a Bose-Einstein condensate as shown in figure 11.11, while keeping its purity. In this example we consider the situation where particle loss is induced at a single site in an extended lattice, e.g. by an electron beam [150,268]. The beam is then slowly scanned through the lattice, such that loss occurs at different sites as illustrated in figure 11.11 (a). Obviously, this leads to the loss of atoms in the lattice. However, the remaining atoms are repelled from the leaky lattice site, which can be understood as another instance of the inhibition of quantum tunneling as discussed in section 11.2. This suppression has a stronger effect on the matter wave than the actual loss of atoms such that the atomic density in the lower part of the lattice *increases* as shown in figure 11.11 (b). Notably, the dissipation at the boundary again induces coherence such that the BEC remains almost completely pure during the complete time evolution as shown in figure 11.11 (c).

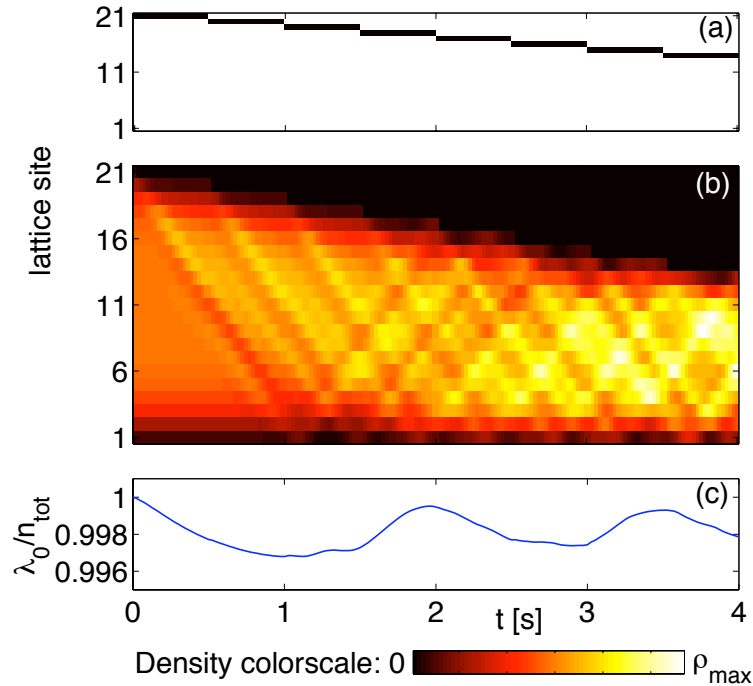


Figure 11.11: Compressing a BEC by moving loss. (a) Loss at a rate $\gamma = 1600 \text{ s}^{-1}$ is induced at one lattice site which is slowly scanned over the lattice. The black lines indicate the position of the leaky lattice site. (b) The BEC is compressed in the lower part of the lattice although a significant fraction of the atoms is lost. Shown is the atomic density assuming a BEC of $n(0) = 1000$ atoms in the GPE ground state at $t = 0$. The maximum atomic density increases to $\rho_{\max} = 113.6$ atoms per site after $t = 4$ s of propagation. (c) The condensate fraction λ_0/n_{tot} remains larger than 99.6% during the whole propagation. The remaining parameters are $J = 40 \text{ s}^{-1}$ and $g = 100 \text{ s}^{-1}$. The dynamics was simulated with the BBR method.

11.6 Outlook

In this chapter we have discussed the influence of particle loss on the dynamics of a Bose-Einstein condensate in a dissipative lattice. Localized loss can generate vacancies and dark solitons, while boundary dissipation facilitates the formation of bright breathers.

Starting from the many-body master equation, we have derived the mean-field approximation and the dissipative Bogoliubov backreaction method, which allows a consistent calculation of the depletion of the condensate. To back up the BBR results, we have analysed the differences to the exact dynamics in a small lattices consisting of only 2 or 3 wells, respectively.

Two important special cases have been studied in detail: Particle loss at the *boundary* leads to localization and the formation of coherent discrete breathers. Surprisingly, dissipation together with interactions can re-purify a BEC. A striking effect of *localized loss* is that strong dissipation can effectively *suppress* decay and induce stable vacancies.

The decay shows a pronounced maximum for intermediate values of the loss rate, when the timescales of the dissipation and the tunneling are matched. Combined with an external potential, these effects can be used to generate stable coherent dark solitons. These examples show that engineering the dissipation is a promising approach for controlling the dynamics in complex quantum many-body systems.

Ultracold atoms provide a distinguished model system for the dynamics of interacting quantum systems, such that the effects discussed here may be observed in different systems, too. In particular, quantum transport of single excitations driven by *local* dissipation has recently been studied in a variety of physical systems ranging from spin chains [279] to light-harvesting biomolecules [280]. On the other hand, it has also been shown on the mean-field level that nonlinear excitations such as discrete breathers play an important role for quantum transport in these systems (cf. [274, 276, 281] and references therein). Thus it is of general interest to further explore the regime which interpolates between the nonlinear mean-field dynamics and the many-body quantum dynamics.

Bibliography

- [1] R. Alicki and M. Fannes, *Quantum Dynamical Systems*, Oxford University Press, Oxford, 2001
- [2] O. Bratteli and D. W. Robinson, *Operator Algebras and Quantum Statistical Mechanics I*, Springer, 1987
- [3] O. Bratteli and D. W. Robinson, *Operator Algebras and Quantum Statistical Mechanics II*, Springer, 1997
- [4] D. Goderis, A. Verbeure, and P. Vets, *Non-commutative central limits*, Prob. Th. Rel. Fields **82** (1989) 527
- [5] D. Goderis and P. Vets, *Central limit theorem for mixing quantum systems and the CCR-Algebra of fluctuations*, Comm. Math. Phys. **122** (1989) 249
- [6] D. Petz, *An Invitation to the Algebra of Canonical Commutation Relations*, Leuven University Press, Leuven, 1989
- [7] H. Kneser, *Sur un théorème fondamental de la théorie des jeux*, C. R. Acad. Sci. Paris **234** (1952) 2418–2420
- [8] M. Reed and B. Simon, *Methods of Modern Mathematical Physics. Volume IV: Analysis of Operators*, Academic Press, London, 1978
- [9] M. Takesaki, *Theory of operator algebras I*, Springer, Berlin Heidelberg New York, 1979
- [10] F. M. Brückler, *Tensor products of C^* -algebras, operator spaces and Hilbert C^* -modules*, Math. Comm. **4** (1999) 257
- [11] G. A. Raggio and R. F. Werner, *Quantum statistical mechanics of general mean field systems*, Helv. Phys. Acta **62** (1989) 980
- [12] N. G. Duffield and R. F. Werner, *Mean-field dynamical semigroups on C^* -algebras*, Reviews in Math. Physics **4** (1991) 383
- [13] N.G. Duffield and R.F. Werner, *Classical Hamiltonian Dynamics for Quantum Hamiltonian Mean-Field Limits*, in A. Truman and I.M. Davies, editors, *Stochastics and Quantum Mechanics*. World Scientific, 1992

-
- [14] K. Hepp and E. H. Lieb, *Phase transitions in reservoir-driven open systems with applications to lasers and superconductors*, Helv. Phys. Act. **46** (1973) 573
- [15] N. G. Duffield and R. F. Werner, *Local dynamical of mean-field quantum systems*, Helv. Phys. Act. **65** (1992) 1016
- [16] G. A. Raggio and R. F. Werner, *The Gibbs variational principle for inhomogenous mean-field models*, Helv. Phys. Acta **64** (1991) 633
- [17] G. A. Raggio and R. F. Werner, *The Gibbs variational principle for general BCS-type models*, Europhys. Lett. **9** (1989) 633
- [18] N. G. Duffield, H. Roos, and R. F. Werner, *Macroscopic limiting dynamics of a class of inhomogenous mean-field quantum systems*, Ann. Inst. Henri Poincaré **56** (1992) 143
- [19] R. F. Werner, *Large deviations ans mean-field quantum systems*, Quantum Probability and Related Topics **3** (1992) 349
- [20] E. Størmer, *Symmetric states on infinite tensor products of C^* -algebras*, J. Func. Anal. **3** (1969) 48–68
- [21] R. L. Hudson and G. R. Moody, *Locally normal symmetric states and an analogue of de Finetti's theorem*, Z. Wahrscheinlichkeitstheorie verw. Gebiete **80** (1976) 7343–351
- [22] M. Fannes and J. T. Lewis und A. Verbeure, *Symmetric states of composite systems*, Lett. Math. Phys. **15** (1988) 255–260
- [23] D. A. Petz, *de Finetti-type theorem wuth m -dependent states*, Prob. Theory Related Fields **85** (1990) 65–72
- [24] C. A. Fuchs C. M. Caves and R. Schack, *Unknown quantum states: The quantum de Finetti representation*, J. Math. Phys. **43** (2001) 4537–4559
- [25] B. De Finetti, *La prévision: Ses lois logiques, ses sources subjectives*, Ann. Inst. H. Poincaré **7** (1937) 1–68
- [26] R. Renner, *Symmetry of large physical systems implies independence of subsystems*, Nature **3** (2007) 645
- [27] P. Monarci and D. Cocci, *Introduction to Bruno de Finetti's Probabilità e Induzione*, Cooperativa Libreria Universitaria Editrice, 1993
- [28] P. Diaconis and D. Freedman, *Finite exchangeable sequences*, Ann. Probab. **8** (1980) 745–764
- [29] R. Koenig and R. Renner, *A de Finetti representation for finite symmetric quantum states*, J. Math. Phys. **46** (2005) 122108

- [30] G. Mitchison M. Christandl, R. König and R. Renner, *One-and-a-half quantum de Finetti theorems*, Comm. Math. Phys. **273** (2007) 473–498
- [31] T. J. Osborne C. D’Cruz and R. Schack, *Finite de Finetti theorems for infinite-dimensional systems*, Phys. Rev. Lett. **98** (2007) 160406
- [32] M. Broidioi, B. Momont, and A. Verbeure, *Lie algebra of anomalously scaled fluctuations*, J. Math. Phys. **36** (1995) 6746
- [33] N. Aneglescu, J. G. Brankov, and A. Verbeure, *General one-particle fluctuations of the ideal Bose gas*, J. Phys. A **29** (1996) 3341
- [34] und A. Verbeure M. Fannes, A. Kossakowski, *Critical Fluctuations for Quantum Mean-Field models*, Journal of Statistical Physics **65** (1991) 801
- [35] A. DasGupta, *Asymptotic Theory of Statistics and Probability*, Springer, Berlin Heidelberg New York, 2008
- [36] C. D. Cushden and R. L. Hudson, *A quantum mechanical central limit theorem*, J. Appl. Prob. **8** (1971) 454
- [37] J. Quaegebeur, *A non-commutative central limit theorem for CCR-algebras*, J. Func. Anal. **57** (1984) 1
- [38] N. Giri and W. von Waldenfels, *An algebraic version of the central limit theorem*, Z. Wahrscheinlichkeitstheorie verw. Gebiete **42** (1978) 129
- [39] L. Accardi and A. Bach, *Quantum central limit theorems for strongly mixing random variables*, Z. Wahrscheinlichkeitstheorie verw. Gebiete **68** (1985) 393
- [40] G. Kuperberg, *A tracial quantum central limit theorem*, Trans. Amer. Math. Soc. **357** (2005) 459
- [41] D. Goderis, A. Verbeure, and P. Vets, *Theory of fluctuations and small oscillations for quantum lattice systems*, J. Math. Phys. **29** (1988) 12
- [42] D. Goderis, A. Verbeure, and P. Vets, *Dynamics of fluctuations for quantum lattice systems*, Commun. Math. Phys. **128** (1990) 533
- [43] E. H. Lieb, R. Seiringer, J. P. Solovej, and J. Yngvason, *The Mathematics of the Bose Gas and its Condensation (Oberwolfach Seminars)*, Birkhäuser, Basel, 2010
- [44] J. Links and K. E. Hibberd, *Bethe Ansatz Solutions of the Bose-Hubbard Dimer*, SIGMA **2** (2006) 095
- [45] R. F. Werner, *Quantum states with Einstein-Podolsky-Rosen correlations admitting a hidden-variable model*, Phys. Rev. A **40** (1989) 4277

- [46] D. Freedman, *A remark on the difference between sampling with and without replacement*, J. Am. Stat. Assoc. **72** (1977) 681
- [47] J. N. Darroch, M. Jirina, and T. P. Speed, *Sampling without replacement: Approximation to the probability distribution*, J. Austral. Math. Soc. (Series A) **44** (1988) 197
- [48] R. T. Rockafellar, *Convex Analysis*, Princeton University Press, Princeton, 1996
- [49] A. M. Perelomov, *Generalized Coherent States and Their Applications*, Springer, Berlin Heidelberg New York, 1986
- [50] C. Brif and A. Mann, *Phase-space formulation of quantum mechanics and quantum-state reconstruction for physical systems with Lie-group symmetries*, Phys. Rev. A **59** (1999) 971
- [51] W.-M. Zhang, D. H. Feng, and R. Gilmore, *Coherent states: Theory and some applications*, Rev. Mod. Phys. **62** (1990) 867
- [52] F. Trimborn, D. Witthaut, and H. J. Korsch, *Exact number conserving phase-space dynamics of the M-site Bose-Hubbard model*, Phys. Rev. A **77** (2008) 043631
- [53] F. Trimborn, D. Witthaut, and H. J. Korsch, *Beyond mean-field dynamics of small Bose-Hubbard systems based on the number-conserving phase space approach*, Phys. Rev. A **79** (2009) 013608
- [54] R. J. Glauber, *The Quantum Theory of Optical Coherence*, Phys. Rev. **130** (1963) 2529
- [55] R. Gilmore, C. M. Bowden, and L. M. Narducci, *Classical-quantum correspondence for multilevel systems*, Phys. Rev. A **12** (1975) 1019
- [56] F. T. Arecchi, E. Courtens, R. Gilmore, and H. Thomas, *Atomic Coherent States in Quantum Optics*, Phys. Rev. A **6** (1972) 2211
- [57] J. M. Radcliffe, *Some properties of coherent spin states*, J. Phys. A **4** (1971) 313
- [58] A. B. Klimov and P. Espinoza, *Moyal-like form of the star product for generalized $SU(2)$ Stratonovich-Weyl symbols*, J. Phys. A **35** (2002) 8435
- [59] C.W. Gardiner and P. Zoller, *Quantum Noise*, Springer Series in Synergetics, Berlin Heidelberg New York, 2004
- [60] A. B. Klimov, *Exact evolution equations for $SU(2)$ quasidistribution functions*, Journal of Mathematical Physics **43** (2002) 2202
- [61] D. Zueco and I. Calvo, *Bopp operators and phase-space spin dynamics: application to rotational quantum Brownian motion*, J. Phys. A **40** (2007) 4635

- [62] D. W. Barry and P. D. Drummond, *Qubit phase space: $SU(n)$ coherent-state P -representations*, Phys. Rev. A **78** (2008) 052108
- [63] R. L. Stratonovich, *On distributions in representation space*, Sov. Phys. JETP **4** (1957) 891
- [64] C. P. Robert and G. Casella, *Monte Carlo Statistical Methods*, Springer, Berlin Heidelberg New York, 2004
- [65] C. W. Gardiner, *Particle-number-conserving Bogoliubov method which demonstrates the validity of the time-dependent Gross-Pitaevskii equation for a highly condensed Bose gas*, Phys. Rev. A **56** (1997) 1414
- [66] H. N. Mülthei and H. Neunzert, *Untersuchung pseudoparabolische Differentialgleichungen mit Hilfe einer verallgemeinerten Riemannschen Integration*, Math. Z. **111** (1969) 257
- [67] H. N. Mülthei and H. Neunzert, *Pseudoparabolische Differentialgleichungen mit charakteristischen Vorgaben im komplexen Gebiet*, Math. Z. **113** (1970) 24
- [68] H. J. Carmichael, *Statistical Methods in Quantum Optics: Master Equations and Fokker-Planck Equations*, Springer, Berlin Heidelberg New York, 1999
- [69] A. Vardi and J. R. Anglin, *Bose-Einstein condensates beyond mean field theory: Quantum backreaction as decoherence*, Phys. Rev. Lett. **86** (2001) 568
- [70] A. Vardi, V. A. Yurovsky, and J. R. Anglin, *Quantum effects on the dynamics of a two-mode atom-molecule Bose-Einstein condensate*, Phys. Rev. A **64** (2001) 063611
- [71] Y. Castin and R. Dum, *Instability and Depletion of an Excited Bose-Einstein Condensate in a Trap*, Phys. Rev. Lett. **79** (1997) 3553
- [72] F. Scheck, *Mechanik*, Berlin Heidelberg New York, Springer, 1996
- [73] V. I. Arnold, *Mathematical Methods of Classical Mechanics*, Springer, Berlin Heidelberg New York, 1978
- [74] T. F. Viscondi and M. A. M. de Aguiar, *Semiclassical propagator for $SU(n)$ coherent states*, JMP **52** (2011) 052104
- [75] A. Sugita, *Proof of the generalized Lieb-Wehrl conjecture for integer indices larger than one*, J. Phys. A **35** (2002) L621
- [76] E. H. Lieb, *The Classical Limit of Quantum Spin Systems*, Commun. Math. Phys. **31** (1973) 327
- [77] F. A. Berezin, *General concept of quantization*, Commun. Math. Phys. **40** (1973) 153

- [78] B. Simon, *The classical limit of quantum partition functions*, Commun. Math. Phys. **71** (1980) 247
- [79] R. Gilmore and D. H. Feng, *Studies of the ground state properties of the Lipkin-Meshkov-Glick model via the atomic coherent states*, Phy. Lett. **76** (1978) 26
- [80] E. Stein and G. Weiss, *Introduction to Fourier Analysis on Euclidean Spaces*, Princeton University Press, 1971
- [81] O. Morsch and M. Oberthaler, *Dynamics of Bose-Einstein condensates in optical lattices*, Rev. Mod. Phys. **78** (2006) 179
- [82] Immanuel Bloch, Jean Dalibard, and Wilhelm Zwerger, *Many-body physics with ultracold gases*, Rev. Mod. Phys. **80(3)** (2008) 885–964
- [83] A. Einstein, *Quantentheorie des einatomigen idealen Gases*, Sitzungsber. preuss. Akad. Wiss. **22** (1924) 261
- [84] A. Einstein, *Quantentheorie des einatomigen idealen Gases. Zweite Abhandlung*, Sitzungsber. preuss. Akad. Wiss. **1** (1925) 3
- [85] S. N. Bose, *Plancks Gesetz und die Lichtquantenhypothese*, Z. Phys. **26** (1924) 178
- [86] N. D. Mermin and H. Wagner, *Absence of Ferromagnetism or Antiferromagnetism in One- or Two-Dimensional Isotropic Heisenberg Models*, Phys. Rev. Lett. **17** (1966) 1133
- [87] P. C. Hohenberg, *Existence of Long-Range Order in One and Two Dimensions*, Phys. Rev. **158** (1967) 383
- [88] S. Grossmann and M. Holthaus, *On Bose-Einstein condensation in harmonic traps*, Phys. Lett. A **208** (1995) 199
- [89] W. Ketterle and N. J. van Druten, *Bose-Einstein condensation of a finite number of particles trapped in one or three dimensions*, Phys. Rev. A **54** (1996) 656
- [90] V. L. Berezinskii, *Destruction of long-range order in one-dimensional and two-dimensional systems possessing a continuous symmetry group. II. Quantum systems*, Sov. Phys. JETP **34** (1972) 610
- [91] J. M. Kosterlitz and D.J. Thouless, *Ordering, metastability and phase-transitions in two-dimensional systems*, J. Phys. C **7** (1973) 1181
- [92] Z. Hadzibabic, P. Krüger, M. Cheneau, B. Battelier, and J. Dalibard, *Berezinskii-Kosterlitz-Thouless crossover in a trapped atomic gas*, Nature **441** (2006) 1118
- [93] O. Penrose and L. Onsager, *Bose-Einstein Condensation and Liquid Helium*, Phys. Rev. **104** (1956) 576

- [94] A. J. Leggett, *Bose-Einstein condensation in the alkali gases: Some fundamental concepts*, Rev. Mod. Phys. **73** (2001) 307
- [95] S. Chu, *Nobel Lecture: The manipulation of neutral particles*, Rev. Mod. Phys. **70** (1998) 685
- [96] C. N. Cohen-Tannoudji, *Nobel Lecture: Manipulating atoms with photons*, Rev. Mod. Phys. **70** (1998) 707
- [97] W. D. Phillips, *Nobel Lecture: Laser cooling and trapping of neutral atoms*, Rev. Mod. Phys. **70** (1998) 721
- [98] H. J. Metcalf and P. van der Straten, *Laser Cooling and Trapping*, Springer, Berlin Heidelberg New York, 1999
- [99] M. H. Anderson, J. R. Ensher, M. R. Matthews, C. E. Wieman, and W. E. Cornell, *Observation of Bose-Einstein Condensation in a Dilute Atomic Vapor*, Science **269** (1995) 198
- [100] C. C. Bradley, C. A. Sackett, J. J. Tollett, and R. G. Hulet, *Evidence of Bose-Einstein Condensation in an Atomic Gas with Attractive Interactions*, Phys. Rev. Lett. **75** (1995) 1687
- [101] K. B. Davis, M. O. Mewes, M. R. Andrews, N. J. van Druten, D. S. Durfee, D. M. Kurn, and W. Ketterle, *Bose-Einstein Condensation in a Gas of Sodium Atoms*, Phys. Rev. Lett. **75** (1995) 3969
- [102] E. A. Cornell and C. E. Wieman, *Nobel Lecture: Bose-Einstein condensation in a dilute gas, the first 70 years and some recent experiments*, Rev. Mod. Phys. **74** (2002) 875
- [103] W. Ketterle, *Nobel lecture: When atoms behave as waves: Bose-Einstein condensation and the atom laser*, Rev. Mod. Phys. **74** (2002) 1131
- [104] W. S. Bakr, A. Peng, M. E. Tai, R. Ma, J. Simon, J. I. Gillen, S. Fölling, L. Pollet, and M. Greiner, *Probing the Superfluid-to-Mott-Insulator Transition at the Single-Atom Level*, Science Express **329** (2010) 547
- [105] J. F. Sherson, C. Weitenberg, M. Endres, M. Cheneau, I. Bloch, and S. Kuhr, *Single-atom-resolved fluorescence imaging of an atomic Mott insulator*, Nature **467** (2010) 68
- [106] W. Ketterle, D. Durfee, and D.M. Stamper-Kurn, *Bose-Einstein Condensation in Atomic Gases*, in *Proceedings of the international School of Physics Enrico Fermi - Course CXL*, pages 67–176. IOS, 1999
- [107] D. G. Fried, T. C. Killian, L. Willmann, D. Landhuis, S. C. Moss, D. Kleppner, and T. J. Greytak, *Bose-Einstein Condensation of Atomic Hydrogen*, Phys. Rev. Lett. **81** (1998) 18

- [108] T. Weber, J. Herbig, M. Mark, H.-C. Nägerl, and R. Grimm, *Bose-Einstein condensation in Caesium*, *Science* **299** (2003) 232
- [109] C. J. Pethick and H. Smith, *Bose-Einstein Condensation in Dilute Gases*, Cambridge University Press, Cambridge, 2008
- [110] L. J. Garay, J. R. Anglin, J. I. Cirac, and P. Zoller, *Sonic black holes in dilute Bose-Einstein condensates*, *Phys. Rev. A* **63** (2001) 023611
- [111] L. V. Hau, S. E. Harris, Z. Dutton, and C. H. Behroozi, *Light speed reduction to 17 metres per second in an ultracold atomic gas*, *Nature* **397** (1999) 594
- [112] M. Fleischhauer, A. Imamoglu, and J. P. Marangos, *Electromagnetically induced transparency: Optics in coherent media*, *Rev. Mod. Phys.* **77** (2005) 633
- [113] S. Jochim, M. Bartenstein, A. Altmeyer, G. Hendl, S. Riedl, C. Chin, J. Hecker Denschlag, and R. Grimm, *Bose-Einstein Condensation of Molecules*, *Science* **302** (2003) 2101
- [114] M. Greiner, C. A. Regal, and D. S. Jin, *Emergence of a molecular Bose-Einstein condensate from a Fermi gas*, *Nature* **426** (2003) 537
- [115] K. Xu, T. Mukaiyama, J.R. Abo-Shaeer, J.K. Chin, D. Miller, and W. Ketterle, *Formation of Quantum-Degenerate Sodium Molecules*, *Phys. Rev. Lett.* **91** (2003) 210402
- [116] S. O. Demokritov, V. E. Demidov, O. Dzyapko, G. A. Melkov, A. A. Serga, B. Hillebrands, and A. N. Slavin, *Bose-Einstein condensation of quasi-equilibrium magnons at room temperature under pumping*, *Nature* **443** (2006) 430
- [117] J. Kasprzak, M. Richard, S. Kundermann, A. Baas, P. Jeambrun, J. M. J. Keeling, F. M. Marchetti, M. H. Szymanski, R. Andr, J. L. Staehli, V. Savona, P. B. Littlewood, B. Deveaud, and Le Si Dang, *Bose-Einstein condensation of exciton polaritons*, *Nature* **443** (2006) 409
- [118] J. Klaers, F. Vewinger, and M. Weitz, *Thermalisation of a two-dimensional photonic gas in a 'white-wall' photon box*, *Nature Physics* **6** (2010) 512
- [119] J. Klaers, J. Schmitt, F. Vewinger, and M. Weitz, *Bose-Einstein condensation of photons in an optical microcavity*, *Nature* **468** (2010) 545
- [120] M. O. Scully and M. S. Zubairy, *Quantum Optics*, Cambridge University Press, Cambridge, 1997
- [121] C. J. Foot, *Atomic physics*, Oxford University Press, 2005
- [122] D. Jaksch, H. J. Briegel, J. I. Cirac, C. W. Gardiner, and P. Zoller, *Entanglement of atoms via cold controlled collisions*, *Phys. Rev. Lett.* **81** (1999) 3108

- [123] A. Görlitz, T. Kinoshita, T. W. Hänsch, and A. Hemmerich, *Realization of bichromatic optical superlattices*, Phys. Rev. A **64** (2001) 011401(R)
- [124] S. Fölling, S. Trotzky, P. Cheinet, M. Feld, R. Saers, A. Widera, T. Müller, and I. Bloch, *Direct Observation of Second Order Atom Tunnelling*, Nature **448** (2007) 1029
- [125] D. Jaksch, C. Bruder, J. I. Cirac, C. W. Gardiner, and P. Zoller, *Cold Bosonic Atoms in Optical Lattices*, Phys. Rev. Lett. **821** (1998) 1975
- [126] C. Bruder, R. Fazio, and G. Schön, *The Bose-Hubbard model: from Josephson junction arrays to optical lattices*, Ann. Phys. (Leipzig) **14** (2005) 566
- [127] M. Greiner, O. Mandel, T. Esslinger, T. W. Hänsch, and I. Bloch, *Quantum phase transition from a superfluid to a Mott insulator in a gas of ultracold atoms*, Nature **415** (2002) 39
- [128] Axel Griesmaier, Jörg Werner, Sven Hensler, Jürgen Stuhler, and Tilman Pfau, *Bose-Einstein Condensation of Chromium*, Phys. Rev. Lett. **94** (2005) 160401
- [129] W. Kohn, *Analytic Properties of Bloch Waves and Wannier Functions*, Phys. Rev. **115** (1959) 809
- [130] M. P. A. Fisher, P. B. Weichman, G. Grinstein, and D. S. Fisher, *Boson localization and the superfluid-insulator transition*, Phys. Rev. B **40** (1989) 547
- [131] L. Pitaevskii and S. Stringari, *Bose-Einstein Condensation*, Oxford University Press, Oxford, 2003
- [132] N. N. Bogoliubov, *On the theory of superfluidity*, J. Phys. USSR **11** (1947) 23
- [133] E.P. Gross, *Structure of a Quantized Vortex in Boson Systems*, Nuovo Cimento **20** (1961) 454
- [134] E.P. Gross, *Hydrodynamics of a superfluid condensate*, J. Math. Phys. **4** (1963) 195
- [135] L.P. Pitaevskii, *Vortex lines in an imperfect Bose gas*, Sov. Phys. JETP **13** (1961) 451
- [136] E. H. Lieb, R. Seiringer, and J. Yngvason, *Bosons in a trap: A rigorous derivation of the Gross-Pitaevskii energy functional*, Phys. Rev. A **61** (2000) 043602
- [137] Y. Castin and R. Dum, *Low-temperature Bose-Einstein condensates in time-dependent traps: Beyond the $U(1)$ symmetry-breaking approach*, Phys. Rev. A **57** (1998) 3008
- [138] E. H. Lieb, R. Seiringer, and J. Yngvason, *Justification of c-Number Substitutions in Bosonic Hamiltonians*, Phys. Rev. Lett. **94** (2005) 080401

- [139] A. Griffin, *Conserving and gapless approximations for an inhomogeneous Bose gas at finite temperatures*, Phys. Rev. B **53** (1996) 9341
- [140] I. Tikhonenkov, J. R. Anglin, and A. Vardi, *Quantum dynamics of Bose-Hubbard Hamiltonians beyond Hartree-Fock-Bogoliubov: The Bogoliubov-backreaction approximation*, Phys. Rev. A **75** (2007) 013613
- [141] J. R. Anglin and A. Vardi, *Dynamics of a two-mode Bose-Einstein condensate beyond mean-field theory*, Phys. Rev. A **64** (2001) 013605
- [142] Y. Khodorkovsky, G. Kurizki, and A. Vardi, *Bosonic amplification of noise-induced suppression of phase diffusion*, Phys. Rev. Lett. **100** (2008) 220403
- [143] Yun Li, Y. Castin, and A. Sinatra, *Optimum spin-squeezing in Bose-Einstein condensates with particle losses*, Phys. Rev. Lett. **100** (2008) 210401
- [144] B. Kraus, H. P. Büchler, S. Diehl, A. Kantian, A. Micheli, and P. Zoller, *Preparation of entangled states by quantum Markov processes*, Phys. Rev. A **78** (2008) 042307
- [145] S. Diehl, A. Micheli, A. Kantian, B. Kraus, H. P. Büchler, and P. Zoller, *Quantum states and phases in driven open quantum systems with cold atoms*, Nat. Phys. **4** (2008) 878
- [146] F. Verstraete, M. M. Wolf, and J. I. Cirac, *Quantum computation, quantum state engineering, and quantum phase transitions driven by dissipation*, Nat. Phys. **5** (2009) 633
- [147] N. Syassen, D. M. Bauer, M. Lettner, T. Volz, D. Dietze, J. J. Garcia-Ripoll, J. I. Cirac, G. Rempe, and S. Dürr, *Strong dissipation inhibits losses and induces correlations in cold molecular gases*, Science **320** (2008) 1329
- [148] J. J. Garcia-Ripoll, S. Dürr, N. Syassen, D. M. Bauer, M. Lettner, and G. Rempe, *Dissipation induced Tonks-Girardeau gas in an optical lattice*, New J. Phys. **11** (2009) 013053
- [149] S. F. Huelga and M. B. Plenio, *Stochastic Resonance Phenomena in Quantum Many-Body Systems*, Phys. Rev. Lett. **98** (2007) 170601
- [150] T. Gericke, P. Würtz, D. Reitz, T. Langen, , and H. Ott, *High Resolution Scanning Electron Microscopy of an Ultracold Quantum Gas*, Nature Physics **4** (2008) 949
- [151] J. Dalibard, Y. Castin, and K. Mølmer, *Wave-function approach to dissipative processes in quantum optics*, Phys. Rev. Lett. **68** (1992) 580
- [152] H. J. Carmichael, *An Open Systems Approach to Quantum Optics*, Springer Lecture Notes in Physics, Berlin Heidelberg New York, 1993

- [153] K. Mølmer, Y. Castin, and J. Dalibard, *Monte-Carlo wave function method in quantum optics*, J. Opt. Soc. Am. B **10** (1993) 542
- [154] J. Anglin, *Cold, Dilute, Trapped Bosons as an Open Quantum System*, Phys. Rev. Lett. **79** (1997) 6
- [155] J. Ruostekoski and D. F. Walls, *Bose-Einstein condensate in a double-well potential as an open quantum system*, Phys. Rev. A **58** (1998) R50
- [156] D. F. Walls and G. J. Milburn, *Effect of dissipation on quantum coherence*, Phys. Rev. A **31** (1985) 2403
- [157] M. Albiez, R. Gati, J. Fölling, S. Hunsmann, M. Cristiani, and M. K. Oberthaler, *Direct Observation of Tunneling and Nonlinear Self-Trapping in a Single Bosonic Josephson Junction*, Phys. Rev. Lett. **95** (2005) 010402
- [158] R. Gati, B. Hemmerling, J. Fölling, M. Albiez, and M. K. Oberthaler, *Noise Thermometry with Two Weakly Coupled Bose-Einstein Condensates*, Phys. Rev. Lett. **96** (2006) 130404
- [159] R. Gati, J. Estève, B. Hemmerling, T.B. Ottenstein, J. Appmeier, A. Weller, and M. K. Oberthaler, *A primary noise thermometer for ultracold bose gases*, New J. Phys. **8** (2006) 189
- [160] S. Trotzky, L. Pollet, F. Gerbier, U. Schnorrberger, I. Bloch, N.V. Prokof'ev, B. Svistunov, and M. Troyer, *Suppression of the critical temperature for superfluidity near the Mott transition*, Nature Physics **6** (2010) 998
- [161] H. Pichler, A. J. Daley, and P. Zoller, *Nonequilibrium dynamics of bosonic atoms in optical lattices: Decoherence of many-body states due to spontaneous emission*, Phys. Rev. A **82** (2010) 063605
- [162] I. Bloch, T. W. Hänsch, and T. Esslinger, *Atom Laser with a cw Output Coupler*, Phys. Rev. Lett. **82** (1999) 3008
- [163] M.B. Plenio and P.L. Knight, *The Quantum jump approach to dissipative dynamics in quantum optics*, Phys. Rev. B **70** (1998) 101
- [164] V. Weisskopf and E. Wigner, *Berechnung der natürlichen Linienbreite auf Grund der Diracschen Lichttheorie*, Z. Phys. **63** (1930) 54
- [165] H.-P. Breuer and F. Petruccione, *The theory of open quantum systems*, Oxford University Press, 2002
- [166] D. F. Walls and G. J. Milburn, *Quantum Optics*, Springer, Berlin Heidelberg New York, 1994

- [167] S. Trotzky, P. Cheinet, S. Fölling, M. Feld, U. Schnorrberger, A. M. Rey, A. Polkovnikov, E. A. Demler, M. D. Lukin, and I. Bloch, *Time-resolved Observation and Control of Superexchange Interactions with Ultracold Atoms in Optical Lattices*, *Science* **319** (2008) 295
- [168] T. Schumm, S. Hofferberth, L. M. Andersson, S. Wildermuth, S. Groth, I. Bar-Joseph, J. Schmiedmayer, and P. Krüger, *Matter-wave interferometry in a double well on an atom chip*, *Nature Physics* **1** (2005) 57
- [169] C. Orzel, A. K. Tuchman, M. L. Fenselau, M. Yasuda, and M. A. Kasevich, *Squeezed States in a Bose-Einstein Condensate*, *Science* **291** (2001) 2386
- [170] Biao Wu and Qian Niu, *Nonlinear Landau-Zener Tunneling*, *Phys. Rev. A* **61** (2000) 023402
- [171] D. Witthaut, E. M. Graefe, and H. J. Korsch, *Towards a Landau-Zener formula for an interacting Bose-Einstein condensate in a two-level system*, *Phys. Rev. A* **73** (2006) 063609
- [172] G. J. Milburn, J. Corney, E. M. Wright, and D. F. Walls, *Quantum dynamics of an atomic Bose-Einstein condensate in a double-well potential*, *Phys. Rev. A* **55** (1997) 4318
- [173] A. Smerzi, S. Fantoni, S. Giovanazzi, and S. R. Shenoy, *Quantum Coherent Atomic Tunneling between Two Trapped Bose-Einstein Condensates*, *Phys. Rev. Lett.* **79** (1997) 4950
- [174] S. Raghavan, A. Smerzi, S. Fantoni, and S. R. Shenoy, *Coherent oscillations between two weakly coupled Bose-Einstein condensates: Josephson Effects, π oscillations, and macroscopic quantum self-trapping*, *Phys. Rev. A* **59** (1999) 620
- [175] M. Albiez, *Observation of nonlinear tunneling of a Bose-Einstein condensate in a single Josephson junction*, Dissertation Universität Heidelberg, 2005
- [176] V. I. Arnold, *Gewöhnliche Differentialgleichungen*, § 5.4, Springer, New York, 1980
- [177] F. Bloch, *Nuclear Induction*, *Phys. Rev.* **70** (1946) 460
- [178] N. Moiseyev and L. Cederbaum, *Resonance solutions of the nonlinear Schrödinger equation: Tunneling lifetime and fragmentation of trapped condensates*, *Phys. Rev. A* **72** (2005) 033605
- [179] P. Schlagheck and S. Wimberger, *Nonexponential decay of Bose-Einstein condensates: a numerical study based on the complex scaling method*, *Appl. Phys. B* **86** (2007) 385–390

- [180] D. Witthaut, E. M. Graefe, S. Wimberger, and H. J. Korsch, *Bose-Einstein condensates in accelerated double-periodic optical lattices: coupling and crossing of resonances*, Phys. Rev. A **75** (2007) 013617
- [181] R. Livi, R. Franzosi, and G.-L. Oppo, *Self-Localization of Bose-Einstein Condensates in Optical Lattices via Boundary Dissipation*, Phys. Rev. Lett. **97** (2006) 060401
- [182] M. Hiller, T. Kottos, and A. Ossipov, *Bifurcations in Resonance Widths of an Open Bose-Hubbard Dimer*, Phys. Rev. A **73** (2006) 063625
- [183] E. M. Graefe, H. J. Korsch, and A. E. Niederle, *Mean-field dynamics of a non-Hermitian Bose-Hubbard dimer*, Phys. Rev. Lett. **101** (2008) 150408
- [184] M. Rigo, G. Alber, F. Mota-Furtado, and P. F. O'Mahony, *Quantum-state diffusion model and the driven damped nonlinear oscillator*, Phys. Rev. A **55** (1997) 1665
- [185] R. Benzi, A. Sutera, and A. Vulpiani, *The mechanism of stochastic resonance*, J. Phys. A **14** (1981) L453
- [186] K. Wiesenfeld and F. Moss, *Stochastic resonance and the benefits of noise: from ice ages to crayfish and SQUIDS*, Nature **373** (1995) 33
- [187] M. I. Dykman, D. G. Luchinsky, R. Mannella, P. V. E. McClintock, N. D. Stein, and N. G. Stocks, *Stochastic resonance in perspective*, Nuovo Cimento D **17** (1995) 661
- [188] L. Gammaitoni, P. Hänggi, P. Jung, and F. Marchesoni, *Stochastic resonance*, Rev. Mod. Phys. **70** (1998) 223
- [189] T. Wellens, V. Shatokhin, and A. Buchleitner, *Stochastic resonance*, Rep. Prog. Phys. **67** (2004) 45
- [190] R. Löfstedt and S. N. Coppersmith, *Quantum stochastic resonance*, Phys. Rev. Lett. **72** (1994) 1947
- [191] R. Löfstedt and S. N. Coppersmith, *Stochastic resonance: Nonperturbative calculation of power spectra and residence-time distributions*, Phys. Rev. E **49** (1994) 4821
- [192] A. Buchleitner and R. N. Mantegna, *Quantum stochastic resonance in a micro-maser*, Phys. Rev. Lett. **80** (1998) 3932
- [193] T. Wellens and A. Buchleitner, *Stochastic resonance in a fundamental quantum system*, J. Phys. A **32** (1999) 2895
- [194] S. F. Huelga and M. B. Plenio, *Quantum Stochastic Resonance in Electron Shelving*, Phys. Rev. A **62** (2000) 052111

- [195] H. H. Adamyan, S. B. Manvelyan, and G. Y. Kryuchkyan, *Chaos in a double driven dissipative nonlinear oscillator*, Phys. Rev. A **63** (2001) 022102
- [196] L. Viola, E. M. Fortunato, S. Lloyd, C.-H. Tseng, and D. G. Cory, *Stochastic Resonance and Nonlinear Response by NMR Spectroscopy*, Phys. Rev. Lett. **80** (2000) 5466
- [197] S. Wimberger, R. Mannella, O. Morsch, E. Arimondo, A. R. Kolovsky, and A. Buchleitner, *Nonlinearity-induced destruction of resonant tunneling in the Wannier-Stark problem*, Phys. Rev. A **72** (2005) 063610
- [198] P. Schlagheck and T. Paul, *Complex scaling approach to the decay of Bose-Einstein condensates*, Phys. Rev. A **73** (2006) 023619
- [199] F. Bloch, *Über die Quantenmechanik der Elektronen in Kristallgittern*, Z. Phys **52** (1928) 555
- [200] E. E. Mendez, F. Agullo-Rueda, and J. M. Hong, *Stark Localizations in GaAs-GaAlAs Superlattices under an Electric field*, Phys. Rev. Lett. **60** (1988) 2426
- [201] P. Voisin, J. Bleuse, C. Bouche, S. Gaillard, C. Alibert, and A. Regreny, *Observation of the Wannier-Stark quantization in a semiconductor superlattice*, Phys. Rev. Lett. **61** (1988) 1639
- [202] J. Feldmann, K. Leo, J. Shah, B. A. B. Miller, J. E. Cunningham, T. Meier, G. von Plessen, A. Schulze, P. Thomas, and S. Schmitt-Rink, *Optical Investigation of Bloch Oscillations in a Semiconductor Superlattice*, Phys. Rev. B **46** (1992) 7252
- [203] K. Leo, *High-Field Transport in Semiconductor Superlattices*, Springer, Berlin Heidelberg New York, 2003
- [204] J. A. Morales, E. Deumens and Y. Öhrn, *On rotational coherent states in molecular quantum dynamics*, J. Math. Phys. **40**(2) (1999) 766
- [205] T. Pertsch, P. Dannberg, W. Elfein, A. Bräuer, and F. Lederer, *Optical Bloch Oscillations in Temperature Tuned Waveguide Arrays*, Phys. Rev. Lett. **83** (1999) 4752
- [206] G. Lenz, I. Talanina, and C. Martijin de Sterke, *Bloch Oscillations in an Array of Curved Optical Waveguides*, Phys. Rev. Lett. **83** (1999) 963
- [207] H. Trompeter, T. Pertsch, F. Lederer, D. Michaelis, U. Streppel, A. Brauer, and U. Peschel, *Visual Observation of Zener Tunneling*, Phys. Rev. Lett. **96** (2006) 023901

- [208] H. Trompeter, W. Krolikowski, D. N. Neshev, A. S. Desyatnikov, A. A. Sukhorukov, Y. S. Kivshar, T. Pertsch, U. Peschel, and F. Lederer, *Bloch Oscillations and Zener Tunneling in Two-Dimensional Photonic Lattices*, Phys. Rev. Lett. **96** (2006) 053903
- [209] M. Ben Dahan, E. Peik, J. Reichel, Y. Castin, and C. Salomon, *Bloch Oscillations of Atoms in an Optical Potential*, Phys. Rev. Lett. **76** (1996) 4508
- [210] B. P. Anderson and M. A. Kasevich, *Macroscopic Quantum Interference from Atomic Tunnel Arrays*, Science **282** (1998) 1686
- [211] O. Morsch, J. H. Müller, M. Cristiani, D. Ciampini, and E. Arimondo, *Bloch Oscillations and Mean-Field Effects of Bose-Einstein Condensates in 1D Optical Lattices*, Phys. Rev. Lett. **87** (2001) 140402
- [212] M. Gustavsson, E. Haller, M. J. Mark, J. G. Danzl, G. Rojas-Kopeinig, and H.-C. Nägerl, *Control of Interaction-Induced Dephasing of Bloch Oscillations*, Phys. Rev. Lett. **100** (2008) 080404
- [213] B. P. Anderson, T. L. Gustavson, and M. A. Kasevich, *Atom Trapping in Nondissipative Optical Lattices*, Phys. Rev. A **53** (1996) R3727
- [214] N. Poli, F.-Y. Wang, M. G. Tarallo, A. Alberti, M. Prevedelli, and G. M. Tino, *Precision Measurement of Gravity with Cold Atoms in an Optical Lattice and Comparison with a Classical Gravimeter*, Phys. Rev. Lett. **106** (2011) 038501
- [215] Quantum Phase Interference and Parity Effects in Magnetic Molecular Clusters, *W. Wernsdorfer and R. Sessoli*, Science **284** (1999) 133
- [216] M. S. Child, *Molecular Collision Theory*, Academic Press, London, 1974
- [217] R. J. C. Spreeuw, N. J. Van Druten, M. W. Beijersbergen, E. R. Eliel, and J. P. Woerdman, *Classical realization of a strongly driven two-level system*, Phys. Rev. Lett. **65** (1990) 2642
- [218] M. Wubs, K. Saito, P. Hänggi, and Y. Kayanuma, *Gauging a quantum heat bath with dissipative Landau-Zener transitions*, Phys. Rev. Lett. **97** (2006) 200404
- [219] S. Kohler, P. Hänggi, and M. Wubs, *Bath-independent transition probabilities in the dissipative Landau-Zener problem*, in W. Janke and A. Pelster, editors, *Path Integrals: New Trends and Perspectives*. World Scientific, 2008
- [220] K. B. Cooper, M. Steffen, R. McDermott, R. W. Simmonds, S. Oh, D. Hite, D. P. Pappas, and J. M. Martinis, *Observation of Quantum Oscillations between a Josephson Phase Qubit and a Microscopic Resonator Using Fast Readout*, Phys. Rev. Lett. **93** (2004) 180401

- [221] G. Ithier, E. Collin, P. Joyez, D. Vion, D. Esteve, J. Ankerhold, and H. Grabert, *Zener Enhancement of Quantum Tunneling in a Two-Level Superconducting Circuit*, Phys. Rev. Lett. **94** (2005) 057004
- [222] W. D. Oliver, Y. Yu, J.C. Lee, K. K. Berggren, L. S. Levitov, and T. P. Orlando, *Mach-Zehnder Interferometry in a Strongly Driven Superconducting Qubit*, Science **310** (2005) 1653
- [223] K. Saito, M. Wubs, S. Kohler, P. Hänggi, and Y. Kayanuma, *Limitation of entanglement due to spatial qubit separation*, Europhys. Lett. **76** (2006) 22
- [224] L. D. Landau, *A theory of energy transfer II*, Phys. Z. Sowjet. **2** (1932) 46
- [225] C. Zener, *Non-Adiabatic Crossing of Energy Levels*, Proc. Roy. Soc. Lond. A **137** (1932) 696
- [226] E. Majorana, *Atomi orientati in campo magnetico variabile*, Nuovo Cim. **9** (1932) 43
- [227] E. C. G. Stückelberg, *Theory of inelastic collisions between atoms*, Helv. Phys. Acta **5** (1932) 369
- [228] O. Zobay and B. M. Garraway, *Time-dependent Tunneling of Bose-Einstein Condensates*, Phys. Rev. A **61** (2000) 033603
- [229] J. Liu, D. Choi, B. Wu and Q. Niu, *Theory of nonlinear Landau-Zener tunneling*, Phys. Rev. A **66** (2002) 023404
- [230] Biao Wu and Qian Niu, *Superfluidity of Bose-Einstein condensates in an optical lattice: Landau-Zener tunneling and dynamical instability*, New J. Phys. **5** (2003) 104
- [231] E. M. Graefe, H. J. Korsch, and D. Witthaut, *Mean-field dynamics of a Bose-Einstein condensate in a time-dependent triple-well trap: Nonlinear eigenstates, Landau-Zener models, and stimulated Raman adiabatic passage*, Phys. Rev. A **73** (2006) 013617
- [232] B. M. Breid, D. Witthaut, and H. J. Korsch, *Manipulation of matter waves using Bloch and Bloch-Zener oscillations*, New J. Phys. **9** (2007) 62
- [233] M. Jona-Lasinio, O. Morsch, M. Cristiani, N. Malossi, J. H. Müller, E. Courtade, M. Anderlini, and E. Arimondo, *Asymmetric Landau-Zener tunneling in a periodic potential*, Phys. Rev. Lett. **91** (2003) 230406
- [234] L. Fallani, L. De Sarlo, J. E. Lye, M. Modugno, R. Sears, C. Fort, and M. Inguscio, *Observation of dynamical instability for a Bose-Einstein condensate in a moving 1D optical lattice*, Phys. Rev. Lett. **93** (2004) 140406

- [235] C. Sias, A. Zenesini, H. Lignier, S. Wimberger, D. Ciampini, O. Morsch, and E. Arimondo, *Resonantly Enhanced Tunneling of Bose-Einstein Condensates in Periodic Potentials*, Phys. Rev. Lett. **98** (2007) 120403
- [236] T. Salger, C. Geckeler, S. Kling, and M. Weitz, *Atomic Landau-Zener tunneling in Fourier-synthesized optical lattices*, Phys. Rev. Lett. **99** (2007) 190405
- [237] A. Zenesini, H. Lignier, G. Tayebirad, J. Radogostowicz, D. Ciampini, R. Mannella, S. Wimberger, O. Morsch, and E. Arimondo, *Time-resolved measurement of Landau-Zener tunneling in periodic potentials*, Phys. Rev. Lett. **103** (2009) 090403
- [238] Y.-A. Chen, S. D. Huber, S. Trotzky, I. Bloch, and E. Altman, *Many-body Landau-Zener dynamics in coupled one-dimensional Bose liquids*, Nature Phys. **7** (2011) 61
- [239] C. Kasztelan, S. Trotzky, Y.-A. Chen, I. Bloch, I. P. McCulloch, U. Schollwöck, and G. Orso, *Landau-Zener sweeps and sudden quenches in coupled Bose-Hubbard chains*, Phys. Rev. Lett. **106** (2011) 155302
- [240] Biao Wu and Jie Liu, *Commutability between semiclassical limit and adiabatic limit*, Phys. Rev. Lett. **96** (2006) 020405
- [241] J. H. Wilkinson, *The Algebraic Eigenvalue Problem*, Oxford University Press, Oxford, 1965
- [242] W. M. Graefe and H. J. Korsch, *Semiclassical quantization of an N-particle Bose-Hubbard model*, Phys. Rev. A **76** (2007) 032116
- [243] K. Smith-Mannschott, M. Chuchem, M. Hiller, T. Kottos, and D. Cohen, *Occupation Statistics of a Bose-Einstein Condensate for a Driven Landau-Zener Crossing*, Phys. Rev. Lett. **102** (2009) 230401
- [244] J. I. Cirac A. Sørensen, L.-M. Duan and P. Zoller, *Many-particle entanglement with Bose-Einstein condensates*, Nature **409** (2001) 63
- [245] J. Estève, C. Gross, A. Weller, S. Giovanazzi, and M. K. Oberthaler, *Squeezing and entanglement in a Bose-Einstein condensate*, Nature **455** (2008) 1216
- [246] T. Hartmann, F. Keck, H. J. Korsch, and S. Mossmann, *Dynamics of Bloch oscillations*, NJP **6** (2004) 2
- [247] M. Glück, A. R. Kolovsky, H. J. Korsch, and N. Moiseyev, *Calculation of Wannier-Bloch and Wannier-Stark states*, Eur. Phys. J. D **4** (1998) 239
- [248] M. Glück, M. Hankel, A. R. Kolovsky, and H. J. Korsch, *Wannier-Stark Ladders in Driven Optical Lattices*, Phys. Rev. A **61** (2000) 061402(R)

- [249] S. R. Wilkinson, C. F. Bharucha, K. W. Madison, Qian Niu, and M. G. Raizen, *Observation of Atomic Wannier-Stark Ladders in an Accelerating Optical Potential*, Phys. Rev. Lett. **76** (1996) 4512
- [250] V. Grecchi and A. Sacchetti, *Acceleration theorem for Bloch oscillators*, Phys. Rev. B **63** (2001) 212303
- [251] M. Abramowitz and I. A. Stegun, *Handbook of Mathematical Functions*, Dover Publications, Inc., New York, 1972
- [252] B. M. Breid, D. Witthaut, and H. J. Korsch, *Bloch-Zener oscillations*, New J. Phys. **8** (2006) 110
- [253] S. Kling, T. Salger, C. Grossert, and M. Weitz, *Atomic Bloch-Zener Oscillations and Stückelberg Interferometry in Optical Lattices*, Phys. Rev. Lett. **105** (2010) 215301
- [254] G. Ritt, C. Geckeler, T. Salger, G. Cennini, and M. Weitz, *Fourier synthesis of optical potentials for atomic quantum gases*, Phys. Rev. A **74** (2006) 063622
- [255] T. Salger, G. Ritt, C. Geckeler, S. Kling, and M. Weitz, *Bloch oscillations of atoms in an optical multiphoton potential*, Phys. Rev. A **79** (2009) 011605(R)
- [256] T. Salger, S. Kling, T. Hecking, C. Geckeler, L. Morales-Molina, and M. Weitz, *Directed Transport of Atoms in a Hamiltonian Quantum Ratchet*, Science **326** (2009) 1241
- [257] D. Witthaut, K. Rapedius, and H. J. Korsch, *The nonlinear Schrödinger equation for the delta-comb potential: quasi-classical chaos and bifurcations of periodic stationary solutions*, J. nonlin. math. Phys. **16** (2009) 207
- [258] A. R. Kolovsky, H. J. Korsch, and E.-M. Graefe, *Bloch oscillations of Bose-Einstein condensates: Quantum counterpart of dynamical instability*, Phys. Rev. A **80** (2009) 023617
- [259] D. Witthaut, M. Werder, S. Mossmann, and H. J. Korsch, *Bloch-oscillations of Bose-Einstein condensates: Breakdown and revival*, Phys. Rev. E **71** (2005) 036625
- [260] S. Longhi, *Klein tunneling in binary photonic superlattices*, Phys. Rev. B **81** (2010) 075102
- [261] S. Longhi, *Field-induced decay of quantum vacuum: visualizing pair production in a classical photonic system*, Phys. Rev. A **81** (2010) 022118
- [262] A. J. Daley, J. M. Taylor, S. Diehl, M. Baranov, and P. Zoller, *Atomic three-body loss as a dynamical three-body interaction*, Phys. Rev. Lett. **102** (2009) 040402

- [263] A. Kantian, M. Dalmonte, S. Diehl, W. Hofstetter, P. Zoller, and A. J. Daley, *An atomic colour superfluid via three-body loss*, Phys. Rev. Lett. **103** (2009) 240401
- [264] M. Roncaglia, M. Rizzi, and J. I. Cirac, *Pfaffian State Generation by Strong 3-Body Dissipation*, Phys. Rev. Lett. **104** (2010) 096803
- [265] S. Diehl, W. Yi, A. J. Daley, and P. Zoller, *Driven Dissipative d-Wave Pairing of Atomic Fermions*, Phys. Rev. Lett. **105** (2010) 227001
- [266] H. Krauter, C. A. Muschik, K. Jensen, W. Wasilewski, J. M. Petersen, J. I. Cirac, and E. S. Polzik, *Entanglement generated by dissipation*, arXiv:1006.4344v1 (2010)
- [267] W. S. Bakr, J. I. Gillen, A. Peng, S. Fölling, and M. Greiner, *A quantum gas microscope for detecting single atoms in a Hubbard-regime optical lattice*, Nature **462** (2009) 47
- [268] P. Würtz, T. Langen, T. Gericke, A. Koglbauer, and H. Ott, *Experimental Demonstration of Single-Site Addressability in a Two-Dimensional Optical Lattice*, Phys. Rev. Lett. **103** (2009) 080404
- [269] G. S. Ng, H. Hennig, R. Fleischmann, T. Kottos, and T. Geisel, *Avalanches of Bose-Einstein Condensates in Leaking Optical Lattices*, New J. Phys. **11** (2009) 073045
- [270] V. A. Brazhnyi, V. V. Konotop, V. M. Perez-Garcia, and H. Ott, *Dissipation-induced coherent structures in Bose-Einstein condensates*, Phys. Rev. Lett. **102** (2009) 144101
- [271] G. Carlo, G. Benenti, G. Casati, S. Wimberger, O. Morsch, R. Mannella, and E. Arimondo, *Chaotic ratchet dynamics with cold atoms in a pair of pulsed optical lattices*, Phys. Rev. A **74** (2006) 033617
- [272] T. Zibold, E. Nicklas, C. Gross, and M. K. Oberthaler, *Classical bifurcation at the transition from Rabi to Josephson dynamics*, Phys. Rev. Lett. **105** (2010) 204101
- [273] J. I. Cirac, A. Schenzle, and P. Zoller, *Inhibition of Quantum Tunneling of an Atom due to the Continuous Observation of Light Scattering*, Europhys. Lett. **27** (1994) 123
- [274] D. K. Campbell, S. Flach, and Y. S. Kivshar, *Localizing Energy Through Nonlinearity and Discreteness*, Phys. Today **57** (2004) 43
- [275] A. Trombettoni and A. Smerzi, *Discrete Solitons and Breathers with Dilute Bose-Einstein Condensates*, Phys. Rev. Lett. **86** (2001) 2353
- [276] S. Flach and A. Gorbach, *Discrete breathers – Advances in theory and applications*, Phys. Rep. **467** (2008) 1

-
- [277] H. Hennig, J. Dorignac, and D. K. Campbell, *Transfer of BECs through discrete breathers in an optical lattice*, Phys. Rev. A **82** (2010) 053604
- [278] J. Denschlag, J. E. Simsarian, D. L. Feder, C. W. Clark, L. A. Collins, J. Cubizolles, L. Deng, E. W. Hagley, K. Helmerson, W. P. Reinhardt, S. L. Rolston, B. I. Schneider, and W. D. Phillips, *Generating Solitons by Phase Engineering of a Bose-Einstein Condensate*, Science **287** (2000) 97
- [279] S. R. Clark, J. Prior, M. J. Hartmann, D. Jaksch, and M. B. Plenio, *Exact matrix product solutions in the Heisenberg picture of an open quantum spin chain*, New J. Phys. **12** (2010) 025005
- [280] M. Sarovar, A. Ishizaki, G. R. Fleming, and K. B. Whaley, *Quantum entanglement in photosynthetic light-harvesting complexes*, Nature Phys. **6** (2010) 462
- [281] Y. Zolotaryuk, S. Flach, and V. Fleurov, *Discrete breathers in classical spin lattices*, Phys. Rev. B **63** (2001) 214422

Lebenslauf

Persönliche Daten:

Name: Friederike Annemarie Trimborn-Witthaut
Geburtsdatum: 15. August 1983
Geburtsort: Ludwigshafen am Rhein
Staatsangehörigkeit: deutsch

Schulbesuch:

1990 - 1994 Carl Bosch Schule, Limburgerhof
1994 - 2003 Geschwister-Scholl-Gymnasium Ludwigshafen a. Rh.
04/2003 Abitur (Note: 1,0 mit Auszeichnung)

Studium:

10/2001 - 03/2002 Früheinstieg ins Physikstudium (FiPS) an der TU Kaiserslautern
04/2003 - 12/2007 Studium der Physik mit den Nebenfächern physikalische Chemie und Mathematik an der TU Kaiserslautern gefördert durch die Studienstiftung des deutsche Volkes
05/2005 Vordiplom in Physik (Note: 1,4) ausgezeichnet mit dem Fachbereichspreis für herausragende Leistungen im Grundstudium
05/2006 Vordiplom in Mathematik (Note: 1,2)
03/2007 - 12/2007 Diplomarbeit „Phasenraumdynamik des Bose-Hubbard-Modells“ in der Arbeitsgruppe von Herrn apl. Prof. Dr. Hans Jürgen Korsch, TU Kaiserslautern
07/2007 - 09/2007 Tutorin am Fachbereich Physik des Kigali Institute for Science and Technology (KIST), Ruanda
12/2007 Diplom in Physik (Note: 1,0) ausgezeichnet mit dem Nachwuchspreis des Fachbereichs Physik für das akademische Jahr 2007

Promotion:

- 01/2008 - 04/2008 Forschungsprojekt, Institut für theoretische Physik, Universität Heidelberg
- seit 05/2008 Promotionsstudent in der Arbeitsgruppe von Herrn Prof. Dr. Reinhard Werner, TU Braunschweig/Leibniz Universität Hannover gefördert durch ein Promotionsstipendium der Studienstiftung des deutschen Volkes
- 08/2008 Forschungsaufenthalt Niels-Bohr Institut Kopenhagen
- 01/2009 - 04/2009 Forschungsaufenthalt Niels-Bohr Institut Kopenhagen

Beruflicher Werdegang:

- seit 07/2010 Referentin im Bundesministerium für Bildung und Forschung, Bonn

Publikationen

1. Friederike Trimborn, Dirk Witthaut, and Hans Jürgen Korsch, *Exact number conserving phase-space dynamics of the M -site Bose-Hubbard model*, Phys. Rev. A **77**, 043631 (2008).
2. Friederike Trimborn, Dirk Witthaut, and Sandro Wimberger, *Mean-field dynamics of a two-mode Bose-Einstein condensate subject to noise and dissipation*, J. Phys. B: At. Mol. Opt. Phys. **41**, 171001(FTC) (2008).
3. Dirk Witthaut, Friederike Trimborn, and Sandro Wimberger, *Dissipation induced coherence of a two-mode Bose-Einstein condensate*, Phys. Rev. Lett. **101**, 200402 (2008).
4. Friederike Trimborn, Dirk Witthaut, and Hans Jürgen Korsch, *Beyond mean-field dynamics of small Bose-Hubbard systems based on the number-conserving phase space approach*, Phys. Rev. A **79**, 013608 (2009).
5. Dirk Witthaut, Friederike Trimborn, and Sandro Wimberger, *Dissipation induced coherence and stochastic resonance of an open two-mode Bose-Einstein condensate*, Phys. Rev. A **79**, 033621 (2009).
6. Friederike Trimborn, Dirk Witthaut, Volker Kegel, and Hans Jürgen Korsch, *Nonlinear Landau-Zener tunneling in quantum phase space*, New J. Phys. **12**, 053010 (2010).
7. Dirk Witthaut, Friederike Trimborn, Volker Kegel, and Hans Jürgen Korsch, *Quantum dynamics of Bose-Einstein condensates in tilted and driven bichromatic optical lattices*, Phys. Rev. A **83**, 013609 (2011).
8. Dirk Witthaut, Friederike Trimborn, Holger Henning, Georgios Kordas, Theo Geisel, and Sandro Wimberger *Beyond mean-field dynamics in open Bose-Hubbard chains*, Phys. Rev. A **83**, 063608 (2011).
9. Friederike Trimborn, Dirk Witthaut, Holger Henning, Georgios Kordas, Theo Geisel, and Sandro Wimberger *Decay of a Bose-Einstein condensate in a dissipative lattice - the mean-field approximation and beyond*, Euro. J. Phys. D **63**, 63 (2011).